PHD

Non-invasive, transdermal, path-selective and highly specific glucose monitoring on a graphene platform

Dupont, Bertrand

Award date:
2015

Awarding institution:
University of Bath

NON-INVASIVE, TRANSDERMAL, PATH-SELECTIVE AND HIGHLY SPECIFIC GLUCOSE MONITORING ON A GRAPHENE PLATFORM

DUPONT BERTRAND

A thesis submitted for the degree of Doctor of Philosophy

University of Bath
Department of Pharmacy and Pharmacology
Septembre 2015

COPYRIGHT

Acknowledgements

I would like to express my gratitude to my supervisors Prof. Rex Tyrrell, Prof. Richard Guy and Dr Adelina Ilie for their insights and support during my doctoral project.

I would like to thank Prof. Frank Marken, Dr Sara Dale and the Frank Marken group for their help and advice in electrochemistry.

I am grateful to Sarah Cordery and to Prof Guy's research group for their assistance with microscopy and skin related experiments.

I would like to thank Dr Ilie's research group; Gavin Jones and Abeer Al-Shammari for their advice and help on using graphene, and in device configurations such as field effect transistors.

I would like to acknowledge Prof. Edmond Magner and Dr Paul De Bank for examining my thesis.

I would also like to express my appreciation to the University of Bath for funding my research project.

Finally, I would like to thank my parents: Dr Gilles Dupont and Marie-Line Dupont as well as my two sisters: Diane Dupont and Claire Dupont Hamm, my cousins: Nicolas Rivals and Damien Rivals and my girlfriend Agnieszka Nawrocka for being there for me, in good and bad times.

I am dedicating this thesis to my grandparents Roger Dupont and Andree Dupont. I am sure they would have been proud to witness that science does indeed run in the family.

"All my life through, the new sights of Nature made me rejoice like a child."

Marie Skłodowska Curie

Abstract

The main technology currently used in diabetic care, monitors blood glucose and involves an invasive "fingerstick" step. However, low patient compliance and non-continuous glucose monitoring imply poor management of diabetes through this technology, which could lead to adverse and potentially life threatening conditions. In this context, non-invasive glucose sensing appears as an alternative that can bring a change in the prevention and management of the diabetic condition, promising to eliminate patient resistance towards more frequent monitoring and, hence, considerably improving diabetic's control over glycaemia. However, no non-invasive technology has yet succeeded on the market over the long term. The research field is therefore open to innovative and performant non-invasive technologies.

This thesis presents the development of a non-invasive biosensor which as a core principle accesses *individual, privileged glucose pathways* in the skin (such as hair follicles), allowing the extraction of glucose directly from the interstitial fluid, *via* reverse iontophoresis (RI). The transdermally extracted glucose is then electrochemically detected in a small size sensor with very high sensitivity. A fully developed technology based on this principle will not require fingerpricking and would thus eliminate users' main barrier to glucose monitoring.

The developed sensor is enzymatic (using glucose oxidase), which electrochemically detects the produced H_2O_2; while the electrode material is graphene produced by Chemical Vapour Deposition, a promising carbon nanomaterial platform for biofunctionalisation and biosensing. The sensor is a miniature one (typically of 9 mm^2 area, containing 24 µL of gel encasing the enzyme), with demonstrated performance parameters that are highly competitive (sensitivity of 2.89 $\mu A.mM^{-1}.cm^{-2}$ and limit of detection down to 1 µM), with high specificity towards glucose. The combination of this sensor with glucose extraction by reverse iontophoresis was then validated (with proportionality between subdermal and extracted glucose concentrations demonstrated); as well as enhanced extraction through targeting of hair follicles with the miniature device. The electrochemical determination of glucose concentration was further confirmed by ^1H quantitative-NMR detection of glucose. Finally, several such sensors were integrated in a multiplex configuration, and independent sensing, with no cross-talk was demonstrated. The steps demonstrated and implemented so far are proof-of-concept of a highly promising non-invasive, transdermal, future technology for diabetic care.

List of abbreviations

1-PBASE: 1-pyrenebutanoic acid succinimidyl ester

3D/2D: 3 Dimensions / 2 Dimensions

AFM: Atomic Force Microscopy

BioFET: Bio-Field Effect Transistor

CE: Counter Electrode

LSCM: Laser Scanning Confocal Microscopy

CV: Cyclic Voltammetry

CVD: Chemical Vapour Deposition

DMF: N,N-dimethylformamide

DMSO: Dimethylsulfoxide

EDTA: Ethylenediaminetetraacetic acid

ENFET: Enzyme Field Effect Transistor

FAD: Flavin Adenine

FDA: Food and Drug Administration

FDM: 1,1'-Ferrocene Dimethanol

FET: Field Effect Transistor

FITC: Fluorescein Isothiocyanate

GOD: Glucose Oxidase

H: Hairy

ICH: International Conference of Harmonization

ISFET: Ion Sensitive Field Effect Transistor

IUPAC: International Union of Pure and Applied Chemistry

LGT: Low Gelling Temperature

LH: Less Hairy

LOD: Limit Of Detection

NMR: Nuclear Magnetic Resonance

PBS: Phosphate-Buffered Saline

PDMS: Polydimethylsiloxane

PMMA: Poly(Methyl Methacrylate)

POD: Horseradish Peroxidase

qNMR: quantitative Nuclear Magnetic Resonance

RE: Reference Electrode

RI: Reverse Iontophoresis

SCE: Saturated Calomel Electrode

SHE: Saturated Hydrogen Electrode

SAM: Self-Assembly Monolayers

SMBG: Self Monitoring Blood Glucose

TMSP-d4: 3-(trimethylsilyl)propionic-2,2,3,3-d4 acid sodium salt

WE: Working Electrode

WHO: World Health Organisation

Table of contents

Chapter 1: Diabetes, glucose sensing and graphene

1.1 Introduction

Diabetes is a growing healthcare problem [1], which needs rapid and efficient addressing. The disease involves abnormal blood glycaemia which can lead to a series of adverse events if the patient doesn't manage the condition adequately. A diabetic individual will therefore require regular blood glucose monitoring in order to assess the glycaemic status and react with the correct therapeutic response. The project aims to benefit individuals suffering from Type 1 and Type 2 diabetes. If the disease is not managed properly, severely damaging adverse effects are apparent. As a result, a number of glucose biosensors of different sorts have been developed that rely upon several detection techniques. The breakthrough achievement was the invention of the oxygen/glucose electrochemical sensor in 1962 [2], triggering an industry that was estimated to be worth billions of $ in the US by 2012 [3]. This included the development of self-monitoring blood glucose devices SMBG (especially fingerstick glucose biosensors [4, 5]) which contributed substantially to the success story [6]. With these simple systems, patients were and are still able to monitor their blood glucose levels with a single drop of blood as low as 0.3 μL [7], radically changing the management of the disease. However, despite this innovation patient self-monitoring shows poor adherence only 46% of patients with type 1 diabetes, and 39% of patients with type 2 diabetes, have been reported to follow their glucose monitoring and treatment carefully, and have fewer adverse effects [8]. This lack of compliance was due to several factors: (1) psychological issues (anxiety, stress, etc.), (2) pain related problems, (3) lack of motivation, (4) poor disease management (particularly difficult at a young age), (5) cost, (6) religious beliefs, and (7) access to medication and to monitoring devices [9].

Consequently, new technologies emerged with the goal of better controlling the disease. Specifically, invasive devices (surgically implanted [10] or subdermal[11]) and non-invasive sensors (tear analysis /contact lenses [12], sweat [13], urine [14], and saliva sensors [15],

optical techniques (near infrared spectroscopy (NIR) [16], optical scattering; spatially-resolved diffuse reflectance [17], Raman scattering [18]), polarimetry, photo acoustic spectroscopy, and transdermal reverse iontophoresis [19]). To date, however, only invasive sensors have achieved an ongoing market presence, while two non-invasive technologies were also commercialized, the GlucoWatch ® Biographer (Cygnus, CA, USA) which received U.S. FDA approval and the PENDRA® (Pendragon Medical Ltd., Zurich, Switzerland). Neither proved to be successful nor are any longer available. PENDRA® is a non-invasive technology based on impedance spectroscopy. It was introduced in Europe (2004) and the detection relied on the measurement of skin impedance. The idea was that changes in skin impedance would be detectable due to glucose concentration-dependent effect on Na^+ and K^+ in gradients [20, 21]. The device, although relatively inexpensive and user friendly had significant limitations including: its indirect detection method; its ineffectiveness in 1/3 of users; the need for a blood glucose calibration [22], and a 60 minutes equilibration before useful blood glucose levels would be determined [23]. The GlucoWatch ® Biographer on the other hand relied on the application of a small direct current across two electrodes positioned on the skin surface to induce the electroosmotic extraction of a very small volume of interstitial fluid containing glucose. However, the innovation suffered several drawbacks, the main ones being: (1) high dilution of the tiny extracted interstitial volume into the large volume of the sensor (typically, 400 µL of gel [24]), resulting in very low (submicromolar) concentrations of glucose and therefore requiring the sensor to operate very close to its limit of detection [25]; (2) sensitivity and accuracy issues especially in hypoglycaemic situations; and (3) the device still required an invasive "finger-pricking" calibration due to variations in the glucose dilution factors between subjects, or for different skin sites on a single individual [26]. These major issues combined with other problems, such as long warm-up time, skipped readings and skin irritation resulted in the withdrawal of the device from the market.

There is, however, potential for a radically revised non-invasive glucose technology based on the reverse iontophoresis extraction technique. The path of electroosmotic fluid flow across the skin under the influence of iontophoresis is privileged through skin appendages, specifically through hair follicles [27]. This fact gave birth to the idea that was followed in this work: to develop a glucose sensor that will specifically target the hair follicles extraction pathways. The glucose concentration at these targeted sites is envisaged to be significantly higher than over a non-follicular part of the dermis, and to approach the glucose

concentration in the interstitial fluid. The electrode/sensor we developed is therefore a miniaturized amperometric glucose oxidase (GOD) biosensor (containing 24 µL volume of gel as receptacle, and of 9 mm^2 geometric area) that will target the preferential extraction. Several such detectors are then multiplexed with the purpose of achieving an improved skin coverage as well as greater accuracy. The work also aimed at improving the sensing technology. Hence, as opposed to the carbon paste/platinum electrochemical glucose sensor involved in the GlucoWatch ® Biographer detection [28], the successful integration of chemical vapour deposited (CVD) graphene as the transducer in a glucose oxidase first generation (i.e. relying on oxygen) biosensor is demonstrated. The reasons behind the choice of CVD graphene as a transducer in the sensor development are in section 1.4.

Using graphene as the base of the research, a visualisation of different enzymatic functionalization and study of the catalytic activity of such coated enzymes will be presented. Two detection platforms will then be investigated in the form of a FET or an amperometric sensor. In parallel amperometric configurations involving detection of glucose via H_2O_2 (first generation sensor) and redox mediators (second generation sensors) or platinum nanoparticles will be studied and the advantage of one technique over the other presented. The optimized sensor will in the end be a CVD graphene-based sensor, enhanced by platinum nanoparticles, and coupled to an agarose gel reservoir containing glucose oxidase.

In order to achieve a non-invasive detection of glucose the developed sensor will then be integrated with reverse iontophoresis to allow both glucose extraction through porcine skin (the closest physiological model to the human skin), and subsequent electrochemical detection. Targeted extraction will also be studied on individual hair follicles in order to confirm privileged path extraction of glucose and subsequent detection. The targeted extraction results will be validated by an independent ^1H quantitative NMR control experiment. An attempt will finally be made to integrate the sensors in a multiplex assay and to demonstrate separated and autonomous glucose sensing, without cross talking.

This thesis is structured as follows:

- **Chapter 1**: (1) Introduction (2) Diabetes mellitus, (3) biosensing, (4) graphene, (5) Analytical and microscopic techniques and (6) aims and objective of the thesis
- **Chapter 2**: Glucose oxidase functionalization on CVD graphene
- **Chapter 3:** Biosensor design and detection principle
- **Chapter 4:** Performance of the sensor
- **Chapter 5:** Non-invasive glucose monitoring
- **Chapter 6:** General conclusion and future work.

1.2 Diabetes Mellitus

1.2.1 Disease pathology

Diabetes mellitus has been defined by the WHO as: "a metabolic disorder of multiple aetiology characterized by chronic hyperglycaemia with disturbance of carbohydrate, fat and protein metabolism resulting from defects in insulin secretion, insulin action or both" [29].
The metabolism of any organism is the sum of biological processes that either produce or consume energy (catabolism and anabolism). The disruption of these mechanisms constitute a metabolic disorder and will cause indirect adverse effects from minor symptoms to life threatening conditions. In the case of diabetes, the disturbed assimilation of glucose by cells causes dysregulation of metabolism inducing hyperglycaemia (high levels of glucose in the bloodstream) [30] and ketoacidosis (caused by incomplete metabolism of fatty acids and accumulation of ketones in the body fluids) [31]. Two types of diabetes (1 and 2) can be distinguished.

1.2.1.1 Type 1 diabetes

Type 1 diabetes is caused by the destruction of pancreatic β cells. This leads to an impaired production of insulin up to the point where insulin injections are required for survival. Type 1 diabetes can be separated into two categories: (1) Type 1A ("immune-mediated") which is characterised by the early presence of antibodies against glutamic acid, islet cells or insulin, and (2) Type 1B ("idiopathic") which is not immunological. In type 1A, the rate of pancreatic β cell destruction is variable and a function of the age of the individual; faster for children,

slower in adults, who can retain a small insulin secretion activiti (so called "latent autoimmune diabetes"). However, ultimately even these diabetes ultimately reach a point at which insulin injections become vital [32, 33].

1.2.1.2 Type 2 diabetes

Type 2 diabetes is the most common form of the disease. It is characterised by impairment of either insulin secretion by the pancreas or insulin detection by receptors or, and most generally, both. Type 2 diabetes involves a progressive degeneration of the pancreatic β cells with time. At least initially, Type 2 diabetics do not require insulin injections. They can remain asymptomatic over a long period of time before the disease is diagnosed, rendering prevention particularly difficult. 90% of the incidence of diabetes can be related to an unhealthy ("western") life-style [34], correlated mainly with obesity, but also with smoking and/or alcohol consumption. A sedentary lifestyle is also associated with the progression of the disease and induced insulin resistance. Other, obvious risk factors include: little or no physical activity, high fat /carbohydrate and low fibre diet, high blood pressure, stress, aging, etc. [35]. Nevertheless, Type 2 diabetes can be reversed through exercise, and a healthier diet and lifestyle, if treated early [36]. Finally, although it is widely agreed that the development of insulin resistance and Type 2 diabetes are mainly due to environmental (life style) factors, a genetic component has also been identified and while the latter account for defective insulin secretion, no clear genetic relationship has yet been established with insulin resistance.[37].

1.2.1.3 Gestational diabetes and other types of diabetes

Gestational diabetes is a life threatening condition for the mother and the child predisposing both individuals and occurs in 7% of all pregnancies in the USA [34]. It manifests during the 3rd trimester of pregnancy and usually terminates with delivery. Women with this condition, however are more likely to develop Type 2 diabetes later in life [34]. Other types of diabetes are related to underlying disorders: (1) diseases of the exocrine pancreas, (2) acute and chronic pancreatitis, (3) genetic defects in insulin action or β cell function, and (4) drug induced diabetes.

1.2.2 Prevalence

Diabetes mellitus is now a worldwide health problem that has dramatically increased in prevalence in the past 30 years (5.6 million against 20.9 million of diagnosed diabetics in the US between 1980 and 2011 [38, 39, 40]). This shows that the disease is a serious and growing problem which has to be addressed. A prevalence schematic is shown in figure 1.1 [1].

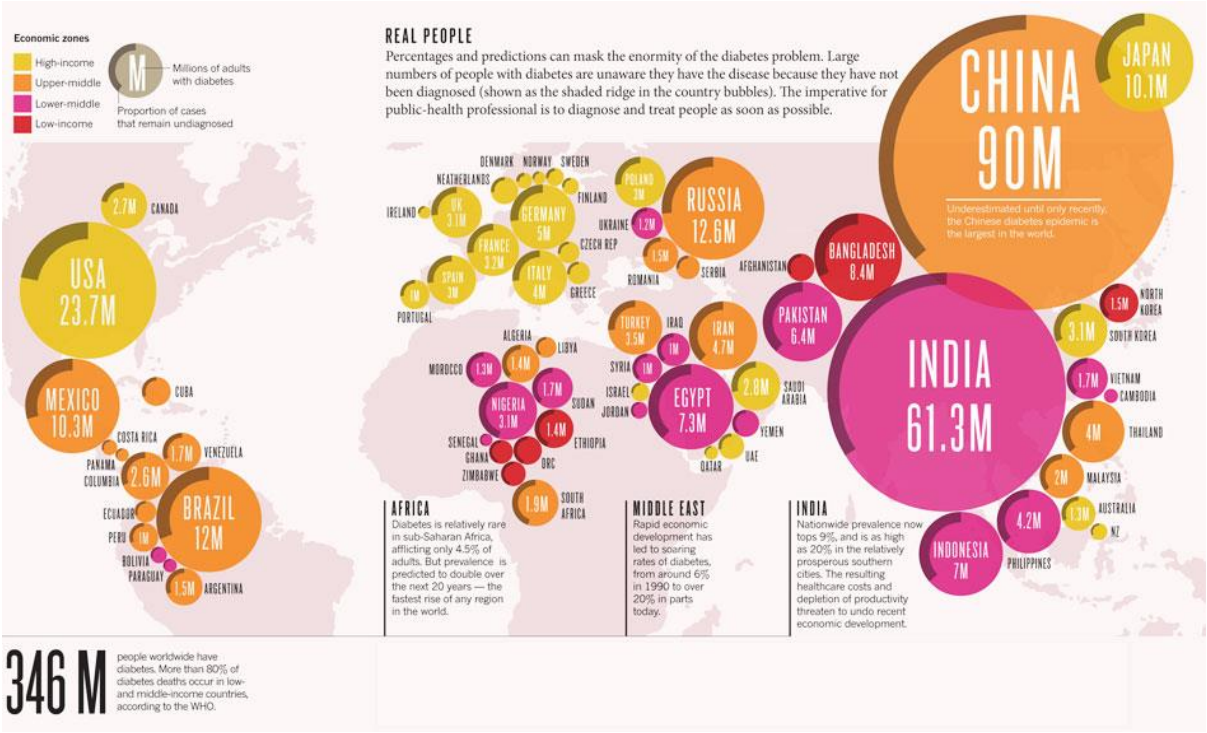

Figure 1.1. Estimated number of diagnosed and undiagnosed cases of diabetes (shaded rings) worldwide in 2012 (reproduced from [1]).

Furthermore, while it would make sense from the description of diabetes as a lifestyle related condition that developed countries would present the highest numbers of diabetics due to their poor "western lifestyle", surprisingly middle to low income countries such as China, India and the Middle-East present the largest cases numbers of cases. This observation has multiple explanations: (1) It has been demonstrated that non-Caucasian ethnic groups present a higher risk of developing Type 2 diabetes [41]. (2) The number of cases can be correlated to economic development. China and India are among the emergent economic powers where the population have gradually changed their lifestyle, becoming more westernised [42]. (3) In

lower income countries, there is less access to preventive treatments, less education, and less infrastructure for early detection of the disease and continuation of treatments. This could explain the high growth rate in Africa, for instance [43].

1.2.3 Diabetes blood glucose levels

1.2.3.1 Fasting plasma glucose, oral glucose tolerance test, HbA1c testing

Three tests are commonly used to diagnose diabetes mellitus:

- **Fasting plasma glucose (FPG)** involves an 8 hour fast and then measuring the blood glucose concentration. The test provides a measurements of the basal glucose level [44].
- **The oral glucose tolerance test (OGTT)** and a measure of blood glucose 2 hours later. The OGTT involves administration of the equivalent of 75 g anhydrous glucose dissolved in water and measurement of the glycaemia after 2 hours [45].
- Thirdly, these two parts are also combined with an analysis of **HbA_{1c}**, a by-product of glucose metabolism (i.e., glycated haemoglobin; the HbA_{1c} complex). HbA_{1c} is expressed as a fraction of total haemoglobin and is proportional (subject to certain individual limitations related to race, age, blood disease [46]) to blood glucose levels. The HbA_{1c} is accepted by the WHO as a diagnosis test for diabetes (i.e., HbA_{1c} ratio ≥ 6.5 %) [47]. However, measurement of HbA_{1c} is not a "spot check" on glucose levels; rather, it provides information on the patient's glycaemic state over a period of approximately the preceding 2 months (see section 1.2.4.1)[48].

1.2.3.2 Blood glucose levels and diabetes diagnosis

1.2.3.2.1 Diabetes

Hyperglycaemia in diabetes has been defined by the following blood glucose level ranges: "fasting plasma glucose ≥7.0 mM (126 mg/dL) or 2 hours plasma glucose (after meal) ≥11.1 mM (200 mg/dL) [44]".

1.2.3.2.2 Pre-diabetes

Prediabetes comprises two physiological states: impaired glucose tolerance (IGT) and impaired fasting glucose (IFG). These are respectively defined as: "fasting plasma glucose

<7.0 mM (126 mg/dL) or 2 hours plasma glucose between 7.8 mM and 11.1 mM (140 and 200 mg/dL)" for IGT, and "fasting plasma glucose between 6.1 and 6.9 mM (110 and 125 mg/dL) or 2 hours plasma glucose <7.8 mM (140 mg/dL)" for IFG [44]. This implies that a normal fasting glycaemia (as defined by WHO) will correspond to "fasting plasma glucose of <6.1 mM and a 2 hours plasma glucose of <7.8 mM" [29]. IGT and IFG are both considered as transition states (i.e., risk factors) leading ultimately to diabetes. An individual experiencing several IFG, IGT and diabetic phases will eventually show hyperglycaemic symptoms which are defined as: (1) polydipsia (excessive thirst), (2) polyuria (frequent urination), (3) blurred vision, and (4) extreme fatigue [49]. These are the acute symptoms of diabetes; however, they are insufficient to make a robust diagnosis, especially in the early stages of the disease when they may be barely perceptible.

1.2.3.2.3 Recommended blood glucose levels in non-pregnant diabetics, as defined by the American Diabetes Association (ADA).

The ADA recommendation for glycaemic measurements with an HbA_{1c} < 7% are: (1) pre-prandial (before a meal) capillary plasma glucose between 3.9 and 7.2 mM (70 and 130 mg/dL), or (2) peak post-prandial (after a meal) capillary plasma glucose < 10 mM (180 mg/dL). The postprandial attribute is defined as 1 or 2 h after the beginning of the meal. These targets have to be moderated according to the following factors [48]: duration of diabetes, age, comorbid conditions, cardiovascular and microvascular diseases, hypoglycaemia unawareness, and other factors

1.2.4 Diabetes management

Today, HbA_{1c} testing, glucose sensing and urine sensing are used to monitor diabetes mellitus.

1.2.4.1 HbA1c testing

Glycation of haemoglobin occurs during the 120 days lifespan of the red blood cell. HbA_{1c} monitoring should therefore be performed on a ≤ 2 monthly regular basis for diabetes management. The measurement of HbA_{1c} should be viewed as a complement to daily blood glucose monitoring and a long term indicator of the outcome of therapeutic interventions [50].

1.2.4.2 Glucose monitoring technologies: Brief historical background

The first glucose meter relied on a colorimetric reaction on a strip ("dextrostics") and on reflectance measurements ("Ames Reflectance Meter: ARM; Miles Laboratories, (Elkhart, IN, USA)") [9]. This laboratory or hospital-based instrument weighed around 1.2 kg, was priced at nearly $500, required a very complicated sample preparation, and provided consistantly overestimated glucose measurements in the low glycaemic range. The first electrochemical biosensor for glucose was developed in 1962 [2]. Its principle of operation involved reaction of glucose with the enzyme glucose oxidase to generate H_2O_2 which was then oxidized electrochemically on an electrode, generating a measurable current proportional to the concentration of glucose present [7]. This led to the development of the widely used fingerstick glucose biosensor (Exactech, first developed by Medisense, (Cambridge, MA, USA) in 1991 [5]) based on a redox mediator (i.e., ferrocene). This development represented a significant improvement in disease management as patients were then able to monitor their own blood glucose. The fingerstick blood sensors became a major commercial success, comprising up to 85% of the market [51]. The American Diabetes Association advised a fingerpricking frequency of 6 to 8 times a day for Type 1 diabetics [48], but this regimen is predictably low [9].

1.2.4.3 Urine glucose sensors, glycosuria monitoring

Glycosuria is the presence of glucose in urine. Below a blood glucose value known as the renal threshold, no glucose is identified in the urine due to renal reabsorption. This threshold varies between individuals and also depends on disease state (long-standing diabetics may have a higher threshold) or physiological condition (young children and pregnant women have reduced thresholds [52]). It is therefore very difficult to correlate blood glucose levels with measurements of glycosuria. Other problems of urine glucose sensing include: (1) Single point measurements and dependence on the frequency of urination. (2) No information about blood glucose levels below the renal threshold. (3) Testing provides an average glucose concentration in urine, not a direct measurement of blood glucose. (4) A negative urine glucose sensing test does not distinguish between hypoglycaemia, euglycaemia and mild or moderate hyperglycaemia. (5) Drugs can affect glycosuria. (6) Fluid intake and urine output modify the glycosuria. (7) Most glucose sensing urine tests are either based on glucose oxidase: Chemstrip (Roche Diagnostics, USA), Clinistix (Bayer, Leverkusen, Germany), Diastix (Bayer, Leverkusen, Germany), and Uristix (Siemens, Munich, Germany)) or copper sulphate reduction: Clinitest, (Bayer, Leverkusen, Germany). The latter is not specific to glucose, however. (8) Several urine sensors are imprecise at low urinary glucose concentrations [52]. Practical issues affecting accuracy have also been identified [53]. Overall, glycosuria does not reliably reflect blood glucose levels and is now rarely used as a surrogate for blood glucose monitoring. In fact, urine analysis is only employed for limited specific cases: (1) Relatively stable type 2 diabetics can gain information from a glycosuria test in conjunction with blood glucose measurements [53]. (2) Glycosuria sensing is sometimes undertaken to assess glucose control and dietary compliance. (3) It is also used with patients for whom blood glucose monitoring is impossible or impractical.

1.3 Biosensing

1.3.1 Biosensing general concept, transducer/bioreceptor

The International Union of Pure and Applied Chemistry (IUPAC) define biosensors (figure 1.2) as a subset of chemical sensors: “A chemical sensor is a device that transforms chemical information, ranging from the concentration of a specific sample component to total

composition analysis, into an analytically useful signal. Chemical sensors usually contain two basic components connected in series: a chemical (molecular) recognition system (receptor) and a physicochemical transducer. Biosensors are chemical sensors in which the recognition system utilizes a biochemical mechanism" [54]. A more extended definition has also been proposed [55, 56]: "Biosensors are defined as analytical devices incorporating a biological material (e.g. tissue, microorganisms, organelles, cell receptors, enzymes, antibodies, nucleic acids, natural products etc.), a biologically derived material (e.g. recombinant antibodies, engineered proteins, aptamers etc.) or a bio-mimic (e.g. synthetic receptors, biomimetic catalysts, combinatorial ligands, imprinted polymers etc.) intimately associated with or integrated within a physicochemical transducer or transducing microsystem, which may be optical, electrochemical, thermometric, piezoelectric, magnetic or micromechanical".

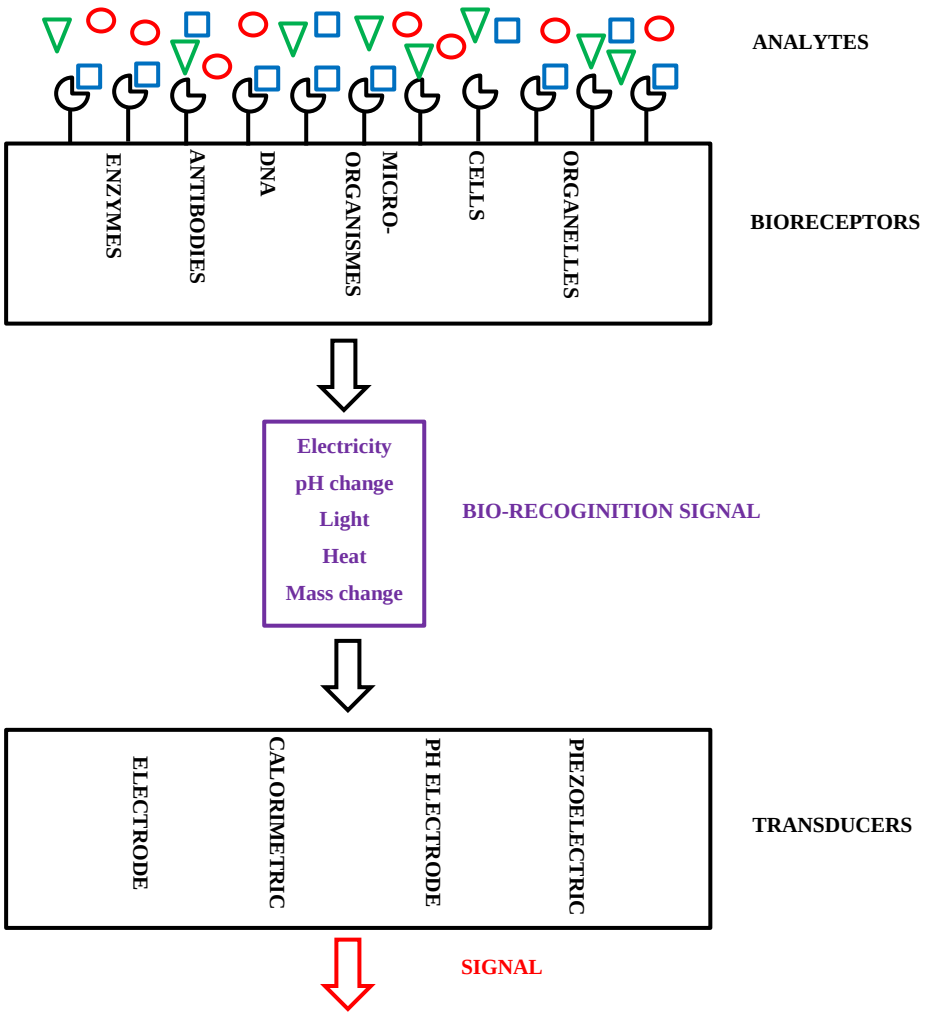

Figure 1.2. Biosensor operation. Two structural components are common to all biosensors: the bioreceptor and the transducer.

1.3.2 Biological entity: Enzymes

Enzymes are the most common element found in biosensors. Glucose oxidase, for instance, is present in almost all glucose biosensors. Enzymes have several advantages for integration into sensing devices: (1) they are relatively stable and retain their catalytic activity when immobilised on an electrode, (2) both the catalytic and substrate affinities of an enzyme can be modified, (3) enzymes are highly substrate specific and follow Michaelis-Menten kinetics [57].

- **Glucose oxidase**

Glucose oxidase (GOD) is the most commonly used enzyme in glucose biosensing. This enzyme catalyses the oxidation of β-D-glucose to D-glucono-1,5-lactone and then gluconic acid in the presence of molecular oxygen producing hydrogen peroxide (H_2O_2). GOD is isolated and produced from many fungal sources (*Aspergillus*, *Penicilium* or *Saccharomyces*) among which *Aspergillus Niger* is the most common. GOD is a dimeric protein composed of two identical polypeptide chains that are linked by disulphide bonds (figure 1.3). Each of the chains contains a tightly bound but non-covalently attached flavin adenine (FAD) moiety at the active site of the enzyme. The catalysis of β-D-glucose involves the reduction of FAD to $FADH_2$ and then the re-oxidation to FAD with molecular oxygen. The FAD cofactors sit inside a funnel shaped active site with a 10Å × 10Å opening.

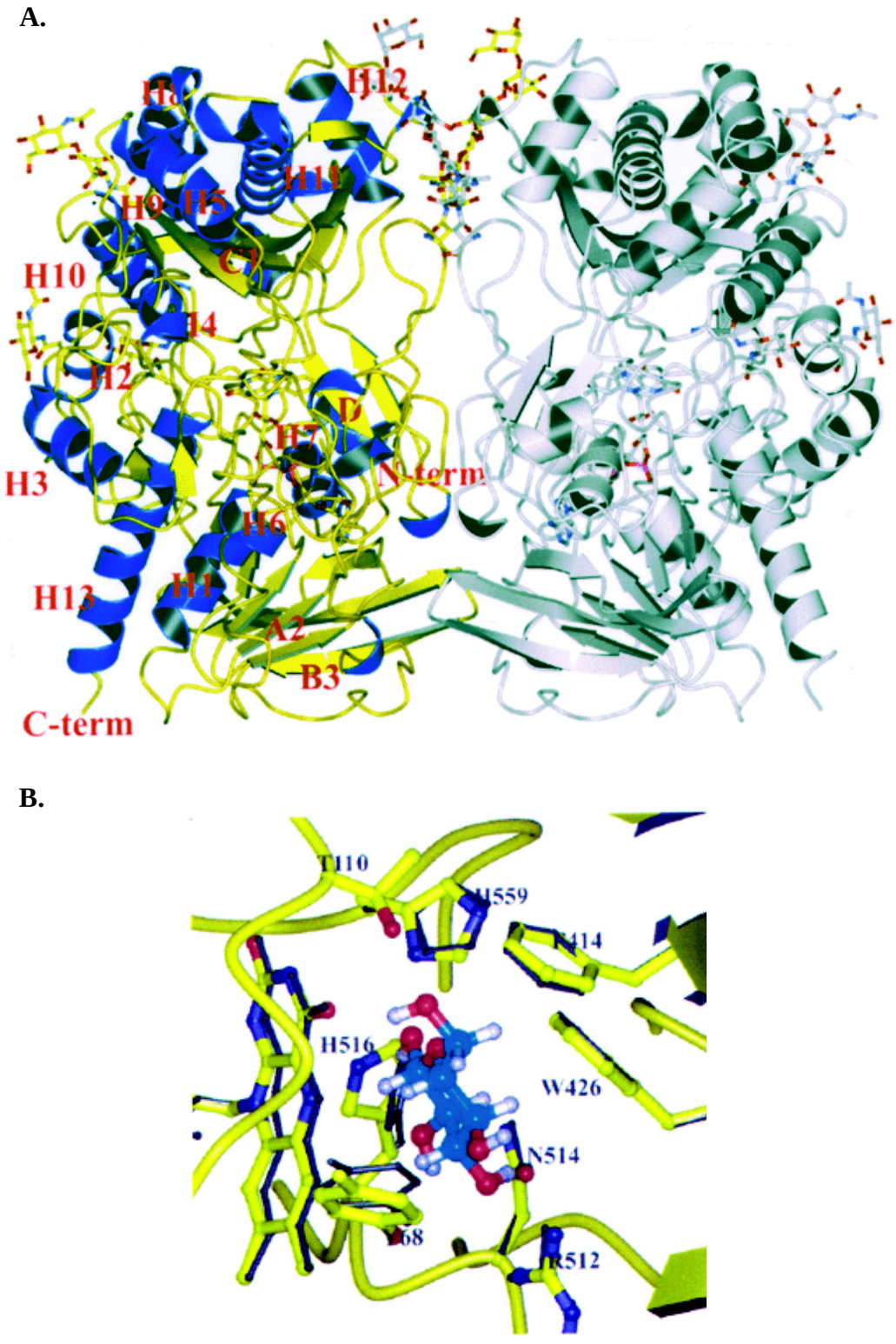

Figure 1.3. Glucose oxidase crystallographic structure (reproduced from [58]). A: Overall structure of the GOD with one subunit in grey and the other coloured. B: Representation of the GOD active site and the amino acids involved in the reaction; the β-D-glucose substrate is shown in pale blue.

GOD has a molecular weight of around 160 kDa and is specific to the β anomer of D-glucose. A number of inhibitors of glucose oxidase have been identified, specifically: chloromecuribenzoate, Ag^{+}, Hg^{2+}, Cd^{2+}, Pb^{2+}, Cu^{2+}, Zn^{2+}, hydroxylamine, hydrazine, phenyl hydrazine, dimedone and sodium bisulphate [59]. Ag^{+} and Hg^{2+} and halide ions are competitive inhibitors towards molecular oxygen [60, 61]. The enzymatic activity is strongly dependent upon the ionic state of the active site amino acid residues. The optimal pH range for GOD is between 3.5 and 6.5 [62]. However, the enzyme is stable enough at physiological pH [63, 64].

1.3.3 Transducer: Electrochemical detection

Electrochemical biosensors are very common, the best example of which is the fingerstick glucose biosensor. These sensors rely on the transformation of a biochemical signal to an electrical signal which is detected at the transducer. Electrochemical biosensors can be separated into catalytic biosensors (enzymes, whole cells, etc…) and affinity sensors (DNA, antibodies etc…). Detection methods are classified in four categories: voltammetry/amperometry, potentiometry, impedance, and conductometry.

1.3.3.1 Voltammetry/amperometry

In voltammetric or amperometric techniques, a potential is applied to a working electrode; WE against a reference electrode; RE (held at a stable potential) and a current is measured that is a function of the electrochemical reaction happening at the WE. Amperometric biosensors are by far the most commonly found electrochemical devices. In amperometry, the potential at the WE is stepped to a constant value with respect to the RE and the change of current (induced by redox reactions at the working electrode) is measured over time (between the WE and a third counter electrode; CE) [65].

1.3.3.2 Potentiometry

A potentiometric sensor is a device that relies on the measurement of the potential of an electrochemical cell while a negligible current is being drawn. Common potentiometric sensors are pH sensors involving the use of two reference electrodes separated by a membrane sensitive to protons or ions in solution. [65]. A specific type of potentiometric devices are field effect transistors (FET), and more precisely ion sensitive field effect transistors (ISFET) and biological field effect transistors (BioFET). These are three electrode

systems comprising a source, a drain and a gate. The source and drain are separated by a semiconductor and the potential applied at the gate will create an electric field that will influence the current flow from source to the drain. Again, any induction of charge at the semiconductor interface will change the potential and generate a signal proportional to the concentration of the analyte of interest (e.g., protons produced during an enzymatic reaction).

1.3.3.3 Impedance

Electrochemical impedance spectroscopy (EIS) is a technique that measures the resistive and capacitive properties of a material when subject to small amplitude sinusoidal Alternating Current. The resistance and capacitance are then obtained [65]. EIS is typically used for affinity biosensors where any binding (DNA, antibody…) will induce a change of impedance on the electrode material. EIS has received much attention from the scientific community in the past few years because it does not require any mediator (as opposed to certain voltammetric/amperometric analysis) and is very sensitive to any biological attachment [66]. The downside of the technique however, is non-specific binding.

1.3.3.4 Conductimetry

Conductimetric experiments measure the change of conductance in solution, due to the migration of ions. While these are among the less described biosensors, they have several advantages including: no requirement for a reference electrode, insensitivity to light, and cheap integration and miniaturization. However, an important drawback is the necessity for the produced ion to induce a conductance change that will be detectable [67]. The most described conductometric biosensors relate to urea detection [68], but some others have been developed to detect bacteria (Mycobacterium avium) [69] or heavy metal ions [70].

1.3.4 Reference technique: fingerstick glucose biosensor

The reference technology and the more successful commercially available biosensor is the fingerstick glucose biosensor. As already introduced in section 1.3.2, the device work on the detection of glucose via enzymes such as glucose oxidase; GOD or glucose dehydrogenase; GDH integrated with redox mediators in so called second generation sensors. The first fingerstick device: Exactech developed by Medisense (Cambridge, MA, USA) in 1991 was based on a GDH/ pyrrole-quinolinequinone (PQQ) enzymatic reaction associated to ferrocene as a redox mediator. PQQ is a cofactor in the enzymatic reaction with glucose and GDH [7].

The transducer was a screen printed carbon electrode [71]. Most of the commercial fingerstick biosensor still work on the same combination of enzyme and redox mediator and are produced via the screen printing process. Table 1.1 is a list of some of the fingerstick devices available commercially along with some of their characteristics such as the sample volumes, the duration of the tests and the assay glucose concentration range [7].

For low blood glucose measurement the reference accepted method would still be the same enzymatic one (i.e. fingerstick biosensor). Of course there are ways to quantify low blood glucose (chromatography, HPLC, qNMR, etc.), see chapter 5 section 5.1.2.2, but these methods are only used punctually and in no way qualified as reference techniques, adapted to patient studies.

Table 1.1. Characteristics of some fingerstick glucose meters

Device	Detection (enzyme)	Sample volume (µL)	Duration of the test (sec)	Assay glucose range (mM)
FreeStyle Freedom Lite (Abbott Diabetes Care, Alameda, CA, USA)	GDH/PQQ	0.3	5	1.1 to 27.8
WaveSense KeyNote (AgaMatrix, Salem, NH, USA)	GOD	0.5	4	1.1 to 33.3
Glucocard X-meter (Arkray, Kyoto, Japan)	GDH	0.3	5	0.6 to 33.3
Accu-Chek Aviva Roche (Indianapolis, IN, USA)	GDH/PQQ	0.6	5	0.6 to 33.3
OneTouch UltraLink (LifeScan part of Johnson & Johnson medical, Livingston, UK)	GOD	1	5	1.1 to 33.3

The technology became the “star” and the major technique for glucose monitoring in only 24 years. Noticeably it is used as a reference for comparison with newly developed techniques such as the transdermal monitoring devices described in the next section [19]. It is also a

fundamental element of diabetes care for many patients around the world. However, this table also brings to light the fundamental problem of each of these devices: the need for a blood sample (the fingerpricking) which is the cause of much stress, discomfort and bad glycaemic control for the majority of patients. The research was therefore oriented towards "next generation devices" separated in two major classes: implanted and non-invasive technologies.

1.3.5 Alternative glucose sensing to the fingerstick meters: implanted and non-invasive technologies

1.3.5.1 Implanted, continuous glucose monitoring system (CGMS)

The following section will give a description of implanted technologies in next generation glucose sensing.

1.3.5.1.1 Intravenously implanted sensors

Intravenously implanted glucose monitoring sensors are for patients who are critically ill and in need of intensive insulin therapy or are in intensive care. The latter experience rapid fluctuations in blood glucose levels, blood flow distribution and temperature. In such situations, traditional fingerstick glucose sensors are insufficient to ensure efficient constant glucose monitoring. The direct intravenous technologies developed include: (1) The Via®Blood (Via Medical Corporation, Austin, TX, USA) [72], OPTImus (IntelliDx Corporation, Santa Clara, CA, USA) [73], and the STG-22™ (Nikkiso, Tokyo, Japan) [74] systems which draw small samples of blood (2 mL per hour) via a catheter [74] that are subsequently analysed with a glucose sensor. [73]. And (2), glucose monitoring devices coupled to central catheters: The GlucoClear™ (Edwards Lifesciences, Irvine, CA, USA) [75], which uses enzymatic (glucose oxidase) amperometric detection, and the GluCath® Intravascular CGM System (GluMetrics Inc., Irvine, CA, USA) [76] which relies on a fluorescent sensor, were developed for continuous intravenous measurements [77].

1.3.5.1.2 Subcutaneous sensors

The other widely developed implanted CGMS are subcutaneous sensors. These are available to a broader patient audience, subcutaneous tissues being more accessible and the implantation of the sensor less prone to complications than the intravascular technologies. The first commercial, FDA-approved subcutaneous CGMS was the Minimed® (Medtronic,

MiniMed Inc., Northridge, CA, USA) [78, 79]. The sensor device is positioned on a needle, inserted subcutaneously [80] to electrochemically detect (via glucose oxidase) subdermal interstitial fluid glucose. Several devices were then commercialized based on the subcutaneous insertion of a needle sensor: (1) The Guardian® Real-Time also developed by Medtronic, MiniMed Inc., Northridge, CA, USA is a real time glycemic monitor unlike its' Minimed® predecessor. It is formed of a platinum electrode/ polyurethane poly urea polymer and also measures glucose amperometrically via GOD (First generation: detection of H_2O_2). It received FDA approval in 2006 [81]. (2) DexCom Inc. (San Diego, CA, USA) also received FDA approval the same year for their device: the DexCom STS™-7. The technology consists of a platinum electrode coupled with a hydrophobic polyurethane and a hydrophilic polyurethane mixture on a 26 gauge insertion needle. The sensor is similarly to the Medtronic devices a GOD/ amperometric device [81]. (3) Finally, the FreeStyle Navigator (Abbott Diabetes Care, Alameda, CA, USA) uses Carbon/ osmium wired electrode to provide a real time monitoring of the glycemia. The needle sensor is an amperometric second generation sensor based on a combination of GOD and an osmium mediator ($Os^{2+/3}$). It received FDA approval in 2008 [81]. The principal limitation to the use of subcutaneous sensors have been identified as: (1) Biocompatibility, which is often a major problem, since any local inflammatory response not only influences the plasma/interstitial glucose concentration ratio but is also deleterious to the patient. (2) Biofouling (disruption of the sensing platform) which is detrimental to the sensing itself and approaches to address this problem are being examined [82]. (3) And the lack of compliance from the patients: the methods involving the placement of a needle underneath the skin [83].

Nevertheless, subcutaneous technologies are the only alternative and approved glucose monitoring approach to the fingerstick method for home use [26]. Advantages and disadvantages of each of the technologies cited are listed in table 1.3 and their performance compared to the developed device in chapter 4, table 4.4.

1.3.5.1.3 Interstitial fluid glucose concentrations/ blood glucose concentration relationship

The subcutaneous technologies presented so far measure interstitial fluid glucose concentrations, not those in the plasma. These two reservoirs can be considered as separated compartments that interact dynamically with each other, see figure 1.4. In the skin, glucose

passes from the capillary endothelium to the interstitial fluid by simple diffusion across a concentration gradient without the need of an active transporter [84].

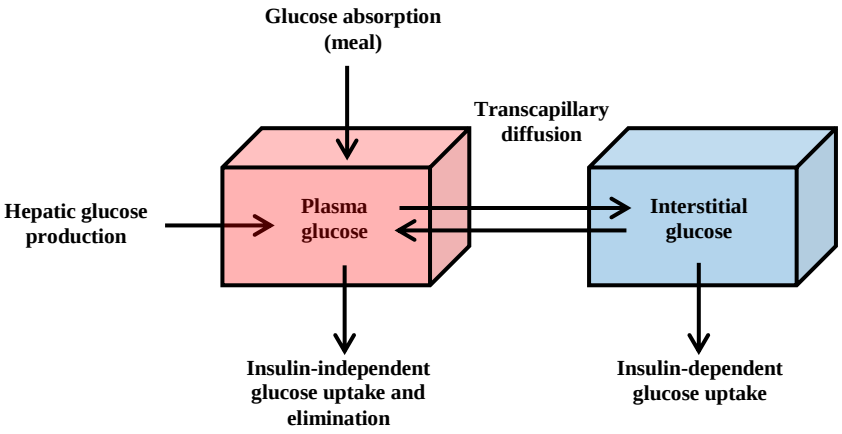

Figure 1.4. Glucose distribution between "plasma glucose" and "interstitial glucose"

The glucose concentration in the interstitial compartment has a proportional relationship with the plasma glucose level [85], the ratio depends on several factors, such as insulin production, blood flow, capillary permeability, etc. There is therefore a lag time (the time required for glucose to diffuse from the capillary to the tissue) [26] before the plasma and interstitial glucose concentrations come into dynamic equilibrium [85]. The lag time varies as a function of glucose concentration, metabolic rate, and glucose uptake. To relate interstitial blood glucose concentration to that in the blood would require a complex algorithm, that may be very patient and situation specific. The question, however, as to whether this conversion is necessary or, indeed, whether the interstitial level is not, in fact, the most relevant clinically for a diabetic, remain open and is the subject of much debate since "there are relatively limited data on dermal interstitial fluid glucose levels" [84]: A study performed on type 1 diabetics on the plasma and interstitial fluid glucose concentrations in pre- and postprandial situations showed that dermal interstitial fluid glucose was highly correlated with plasma glucose [86]. The lag time between the two compartments however varies from study to study depending on the technique used to measure the glucose, the different tested conditions and the model studied (animal or human, diabetic or not) [84]. It has also been suggested that interstitial fluid glucose may decrease before plasma glucose due to a phenomenon called the "push-pull" during which the glucose is pushed from the blood to the interstitial fluid at times of increased blood glucose, and later on glucose is pulled from the interstitial fluid to the surrounding cells during decreasing blood glucose levels. However, this phenomenon is also the matter of debate at the moment with other studies demonstrating a compensation of the

increased passage of glucose in the interstitial fluid by increased delivery of glucose to the plasma as well as a decrease of the effect of glucose removal from the interstitial fluid [84, 87].

1.3.5.2 Other invasive technologies

1.3.5.2.1 Microdialysis

The GlucoDay® (A. Menarini Diagnostics, Florence, Italy), and its later version, the GlucoMenDay® [88], are alternatives for continuous subcutaneous glucose monitoring that use a microdialysis setup. The devices have been commercialised in Europe but have not received FDA approval [89]. The technique requires implantation of a microdialysis probe in the periumbilical region, via which interstitial fluid is collected with a perfusion solution. The latter then passes into a biosensor cell on the abdomen of the patient, where a GOD amperometric biosensor measures the glucose.

1.3.5.2.2 The "artificial pancreas"

The main function of the pancreas is to control glycaemia through the release of insulin and the production of the glucagon. Both glucose biosensing and insulin delivery technologies exist. The design of an "artificial pancreas" is therefore (at least in theory) possible. The holy grail, of course, is "closing the loop" with sensing and delivery operated automatically via an algorithmic feedback system. Nowadays, implantable CGMS [90], and insulin pumps [91], together with closed looped algorithms [92] are available but the ultimate prize is yet to be achieved. The closest approach to date is the Medtronic 530G with Enlite technology system (Medtronic, Northridge, CA, USA) which received FDA approval in 2013 [93]. This system provides "a threshold suspend feature that automatically stops insulin delivery when a pre-set low blood glucose value is detected by the continuous glucose monitor" [94]. It is not however an artificial pancreas as presented in table 1.2, along with the issues that would be associated with the design of such an artificial pancreas.

1.3.5.3 Advantages and disadvantages of implanted glucose sensor

Table 1.2 describes the advantages and disadvantages of several implanted sensor and technologies. It is split into three categories: (1) intraveneously implanted devices, (2) subcutaneous devices and (3) other invasive technologies.

Table 1.2. Advantages and disadvantages of implanted glucose sensing devices

Techniques	Advantages	Disadvantages	References
Intravenously implanted devices			
Via®Blood **(Via Medical Corporation, Austin, TX, USA)** **OPTImus** **(IntelliDx Corporation, Santa Clara, CA, USA)** **STG-22™** **(Nikkiso, Tokyo, Japan)**	• Use in intensive care units (ICU) • Reduced workload for ICU staff • STG-22™: ➢ Minimal patient glucose variability: standard deviation of 19.9 ± 10.9 mg/dl ➢ Good detection and prevention of hypoglycaemia when integrated with an insulin/glucose delivery system	• Blood sampling • Small negative pressure necessary to avoid blood vessels to collapse • Requirement to stop other intravenous infusions to be stopped periodically • Interruption of glycaemic control due to poor blood removal • Problems of cost and device preparation	[73, 74]
GlucoClear™ **(Edwards Lifesciences, Irvine, CA, USA)**	• Blood automatically drawn every five minutes and then returned to the patient • Real time graphical display • System self-calibration	• Biofouling of the sensor surfaces, i.e., the formation and accumulation of proteins and biological elements on the sensor creating a "barrier" that impairs performance • Invasive, surgical monitoring only applicable to ICU	[77, 95]
GluCath® Intravascular CGM System **(GluMetrics Inc., Irvine, CA, USA)**	• Optical measurements made every 10 seconds • Use in post-cardiothoracic surgery patients in whom glycaemic control is indicated		

Techniques	Advantages		Disadvantages		References
Subcutaneous devices					
	Specific	*General*	*Specific*	*General*	
Minimed® **(Medtronic, MiniMed Inc., Northridge, CA, USA)**	• "Primitive device and gold standard for the improved guardian version"	• Fewer finger pricking sensing • Safe and easy to use system • Real time sensing coupled with an alarm to warn of out of range sensing • Improvement in glycemic control in motivated children, adolescents and patients with poorly controlled type 1 diabetes • Better determination of asymptomatic hypoglycaemia than self-monitoring blood glucose • Increased patient motivation	• No real time glucose monitoring • Requires to download datas on a computer every 72 hours	• **Lag time:** "There is currently controversy surrounding the delay in the recognition of and recovery from hypoglycaemia" [98] • **Calibration:** the systems are not yet accurate enough to replace finger-pricking, hence necessity to draw blood samples one to three times a day • **Overestimation of hypoglycaemia:** High false alarm rate • Disconfort, skin irritation/puritis, interruption of the signal between the sensor and the receiver	[81, 96-99]
Guardian® Real-Time **(Medtronic, MiniMed Inc., Northridge, CA, USA)**	• Real time glucose monitor • Numerical and graphic depictions • Wireless: 6 feet		• Three finger pricking calibration indicated • 47% false alarms in hypoglycemia		
DexCom STS™-7 **(DexCom Inc. San Diego, CA, USA)**	• Glucose concentration measured every 5 minutes • 7 days sensor		• 1 invasive calibration after 2 hours of the sensor insertion and then 1 every 12 hours		
FreeStyle Navigator® **(Abbott Diabetes Care Alameda, CA, USA)**	• The addition of the TRUstart algorithm correct for the effect of interstitial lag and the acceptable range for calibration was increased from 60-300 to 60-400 mg/dL		• First generation device: 10 hours warm-up period, inaccurate glucose readings because of insertion trauma and wound-healing processes Second generation device: 1 hour warm up period • Finger pricking calibration necessary		

Techniques	Advantages	Disadvantages	References
Other invasive technologies			
Microdialysis **GlucoDay® (A. Menarini Diagnostics, Florence, Italy)**	• Linear response up to 30 mM glucose • Continuous monitoring for up to 48 hours	• Invasive technique: reduced patient compliance • Daily fingerprick blood glucose calibration • Significant inter-individual variability • Lag time of 10 to 12 minutes • Sensor prone to interference and biofouling • Expensive system • Not commercially available	[88, 100, 101]
"Artificial pancreas"	• "Holy grail": "closing the loop" with sensing and delivery operated automatically via an algorithmic feedback system. • Technologies available to achieve such a goal • The closest approach to date is the Medtronic 530G with Enlite technology system (Medtronic, Northridge, CA, USA)	• The Medtronic 530G with Enlite technology system (Medtronic, Northridge, CA, USA) is not an artificial pancreas: it is not coupled with an automatic insulin delivery, and fingerstick testing and glucose self-management are still required. • Type 2 diabetes isn't treated via insulin treatment (except at a late stage of the disease) • Algorithm don't take into account punctual events influencing the glycaemia such as (i.e., stress, physical activity, meals, intercurrent illness, etc.) and the lag time for the plasma and interstitial glucose concentrations to come into dynamic equilibrium. • Glucose biosensing devices still suffer from sensitivity problems or reproducibility issues • The cost and accessibility of the technologies would also be a limiting factor	[94, 102-105]

Following the observations listed in table 1.2, it appears that implanted technologies are favourable to provide a real time monitoring of the glycemia, with alerts systems in place when the levels of blood glucose fall out of the normal range. Most of the devices are relatively safe and easy to use. Moreover, the subcutaneous and intraveneous sensors are the only alternative technologies to the finger pricking meters that are commercially available [106]. However, they also involve invasive insertion of the sensor and hence poor patient compliance, multiple fingerstick calibration per day, overestimation of hypoglycaemia, false alerts, etc. Research has therefore focused in recent years on the development of a non-invasive technology that will tackle some of the cited issues.

1.3.5.4 Non-invasive glucose sensing: Transdermal technologies

1.3.5.4.1 Minimally and non-invasive sensing

With respect to transdermal glucose monitoring, two approaches have been taken:

(1) First the "minimally invasive" extraction of interstitial fluid by reversibly compromising the integrity of the stratum corneum (the outmost skin layer) through the application of physical energy or mechanical force (e.g., sonophoresis, microporation) [107].

(2) Second, "non-invasive" optical techniques (Raman spectroscopy, polarimetry, photo acoustic spectroscopy, and spatially-resolved diffuse reflectance and NIR spectroscopy) that do not involve physical perturbation of the skin or withdrawal of interstitial fluids.

Reverse iontophoresis has been described by some as "minimally invasive" and other "non-invasive" and there is much debate around the terminology [107].

1.3.5.4.2 Reverse iontophoresis (RI)

Iontophoresis imposes a small intensity current between two electrodes placed on the top of the skin surface leading to the delivery of charged and uncharged therapeutic molecules for example. The phenomenon has been developed and used for many years. Indeed, the notion of iontophoresis emerged in the 18^{th} century with the study of Galvani and Volta on electrical motion of metallic ions [108], and was applied to skin delivery of therapeutics through the work of Leduc who proposed a theory for the process in 1900 [109]. Iontophoresis is a symmetrical process which creates flux of ions inside and out the skin. There is potential therefore to extract charged and uncharged molecules in the so called reverse iontophoresis process. This would be a great diagnostic tool since "information" (such as glucose) could be

extracted from the skin without the need for a blood sample [110]. Any iontophoretic transdermal process includes three fundamental phenomena: electromigration, electroosmosis and passive diffusion.

1.3.5.4.2.1 Electromigration (EM)

Electromigration describes the direct effect of the applied electric field inducing the movement of ions through the skin. This induced flux will carry the imposed current while the electro-neutrality of the system is maintained. The electromigration process can be described by equation 1.1, relating the electromigration flux to the total iontophoretic current I:

$$J_{EM} = \frac{t_i\, I}{F\, z_i} \qquad (1.1)$$

Where J_{EM} is the electromigration flux expressed in mol/sec, F is the Faraday constant equal to 9.64×10^4 C/mol, I is the iontophoretic current expressed in Amperes, while t_i and z_i are the transport numbers (fraction of the total current carried by a defined ion and charges of the ions involved in the process, respectively). The electromigration flux is highly dependent on the capacity of the ion of interest to carry the current [111].

1.3.5.4.2.2 Electroosmosis (EO)

At physiological pH the skin presents a net negative charge (isoelectric point ranging from 3.5 to 4.8) and it therefore acts as a cation permselective membrane. The iontophoretic current hence induces a net convective solvent flow (H_2O in majority) from anode to cathode which carries the uncharged and high molecular weight molecules with it [112]. Cations flow towards the cathode under the combined influence of electromigrations and electroosmosis. However, although electromigration dominates for low molecular weight cations [113], electroosmosis is the dominant phenomenon for the extraction of the uncharged molecules and large cations [114]. The electroosmotic flux J_{EO} (see equation 1.2) and is expressed in mol. $sec^{-1}.cm^{-2}$. J_v is the volume flow expressed in $cm^2.s^{-1}$ and c_a the concentration of a molecule "*a*" expressed in mol, to be extracted. The volume flow component J_v is function of the characteristics of the permselective membranes , such as pH, NaCl concentration [115].

$$J_{EO} = J_V\, c_a \qquad (1.2)$$

1.3.5.4.2.3 Passive diffusion

The last notion to be introduced is the passive diffusion of analytes through the skin. Passive diffusion refers to the transport of molecules through the skin membrane without any external actions. It is described by equation 1.3 and is dependent on the diffusivity, D_j, and the gradient of concentration, ΔC_j, through the skin of thickness, h [116]:

$$J_p = D_j \frac{\Delta C_j}{h} \tag{1.3}$$

1.3.5.4.2.4 Total iontophoretic flux

The total flux of any iontophoretic operation will thereafter be defined as the sum of the electromigration flux, J_{EM}, the electroosmosis flux, J_{EO}, and the passive diffusion, J_p. However, the electromigration can be ruled out in the case of glucose, the interest being focused on the extraction of an uncharged molecule at the cathode. Moreover, the extraction of glucose is much faster by electroosmosis than by passive diffusion [117]. Passive diffusion is therefore considered as negligible compared to electroosmosis during RI of glucose [118]. The RI flux is therefore approximated as J_{EO}. A typical reverse iontophoretic schematic is displayed in figure 1.5:

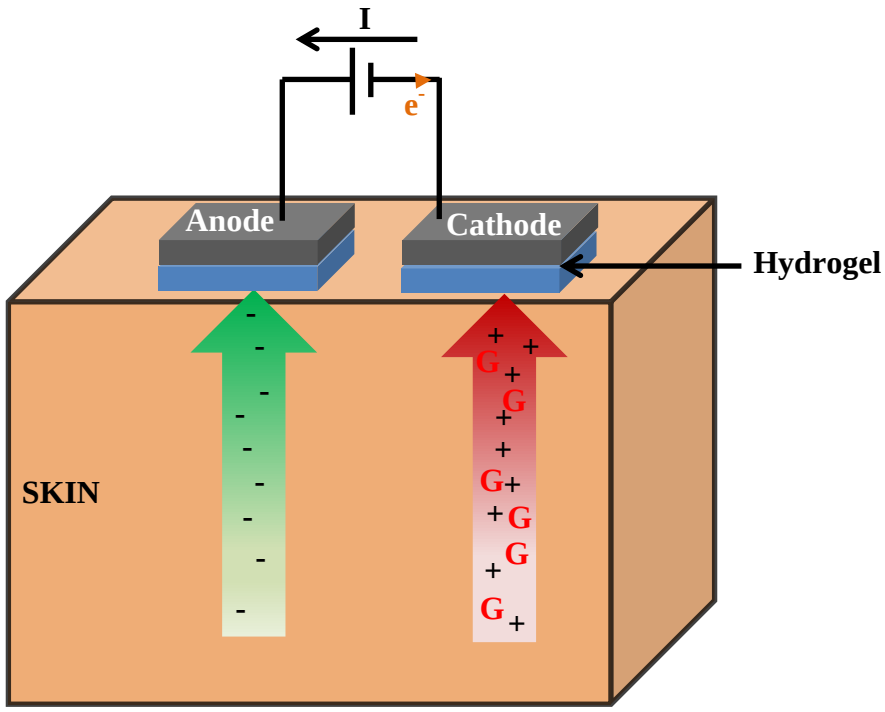

Figure 1.5. Reverse iontophoresis schematics. A current *I* is created between two electrodes placed on top of two hydrogel reservoirs inducing a stream of ions through the skin that enables the glucose molecule (*G*) to be extracted at the cathode via electroosmosis.

1.3.5.4.3 The GlucoWatch ® Biographer

Reverse iontophoresis is the principle behind the only non-invasive glucose extraction technology to have received FDA approval: the GlucoWatch ® Biographer (Cygnus, CA, USA). It combined the reverse iontophoresis extraction principle with electrochemical glucose detection. The device received FDA approval in 1999 and was briefly commercialised before becoming unavailable in the early 2000s [28, 119]. The advantages of the GlucoWatch were in principle multiple: better patient compliance, fewer finger pricks, continuous monitoring and hence better diabetes management, better control of hypoglycaemia [120], practicality of a wrist worn device, cost effective technology [121]. The device also had additional advantages with respect to the glucose biosensing: high molecular weight molecules responsible for electrode fouling were filtered by the skin, molecular oxygen was not a detection limitation factor, and common glucose sensor interferents were extracted towards the other, nonsensing electrode (anode) [107]. Unfortunately, the device was not commercially successful because of several limitations already listed in section 1.1 [121-123]. The technology developed in this thesis aims to tackle some of these limitations to achieve improved transdermal glucose monitoring. This will be achieved by designing an improved and miniaturized biosensing platform as well as targeting hair follicle glucose extraction pathways.

1.3.5.4.4 Reverse iontophoresis and privileged extraction through hair follicles

1.3.5.4.4.1 Skin structure

The human skin is formed by a succession of layers ensuring its fundamental role as a barrier, namely the hypodermis, dermis and epidermis. Their typical thicknesses are respectively 1 mm to 5cm, 1 mm [124] and 100 µm [125]. The hypodermis comprises primarily adipocytes and reticulated blood vessels and serves a fundamental structural function. It is easily distinguished from the fibrous connective tissues of the dermis, which confer the skin's elastic tensile strength and pliability properties. Cell density in the dermis is less than that in the epidermis and the extracellular space is therefore larger. The dermal layer shows good integration with the skin appendages and supports the vascular and sensory networks. The epidermis is the external part of the skin and is mostly composed of keratinocytes. It is structured in layers: (1) the stratum basale, (2) the stratum spinousum, (3) the stratum granulosum and (4) the stratum corneum.

(1) The stratum basale is the deepest and is formed of mitotic and migrant cells. 10% of the cells found in the stratum basale are stem cells that have the potential to differentiate, multiply and regenerate the epidermal cell content. It has been estimated that it takes a keratinocyte 14 days to travel from the stratum basale to the stratum corneum and another 14 days until desquamation [126].
(2) Next, the stratum spinousum is named after the polyhedral histological appearance of the cells.
(3) The stratum granulosum is formed of larger and flatter keratinocytes with kerotohyalin granules and a high density of desmosomes. Lamellar bodies are also present that release lipids into the extracellular space at the base of the outmost epidermal layer, the stratum corneum (SC).
(4) The SC is composed of "dead" terminally differentiated keratinocytes named corneocytes. These cells are surrounded by extracellular lipids in a "bricks and mortar" configuration and performs a fundamental barrier role (water loss prevention, selective absorption of molecules, etc.). Homeostasis of the SC is maintained by desquamation of approximately one layer of cells per day [127].

Skin appendages include sweat glands (eccrine and apocrine), sebaceous glands, hair follicles and nails. Hair follicles are present all over the body with the exception of the lips, palms and soles. They originate in the deep layer of the reticular dermis, and are associated with sebaceous glands that secrete sebum (wax esters, squalene, triglycerides, cholesterol and free fatty acids).
Eccrine glands are responsible for sweat production and therefore play a role in thermoregulation. Apocrine glands are specialised sweat glands found in specific body sites (axillae, groin, etc.) and develop in association with hair follicles, and open into them. Nails are composed of compact flatten keratinized cells with low lipid content 0.1 to 1% [128].

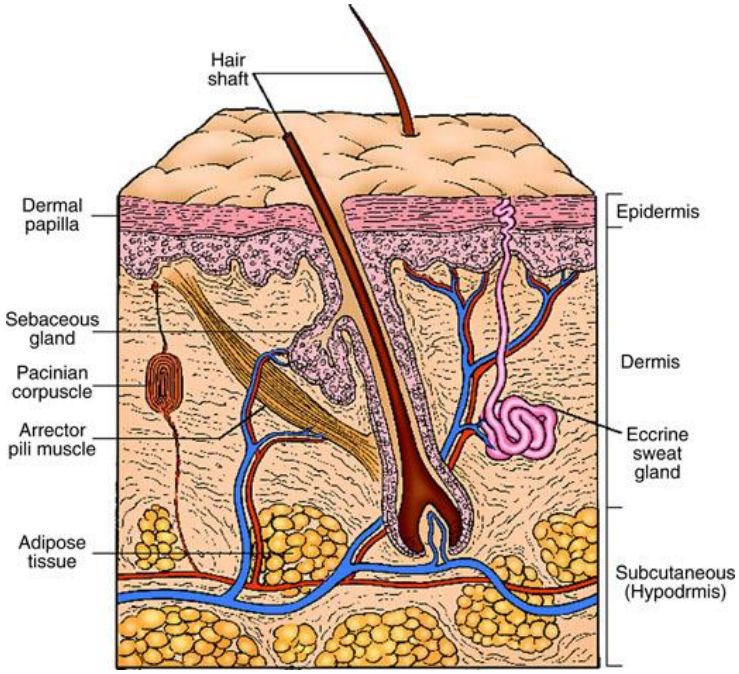

Figure 1.6: Skin structure (Reproduced from [129])

1.3.5.4.4.2 Preferential reverse iontophoresis pathway through hair follicles

During iontophoresis, 3 pathways across the skin may be identified: intercellular (between the corneocytes in the epidermis), transcellular (through the cells) and appendageal [130], (figure 1.7).

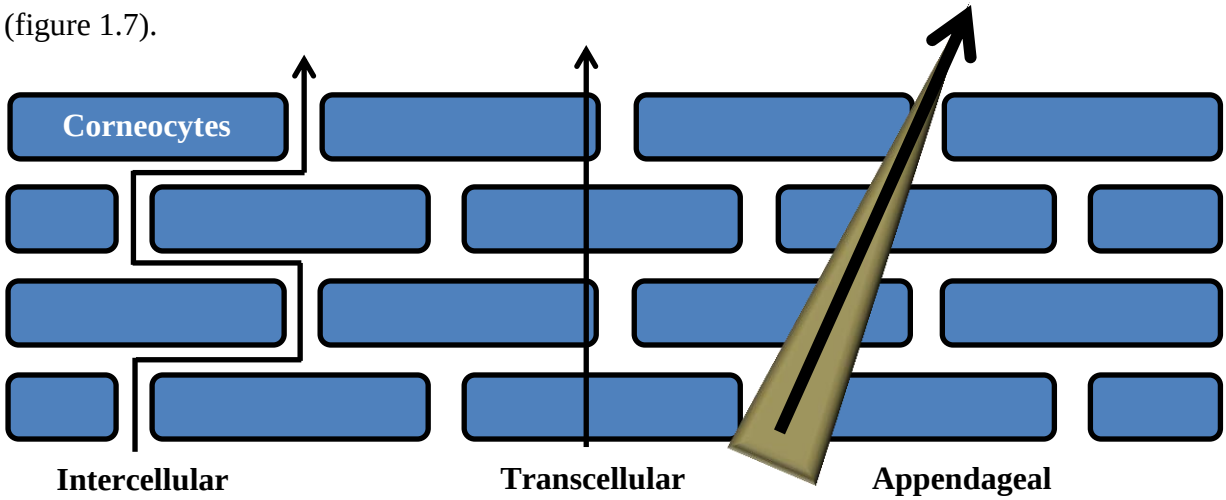

Figure 1.7. Extraction pathways through the skin during RI. The principal anticipated pathway for glucose and large ions during reverse iontophoresis is appendageal because of its low electrical resistance [131].

The dominant role of the appendageal (follicles, sweat glands) iontophoretic route, has been demonstrated in a number of studies [132-135] and it is likely that electroosmotic flow will also take place via this low resistance pathway: One study introduced for example the preferential iontophoretic delivery of calcein (a negatively charged fluorescent compound) through hair follicles [136]. In another study the preferential extraction of a neutral molecule, hydroquinone, through hair follicles via RI was also successfully confirmed [134]. Hence, it would appear reasonable to assume that the uncharged glucose molecules will follow the same extraction pathway in majority.

1.3.5.5 Non-invasive glucose sensing: ocular detection

Although some research is ongoing in ocular glucose sensing, no device have so far been commercialized or received accreditation. Google, very recently (July 2014), filed a patent in collaboration with Novartis on the development of a smart glucose sensing contact lens [137]. This general announcement does not appear to be a real technological or a scientific achievement: the technology is described as a contact lens that will collect tear fluid and analyse it through biosensing, electrochemical, amperometric or pressure sensor detections without distinctions. Furthermore, no clear proportionality has been demonstrated between tear and blood good glucose [138, 139]. Research in ocular glucose sensing is ongoing as presented in figure 1.8, but just like the transdermal one, no commercial device as yet successfully emerged in the market.

1.3.5.6 Summary

Figure 1.8 attempts to summarise the state of the "new" glucose monitoring art at the present time. While continuous monitoring has been proven possible, current use of the available technology is limited by its invasive nature. Less invasive approaches have been developed but, for one reason or another, have not been able to make any significant impact in terms of sustained, practical use. There remains a real opportunity, therefore, for a non-invasive glucose monitoring technique that is accurate, user friendly and cost-effective.

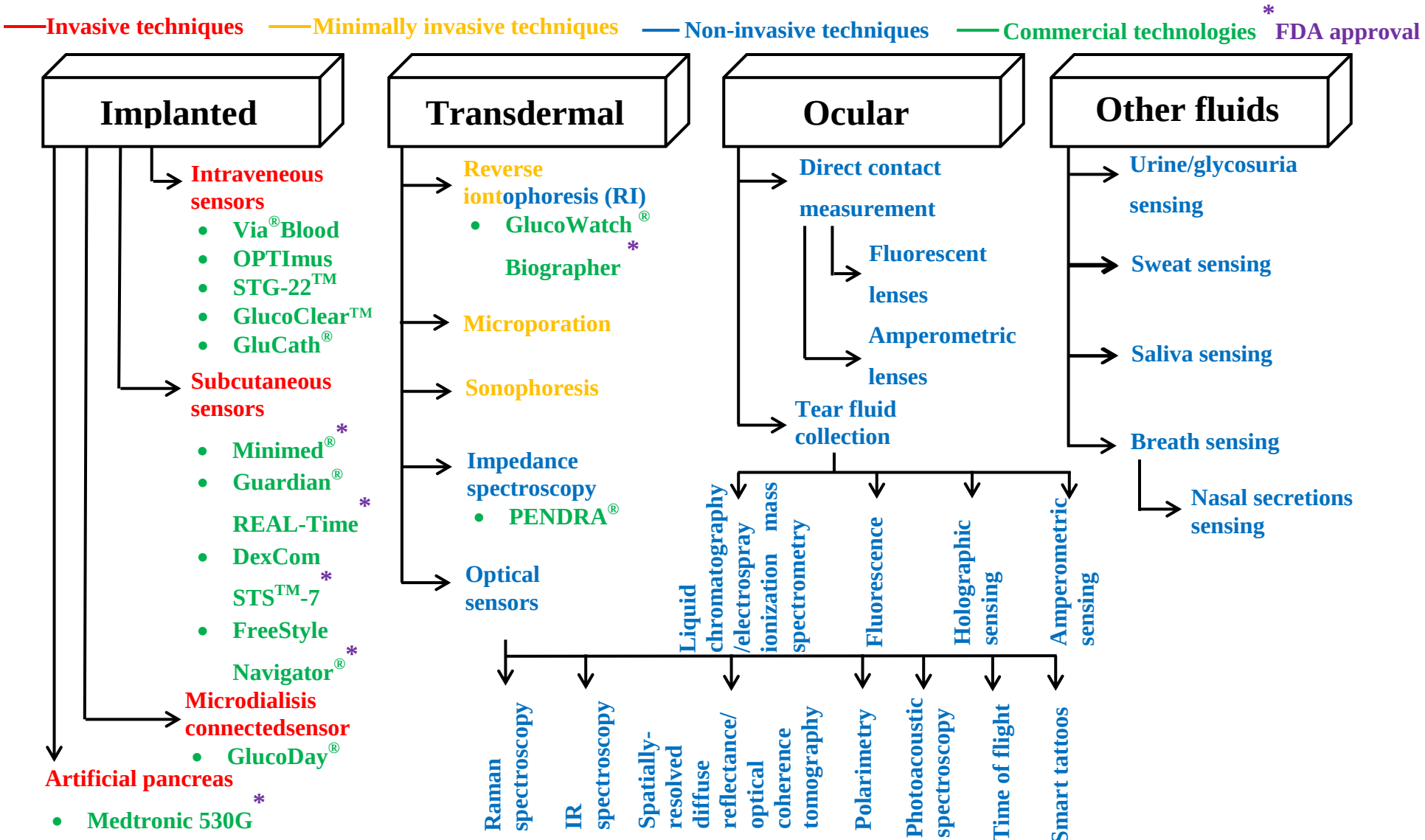

Figure 1.8. Alternative glucose sensing technologies to the fingerstick glucose reference sensor

1.4 Graphene

1.4.1 Graphene as a nanomaterial of interest for integration in a glucose biosensor

Graphene has recently been isolated in a free standing form by Geim and Novoselov [140] and this led to an exponential growth in research and applications. The authors (who received the nobel prize of physics in 2010, for "groundbreaking experiments regarding the two-dimensional material graphene" [141]) characterized the nanomaterial as: "A flat monolayer of carbon atoms tightly packed into a two-dimensional (2D) honeycomb lattice and a basic building block for graphitic materials of all other dimensionalities [140]". The authors did not discover the nanomaterial per se, graphene having been studied and characterised theoretically as early as 67 years ago [142]. But, for many years graphene was described as an academic material since scientists did not believe that such a material could exist in the free state (being considered as thermodynamically unstable [140]). Atomic monolayers (part of a 3D lattice) were deemed impossible to isolate until 2004 when Geim and Novoselov characterised free standing graphene (defined as a 2D atomic crystal) that could be obtained on top of non-crystalline substrates, in liquid suspension and as suspended membrane [140]. Graphene is defined as a 2 dimensional nanomaterial and will approach the 3 dimensional aspect past 10 stacking graphene layers. The graphene carbons are arranged in hexagonal configurations and are linked with together with sp^2 bonding (orbital hybridisation) forming the typical 2D honeycombe nanomaterial structure (figure 1.9). Other carbon nanomaterial have also been studied in the literature (single wall carbon nanotubes, fullerenes) that are "folded" sheets of graphene, and have remarkably been introduced into biosensing devices [143, 144]. Both configurations are presented in figure 1.9.

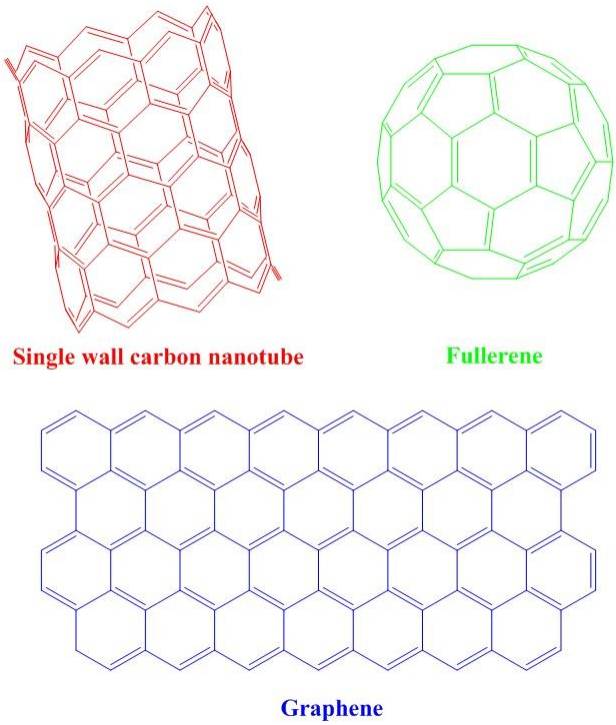

Figure 1.9. Schematic depictions of graphene fullerene, and single wall carbon nanotubes.

These carbon nanomaterials but also other structures such as graphite or glassy carbon electrodes (GCE) are commonly used in biosensing. Following is a table comparing some of these materials properties to the graphene ones.

Table 1.3 Comparison of carbon based sensing material properties

Electrode material	Conductivity	Other physical properties	Integration in biosensing	Large scale production	Level of difficulty of fabrication	Other interesting features	References
Graphene	Charge carriers mobility extremely high: 200,000 cm^2 V^{-1} s^{-1}	• Strongest material ever measured: tensile strength of 130 GPa • Optically invisible (except on selected wafers) • Highly flexible: "zero bending" stiffness • "zero gap" semiconductor	• **Graphene oxide**: Extensively studied bio-integration, but impaired conductivity • **Other graphene types:** Fewer bio-functionalization, diverse techniques investigated *(See chapter 2 for a more extensive description of the different bio-integrations)*	• **CVD graphene:** Demonstrated • **Other graphene types:** More difficult to impossible	Dependent on the production technique. **CVD graphene:** Demanding production involving the use of gas and controlled temperature/pressure but easy transfer onto any chosen wafer	• Low production cost of CVD graphene • Graphene is being studied as the "star" novel nanomaterial in other areas that could be coupled with biosensing • Graphene can easily be patterned (via oxygen plasma treatment for instance)	[140, 145-153]

Electrode material	Conductivity	Other physical properties	Integration in biosensing	Large scale production	Level of difficulty of fabrication	Other interesting features	References
Single wall carbon nanotubes (SWCN)	High charge carriers mobility: >100,000 cm^2 V^{-1} s^{-1}	• Strong material: tensile strength up to 63 GPa • Transparent and flexible properties like graphene • Electrochemical, optical and electric properties function of the heterogeneity in length, diameters, chiralities	• Extensive literature on carbon nanotubes bio-integration. • Large functionalizable area	Large scale production of SWCN is possible but it is still challenging to obtain homogeneity in the nanomaterial geometry (length diameter, etc.), chirality and alignment	Different technique are available for production of carbon nanotubes (arc discharge, CVD, etc.) that present more or less complexity but won't be developed here	Nanomaterial studied for many years in a wide variety of applications: medical, electronic, composite material, etc.	[154-161]
Fullerenes	Carriers mobility: ~ 3×10^{-3} cm^2 V^{-1} s^{-1}	• Lower tensile strength than the previous nanomaterials: ~ 10 MPa • Non-toxic and soluble in several organic solvents • Integration on transparent electrodes	• Spherical structure that act as carriers for genes and drugs for instance • Good electronic mediator • Functionalization dependent mostly on addition of functional chemical groups	The main issue with fullerenes production is the poor production yield obtained: ~ 8-15% in most production facilities	Similarly to carbon nanotubes and graphene several techniques are used to produce fullerenes: carbon arc, hydrocarbon flame or field-induced hot carbon plasma	The spherical carbon structures can be used in other applications than biosensing: drug carriers, solar cells, etc.	[162-168]

Electrode material	Conductivity	Other physical properties	Integration in biosensing	Large scale production	Level of difficulty of fabrication	Other interesting features	References
Graphite	Carriers mobility: 15,000 $cm^2 V^{-1} s^{-1}$	• Low tensile strength: ~ 11 MPa • Very opaque and rigid material	• Extensive literature on graphite bio-integration • Wide range of functionalization techniques • Considered as an interesting an element for bio-amperometric applications but the question remains debatable *(See section 1.4.4)*	Easy to produce in large scale	Graphite can either be extracted or artificially produced. Its' production is cheap and thoroughly documented	-	[169-171]
Glassy carbon electrodes	-	• Tensil strength of 870 MPa demonstrated with thin films glassy carbon electrodes, but the strength seems to be highly dependent on the size of the electrode • Very opaque and rigid material	• Usually used as an adjunct to some of the carbon nanomaterial cited above for biosensing • Very few interest and less biocatalytic activity when used on its' own	Easy to produce in large scale	Glassy carbon electrode have been available commercially for a long time at a cheap price and their production is well documented	-	[172-175]

From table 1.3 two conclusions can be drawn. (1) Firstly, on the comparison of graphene with other carbon nanomaterials (SWCN, fullerenes) and commonly used electrochemical electrodes (GCE, graphite). Each of the materials presents specific interesting qualities: the carbon nanomaterial have good bio functionalization and physical properties. GCE and graphite have extensively been studied and are easy to produce. However, they also present major drawbacks such as uneven and difficult production methods (SWCN and fullerenes) or rigidity and opacity (GCE and graphite electrodes). (2) Secondly, graphene as described in section 1.4.3, can be produced via different methodologies that give slightly different qualities to the nanomaterial. The type of graphene used here is CVD graphene. It is of particular interest when compared to other types of graphene because it can be produced in big quantities, it is quite cheap and easily transferrable to many substrates (flexible ones for instance). It is also one of the purest (less defects or impurity) form of graphene produced which means that it will display exquisite conductivity that will be of great interest in potentiometric sensors such as field effect transistors (FET) [176] (see chapter 3).

1.4.2 Characterisation and structure

Graphene has unique mechanical, optical, electrical/conductive and functionalization properties.

1.4.2.1 Mechanical properties

The measured experimental breaking strength of 42 N/m for a single graphene sheet [177] corresponds to the theoretical intrinsic strength of a defect free nanomaterial making graphene the strongest material ever measured. A 2D graphene membrane has a “zero bending” stiffness [177], and demonstrates stable conductive properties at 11% stretching. It follows that graphene may be transferred on flexible substrates thereby offering a wide range of potential applications (e.g. flexible solar cells [178], flexible biosensors [145] or flexible touchscreens [179]). This high flexibility will be of major interest in the developed technology, the ultimate aim being the integration on the skin (a highly flexible membrane).

1.4.2.2 Optical properties

Graphene is optically invisible on most wafers [140], however the nanomaterial becomes visible when deposited on silicon dioxide (SiO_2) with an oxide layer of 300 nm (i.e. substrate used in the design of the presented sensor). The visualisation is possible due to the feeble interference contrast with light on an empty wafer and is highly dependent on the thickness of the oxide. The transparent properties of graphene could be exploited for future development of the introduced technology, (i.e. integration on a transparent substrate).

1.4.2.3 Electrical/conductive properties

Charge carriers (holes and electrons) have an extremely high mobility in a graphene structure which exceed 15,000 $cm^2 V^{-1} s^{-1}$ [140]. Graphene is described as a zero-gap semiconductor. In graphene, the energy bands (conduction and valence bands) are conical and connects at the Dirac point (see figure 1.14). As a result, no threshold energy is necessary to move charge carriers from the valence band to the conduction band [147].

1.4.2.4 Functionalization properties

The "high surface to volume" of the nanomaterial provides a very large area for biofunctionalization (e.g. with a protein or enzyme) [149]. Across the broad area of graphene biosensing research, the following examples can be identified: DNA [150], bacteria/cells [151], protein/antibody [180], enzymatic biosensors [181], etc., using amperometric [182], potentiometric (FET) [180], and impedance [183] detection.

1.4.3 Graphene production

Two graphene production techniques may be differentiated. The first is a "top down" approach and includes mechanical exfoliation, solution based exfoliation, chemical oxidation (production of graphene oxide), electrochemical exfoliation of graphite, and opening/unzipping carbon nanotubes. The second "bottom up" approach involves building up graphene from smaller organic entities [184] and includes: chemical synthesis, epitaxial growth on SiC and chemical vapour deposition.

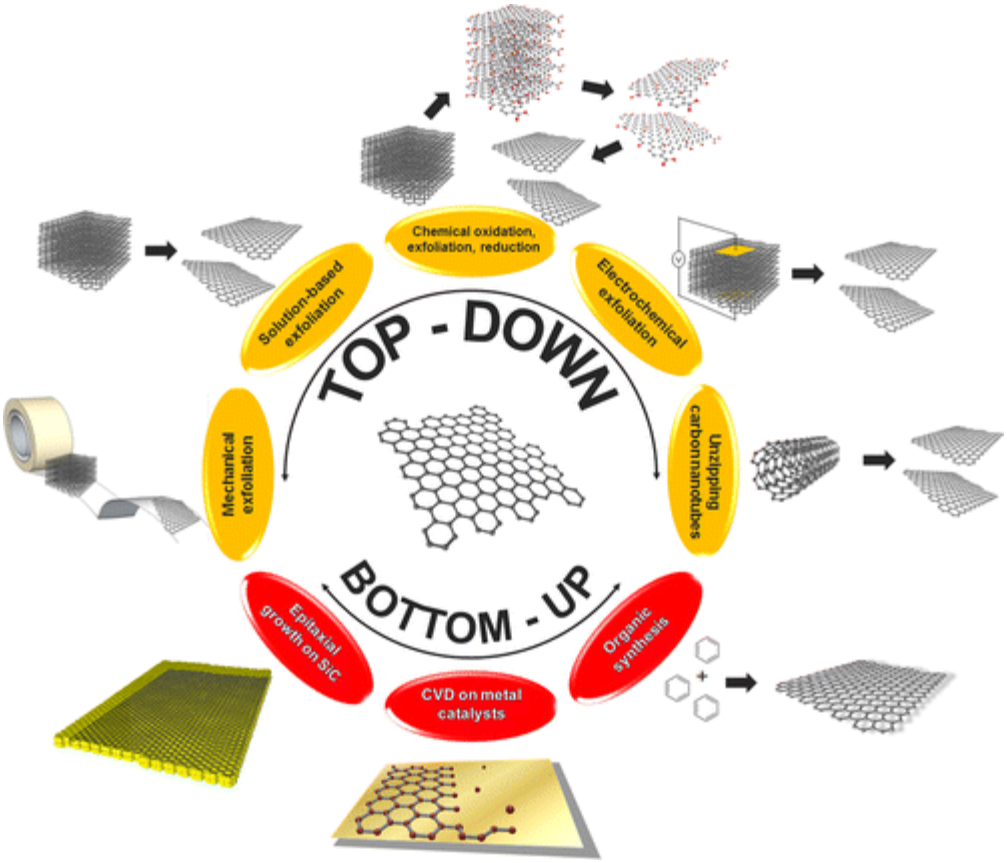

Figure 1.10. Graphene production techniques (reproduced from [184])

1.4.3.1 Top down techniques

1.4.3.1.1 Mechanical exfoliation

Micro-mechanical cleavage of highly oriented pyrolytic graphite (HOPG) was the first technique to be introduced by Geim and novoselov in 2004 [185]. The technique was relatively straight forwards since it involved the pealing down of graphite until obtaining few-layers or monolayer graphene (the technique is also commonly referred to as the "scotch tape technique"). This technique enables to obtain the highest graphene quality of all existing techniques and is at the basis of most of the research on the fundamental physical properties of the nanomaterial. But the procedure is limited in applications and scaling up: it has low reproducibility and it is impossible to implement in a large scale production process [184].

1.4.3.1.2 Solution based exfoliation

Considering that exfoliated graphene is of high quality and therefore high interest, scientists have tried to exfoliate HOPG in solution. Most of the attempts involved the combination of organic solvents and ultrasonication. Examples of solvent based exfoliated graphene include: ultrasonication of graphite in N,N dimethylformamide [186] or the use of N-methylpyrrolidone and the same ultrasonicating process [187]. Other solution based exfoliation involved the use of surfactants in aqueous solution in combination with ultrasonication [188]. The techniques however suffer significant drawbacks: (1) the production yield is fairly low, (2) the majority of the produced flakes are multi-layered, (3) the ultrasounds have the adverse effect of breaking the graphene sheets in small flakes and graphitic impurities, and finally (4) exfoliating agents can intercalate in the produced nanomaterial impairing therefore its' purity and properties [184].

1.4.3.1.3 Chemical oxidation: production of graphene oxide

Chemical oxidation of graphite has also been described to produce the well documented graphene oxide. Graphene oxide is a graphene like structure onto which oxygen groups have been intercalated (see figure 1.11).

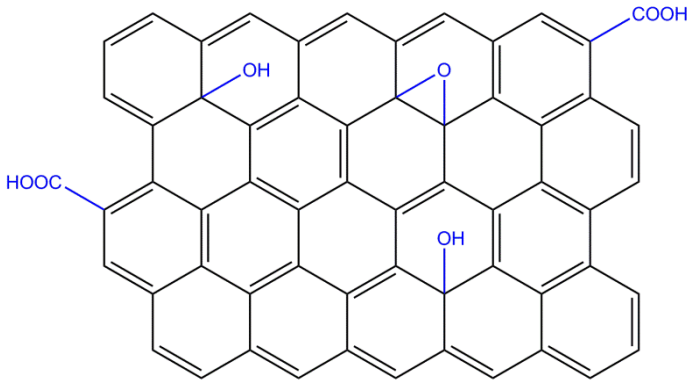

Figure 1.11 Graphene oxide structure. The oxygen groups intercalated inside the graphene structure are represented in blue.

Graphene oxide is produced by using strong oxidising agents in the presence of strong acids such as concentrated sulphuric or nitric acids. Several techniques have been developed based on the use of potassium chlorate as described by Brodie in 1859 [189] and further improved by Staudenmayer in 1898 [190, 191] or the less dangerous (since it doesn't involve the production of ClO_2 gas) use of potassium permanganate developed by Hummers and Offeman in 1958 [192]. However advantageous the intercalation of oxygen species might be

(for biofonctionalisation for example [193]), it also reduces considerably the graphene conductive and electronic properties (as well as modifying the optical characteristics [184]). The use of such a material loses the original purpose of benefiting from the amazing properties of pristine graphene. Further graphene oxide treatments using thermal [194], electrochemical [195] or chemical [196] methods have been implemented to reduce the amount of intercalated oxygen, none of which displayed total efficiency (presence of residual oxygen groups and defects originating from the oxidation of graphite). Other inconvenient of graphene oxide includes: (1) the solution based product, (2) the use of strong solvents, acids and (3) the limited large scale production.

1.4.3.1.4 Electrochemical exfoliation

During electrochemical exfoliation, a working electrode of graphite is introduced in a three electrode setup with a counter and a reference electrode. The supporting electrolytes solution used in the experiments vary (sulphuric acid, poly(styrenesulfonate), perchloric acid etc…). By applying a positive potential on the working electrode, the graphite is oxidised which induces the intercalation of negatively charged ions between the graphene sheets. The further application of a negative potential will complete the exfoliation process. This production technique presents the advantage of being a simple procedure that doesn't necessarily involve strong chemicals. It does however have the same drawbacks as graphene oxide since the produced graphene have oxygen groups intercalated in its' lattice. It is also very difficult to produce graphene with homogeneous size and few layers. Finally this technique sometimes involves the use of surfactants impairing the quality of the final material product [184].

1.4.3.1.5 Opening carbon nanotubes

The opening of carbon nanotubes is slightly different from the previously presented techniques in the sense that graphite is not the starting point of the production process. This technique is associated with carbon nanotube research and produces high aspect ratio (length/width higher than 10) entities named graphene nanoribbons (GNR) that presents a typical width of <50 nm [197]. The width and length of GNRs is tuneable by controlling the carbon nanotubes circumference and length respectively. Different techniques have been used to produce GNRs: (1) Firstly, a controlled unzipping of carbon nanotubes was presented using the Hummers and Offeman technique [192]. The GNRs were further thermally treated at 900°C in argon in order to reduce the amount of oxygen functionalities on the carbon

nanomaterial (2) Secondly, carbon nanotubes were half embedded in a bed of poly(methyl methacrylate), PMMA, and further treated with oxygen plasma inducing their opening [198]. And finally, (3) a zinc treatment was also used to trigger the unzipping of the nanotubes entities [199]. The major issue behind opening carbon nanotubes is the induction of structural defects during the opening phase either by introducing oxygen functional groups or simply by compromising the graphene structure. These techniques will also suffer from carbon nanotubes production drawbacks (presence of metallic or carbonaceous impurities [184]).

1.4.3.1.6 Arc discharge/ Laser ablation

Arc discharge involves applying very high voltages on graphitic electrodes separated by small distances. A high electric field will be formed that induces an instantaneous spark in a welding process. The falling entities during the discharged will be the graphene flakes. This process however demonstrates very poor selectivity (large amount of unwanted products formed/ debris) [200]. Laser ablation involves the use of a laser beam to cleave graphite in a so called "photoexfoliation" process. The production of fine numbers of graphene layers have been demonstrated by changing the laser energy density. This process is still underdeveloped and laboratory based [201].

Both techniques where presented together because they suffer the same general limitations: (1) they require a large amount of graphite source and (2) an important amount of energy is necessary to produce the arc discharge or power the laser ablation, rendering large scale production impossible [160].

1.4.3.2 Bottom up techniques

1.4.3.2.1 Organic synthesis

Graphene is formed of fundamental polycyclic aromatic hydrocarbon units, it should hence be possible to create a graphene sheet by organic synthesis (linking these units together). This process is however very limited since, when exceeding a few nanometers, graphene sheets become highly insoluble in organic solvents. This will reduce further organic growth as well as induce unwanted side reactions [184]. This technique, however interesting for the production of pristine graphene, is hence dramatically impaired by the production size of the graphene sheets and research is ongoing to improve this crucial aspect (recently the organic synthesis of GNRs of 500 nm in length was presented [202]).

1.4.3.2.2 Epitaxial growth on SiC

Another way of growing graphene is through the heating treatment of SiC substrates under ultrahigh vacuum conditions. During the thermal process, the Si atoms sublimates to leave graphene layers which can be tuned to very few layers by controlling the operating conditions [203]. The properties of epitaxially grown graphene from SiC however differs from pristine graphene because of surface induced corrugation and irregular orientations of graphene layers. The expensive aspect of the technique will also be an important limitation which will limit the large scale application of the production method [184].

1.4.3.2.3 Chemical vapour deposition

Chemical vapour deposition (CVD) is by far the "most promising techniques for industrial-scale fabrication of graphene" [184]. It involves a high temperature decomposition of gaseous hydrocarbon precursors (methane, ethane, propane) into carbon radicals that organise in the graphene honeycombed configuration on top of a metal sheet (Cu or Ni). During the growth, the supporting metal not only acts as a catalyst to lower the activation energy barrier of the reaction but also dictates the deposition mechanism that affects the quality of the nanomaterial [204]. The CVD process produces large, close to pristine, and mostly monolayer graphene sheets in a cost effective and scaled up manner [184]. It has already been applied to diverse developments such as electronic transistors, transparent conductive electrodes, electrochemical detection, corrosion inhibiting coating, solar cells etc. The technique does however suffer some drawbacks: (1) Graphene growth on the metal surfaces occurs via the fusion of graphene "islands", a process that sometimes induces defects and impairs therefore the resulting conductive properties. (2) The transfer of the graphene sheet onto a substrate is a potential cause of defects and folding.

1.4.4 Benefit of CVD graphene introduction in a biosensor device

The benefit of using CVD graphene in biosensing device depends essentially on the detection principle. Hence a field effect transistor (FET) devices would benefit from the pristine quality of CVD graphene displaying an exquisite conductivity since any change at the surface of the semiconductor will induce a change of gating potential (see chapter 3). This lead to the development, in recent years, of hybridization sensor (DNA, cell [205]) or enzymatic FET (ENFET [145]) CVD graphene sensor. On the other hand the nanomaterial has been deemed less interesting in electrochemical applications, the catalytic activity being increased at edges

and decreased on the basal plane of the graphene (i.e. table 1.3) [206]. This last observation is however the subject of much debate in the scientific community, and CVD graphene is still implemented in amperometric biosensors [207] mostly combined with nanoparticles that provide an increased electron transfer and catalytic activity (see chapter 3) [208, 209]. The developed amperometric device will benefit from the electrochemical deposition of platinum nanoparticles on the surface of the graphene acting as "electron wires" for the GOD catalytic reaction. As demonstrated in chapter 4, the sensitivity and limit of detection thereby achieved will be highly competitive compared to comparable devices found in the literature. Further and foremost CVD graphene possesses exceptional qualities compared to other graphene types and commonly used electrodes that are listed in table 1.1 that will be fundamental attributes of the developed technology (flexibility, large scale production, etc.). Moreover, a comparison of the performance of CVD graphene glucose sensor found in the literature to the developed sensor is provided in chapter 4, table 4.3. It presents some of the designs for amperometric glucose sensing based on the nanomaterial and metallic nanoparticles. The literature study was narrowed down to these characteristics but other glucose biosensor based on graphene exist such as amperometric biosensors based on CVD graphene (without nanoparticles) [207] or else FET CVD graphene glucose biosensors [145, 181].

1.5 Analytical and microscopic techniques: principles

A wide range of microscopic and analytical techniques have been used throughout the thesis the principles of which are described in this section.

1.5.1 Microscopic techniques

1.5.1.1 Laser scanning confocal microscopy

Laser scanning confocal microscopy (LSCM) is a visualisation technique that measures the fluorescence emitted by the sample. A laser beam is directed to and focused on the sample via an objective lens. Fluorophores in the sample are then excited and emit fluorescent signals. Part of this fluorescence is collected through the lens, filtered by the dichroic mirror and focused onto a pinhole in front of the detector (figure 1.12) [210, 211].

LSCM enables high resolution (and 3 dimensional) imaging of the sample, with the specific attributes that the light source is focused onto a single point in the focal plane, and that the pinhole in front of the detector effectively blocks any out of focus fluorescent signal. The image is acquired by scanning the laser across the sample in the focal plane, and then layer by layer for acquisition of a 3D image [212].

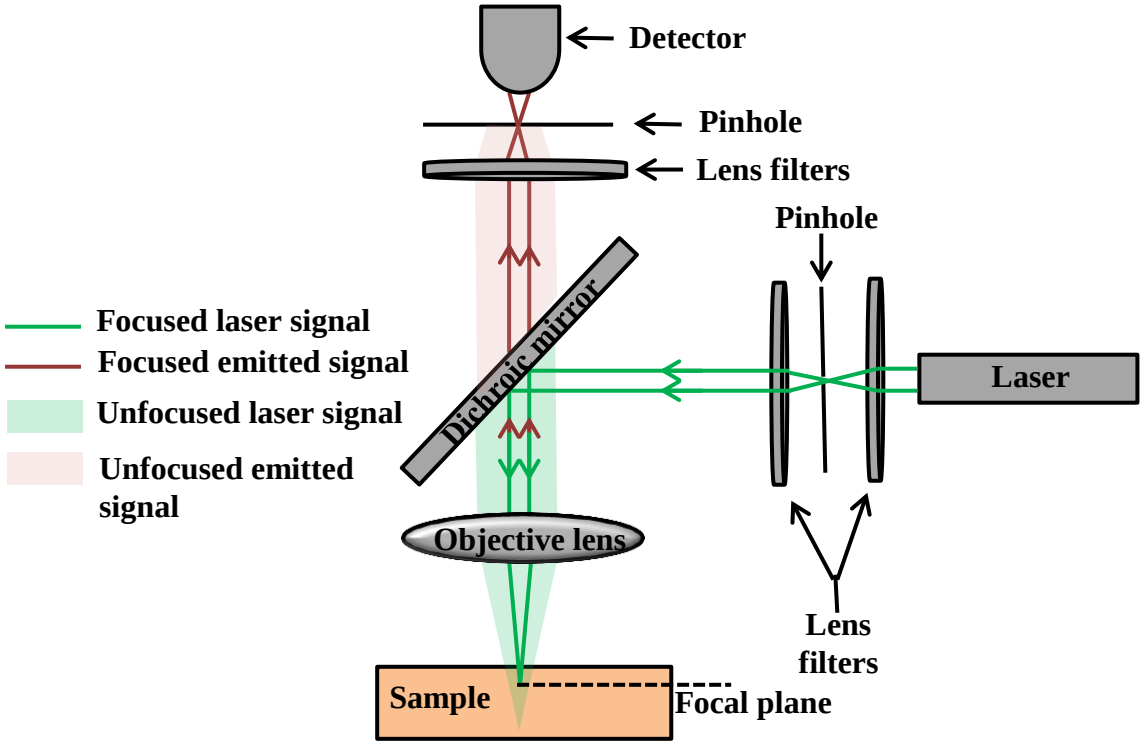

Figure 1.12. Schematic diagram of LSCM. Green and brown arrows indicate respectively the direction of the incident laser light and the emitted fluorescence, [213].

1.5.1.2 Atomic Force Microscopy (AFM)

AFM enables non-destructive imaging under ambient conditions. It can be applied to hard or soft, synthetic or natural compounds and surfaces. Unlike electron microscopy, sample visualisation by AFM relies on the mechanical approach of the probe to the sample [214]. The resolution of an AFM image is on the order of 0.1 nm (height) and 1 nm (lateral). The AFM principle is illustrated in figure 1.13. [215].

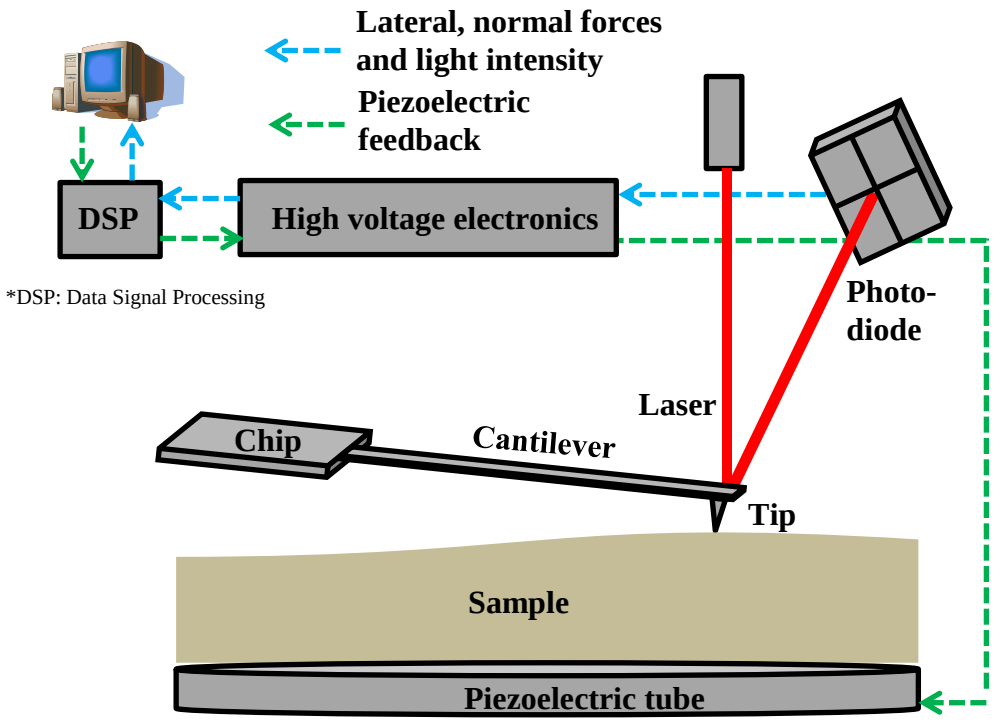

Figure 1.13. Schematic representation of atomic force microscopy

1.5.2 Potentiometric operations

1.5.2.1 Field effect transistors (FET)

A potentiometric device relies on the measure of a potential change with respect to a reference electrode. A typical field effect transistor (FET), or voltage control device, comprises three electrical conductors (a source, a drain and a gate). The source and the drain are separated by a semiconductor. The current flows from the source to the drain. It is modulated by the movement of charge carriers (holes or electrons) that are under the influence of a magnetic field created by the gate and separated from the system by an insulator. figure 1.14-A presents the electrical double layer formed when applying a positive potential on the gate with the ions in solution, while figure 1.14-B is a representation of the FET setup studied in this chapter.

A change of charge around the semiconductor (graphene), following an enzymatic reaction for example, will have for consequence to change the "gating" of the FET. This will cause a displacement of the source to drain current characteristics as a function of the gate potential (see chapter 3, figure 3.3 to 3.5).

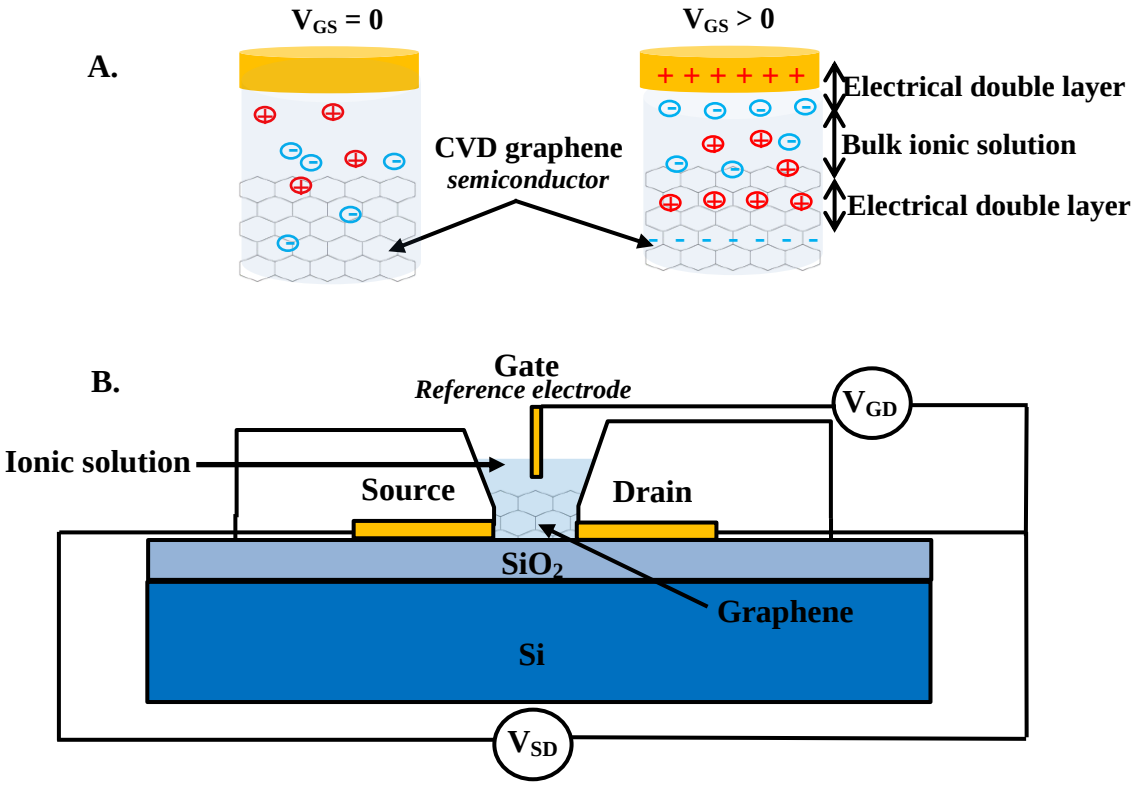

Figure 1.14. Electrical double layer and schematic diagram of the FET. A: The electrical double layer formed in an ionic solution when a gate voltage V_{GS} is imposed. B: Diagrammatic representation of the FET.

1.5.2.2 Graphene electrical properties; "zero-gap semiconductor"

Recently, graphene has been introduced as an alternative for integration in FET devices. The use of graphene in field effect transistors has been widely studied due to the ability to control its electrical transport properties with the gate electrode [216]. Graphene is defined as a zero-gap semiconductor, approaching the properties of semi-metals in that electron passage between energy bands is facilitated and even enhanced [147]. In the low energy range, the conduction and valence bands form conical shapes and meet at the Dirac point facilitating electron mobility in the nanomaterial and enabling small changes at its surface (when integrated with biological molecules in a FET device) to be detected [217].

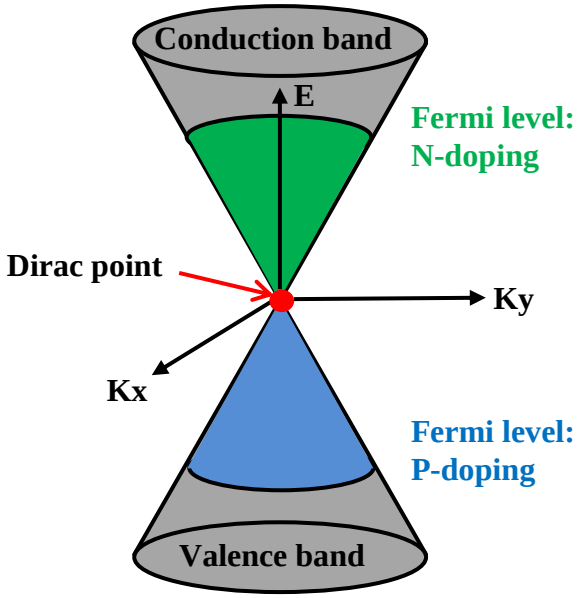

Figure 1.15. Representation of the conduction and valence band in graphene.

1.5.3 Voltammetric operations

A potentiometric and an amperometric approach were envisaged for the sensor development. Promising preliminary results were obtained with a Field Effect Transistor (FET), (see chapter 3). A voltammetric detection was however preferred, the transistor suffering from drawbacks such as: complicated integration with non-invasive detection techniques and limitations associated to buffer strength, storage, stability etc.

The electrochemical procedures described in the thesis rely on the use of electrochemical cell setups including three electrodes: a working electrode (WE), a counter electrode (CE) and a reference electrode (RE). The application of a potential between the WE and the RE (displaying a stable potential) induces the oxidation or reduction of a compound of interest (at the WE) in an aqueous solution which translates in a change of current measured between the WE and the CE. The role of supporting electrolytes in the aqueous solution will be to reduce the Ohmic (or *IR*) drop in the cell and to eliminate the contribution of migration current from the redox species of interest.

1.5.3.1 The Electrochemical cell

In a typical electrochemical experiment a redox reaction signal is acquired at a working electrode (WE), while the other half of the cell is a reference electrode (RE) which will be maintained at a constant potential [218]. When a potential is applied between WE and RE a voltage drop *IR* is observed that follows Ohm's law, equation 1.4.

$$V = IR \tag{1.4}$$

This equation describes the Ohmic relationship between the cell potential (*V*, Volts), current passing through the cell (*I*, Amps) and solution resistance (*R*, Ohms).

When $IR \leq$ 1-2 mV, a two electrode system (RE and WE) might be used to detect the redox current signal, however, the RE potential need to stay stable while current passes through it which isn't achievable with high *IR*. Two electrode cells have been used with micro-working electrodes and low *IR* processes but are not commonly applied in electrochemistry. The introduction of a third electrode in the system is preferred in order to maintain a stable potential at the RE (approaching ideal non-polarisable characteristics). The current is then measured between the newly introduced counter electrode (CE) and the working electrode (WE). This situation, displayed in figure 1.16 is the most commonly found in typical volatmmetric and amperometric configurations [219].

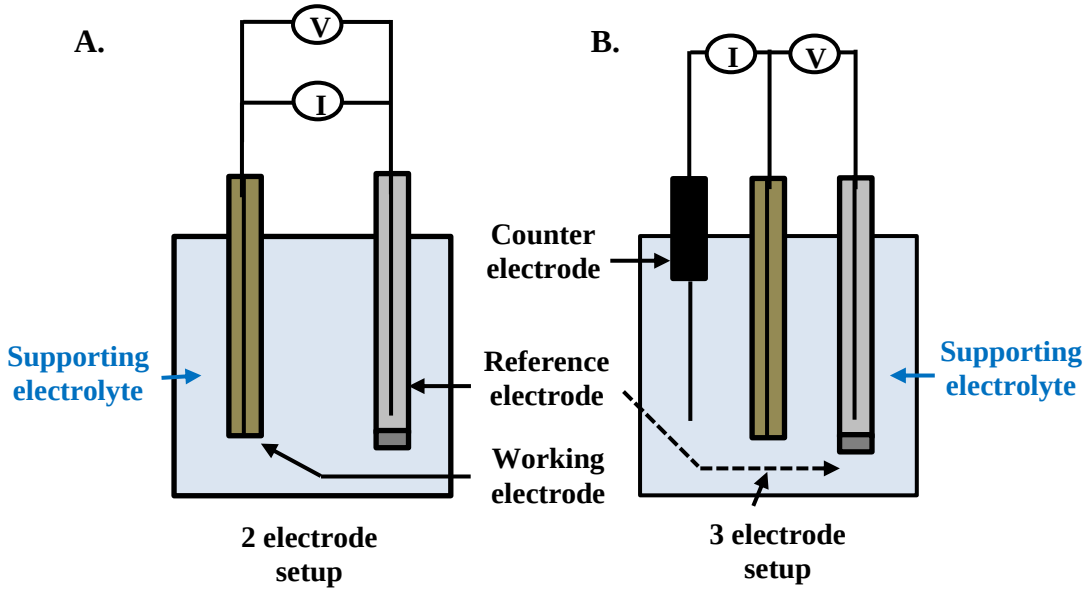

Figure 1.16. Electrochemical cell configurations. A: 2 electrodes setup; the potential is applied and current measured between a RE and a WE. B: 3 electrodes setup; the potential is applied between a RE and a WE while current is acquired between WE and CE.

The voltage and current between the three electrodes in situation B are controlled and measured by a device called a potentiostat. Finally, a fundamental feature of any electrochemical cell will be the presence of supporting electrolytes in sufficient concentration to support the redox reactions (see section 1.5.3.5).

1.5.3.2.Reference electrodes (RE)

Several electrodes are commonly used:

1.5.3.2.1The standard hydrogen electrode (SHE)

The SHE is the reference electrode that serves as a globally accepted standard for electrochemical literature as defined by the International Union of Pure and Applied Chemistry (IUPAC) [220]. This electrode should display the noticeable electrode potential $E_0(H^+/H_2) = 0$, at any temperature making it a reliable comparative system. A SHE comprises of a platinum black electrode which is dipped in a solution of hydrochloric acid. Hydrogen gas is bubbled through the system giving rise to the following equilibrium:

$$H^+(aq) + e^- \rightleftharpoons 1/2\ H_2(g) \qquad 1.5$$

aq: aqueous, g: gas

1.5.3.2.2 The saturated silver/silver chloride electrode

This electrode (as well as the saturated calomel electrode) is more applicable than the SHE which requires a constant flux of hydrogen gas. Results obtained with these two electrodes could however be corrected in order to be expressed against SHE following figure 1.17:

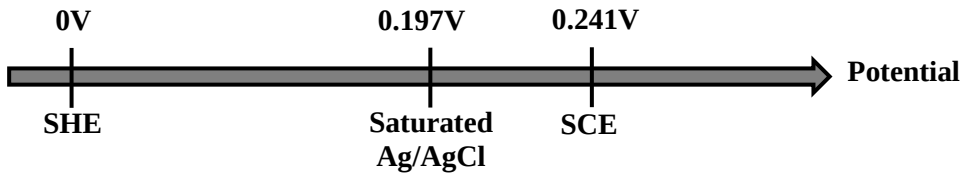

Figure 1.17. Reference electrode potential variations with respect to the standard hydrogen electrode.

A saturated Ag/AgCl electrode is formed of a silver wire coated with porous silver chloride, itself dipped in a saturated KCl solution. The porosity of the AgCl chloride layer is of high importance for the KCl solution to reach the silver wire. The equilibrium involved in this reference electrode is:

$$AgCl(s) + e^- \rightleftharpoons Ag(s) + Cl^-(aq) \qquad 1.6$$

s: solid, aq: aqueous

The Ag/AgCl electrode used in chapter 4 and 5 is not saturated (either pseudo Ag metallic wire, or micro Ag/AgCl electrode in 0.1 M KCl). This was done intentionally since the enzyme glucose oxidase is inhibited by halide (chloride) ions [61, 221].

1.5.3.2.3 The Saturated Calomel electrode (SCE)

The SCE is the other very frequently used reference electrode and is used in part of the thesis electrochemical analysis. It is formed of liquid mercury contacting insoluble di-mercury (I) chloride (also called "calomel"). This assembly is in direct contact with a saturated KCl solution. The redox equilibrium of a calomel electrode is presented thereof [218]:

$$1/2\ Hg_2Cl_2(s) + e^- \rightleftharpoons Hg(l) + Cl^-(aq) \qquad 1.7$$

s: solid, l: liquid, aq: aqueous

1.5.3.3 Counter electrode (CE)

The role of a counter electrode is to act as a current flowing counterpart for the working electrode. The active area of the counter electrode should preferably be large (coiled wire) in order to avoid influences on the charge flow (small current density). The most noticeable structural characteristic of such an electrode, however, is that it must be inert regarding the redox reaction happening in the electrochemical cell. Several techniques can be implemented in order to avoid reaction at the CE (use of a frit or a side arm to the electrochemical cell to separate the electrode from the working solution), but usually, the choice of an inert metal such as platinum will be sufficient to reduce considerably undesirable interactions, especially when working under normal voltammetric conditions where tiny quantities of material are consumed [218].

1.5.3.4 Working electrode (WE)

The working electrode is the core component of the system where the electrochemical reaction occurs. The oxidation or reduction happening at the WE will cause current to be drawn in or out of the CE producing a signal function of the potential imposed with respect to the RE. The efficiency of a WE will be dependent on multiple factors; electrode material, geometry, liquid/solid interphase etc. Some of the most common materials used for working electrodes can be listed as: metallic electrodes (gold, platinum, silver), carbon electrodes (glassy carbon, graphite, carbon paste, carbon nanomaterials) and liquid mercury electrodes (dropping mercury electrodes, hanging mercury drop electrodes, static mercury drop electrodes, mercury thin film electrode). The following characteristics have been defined to obtain an optimal WE: "(1) Small noise levels (for high sensitivity) (2) Reproducibility and stability of the electrode (3) Good redox active surface and interphase (4) Large working potential range and (5) Easy handling of the electrode assembly" [222]. All these criteria are considered and improved in the electrode development described in chapter 4.

1.5.3.5 Supporting electrolytes

Supporting electrolytes have been defined by the IUPAC as: "An electrolyte solution, whose constituents are not electroactive in the range of applied potentials being studied, and whose ionic strength (and, therefore, contribution to the conductivity) is usually much larger than the concentration of an electroactive substance to be dissolved in it [223]." Most buffers

satisfy this definition at concentrations between 1 and 0.1 M. Typical electrolytes are identified as: chlorides, sulphates, potassium, sodium, phosphate etc. The role of the supporting electrolytes will be to reduce the Ohmic (or *IR*) drop in the cell and to eliminate the migration current contribution from the redox species of interest [222]. Without supporting electrolyte, no voltammetric operation could occur as there wouldn't be any ionic entity to counter the migration of the redox analyte. The supporting electrolyte solution used in the electrochemical experiments is 0.1 M phosphate buffer pH 7.4, which is adequate for maintaining an appropriate pH around biological entities (enzyme: GOD) as well as being used widely in electrochemistry [224, 225].

1.5.3.6 Cyclic voltammetry (CV)

The principle of CV operations, as the name implies, involves varying the potential between a WE and a RE in a cyclic manner, and measuring the catalytic current. The imposed potential therefore has a triangular shape over time, starting at E_1, then increasing to a second E_2 and finally coming back to E_1 [218, 226] (figure 1.18). A cyclic voltammogram displays catalytic current = f(potential vs RE), (chapter 2, figure 2.10).

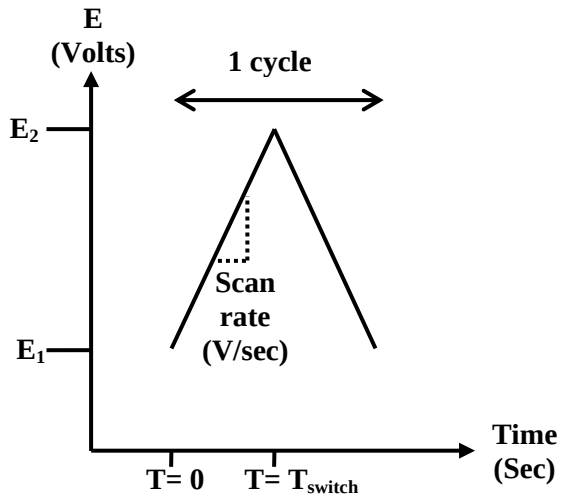

Figure 1.18. Potential sweep over time during cyclic voltammetry. The slope of the linear increase from E_1 to E_2 is the scan rate expressed in V/sec.

1.5.3.7 Chronoamperometry

The chronoamperometric measurement involves stepping the potential from a value at which no redox reaction occurs to one where a current relating to a specific redox reaction is observed, (figure 1.19). Chronoamperometry curves display, catalytic current = f(time) at a set potential against the RE (chapter 2, figure 2.11).

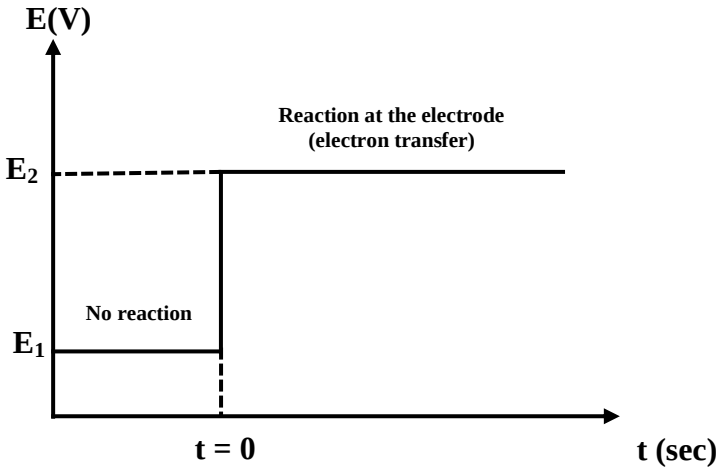

Figure 1.19. Stepping the potential in chronoamperometry

The diffusion of reactant to the electrode surface is described by the Cottrell equation [227] and is only applicable in the first few seconds of the chronoamperometric step where there is a current spike and a decay.

$$I_P = \frac{nFAC'\sqrt{D}}{\sqrt{\pi t}} \qquad (1.8)$$

I_P is the analytic current expressed as a function of the number of electrons *n*, the electrode area *A*, the concentration *C',* the diffusion coefficient *D* and the time *t*.

The diffusion field is a concentration gradient which extends out perpendicularly from the working electrode surface. Close to the working electrode surface, the redox species of interest (A) is depleted due to its uptake of either electrons or holes and therefore its conversion to another species (B).

$$A + e^- \rightarrow B \qquad (1.9)$$

This diffusion field is time dependent and at very short time scales, of the order of milliseconds, this diffusion field has not had time to establish. Therefore the depletion layer

close to the electrode surface is very small. Conversely, at longer time scales the diffusion field has time to establish and a thick diffusion field is created extending out into bulk solution (figure 1.20-A). This effect can be seen from the shape of the chronoamperometry curve (figure 1.20-B). At short time scales, the current can be seen to initially increase. This is because of the high concentration of redox species close to the electrode surface and its immediate conversion to another species. After a time, there is a peak in the current. This indicates that the diffusion field has now established and the redox species of interest cannot reach the working electrode surface fast enough to pick up the electrons or holes. After this peak, the current then falls and eventually stabilises as the diffusion field has reached a steady-state where it does not continue extending into the solution because of convection as well as Brownian motion limiting the size of the diffusion field [227].

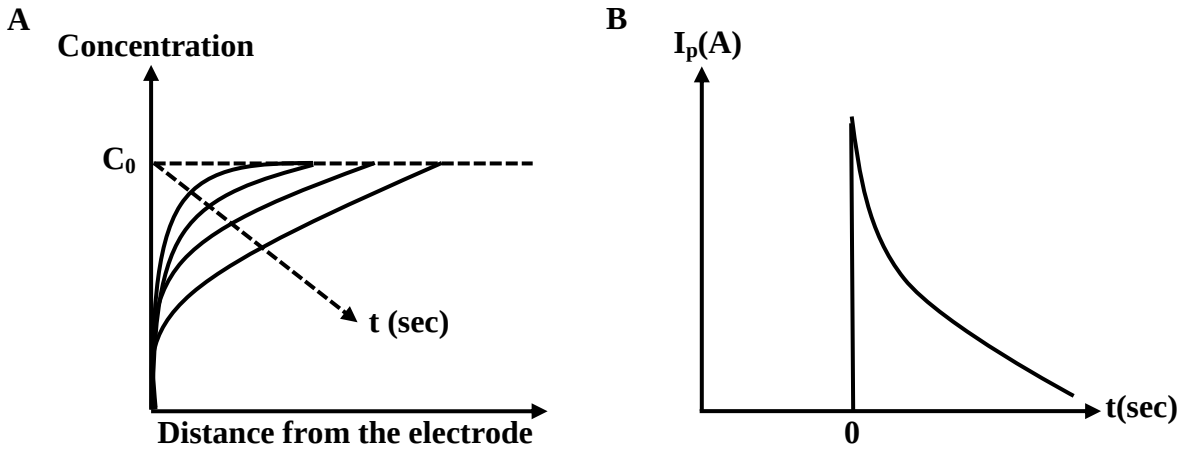

Figure 1.20. Chronoamperometry is diffusion dependent. A: Decrease of reactant concentration as a function of time and distance from the electrode. B: Current I_P response as a function of time.

1.6 Aims and objectives of the project

This chapter raises concern regarding the rising evolution of diabetes and the fundamental need for improved glucose sensing technologies (as opposed to the commonly used fingerstick sensor). An emphasis is therefore brought on alternative technologies and more specifically on non-invasive technologies that seems to be the future of the glucose biosensing industry. However, no such device has managed so far to be a commercial success. There is therefore opportunities for new non-invasive research to emerge.

Accordingly, the project therefore aims to develop a new non-invasive technology based on reverse iontophoresis. It will follow two principal axes: (1) the development of a highly sensitive and specific glucose biosensing platform and (2) the integration with reverse iontophoresis on a pig skin model and the targeting of hair follicles glucose extraction pathways.

(1) Based on the choice of CVD graphene as the transducer electrode, two characteristics will be considered in chapter 2 and 3. First, the biofunctionalization of the nanomaterial with GOD. This step is fundamental because it will ensure whether or not the enzyme will be retained on the sensor and keep its' catalytic activity intact. Two coatings will be investigated a non-covalent coating of graphene via a linker and the entrapment of the enzyme into an agarose gel. Then the detection principle will be considered and two sensing operations studied: a FET and an amperometric design. This will lead to the design of a specific and sensitive amperometric glucose biosensor in chapter 4. This chapter will more precisely describe how the results obtained from chapter 2 and 3 managed to create a performant biosensor benefiting from improvements such as the miniaturization of the setup or the additions of platinum nanoparticles.

(2) Having developed a performant and competitive sensing platform. The following aim will be to integrate it with reverse iontophoresis which will be successfully achieved in chapter 5. The preferential extraction of glucose through hair follicles and detection on the miniature sensor will then be demonstrated. This will be validated by an independent ^{1}HqNMR test of extracted glucose through the same pathways. Finally a first attempt will be made at multiplexing the sensor and cross talking between the different detection units investigated.

The overall objective of the project is therefore to design a miniature highly sensitive and specific glucose biosensor based on CVD graphene and integrate it to reverse iontophoresis as well as target reverse iontophoresis pathways where the extraction of neutral molecules such as glucose is preferential.

1. Scully, T., *Diabetes in numbers.* Nature, 2012. **485**(7398): p. S2-S3.
2. Clark, L.C. and C. Lyons, *Electrode systems for continuous monitoring in cardiovascular surgery.* Annals of the New York Academy of Sciences, 1962. **102**(1): p. 29-45.
3. Turner, A.P.F., *Biosensors: sense and sensibility.* Chemical Society Reviews, 2013. **42**(8): p. 3184-3196.
4. Higgins, I.J., H.A.O. Hill, and E.V. Plotkin, *Enzyme for catalysis, ferrocene mediator,* 1985, US Patent 4545382 A.
5. Hilditch, P.I. and M.J. Green, *Disposable electrochemical biosensors.* Analyst, 1991. **116**(12): p. 1217-1220.
6. Vadgama, P., et al., *Chemical sensors and biosensors: nearer the patient*, in *Pure and Applied Chemistry*1991. p. 1147.
7. Yoo, E.-H. and S.-Y. Lee, *Glucose Biosensors: An Overview of Use in Clinical Practice.* Sensors, 2010. **10**(5): p. 4558.
8. Peyrot, M., et al., *Psychosocial problems and barriers to improved diabetes management: results of the Cross-National Diabetes Attitudes, Wishes and Needs (DAWN) Study.* Diabetic Medicine, 2005. **22**(10): p. 1379-1385.
9. Clarke, S.E. and J.R. Foster, *A history of blood glucose meters and their role in self-monitoring of diabetes mellitus.* British Journal of Biomedical Science, 2012. **69**(2): p. 83-93.
10. Zhou, D.D. and R.J. Greenberg, *Implantable Electrochemical Biosensors for Retinal Prostheses,* 2014, US Patent 20140249395 A1.
11. Vaddiraju, S., et al., *Enhancing the Sensitivity of Needle-Implantable Electrochemical Glucose Sensors via Surface Rebuilding.* Journal of Diabetes Science and Technology, 2013. **7**(2): p. 441-451.
12. Badugu, R., J. Lakowicz, and C. Geddes, *A Glucose Sensing Contact Lens: A Non-Invasive Technique for Continuous Physiological Glucose Monitoring.* Journal of Fluorescence, 2003. **13**(5): p. 371-374.
13. Potts, R.O. and J.W. Moyer, *Sweat glucose sensors and collection devices for glucose measurement,* 2010, WO Patent 2010045247 A1.
14. Kim, H.Y., et al., *Reusable urine glucose sensor based on functionalized graphene oxide conjugated Au electrode with protective layers.* Biotechnology Reports, 2014. **3**(0): p. 49-53.

15. Zhang, W. and M.L. Wang, *Saliva Glucose Monitoring System*, 2014, US Patent 20140197042 A1.
16. Burmeister, J.J. and M.A. Arnold, *Evaluation of Measurement Sites for Noninvasive Blood Glucose Sensing with Near-Infrared Transmission Spectroscopy.* Clinical Chemistry, 1999. **45**(9): p. 1621-1627.
17. Bruulsema, J.T., et al., *Correlation between blood glucose concentration in diabetics and noninvasively measured tissue optical scattering coefficient.* Optics Letters, 1997. **22**(3): p. 190-192.
18. Tarr, R.V. and P.G. Steffes, *Non-invasive blood glucose measurement system and method using stimulated raman spectroscopy*, 1993, US Patent 5243983 A.
19. Tierney, M.J., et al., *Clinical evaluation of the GlucoWatch® biographer: a continual, non-invasive glucose monitor for patients with diabetes.* Biosensors and Bioelectronics, 2001. **16**(9–12): p. 621-629.
20. Ermolina, I., Y. Polevaya, and Y. Feldman, *Analysis of dielectric spectra of eukaryotic cells by computer modeling.* European Biophysics Journal, 2000. **29**(2): p. 141-145.
21. So, C.F., et al., *Recent advances in noninvasive glucose monitoring.* Med Devices (Auckl), 2012. **5**: p. 45-52.
22. Weinzimer, S.A., *Analysis: PENDRA: The Once and Future Noninvasive Continuous Glucose Monitoring Device?* Diabetes Technology & Therapeutics, 2004. **6**(4): p. 442-444.
23. Caduff, A., et al., *First human experiments with a novel non-invasive, non-optical continuous glucose monitoring system.* Biosensors and Bioelectronics, 2003. **19**(3): p. 209-217.
24. Leboulanger, B., R.H. Guy, and M.B. Delgado-Charro, *Reverse iontophoresis for non-invasive transdermal monitoring.* Physiological Measurement, 2004. **25**(3): p. R35.
25. Tierney, M.J., *Electrochemical sensor with dual purpose electrode*, 2002, US Patent 5954685 A.
26. Rossetti, P., et al., *Estimating Plasma Glucose from Interstitial Glucose: The Issue of Calibration Algorithms in Commercial Continuous Glucose Monitoring Devices.* Sensors, 2010. **10**(12): p. 10936-10952.
27. Bath, B.D., et al., *Scanning electrochemical microscopy of iontophoretic transport in hairless mouse skin. Analysis of the relative contributions of diffusion, migration, and*

electroosmosis to transport in hair follicles. Journal of Pharmaceutical Sciences, 2000. **89**(12): p. 1537-1549.

28. Chan, M.-S., et al., *Materials for Fabricating Biosensors for Transdermal Glucose Monitoring.* Clinical Chemistry, 1999. **45**(9): p. 1689-1690.
29. Alberti, K.G. and P.Z. Zimmet, *Definition, diagnosis and classification of diabetes mellitus and its complications. Part 1: diagnosis and classification of diabetes mellitus provisional report of a WHO consultation.* Diabet Med, 1998. **15**(7): p. 539-53.
30. DeBerardinis, Ralph J. and Craig B. Thompson, *Cellular Metabolism and Disease: What Do Metabolic Outliers Teach Us?* Cell, 2012. **148**(6): p. 1132-1144.
31. Schrier, R.W., *Diseases of the Kidney and Urinary Tract*. 2007: Wolters Kluwer Health/Lippincott Williams & Wilkins.
32. Joslin, E.P. and C.R. Kahn, *Joslin's Diabetes Mellitus: Edited by C. Ronald Kahn et al*. 2005: Lippincott Williams & Willkins.
33. LeRoith, D., S.I. Taylor, and J.M. Olefsky, *Diabetes Mellitus: A Fundamental and Clinical Text*. 2004: Lippincott Williams & Wilkins.
34. Serrano-Ríos, M., *Type 2. Diabetes Mellitus*. 2010: Elsevier.
35. Goldstein, B.J. and D. Mueller-Wieland, *Type 2 Diabetes: Principles and Practice, Second Edition*. 2007: Taylor & Francis.
36. Eriksson, K.F. and F. Lindgärde, *Prevention of Type 2 (non-insulin-dependent) diabetes mellitus by diet and physical exercise The 6-year Malmö feasibility study.* Diabetologia, 1991. **34**(12): p. 891-898.
37. Ferrara, C.T. and D.U. Pharmacology, *Metabolic Pathways of Type 2 Diabetes: Intersection of Genetics, Transcriptomics, and Metabolite Profiling*. 2008: Duke University.
38. CDC. *Diabetes surveillance system*. 2014 [cited 2014]; Available from: http://www.cdc.gov/nchs/fastats/diabetes.htm.
39. Engelgau, M.M., et al., *The Evolving Diabetes Burden in the United States.* Annals of Internal Medicine, 2004. **140**(11): p. 945-950.
40. Jain, S. and S. Saraf, *Type 2 diabetes mellitus—Its global prevalence and therapeutic strategies.* Diabetes & Metabolic Syndrome: Clinical Research & Reviews, 2010. **4**(1): p. 48-56.
41. Oldroyd, J., et al., *Diabetes and ethnic minorities.* Postgraduate Medical Journal, 2005. **81**(958): p. 486-490.

42. Hu, F.B., *Globalization of Diabetes: The role of diet, lifestyle, and genes.* Diabetes Care, 2011. **34**(6): p. 1249-1257.
43. Alhabib, S., M. Aldraimly, and A. Alfarhan, *An evolving role of clinical pharmacists in managing diabetes: Evidence from the literature.* Saudi Pharmaceutical Journal, 2014(0).
44. WHO. *definition and diagnosis of diabetes mellitus and intermediate hyperglycemia*. Report of a WHO/IDF consultation 2006 [cited 2015]; Available from: http://www.who.int/diabetes/publications/Definition%20and%20diagnosis%20of%20diabetes_new.pdf.
45. WHO. *Screening for type 2 diabetes: Report of a WHO and IDF meeting*. World Health Organization, Geneva 2003 [cited 2015]; Available from: http://www.who.int/diabetes/publications/en/screening_mnc03.pdf.
46. Reynolds, T.M., W.S.A. Smellie, and P.J. Twomey, *Glycated haemoglobin (HbA1c) monitoring*. Vol. 333. 2006. 586-588.
47. WHO, *Use of glycated haemoglobin (HbA1c) in the diagnosis of diabetes mellitus.* Diabetes Research and Clinical Practice, 2011. **93**(3): p. 299-309.
48. Association, A.D., *Standards of Medical Care in Diabetes—2014.* Diabetes Care, 2014. **37**(Supplement 1): p. S14-S80.
49. Mera, S.L., *Understanding Disease: Pathology and Prevention*. 1997: Stanley Thornes.
50. Gribovschi, M., et al., *Assessing Glycemic Control in Diabetes: From Self Monitoring of Blood Glucose to Continuous Glucose Monitoring System*, in *International Conference on Advancements of Medicine and Health Care through Technology*, S. Vlad, R. Ciupa, and A. Nicu, Editors. 2009, Springer Berlin Heidelberg. p. 29-32.
51. Wang, J., *Electrochemical Glucose Biosensors.* Chemical Reviews, 2007. **108**(2): p. 814-825.
52. Goldstein, D.E., et al., *Tests of Glycemia in Diabetes.* Diabetes Care, 2004. **27**(7): p. 1761-1773.
53. Cowart, S.L. and M.E. Stachura, *Glucosuria*, in *Clinical Methods: The History, Physical, and Laboratory Examinations*, H.K. Walker, W.D. Hall, and J.W. Hurst, Editors. 1990: Boston.
54. Thevenot, D.R., et al., *Electrochemical biosensors: recommended definitions and classification.* Biosens Bioelectron, 2001. **16**(1-2): p. 121-31.

55. Turner, A.P.F., I. Karube, and G.S. Wilson, *Biosensors: fundamentals and applications*. 1987: Oxford University Press.
56. Turner, A.P.F. *Biosensors and Bioelectronics*. 2014 [cited 2014]; Available from: http://www.journals.elsevier.com/biosensors-and-bioelectronics/.
57. Mascini, M., I. Palchetti, and R.S.o. Chemistry, *Nucleic Acid Biosensors for Environmental Pollution Monitoring*. 2011: Royal Society of Chemistry.
58. Wohlfahrt, G., et al., *1.8 and 1.9 A resolution structures of the Penicillium amagasakiense and Aspergillus niger glucose oxidases as a basis for modelling substrate complexes.* Acta Crystallographica Section D, 1999. **55**(5): p. 969-977.
59. Bankar, S.B., et al., *Glucose oxidase — An overview.* Biotechnology Advances, 2009. **27**(4): p. 489-501.
60. Nakamura, S. and Y. Ogura, *Mode of Inhibition of Glucose Oxidase by Metal Ions.* Journal of Biochemistry, 1968. **64**(4): p. 439-447.
61. Rogers, M.J. and K.G. Brandt, *Multiple inhibition analysis of Aspergillus niger glucose oxidase by D-glucal and halide ions.* Biochemistry, 1971. **10**(25): p. 4636-4641.
62. Nakamura, S. and S. Fujiki, *Comparative Studies on the Glucose Oxidases of Aspergillus niger and Penicillium amagasakiense.* Journal of Biochemistry, 1968. **63**(1): p. 51-58.
63. Selvakumar, P., V.A.T. Ezhil, and C. Shen-Ming, *Direct Electrochemistry of Glucose Oxidase at Reduced Graphene Oxide/Zinc Oxide Composite Modified Electrode for Glucose Sensor.* International Journal of Electrochemical Science, 2012. **7**(3): p. 2153.
64. Vogt, S., et al., *Determination of the pH Dependent Redox Potential of Glucose Oxidase by Spectroelectrochemistry.* Analytical Chemistry, 2014. **86**(15): p. 7530-7535.
65. Ronkainen, N.J., H.B. Halsall, and W.R. Heineman, *Electrochemical biosensors.* Chemical Society Reviews, 2010. **39**(5): p. 1747-1763.
66. Hu, Y., P. Zuo, and B.-C. Ye, *Label-free electrochemical impedance spectroscopy biosensor for direct detection of cancer cells based on the interaction between carbohydrate and lectin.* Biosensors and Bioelectronics, 2013. **43**(0): p. 79-83.
67. Zourob, M., *Recognition Receptors in Biosensors*. 2010: Springer.
68. Lee, W.-Y., et al., *Microfabricated Conductometric Urea Biosensor Based on Sol-Gel Immobilized Urease.* Electroanalysis, 2000. **12**(1): p. 78-82.

69. Okafor, C., et al., *Fabrication of a Novel Conductometric Biosensor for Detecting Mycobacterium avium subsp. paratuberculosis Antibodies.* Sensors, 2008. **8**(9): p. 6015-6025.
70. Soldatkin, O.O., et al., *Novel conductometric biosensor based on three-enzyme system for selective determination of heavy metal ions.* Bioelectrochemistry, 2012. **83**(0): p. 25-30.
71. Eggins, B.R., *Chemical Sensors and Biosensors*. 2002: Wiley.
72. Ganesh, A., et al., *Evaluation of the VIA® Blood Chemistry Monitor for Glucose in Healthy and Diabetic Volunteers.* Journal of Diabetes Science and Technology, 2008. **2**(2): p. 182-193.
73. Torjman, M.C., N. Dalal, and M.E. Goldberg, *Glucose monitoring in acute care: technologies on the horizon.* J Diabetes Sci Technol, 2008. **2**(2): p. 178-81.
74. Yatabe, T., K. Hanazaki, and M. Yokoyama, *Automating Blood Glucose Control.* J Anesthe Clinic Res, 2012. **3**(1).
75. Scawn, N., et al., *First clinical study data from therapeutic use of a novel continuous glucose monitoring system in the ICU.* Critical Care, 2014. **18**(Suppl 1): p. P443.
76. Bird, S., et al., *Initial experience with continuous intra-arterial fluorescent glucose monitoring in patients in the ICU following cardiac surgery.* Critical Care, 2012. **16**(Suppl 1): p. P174.
77. Chee, F. and T. Fernando, *Closed-Loop Control of Blood Glucose*. 2007: Springer.
78. Mastrototaro, J.J., *The MiniMed Continuous Glucose Monitoring System.* Diabetes Technology & Therapeutics, 2000. **2**(1).
79. Ginsberg, B.H., *The FDA Panel Advises Approval of the First Continuous Glucose Sensor.* Diabetes Technology & Therapeutics, 1999. **1**(2): p. 203-204.
80. Holker, J.D., et al., *Analyte sensor and method of making the same*, 2006, US Patent 20020032374 A1.
81. Mamkin, I., et al., *Real-Time Continuous Glucose Monitoring in the Clinical Setting: The Good, the Bad, and the Practical.* Journal of diabetes science and technology (Online), 2008. **2**(5): p. 882-889.
82. van den Bosch, E.E., et al., *A promising solution to enhance the sensocompatibility of biosensors in continuous glucose monitoring systems.* J Diabetes Sci Technol, 2013. **7**(2): p. 455-64.

83. Maia, F.F. and L.R. Araujo, *[Accuracy, utility and complications of continuous glucose monitoring system (CGMS) in pediatric patients with type 1 diabetes]*. J Pediatr (Rio J), 2005. **81**(4): p. 293-7.
84. Cengiz, E. and W.V. Tamborlane, *A Tale of Two Compartments: Interstitial Versus Blood Glucose Monitoring.* Diabetes Technology & Therapeutics, 2009. **11**(Suppl 1): p. S-11-S-16.
85. Boyne, M.S., et al., *Timing of Changes in Interstitial and Venous Blood Glucose Measured With a Continuous Subcutaneous Glucose Sensor.* Diabetes, 2003. **52**(11): p. 2790-2794.
86. Bantle, J.P. and W. Thomas, *Glucose measurement in patients with diabetes mellitus with dermal interstitial fluid.* Journal of Laboratory and Clinical Medicine, 1997. **130**(4): p. 436-441.
87. Steil, G.M., et al., *Interstitial fluid glucose dynamics during insulin-induced hypoglycaemia.* Diabetologia, 2005. **48**(9): p. 1833-1840.
88. Valgimigli, F., et al., *Evaluating the clinical accuracy of GlucoMen(R)Day: a novel microdialysis-based continuous glucose monitor*. J Diabetes Sci Technol, 2010. **4**(5): p. 1182-92.
89. Larson, N.S. and J.E. Pinsker, *The role of continuous glucose monitoring in the care of children with type 1 diabetes.* International Journal of Pediatric Endocrinology, 2013. **2013**(1): p. 8-8.
90. Heo, Y.J. and S. Takeuchi, *Towards Smart Tattoos: Implantable Biosensors for Continuous Glucose Monitoring.* Advanced Healthcare Materials, 2013. **2**(1): p. 43-56.
91. Zazworsky, D., J.N. Bolin, and V. Gaubeca, *Handbook of Diabetes Management*. 2007: Springer.
92. Cormerais, H. and P.Y. Richard, *Artificial pancreas for type 1 diabetes: Closed-loop algorithm based on Error Dynamics Shaping.* Journal of Process Control, 2012. **22**(7): p. 1219-1227.
93. FDA. *MiniMed 530G System*. 2013 [cited 2014]; Available from: http://www.accessdata.fda.gov/cdrh_docs/pdf12/p120010a.pdf.
94. Sorli, C., *New Developments in Insulin Therapy for Type 2 Diabetes.* The American Journal of Medicine, 2014. **127**(10, Supplement): p. S39-S48.
95. Wernerman, J., et al., *Continuous glucose control in the ICU: report of a 2013 round table meeting.* Crit Care, 2014. **18**(3): p. 226.

96. Geoffrey, M., R. Brazg, and W. Richard, *FreeStyle Navigator Continuous Glucose Monitoring System with TRUstart Algorithm, a 1-Hour Warm-Up Time.* Journal of Diabetes Science and Technology, 2011. **5**(1): p. 99-106.
97. Burge, M.R., et al., *Continuous Glucose Monitoring: The Future of Diabetes Management.* Diabetes Spectrum, 2008. **21**(2): p. 112-119.
98. Tubiana-Rufi, N., J.P. Riveline, and D. Dardari, *Real-time continuous glucose monitoring using Guardian®RT: from research to clinical practice.* Diabetes & Metabolism, 2007. **33**(6): p. 415-420.
99. Bode, B., et al., *Alarms Based on Real-Time Sensor Glucose Values Alert Patients to Hypo- and Hyperglycemia: The Guardian Continuous Monitoring System.* Diabetes Technology & Therapeutics, 2004. **6**(2): p. 105-113.
100. Poscia, A., et al., *A microdialysis technique for continuous subcutaneous glucose monitoring in diabetic patients (part 1).* Biosensors and Bioelectronics, 2003. **18**(7): p. 891-898.
101. Kubiak, T., et al., *Microdialysis-Based 48-Hour Continuous Glucose Monitoring with GlucoDay™: Clinical Performance and Patients' Acceptance.* Diabetes Technology & Therapeutics, 2006. **8**(5): p. 570-575.
102. Guerci, B., et al., *Clinical Performance of CGMS in Type 1 Diabetic Patients Treated by Continuous Subcutaneous Insulin Infusion Using Insulin Analogs.* Diabetes Care, 2003. **26**(3): p. 582-589.
103. Maia, F.F.R. and L.R. Araújo, *Efficacy of continuous glucose monitoring system (CGMS) to detect postprandial hyperglycemia and unrecognized hypoglycemia in type 1 diabetic patients.* Diabetes Research and Clinical Practice, 2007. **75**(1): p. 30-34.
104. Schoonen, A.J.M. and K.J.C. Wientjes, *A Model for Transport of Glucose in Adipose Tissue to a Microdialysis Probe.* Diabetes Technology & Therapeutics, 2003. **5**(4): p. 589-598.
105. Kudva, Y.C., et al., *Closed-Loop Artificial Pancreas Systems: Physiological Input to Enhance Next-Generation Devices.* Diabetes Care, 2014. **37**(5): p. 1184-1190.
106. Sadana, A. and N. Sadana, *Biomarkers and Biosensors: Detection and Binding to Biosensor Surfaces and Biomarkers Applications*. 2014: Elsevier Science.
107. Sieg, A., R.H. Guy, and M.B. Delgado-Charro, *Noninvasive and Minimally Invasive Methods for Transdermal Glucose Monitoring.* Diabetes Technology & Therapeutics, 2005. **7**(1): p. 174-197.

108. Khan, A., et al., *Iontophoretic drug delivery: History and applications.* Journal of Applied Pharmaceutical Science 2011. **1**(3): p. 11-24.
109. Rawat, S., et al., *Transdermal delivery by iontophoresis.* Indian J Pharm Sci, 2008. **70**(1): p. 5-10.
110. Merino, V., Y.N. Kalia, and R.H. Guy, *Transdermal therapy and diagnosis by iontophoresis.* Trends in Biotechnology. **15**(8): p. 288-290.
111. Mudry, B., R.H. Guy, and M.B. Delgado-Charro, *Transport Numbers in Transdermal Iontophoresis.* Biophysical Journal, 2006. **90**(8): p. 2822-2830.
112. Marro, D., et al., *Contributions of electromigration and electroosmosis to iontophoretic drug delivery.* Pharm Res, 2001. **18**(12): p. 1701-8.
113. Pikal, M.J., *The role of electroosmotic flow in transdermal iontophoresis.* Advanced Drug Delivery Reviews, 2001. **46**(1–3): p. 281-305.
114. Sieg, A., R.H. Guy, and M. Begoña Delgado-Charro, *Electroosmosis in Transdermal Iontophoresis: Implications for Noninvasive and Calibration-Free Glucose Monitoring.* Biophysical Journal, 2004. **87**(5): p. 3344-3350.
115. Pikal, M.J. and S. Shah, *Transport mechanisms in iontophoresis. II. Electroosmotic flow and transference number measurements for hairless mouse skin.* Pharm Res, 1990. **7**(3): p. 213-21.
116. Hadgraft, J. and R. Guy, *Biotechnological Aspects of Transport Across Human Skin.* Biotechnology and Genetic Engineering Reviews, 2004. **21**(1): p. 183-196.
117. Degim, T., et al., *Method for measuring blood urea level by reverse iontophoresis*, 2003, WO Patent 2003084604 A1.
118. Nandy, B.C., et al., *Transdermal electronically assisted technologies: current approaches on iontophoretic delivery system.* 2011. **2**(4).
119. Sage, B.H., Jr., *FDA panel approves Cygnus's noninvasive GlucoWatch.* Diabetes Technol Ther, 2000. **2**(1): p. 115-6.
120. Chan, N.N. and S.J. Hurel, *Potential impact of a new blood glucose monitoring device: the GlucoWatch® Biographer.* Practical Diabetes International, 2002. **19**(4): p. 97-100.
121. Eastman, R.C., A.D. Leptien, and H.P. Chase, *Cost-effectiveness of use of the GlucoWatch® Biographer in children and adolescents with type 1 diabetes: a preliminary analysis based on a randomized controlled trial.* Pediatric Diabetes, 2003. **4**(2): p. 82-86.

122. Gandrud, L.M., et al., *Use of the Cygnus GlucoWatch Biographer at a Diabetes Camp.* Pediatrics, 2004. **113**(1): p. 108-111.
123. Iafusco, D., et al., *Usefulness or Uselessness of GlucoWatch in Monitoring Hypoglycemia in Children and Adolescents.* Pediatrics, 2004. **113**(1): p. 175-176.
124. Agache, P.G., et al., *Measuring the Skin*. 2004: Springer.
125. Touitou, E. and B.W. Barry, *Enhancement in Drug Delivery*. 2006: Taylor & Francis.
126. Adkinson, N.F., et al., *Middleton's Allergy: Principles and Practice*. 2013: Elsevier Health Sciences.
127. Freinkel, R.K. and D.T. Woodley, *The Biology of the Skin*. 2001: Taylor & Francis.
128. Ehrhardt, C. and K.J. Kim, *Drug Absorption Studies: In Situ, In Vitro and In Silico Models*. 2007: Springer.
129. Farage, M., K. Miller, and H. Maibach, *Degenerative Changes in Aging Skin*, in *Textbook of Aging Skin*, M. Farage, K. Miller, and H. Maibach, Editors. 2010, Springer Berlin Heidelberg. p. 25-35.
130. Cullander, C., *What are the pathways of iontophoretic current flow through mammalian skin?* Advanced Drug Delivery Reviews, 1992. **9**(2–3): p. 119-135.
131. Dhote, V., et al., *Iontophoresis: a potential emergence of a transdermal drug delivery system.* Sci Pharm, 2012. **80**(1): p. 1-28.
132. Turner, N.G. and R.H. Guy, *Visualization and Quantitation of Iontophoretic Pathways Using Confocal Microscopy*. J Invest Derm Symp P, 1998. **3**(2): p. 136-142.
133. Craane-van Hinsberg, W.H.M., et al., *Role of Appendages in Skin Resistance and Iontophoretic Peptide Flux: Human Versus Snake Skin.* Pharmaceutical Research, 1995. **12**(10): p. 1506-1512.
134. Bath, B., H. White, and E. Scott, *Visualization and Analysis of Electroosmotic Flow in Hairless Mouse Skin.* Pharmaceutical Research, 2000. **17**(4): p. 471-475.
135. Turner, N.G. and R.H. Guy, *Iontophoretic transport pathways: Dependence on penetrant physicochemical properties.* Journal of Pharmaceutical Sciences, 1997. **86**(12): p. 1385-1389.
136. Turner, N.G. and R.H. Guy, *Visualization and quantitation of iontophoretic pathways using confocal microscopy.* J Investig Dermatol Symp Proc, 1998. **3**(2): p. 136-42.
137. Liu, Z. and J. Etzkorn, *In-situ tear sample collection and testing using a contact lens*, 2014, US Patent 20140194706 A1.

138. Sen, D.K. and G.S. Sarin, *Tear Glucose-Levels in Normal People and in Diabetic-Patients.* British Journal of Ophthalmology, 1980. **64**(9): p. 693-695.
139. LeBlanc, J., et al., *Evaluation of lacrimal fluid as an alternative for monitoring glucose in critically ill patients.* Intensive Care Medicine, 2005. **31**(10): p. 1442-1445.
140. Geim, A.K. and K.S. Novoselov, *The rise of graphene.* Nat Mater, 2007. **6**(3): p. 183-191.
141. *It's still all about graphene.* Nat Mater, 2011. **10**(1): p. 1-1.
142. Wallace, P.R., *The Band Theory of Graphite.* Physical Review, 1947. **71**(9): p. 622-634.
143. Lin, Y., et al., *Glucose Biosensors Based on Carbon Nanotube Nanoelectrode Ensembles.* Nano Letters, 2003. **4**(2): p. 191-195.
144. Lanzellotto, C., et al., *Nanostructured enzymatic biosensor based on fullerene and gold nanoparticles: Preparation, characterization and analytical applications.* Biosensors and Bioelectronics, 2014. **55**(0): p. 430-437.
145. Kwak, Y.H., et al., *Flexible glucose sensor using CVD-grown graphene-based field effect transistor.* Biosensors and Bioelectronics, 2012. **37**(1): p. 82-87.
146. Pop, E., V. Varshney, and A.K. Roy, *Thermal properties of graphene: Fundamentals and applications.* MRS Bulletin, 2012. **37**(12): p. 1273-1281.
147. Wang, X.-L., S.X. Dou, and C. Zhang, *Zero-gap materials for future spintronics, electronics and optics.* NPG Asia Mater, 2010. **2**: p. 31-38.
148. Obeng, Y.S. and P. Srinivasan, *Graphene - Is it the future for Semiconductors? A High Level Overview of Materials, Devices and Applications.* The electrochemical society's interface, 2011. **20**(1): p. 47-52.
149. Yusoff, A.R.M., *Graphene Optoelectronics: Synthesis, Characterization, Properties, and Applications*. 2014: Wiley.
150. Gao, H., et al., *Electrochemical DNA Biosensor Based on Graphene and TiO2 Nanorods Composite Film for the Detection of Transgenic Soybean Gene Sequence of MON89788.* Electroanalysis, 2012. **24**(12): p. 2283-2290.
151. Hernández, R., et al., *Graphene-based potentiometric biosensor for the immediate detection of living bacteria.* Biosensors and Bioelectronics, 2014. **54**(0): p. 553-557.
152. Gogotsi, Y. and V. Presser, *Carbon Nanomaterials, Second Edition*. 2013: CRC Press.
153. Tsoukleri, G., et al., *Subjecting a Graphene Monolayer to Tension and Compression.* Small, 2009. **5**(21): p. 2397-2402.

154. Dürkop, T., et al., *Extraordinary Mobility in Semiconducting Carbon Nanotubes.* Nano Letters, 2004. **4**(1): p. 35-39.
155. Yu, M.-F., et al., *Strength and Breaking Mechanism of Multiwalled Carbon Nanotubes Under Tensile Load.* Science, 2000. **287**(5453): p. 637-640.
156. Mirri, F., et al., *High-Performance Carbon Nanotube Transparent Conductive Films by Scalable Dip Coating.* ACS Nano, 2012. **6**(11): p. 9737-9744.
157. Sun, D.-M., et al., *A Review of Carbon Nanotube- and Graphene-Based Flexible Thin-Film Transistors.* Small, 2013. **9**(8): p. 1188-1205.
158. Morris, J.E. and K. Iniewski, *Graphene, Carbon Nanotubes, and Nanostructures: Techniques and Applications*. 2013: CRC Press.
159. Huang, J., et al., *A review of the large-scale production of carbon nanotubes: The practice of nanoscale process engineering.* Chinese Science Bulletin, 2012. **57**(2-3): p. 157-166.
160. Rafique, M. and J. Iqbal, *Production of Carbon Nanotubes by Different Routes-A Review.* Journal of Encapsulation and Adsorption Sciences, 2011. **1**(2): p. 29-34.
161. De Volder, M.F.L., et al., *Carbon Nanotubes: Present and Future Commercial Applications.* Science, 2013. **339**(6119): p. 535-539.
162. Nakanishi, T., *Supramolecular Soft Matter: Applications in Materials and Organic Electronics*. 2011: Wiley.
163. Tanaka, S., *Fullerene composite*, 1997, US Patent 5648056 A.
164. Bakry, R., et al., *Medicinal applications of fullerenes.* Int J Nanomedicine, 2007. **2**(4): p. 639-49.
165. Schubert, S., et al., *Highly doped fullerene C60 thin films as transparent stand alone top electrode for organic solar cells.* Solar Energy Materials and Solar Cells, 2013. **118**(0): p. 165-170.
166. Afreen, S., et al., *Functionalized fullerene (C60) as a potential nanomediator in the fabrication of highly sensitive biosensors.* Biosensors and Bioelectronics, 2015. **63**(0): p. 354-364.
167. Omacrsawa, E., *Perspectives of Fullerene Nanotechnology*. 2012: Springer Netherlands.
168. Thompson, B.C. and J.M. Frechet, *Polymer-fullerene composite solar cells.* Angew Chem Int Ed Engl, 2008. **47**(1): p. 58-77.
169. Sun, S.S. and L.R. Dalton, *Introduction to Organic Electronic and Optoelectronic Materials and Devices*. 2008: Taylor & Francis.

170. Manhani, L.G.B., L.C. Pardini, and F. Levy Neto, *Assessement of tensile strength of graphites by the Iosipescu coupon test.* Materials Research, 2007. **10**: p. 233-239.
171. Brownson, D.A.C. and C.E. Banks, *Graphene electrochemistry: an overview of potential applications.* Analyst, 2010. **135**(11): p. 2768-2778.
172. Manoharan, M.P., et al., *Elastic Properties of 4–6 nm-thick Glassy Carbon Thin Films.* Nanoscale Research Letters, 2010. **5**(1): p. 14-19.
173. Tang, W., et al., *Glucose Biosensor Based on a Glassy Carbon Electrode Modified with Polythionine and Multiwalled Carbon Nanotubes.* PLoS ONE, 2014. **9**(5): p. e95030.
174. Wang, J., A.N. Kawde, and M. Musameh, *Carbon-nanotube-modified glassy carbon electrodes for amplified label-free electrochemical detection of DNA hybridization.* Analyst, 2003. **128**(7): p. 912-6.
175. Braun, A., *Development and Characterization of Glassy Carbon Electrodes for a Bipolar Electrochemical Double Layer Capacitor*. 2002: Diplom.de.
176. Zhu, Y., et al., *Graphene and graphene oxide: synthesis, properties, and applications.* Adv Mater, 2010. **22**(35): p. 3906-24.
177. Lee, C., et al., *Measurement of the elastic properties and intrinsic strength of monolayer graphene.* Science, 2008. **321**(5887): p. 385-8.
178. Park, H., et al., *Flexible Graphene Electrode-Based Organic Photovoltaics with Record-High Efficiency.* Nano Letters, 2014. **14**(9): p. 5148-5154.
179. Ahn, J.-H. and B.H. Hong, *Graphene for displays that bend.* Nat Nano, 2014. **9**(10): p. 737-738.
180. Mao, S., et al., *Highly sensitive protein sensor based on thermally-reduced graphene oxide field-effect transistor.* Nano Research, 2011. **4**(10): p. 921-930.
181. Huang, Y., et al., *Nanoelectronic biosensors based on CVD grown graphene.* Nanoscale, 2010. **2**(8): p. 1485-1488.
182. Dey, R.S. and C.R. Raj, *Development of an Amperometric Cholesterol Biosensor Based on Graphene−Pt Nanoparticle Hybrid Material.* The Journal of Physical Chemistry C, 2010. **114**(49): p. 21427-21433.
183. Kim, K.S., et al., *Highly Sensitive Reduced Graphene Oxide Impedance Sensor Harnessing π-Stacking Interaction Mediated Direct Deposition of Protein Probes.* ACS Applied Materials & Interfaces, 2013. **5**(9): p. 3591-3598.
184. Ambrosi, A., et al., *Electrochemistry of Graphene and Related Materials.* Chemical Reviews, 2014. **114**(14): p. 7150-7188.

185. Novoselov, K.S., et al., *Electric Field Effect in Atomically Thin Carbon Films.* Science, 2004. **306**(5696): p. 666-669.
186. Blake, P., et al., *Graphene-Based Liquid Crystal Device.* Nano Letters, 2008. **8**(6): p. 1704-1708.
187. Hernandez, Y., et al., *High-yield production of graphene by liquid-phase exfoliation of graphite.* Nat Nano, 2008. **3**(9): p. 563-568.
188. Wang, S., et al., *Adding ethanol can effectively enhance the graphene concentration in water-surfactant solutions.* RSC Advances, 2014. **4**(48): p. 25374-25378.
189. Brodie, B.C., *On the Atomic Weight of Graphite.* Philosophical Transactions of the Royal Society of London, 1859. **149**: p. 249-259.
190. Dreyer, D.R., et al., *The chemistry of graphene oxide.* Chemical Society Reviews, 2010. **39**(1): p. 228-240.
191. Staudenmaier, L., *Verfahren zur Darstellung der Graphitsäure.* Berichte der deutschen chemischen Gesellschaft, 1898. **31**(2): p. 1481-1487.
192. Hummers, W.S. and R.E. Offeman, *Preparation of Graphitic Oxide.* Journal of the American Chemical Society, 1958. **80**(6): p. 1339-1339.
193. Chen, D., H. Feng, and J. Li, *Graphene Oxide: Preparation, Functionalization, and Electrochemical Applications.* Chemical Reviews, 2012. **112**(11): p. 6027-6053.
194. McAllister, M.J., et al., *Single Sheet Functionalized Graphene by Oxidation and Thermal Expansion of Graphite.* Chemistry of Materials, 2007. **19**(18): p. 4396-4404.
195. Ambrosi, A. and M. Pumera, *Precise Tuning of Surface Composition and Electron-Transfer Properties of Graphene Oxide Films through Electroreduction.* Chemistry – A European Journal, 2013. **19**(15): p. 4748-4753.
196. Stankovich, S., et al., *Synthesis of graphene-based nanosheets via chemical reduction of exfoliated graphite oxide.* Carbon, 2007. **45**(7): p. 1558-1565.
197. Chen, L., et al., *From Nanographene and Graphene Nanoribbons to Graphene Sheets: Chemical Synthesis.* Angewandte Chemie International Edition, 2012. **51**(31): p. 7640-7654.
198. Jiao, L., et al., *Narrow graphene nanoribbons from carbon nanotubes.* Nature, 2009. **458**(7240): p. 877-880.
199. Wei, D., et al., *Controllable unzipping for intramolecular junctions of graphene nanoribbons and single-walled carbon nanotubes.* Nat Commun, 2013. **4**: p. 1374.

200. Hu, Y. and X. Sun, *Chemically Functionalized Graphene and Their Applications in Electrochemical Energy Conversion and Storage*, *Advances in Graphene Science*, M. Aliofkhazraei, Editor 2013, InTech.
201. Bonaccorso, F., et al., *Production and processing of graphene and 2d crystals.* Materials Today, 2012. **15**(12): p. 564-589.
202. Hartley, C.S., *Graphene synthesis: Nanoribbons from the bottom-up.* Nat Chem, 2014. **6**(2): p. 91-92.
203. Ruan, M., et al., *Epitaxial graphene on silicon carbide: Introduction to structured graphene.* MRS Bulletin, 2012. **37**(12): p. 1138-1147.
204. Zhang, Y., L. Zhang, and C. Zhou, *Review of Chemical Vapor Deposition of Graphene and Related Applications.* Accounts of Chemical Research, 2013. **46**(10): p. 2329-2339.
205. Aniket, K., et al., *Detection of DNA and poly-l-lysine using CVD graphene-channel FET biosensors.* Nanotechnology, 2015. **26**(12): p. 125502.
206. Brownson, D.A.C. and C.E. Banks, *CVD graphene electrochemistry: the role of graphitic islands.* Physical Chemistry Chemical Physics, 2011. **13**(35): p. 15825-15828.
207. Hai Binh, N., et al., *Graphene patterned polyaniline-based biosensor for glucose detection.* Advances in Natural Sciences: Nanoscience and Nanotechnology, 2012. **3**(2): p. 025011.
208. Gutés, A., C. Carraro, and R. Maboudian, *Single-layer CVD-grown graphene decorated with metal nanoparticles as a promising biosensing platform.* Biosensors and Bioelectronics, 2012. **33**(1): p. 56-59.
209. Rengaraj, A., et al., *Electrodeposition of flower-like nickel oxide on CVD-grown graphene to develop an electrochemical non-enzymatic biosensor.* Journal of Materials Chemistry B, 2015.
210. Pawley, J., *Handbook of Biological Confocal Microscopy*. 2010: Springer.
211. Price, R.L. and W.G. Jerome, *Basic Confocal Microscopy*. 2011: Springer.
212. Muller, M., *Introduction to Confocal Fluorescence Microscopy*. 2006: Society of Photo Optical.
213. Gu, M., *Principles of Three Dimensional Imaging in Confocal Microscopes*. 1996: World Scientific.
214. Haugstad, G., *Atomic Force Microscopy: Understanding Basic Modes and Advanced Applications*. 2012: Wiley.

215. Wilson, R.A., and Bullen H. A. *Introduction to Scanning Probe Microscopy (SPM)Basic Theory Atomic Force Microscopy (AFM)*. 2006 20-09-2012].
216. Schwierz, F., *Graphene transistors.* Nat Nano, 2010. **5**(7): p. 487-496.
217. Avouris, P., *Graphene: Electronic and Photonic Properties and Devices.* Nano Letters, 2010. **10**(11): p. 4285-4294.
218. Compton, R.G. and C.E. Banks, *Understanding Voltammetry*. 2011: Imperial College Press.
219. Zoski, C.G., *Handbook of Electrochemistry*. 2007: Elsevier.
220. Trasatti, S., *The absolute electrode potential: an explanatory note (Recommendations 1986).* Journal of Electroanalytical Chemistry and Interfacial Electrochemistry, 1986. **209**(2): p. 417-428.
221. Kumar, M. and A.J. Poulose, *Detergents with stabilized enzyme systems*, 2008, WO Patent 2008005571 A2.
222. Thomas, F.G. and G. Henze, *Introduction to Voltammetric Analysis: Theory and Practice*. 2000: CSIRO Pub.
223. McNaught, A.D., et al., *Compendium of Chemical Terminology: IUPAC Recommendations*. 1997: Blackwell Science.
224. Jalit, Y., et al., *Glassy Carbon Electrodes Modified with Multiwall Carbon Nanotubes Dispersed in Polylysine.* Electroanalysis, 2008. **20**(15): p. 1623-1631.
225. Stefan, R.I., *Electrochemical Sensors in Bioanalysis*. 2001: Taylor & Francis.
226. Kissinger, P.T. and W.R. Heineman, *Cyclic voltammetry.* Journal of Chemical Education, 1983. **60**(9): p. 702.
227. Brownson, D.A.C., *Handbook of Graphene Electrochemistry*. 2014: Springer London, Limited.

Chapter 2: Glucose oxidase functionalization on chemical vapour deposited (CVD) graphene

2.1 Introduction

When designing a biosensor two aspects are to be considered: (1) the biological element and its' functionalization on the transducer and (2) the transducer and the detection principle. The first point will be detailed in this chapter while the second will be investigated in chapter 3. When functionalising an electrode with proteins (i.e., the GOD enzyme in this case) several techniques can be identified: (1) electromagnetic coating, (2) covalent functionalization, (3) non-covalent coating and (4) entrapment in a polymeric matrix or a hydrogel, (see figure 2.1). (1) Covalent coating involves chemical modification of the transducer or reaction via functional groups already present thereon (as is the case for graphene oxide, for example). This results in strong and organised coupling but can affect the properties of the transducer and/or the enzyme [1]. Graphene, must remain chemically unmodified to retain its' conductive properties [2]; equally, linking an enzyme covalently may alter its activity/structure and, self-evidently, the linkage must not involve the catalytic site [3]. A common way to covalently attach enzymes on an electronic support is to use self-assembly monolayers (SAM) involving long chain molecules that associate with the electrode via chemisorption or physisorption [4]. The approach provides strong and organised functionalization but can sometimes change the physical properties of the transducer and reduce the efficiency of electron transfer due to reduced enzyme activity [5]. Covalent bonding has also been used with graphene oxide [6], but this strategy has not been investigated here due to the frequently impaired physical properties of the nanomaterial as well as the difficulty of scaling-up the production of such sensors. (2) The approach based on electrostatic interactions, for example between a positively charged polymer and the negatively charged GOD [7], is relatively easy to implement and does not require chemical

modification of the transducer. The binding is, however, weak and will be subject to any changes in pH or ionic strength that are likely in an electrochemical-based biomedical device. (3) With the introduction of carbon nanomaterials such as fullerenes, carbon nanotubes and graphene, a new type of functionalization has emerged that provides a uniform coating and is minimally disruptive to the transducer and to the enzyme: namely, non-covalent binding via π-π interactions [8, 9]. The quality of the coating will however rely strongly on the ability to obtain a strong non covalent adhesion (via 1-pyrene butanoic succinimidyl ester: 1-PBASE here). (4) Finally, polymeric or gel entrapment, enables the largest quantity of proteins to be coated without disrupting the properties of the electrode [10]. Polymeric entrapment has been described using polypyrrole [11], chitosan [12] or nafion [13] and results in a thin (sometimes conductive) layer in which a high enzymatic loading can be achieved. The use of a hydrogel is further explored in the next chapter. This approach also eliminates any electrode coating issues and problems related to enzyme stability on long-term storage (i.e., it allows the enzyme containing gel to be readily removed and replaced while, leaving the transducer untouched). This type of functionalization was used in the GlucoWatch ® Biographer device [14]. The presented biosensor development focuses on the last two functionalizations for the following reasons:

(i) Non-covalent coating is minimally disruptive, allowing graphene to retain its electrical properties [15]. A uniform layer of enzyme can be formed on the transducer (see figure 2.12) [16]. And the enzyme can be patterned on the graphene sheet, by means of micro-contact printing, for example [8], (see figure 2.11).

(ii) Hydrogel entrapment is also minimally disruptive and will be preferred in the second part because it doesn't require any treatment of the graphene, the graphene electrodes can be stored at room temperature, and the enzymatic loading (and hence catalytic signal) increased (see section 2.3.2).

Laser confocal scanning microscopy and electrochemical measurements (cyclic voltammetry and chronoamperometry) will be used to characterise the entrapments. (1) The first microscopic technique helped to visualise the non-covalent coating (on the graphene) of a GOD-linker complex on which Fluorescein isothiocyanate had been attached. The coverage of the entire graphene surface was visualised as well as the patterned deposition of the enzyme via microcontact printing. Both these images allowed to assess the quality of the non-covalent enzymatic coating. The GOD activity was further investigated by coupling an

electrochemical experiment with LSCM visualization (figure 2.8). (2) Attention was then focused on developing a first generation biosensor relying on O_2 during the enzymatic catalysis reaction of glucose oxidase in the presence of the substrate β-D glucose [17]. H_2O_2 is formed from the reduction of O_2 in the FAD active cofactor centre of the enzyme and then oxidised against the electrode. This oxygen-based detection was first introduced in 1962 by Clark and Lyons [18] and remains the basic principle for many bio-electrochemical sensors [19]. Enzyme immobilization in biosensing applications should ensure efficient physical attachment of the enzyme without perturbation of structure and activity. It must allow for good electron transfer, and easy diffusional access for the substrate [20]. The enzymatic catalytic activity is influenced by several factors. (1) The electron transfer between the active site of the enzyme and the electrode. This is highly dependent on the distance between them: the closer the enzyme's active site to the transducer, and the more conductive the supporting matrix, the better the delivery of the signal. (2) The retention of the enzyme and diffusional access for the substrate. The sensor must be designed so that the enzyme is efficiently retained on the transducer while allowing the substrate (glucose) and product (H_2O_2) to diffuse efficiently. (3) The signal will be proportional to the quantity of active enzymes on the transducer. (4) The enzyme receptacle or functionalized transducer must be kept under conditions that are not stringent for the protein (appropriate pH, temperature).

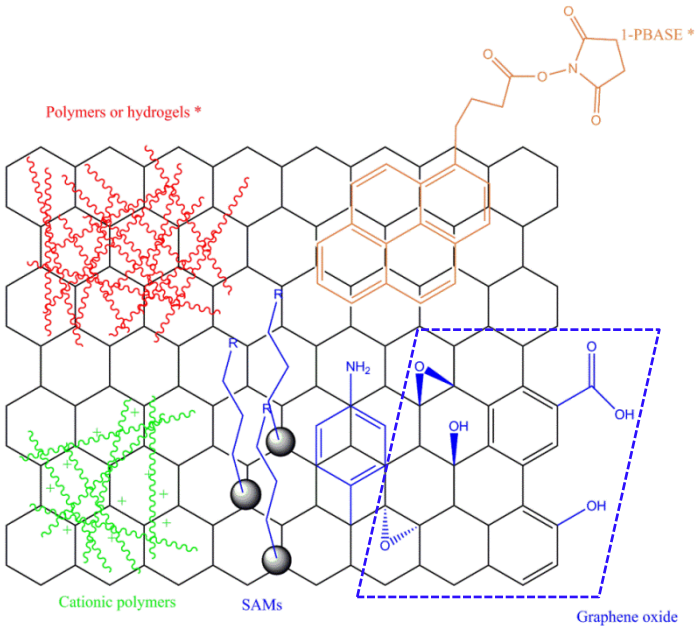

Figure 2.1. Graphene functionalization. The four principal methods used to functionalize graphene with biomolecules are presented: polymeric or hydrogel entrapment (red), cationic coating (green), covalent functionalization and chemical modification of the graphene lattice (or use of graphene oxide) (blue), and non-covalent functionalization via π-π interaction (orange). Asterisks (*) signify techniques pursued in this work.

2.2 Materials and experimental methods

2.2.1 Materials

Two glucose oxidase were used in this chapter: (1) glucose oxidase type VII, (EC 1.1.3.4), lyophilized powder, ≥100,000 units/g solid (without added oxygen) for the microscopic experiments and (2) glucose oxidase type X-S, (EC 1.1.3.4), 100,000-250,000 units/g solid (without added oxygen) for the electrochemical experiments. The two enzymes are structurally the same (the difference in numbers (VII and X-S) was introduced by the manufacturer as an internal classification). D-glucose, Na_2HPO_4, NaH_2PO_4, $NaHCO_3$, Na_2CO_3, NH_4Cl, $FeCl_3$, 1-pyrene butanoic succinimidyl ester (1-PBASE), *N*,*N*-dimethylformamide (DMF), dimethylsulfoxide (DMSO), silicon master 200® fluid, fluorescein isothyocyanate (FITC) and rhodamine isothyocyanate were purchased from Sigma-Aldrich (Dorset, UK). Agarose was purchased from Fisher Scientific (Loughborough, UK). Phosphate buffer 0.1 M pH 7.4 (our standard electrochemical buffer) was prepared from Na_2HPO_4 and NaH_2PO_4 salts. MiliQ-water was used for all solutions. CVD graphene on copper and deposited on a silicon dioxide wafer, or on glass with a wet etching technique, was provided by the Univeristy of Bath, UK. Silicon dioxide (300 nm oxide) was acquired from IDB technology (Whitley, UK), 495 PMMA A3 (poly(methyl metacrylate)) from Microchem (Rugby, UK), Silcoset 151 silicone rubber from Farnell (Leeds, UK), Amicon ultracel 10K centrifugal tubes with regenerated cellulose from Merck Millipore (Darmstadt, Germany), PD-10 Desalting Columns from GE healthcare (Little Chalfont, UK), conductive silver paint from Agar Scientific (Stansted, UK), S-18-13 photoresist from AZ Electronic Materials, Merck (Darmstadt, Germany) and curing PDMS (polydimethylsiloxane) curing agent (Elastomer Sylgard 184) from Dow Corning (Midland, MI, USA). The confocal laser microscope was a LSM 510 from Zeiss (Cambridge, UK) and the AFM, an Asylum Research (High Wycombe, UK) MFP-3D microscope.

2.2.2 Experimental methods

2.2.2.1 Graphene wet etching and transfer

A wet etching technique [21] was used in order to transfer CVD graphene (which had already been deposited on copper) onto Si/SiO_2 (300 nm thickness). The procedure involved the deposition of a 495 PMMA A3 layer on the top of the graphene by spin coating at 301 *g* for 30 seconds: a drop of PMMA was used between the back of the graphene sample and a glass coverslip and was cured at 115 ˚C for 25 seconds to fix the sample during spin coating. The sample was then cured at 120 ˚C for 2 minutes before being placed in a bath of 1 M $FeCl_3$ and left to etch overnight. The sample was further washed 3 times with milliQ water for 30 minutes. It was subsequently deposited on Si/SiO_2 and left to air-dry for 10 to 15 minutes before a 10 µL drop of PMMA was added to relax the pre-existing polymer layer for 20 minutes. Finally, the sample was washed and incubated in acetone for 1 hour.

2.2.2.2 Non-covalent graphene functionalization by π-π stacking

Graphene was then treated with 5 mM 1-PBASE in DMF. This molecule binds to graphene via π-π interactions, and to the amine groups on glucose oxidase (GOD) via a nucleophilic reaction. The resulting product was then washed with DMF and milliQ water before being incubated overnight in a 6.25 mg/mL solution of GOD in 0.1 M sodium carbonate/sodium bicarbonate buffer (pH 9.0) at 4 °C. The reaction between the succinimidyl ester group of 1-PBASE and the NH_2 of the enzyme is displayed in figure 2.2. Finally, it was rinsed in phosphate buffer (pH 7.4) and milliQ water.

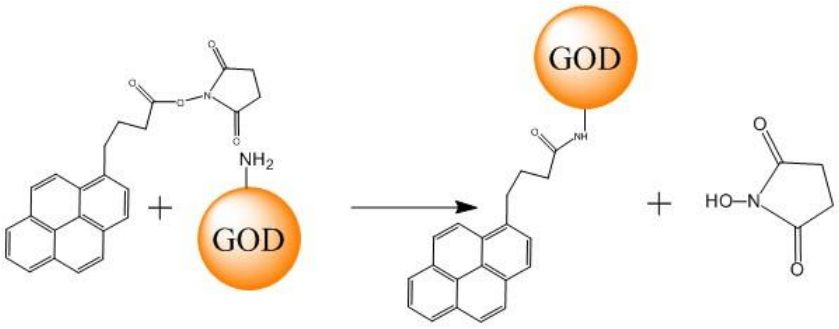

Figure 2.2. Reaction between the succinimidyl ester group of the linker and the NH_2 of the enzyme.

2.2.2.3 Glucose oxidase fluorescent FITC labelling

Glucose oxidase was covalently conjugated with FITC following a protocol described in [22]: A solution of 4 mg/mL of GOD was prepared in 1 mL of 0.1 M sodium bicarbonate pH 9. In parallel, a 1 mg/mL solution of FITC was prepared in anhydrous DMSO. 200 µL of the FITC solution was then very gently added to the GOD solution in 5 µL aliquots while stirring. The mixture was subsequently incubated in the dark, overnight at 4 ˚C, under constant stirring. NH_4Cl was then added to a final concentration of 50 mM, incubated for 2 hours at 4 ˚C, and supplemented with 5% glycerol. The unbound FITC was further separated from the labelled protein with a PD-10 sephadex desalting column. The column was equilibrated with 4 washes of 5 mL bicarbonate buffer. 1 mL of the fluorescent mixture was then introduced onto the column with another 2.5 mL of buffer. Finally, 3.5 mL of buffer were added to elute the protein. The operation was repeated to collect the maximum amount of labelled protein. The obtained concentration of FITC/GOD was estimated as 0.57 mg/mL. It was concentrated down using membrane filtration/centrifugation: The eluate was introduced in a falcon tube with a 10,000 Da exclusion membrane and centrifuged at 4,900 g for 10-15 minutes. The total concentration of enzyme was therefore approximated as 6.25 mg/mL (considering a 100% recovery of proteins).

2.2.2.4 Micro-contact printing

Micro-contact printing of glucose oxidase on CVD graphene was used to check the integrity of the coating.

2.2.2.4.1 Production of a PDMS stamp

A poly(dimethylsiloxane) (PDMS) stamp was prepared from a predesigned pattern by photolithography. A photoresist (S-18-13) was spin coated onto a Si/SiO_2 wafer at 8 *g* for 5 seconds and at 134 *g* for 45 seconds. Subsequently, a negative "line shaped" mask was used to obtain a positive pattern on the resist which was exposed for 6 seconds at 45 mJ under UV light. A Microposit ™ 351 developer (Dow electronic material, Berlin, Germany) was prepared (10 into 35 mL into water) and the sample was gently stirred in the solution for 30 seconds until a pattern appeared. It was then placed into deionized water to stop the developing reaction. The PDMS polymer stamp was then obtained by adding a curing agent, Elastomer Sylgard 184 (Dow Corning, Midland, MI, USA) to a silicone master at a ratio of 1:7 [23]. The polymeric mix was poured into a mould in contact with the photolithographic

pattern, degassed under vacuum for 30 minutes, and incubated at 90 °C overnight. It was then gently peeled off, ready to use.

2.2.2.4.2 Micro-contact printing

CVD graphene sheets were transferred onto Si/SiO_2 wafers, incubated with 5 mM of 1-PBASE in DMF for 2 hours at room temperature and thoroughly washed with DMF and milliQ water. In the meantime, PDMS stamps were incubated with FITC-labelled GOD in bicarbonate buffer at 4 °C for 1 h - the enzyme was retained on the stamp via hydrophobic interactions. The stamp was then pressed against the graphene sheet for a short period of time (0.5 - 1 minute) and washed thoroughly with PBS (figure 2.3) [8].

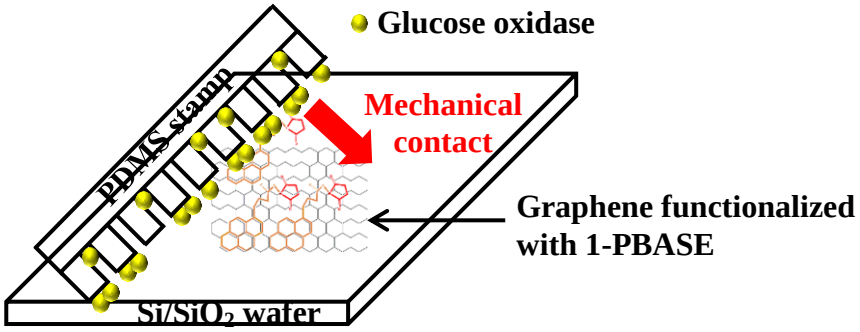

Figure 2.3. Micro-contact printing. A PDMS stamp was inked with a protein solution (GOD) and brought to mechanical contact with graphene functionalised with 1-PBASE for non-covalent coating.

2.2.2.5 Visualisation of the GOD activity

GOD was labelled with rhodamine isothiocyanate in the same way as the fluorescein functionalization described in section 2.2.2.3, the final enzyme concentration was therefore estimated to be similar to the FITC-GOD (i.e. 6.25 mg/ml). Gold and titanium were evaporated onto part of a graphene sample to generate a working electrode, which was insulated by depositing silicone rubber onto the gold. The rhodamine labelled GOD was then micro-contact printed on CVD graphene following the protocol presented in section 2.2.2.4.2. A Pt counter electrode and Ag pseudo-reference electrode were then inserted in the small drop of buffer containing 20 µM of fluorescein. The setup was mounted in the fluorescence microscope and the electrodes connected to a potentiostat (Autolab, Metrohom, Utrecht, The Netherland). Cyclic voltammograms were acquired, at 20 mV/sec, between -0.4 and 0.8 V against the Ag reference electrode before and after each addition of glucose. The imaging was acquired after each cyclic voltammetric operation (corresponding to the addition of glucose, see figure 2.8).

2.2.2.6 LSCM parameters

Two fluorophores were used, rhodamine and fluorescein with excitation/emission wavelengths at 543 nm/580 nm and 490 nm/525 nm respectively, with two different lasers: argon (which excites fluorescein at 488 nm (green fluorescence)), and HeNe (exciting rhodamine at 543 nm (red fluorescence)), in conjunction with the specific filters BP 505-530 nm for fluorescein emission and LP 560 nm for rhodamine. The objective lens used for imaging the protein coating had a magnification of 20×.

2.2.2.7 Electrochemistry: experimental methods

2.2.2.7.1 Electrode design

The electronic connection between the graphene flake and the potentiostat was achieved via thermal evaporation of successively titanium and gold (10 and 60 nm thickness, respectively) or by application of silver paint. Both connections were completed with gold wire making a gold-gold or silver-gold contact. The graphene squares were insulated from the gold or silver contacts via the deposition of ACC silicone rubber (see [4α] footnote). The target graphene square dimensions were set as 9 mm^2; those achieved were 9 mm^2 ± 2.25 mm^2 (the error originating from the metallic contact with the graphene flake). The devices were left dry at room temperature in petri dishes before use.

2.2.2.7.2 Gel casting

The enzymatic coating entrapped GOD was built in a 0.5% agarose gel matrix. 250 µL of a clear 1% w/v solution of agarose in 0.1 M phosphate buffer pH 7.4 was created by warming above 80 ˚C and then cooling down to 28 ˚C (a temperature low enough to maintain the enzyme's catalytic and structural properties [24] while enabling efficient entrapment in the gel, i.e., below the gelling temperature of ~ 36 ˚C). 250 µL of an 8 mg/mL solution of GOD in 0.1 M phosphate buffer was then added to the gel and left for 1 hour at 4˚C; the resulting mixture therefore comprised 500 µL of 0.5% agarose gel with 4 mg/mL enzyme. A section was excised with a glass capillary of 1.5 mm radius which corresponded to 24 µL +/- 2µL in volume, and placed on top of the working graphene electrode for analysis. This gel entrapment technique will be designated as *entrapment 1*, as opposed to other improved entrapment presented further in the thesis (chapter 3 and 4: *entrapment 2 and 3*).

[4.α] The silicone rubber, when dry, provides good insulation while releasing a small quantity of acetic acid. It is believed that the acetic acid is removed in the washing step and does not therefore interfere with the sensing. No interference has been identified from acetic acid when studying the catalytic activity of the electrode as shown in chapter 4, figure 4.15.

2.2.2.7.3 Electrochemical set-up

A potentiostat (Metrohom, autolab, Utrecht, The Netherland) was used for all electrochemical analyses. Fine manipulation of the apparatus and better insulation from electromagnetic interference was provided by a circuit board built in house (Jules Hammond, Department of Electronic & Electrical Engineering, University of Bath, UK). Two platinum wires of 0.5 mm diameter, 99.95% pure (Advent, Oxford, UK) were used as a counter electrode and as a pseudo-reference electrode. The pseudo platinum reference electrode was used for practical reasons in the set-up; to allow easier measurements in the 24 µL volume of gel.

2.2.2.7.4 Substrate glucose solution

For glucose sensing experiments, stock glucose solutions were prepared in 0.1 M phosphate buffer pH 7.4 and left to mutarotate overnight at room temperature. GOD only catalyses the reaction with the β cyclic anomer of glucose. A glucose solution comprises about 64% of the β form at equilibrium [25]. If not used immediately, the glucose stock solutions and dilutions thereof were kept at 4˚C and, in any case, were used within two weeks of their preparation. Glucose stability was checked using the colorimetric enzymatic assay described in section 2.3.2.1.

2.2.3 Data analysis: glucose calibration curves

2.2.3.1 Cyclic voltammetry

For cyclic voltammograms, calibration curves were built for the oxidative signal in order to assess the proportionality of the current obtained with additions of glucose: catalytic current = f(glucose concentration). The catalytic current was taken at 0.7 V against the reference electrodes and subtracted to the control oxidative signal (obtained at 0.7 V with no glucose). The calibration curves were fitted with a linear regression and R^2 calculated with Microsoft Excel following the statistic formula for the data points [26]:

$$R^2 = \frac{SSR}{SST} \qquad (2.1)$$

$$SST = SSE + SSR$$

Where SSR is the regression sum of square; the variation explained by the linear relationship between x and y:

$$SSR = \sum (Predicted\ Y\ value - Mean\ Y\ value)^2 \qquad (2.2)$$

And SSE is the error sum of squares; the variation associated with other factors besides the linear relationship:

$$SSE = \sum (observed\ Y\ value - predicted\ Y\ value)^2 \qquad (2.3)$$

From this point forwards all the calibrations data will be fitted with linear regression and R^2 calculated with Microsoft Excel in the same way.

2.2.3.2 Chronoamperometry

The catalytic current was approximated as the background-corrected current, averaged (over 10 seconds) determined for each chronoamperometric step (plateau, i.e. equation 2.4). This allowed the calibration curves to be derived (catalytic current = f(concentration)) and to be fitted with linear regression (and calculated R^2) as previously explained.

$$Catalytic\ current = I[Chronoamp.step_{(\ averaged\ 10\ sec)}] - I[Background_{(\ averaged\ 10\ sec)}] \qquad (2.4)$$

2.2.4 Colorimetric enzymatic assay for control of the enzyme activity and glucose stability

Glucose oxidase activity was regularly assessed using a standard colorimetric assay involving: horseradish peroxidase (POD). This test was also used to check glucose stability over time. The reactions involved are depicted in figure 2.4.

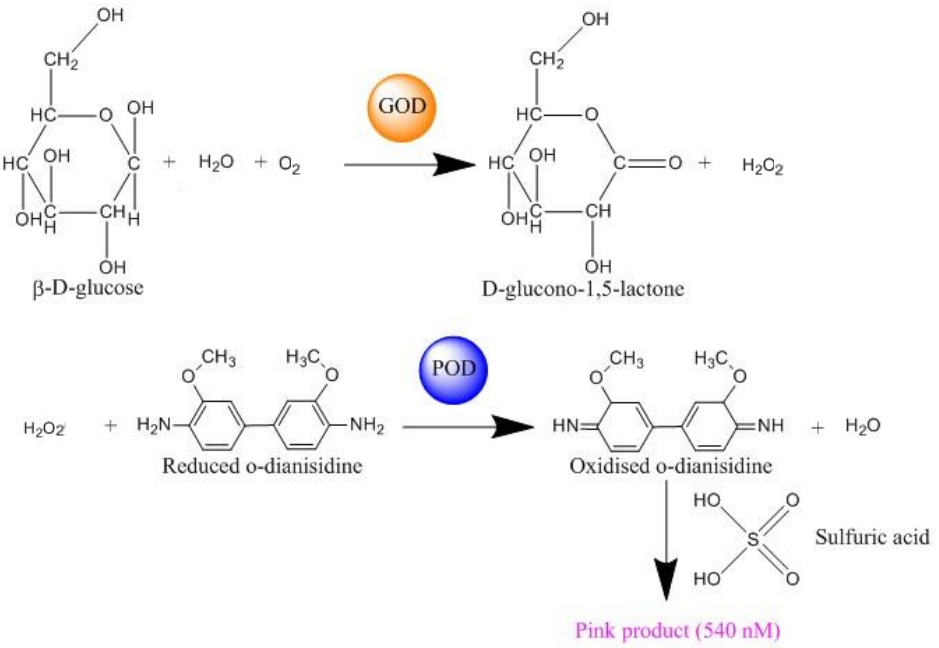

Figure 2.4. Colorimetric enzymatic reaction for the quantitative analysis of glucose and/or assessment of the glucose oxidase enzyme activity. Glucose oxidase (GOD) reacts with glucose in the presence of oxygen producing H_2O_2 that then reacts with horseradish peroxidase (POD) and reduced o-dianisidine forming oxidised o-dianisidine. This, in turn produces a more stable oxidised o-dianisidine that displays a pink colour in the presence of sulphuric acid which can be monitored spectrophotometrically giving a signal proportional to the concentration of glucose in solution.

500 units of GOD and 100 units of POD were dissolved in milliQ water to a volume of 39.2 mL. The o-dianisidine reagent was prepared at 5 mg/mL in milliQ water and added to the enzymatic solution forming the reagent mix. A series of glucose solutions were prepared from a standard of 1 mg/mL in 0.1% benzoic acid (benzoic acid is used here as a conservator for the glucose solution against degradation by microorganisms [27]). Their concentration were: 20, 40, 60 and 80 µg/mL plus a blank control. The reaction was started by adding 2 mL of the reagent mix to the glucose standards, the "unknown" sample and the blank. The reaction was allowed to proceed for 30 min at 37˚C and then stopped by adding 2 mL of 12 N H_2SO_4. The absorbance was read at 540 nm. For enzyme activity and glucose stability tests, the glucose concentration was known and set at 0.054 mg/mL.

2.3 Results

2.3.1 Microscopy results

2.3.1.1 LSCM imaging of GOD/micro-contact printed CVD graphene on Si/SiO_2

A CVD graphene sample deposited on Si/SiO_2 was treated with 1-PBASE and stamped with fluorescently (FITC) labelled GOD. The pattern of the stamp comprised five lines (see figure 2.5) showing good adhesion of the FITC labelled GOD to the 1-PBASE.

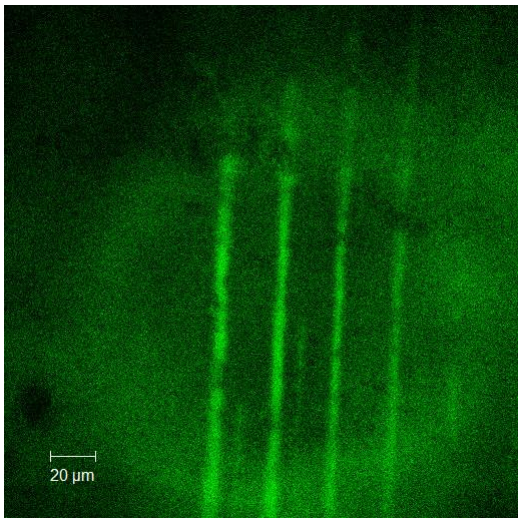

Figure 2.5. Micro-contact printing of FITC functionalized GOD on CVD graphene. The protein was successfully retained on the nanomaterial and the efficiency of the microcontact printing technique was demonstrated. The background auto-fluorescence acted as a control.

2.3.1.2 LSCM imaging of FITC labelled GOD-coverage of the entire CVD graphene area

FITC labelled GOD functionalization of a CVD graphene sample deposited on glass was imaged and displayed uniform fluorescence of the FITC labelled GOD (see figure 2.6). This shows that the FITC has been evenly distributed on the GOD enzyme.

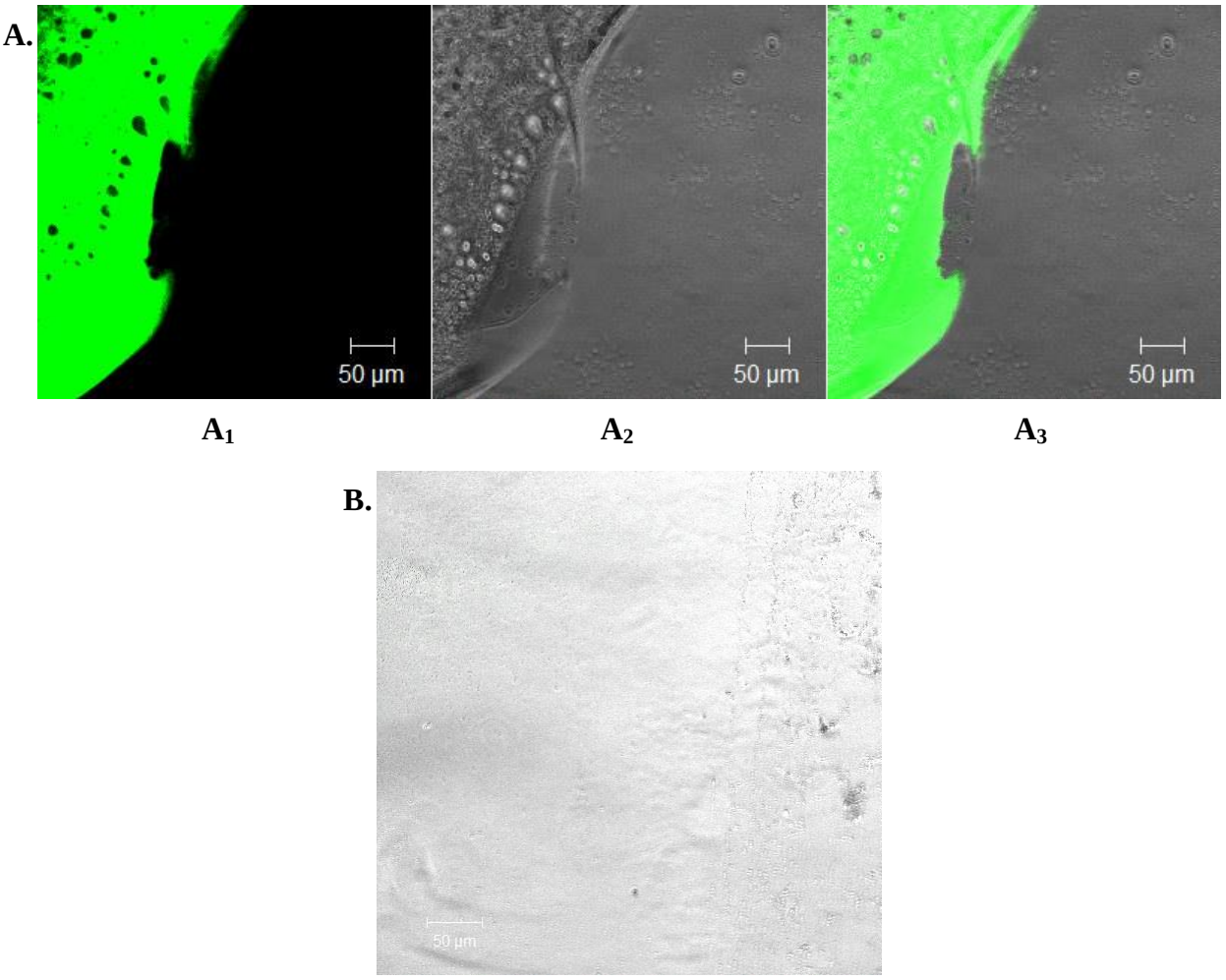

Figure 2.6. Functionalization of CVD graphene with FITC labelled GOD. A: LSCM image of the protein coating (A_1: fluorescent signal; A_2: white light image; and A_3: combination of A_1+A_2). B: Control P-BASE treated CVD graphene (i.e., without GOD).

2.3.1.3 LSCM combined with microcontact printing as a tool for glucose sensing

Fluorescein is fluorescently inactivated in acidic conditions [28]. When in the presence of glucose and under specific electrochemical conditions (0.7 V against a Ag pseudo-reference electrode), GOD reacts as shown in figure 2.7 leading to the production of 3 protons

(displayed in red in figure 2.7), acidifying the nearby medium, and causing fluorescein fluorescence to decrease.

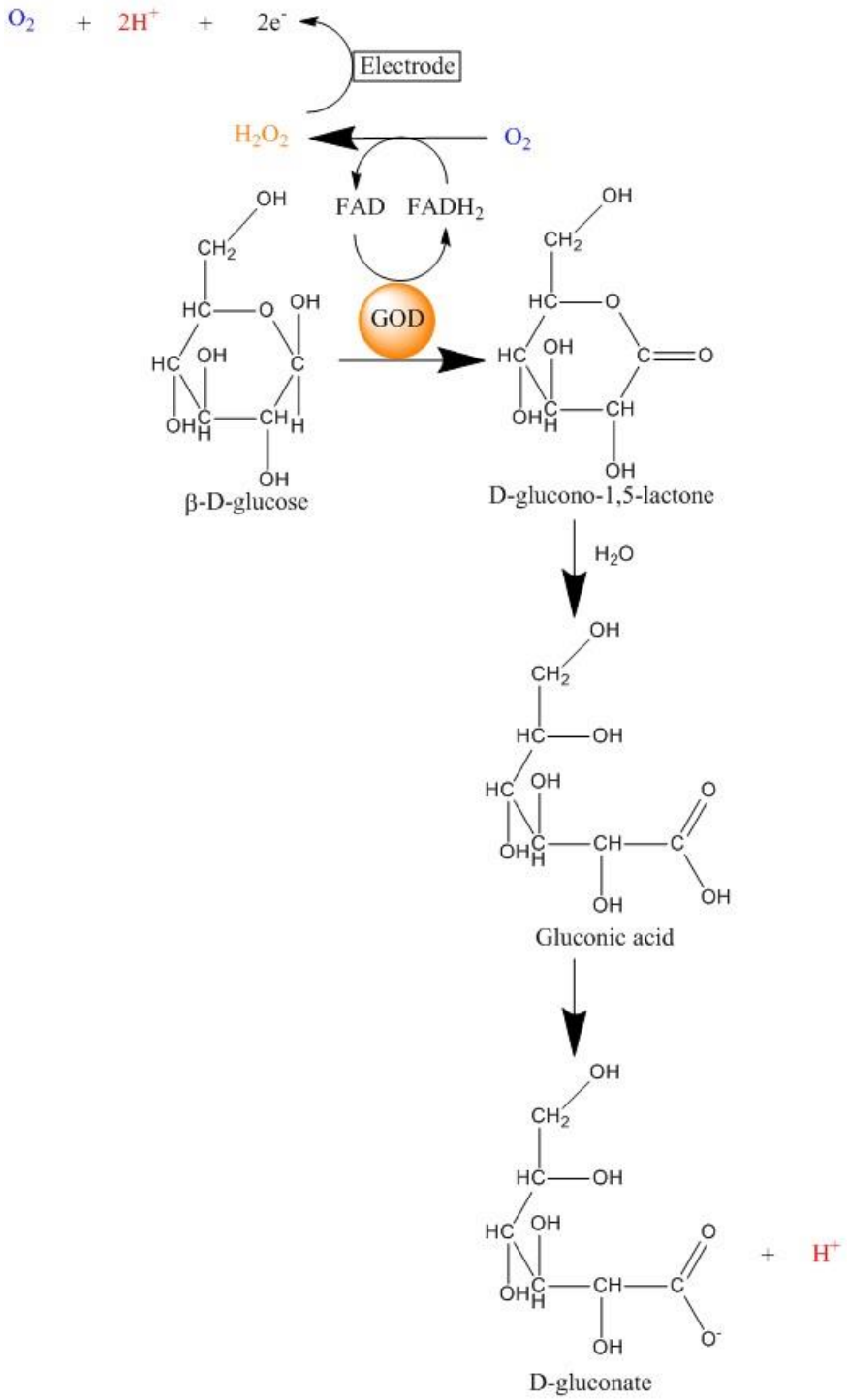

Figure 2.7. Glucose oxidase reaction mechanism: catalytic reaction in the presence of β-D-glucose and under specific electrochemical conditions where H_2O_2 is oxidised at the working electrode (i.e., commonly 0.7 V against SCE). The protons produced that acidify the medium are depicted in red.

To distinguish between the GOD enzyme and the pH conditions, GOD was coated with rhodamine, another fluorescent molecule which is insensitive to pH conditions, and a 20 µL phosphate buffer drop containing 20 µM of fluorescein put on top of the sample. Cyclic voltammetry was performed during fluorescent imaging to produce protons and change the pH conditions. Figure 2.8 shows rhodamine coated GOD micro-contact printed on CVD graphene (in red) and surrounded in fluorescein solution (in green). These results show that the rhodamine labelled GOD can be easily distinguished from the surrounding fluorescein solution. At high glucose concentrations, the fluorescence of the fluorescein was depleted close to where the GOD enzyme is immobilised indicating production of protons and therefore low pH conditions.

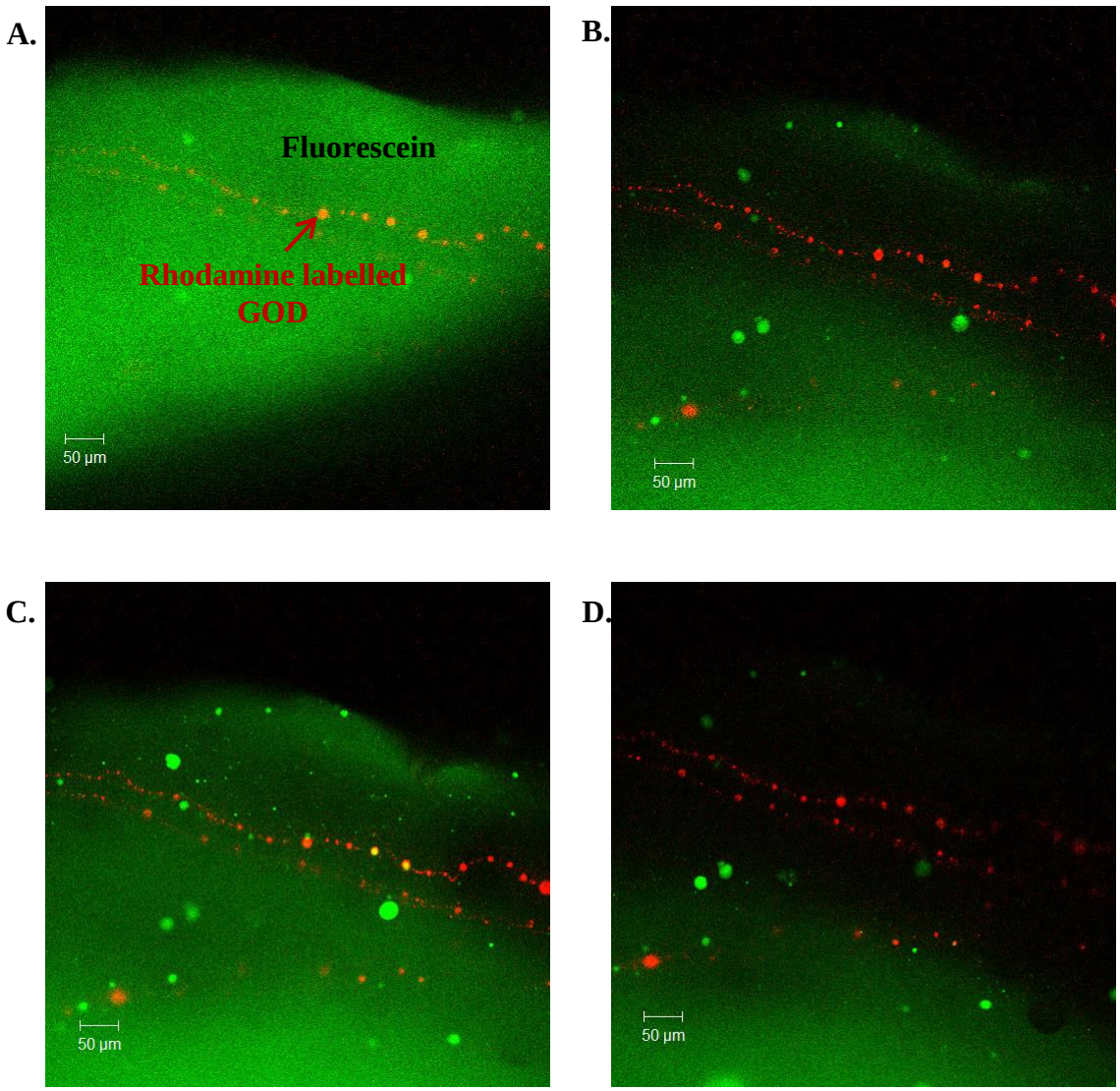

Figure 2.8. Real time LSCM glucose sensing via GOD microcontact printing and cyclic voltammetry. Glucose concentrations are: A: 0 mM; B: 5 mM; C: 10 mM; and D: excess (>2 M).

2.3.2 Electrochemistry results

2.3.2.1 Assessment of glucose stability in phosphate buffer (stored at 4 °C)

Glucose solutions were stored for two weeks in phosphate buffer at 4 °C, while operating electrochemical experiments for practical reasons. It was therefore of importance to monitor the stability of such solutions over time. This was done by measuring a set concentration of glucose (0.054 mg/mL) stored at 4 °C after 2, 10 and 41 days with the colorimetric assay presented in section 2.2.4 and measuring the solution absorbance at a wavelength of 540 nm. Figure 2.9 presents calibration plots of glucose obtained via the colorimetric test with known amounts of fresh solutions of glucose (black curves representing absorbance=f(concentration)). The absorbance of the studied stored sample was then obtained and reported on the calibration curves in order to obtain the concentration for each of the analysed times. The results indicate that the sample concentration of glucose increases but only by a very small amount over a period of 41 days showing the glucose to be relatively stable.

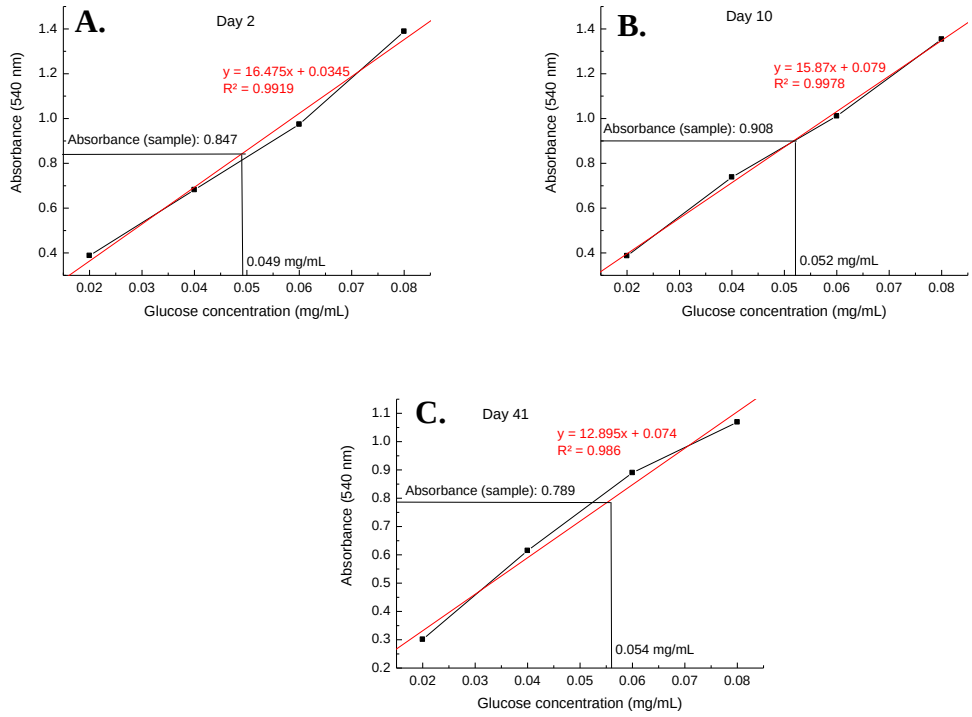

Figure 2.9. Glucose stability in phosphate buffer pH 7.4 stored at 4 °C, over 41 days. Glucose concentration calibration curves vs absorbance (black curves) obtained through a horseradish peroxidase/glucose oxidase colorimetric assay. The original sample concentration was fixed at 0.054 mg/mL and reported on the gradients. A: day 2, B: day 10 and C: day 41

2.3.2.2 Response to glucose of CVD graphene electrode coated with GOD through an agarose gel

The study was performed on samples (22 µL +/- 2 µL) of 0.5% agarose gel, to which 10 µL of buffer were added at the start of the experiment (the initial gel volume was therefore considered to be 32 µL +/- 2 µL and the glucose concentrations calculated accordingly). The gel was then placed on the GOD coated CVD graphene electrode. A cyclic voltammogram was then acquired before serial additions of glucose were made, after each of which another cyclic voltammogram was recorded (see figure 2.10). A more quantitative test was also undertaken by fixing the potential at 0.7 V against a Pt pseudo-reference electrode and measuring the variation of current with each glucose addition as a function of time, in a chronoamperometric experiment (see figure 2.11).

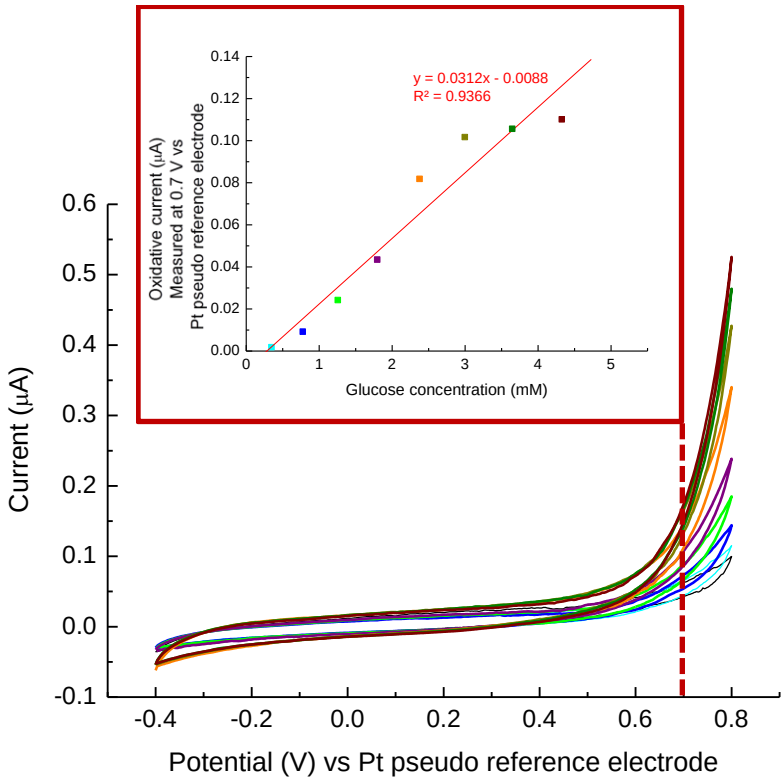

Figure 2.10. Response of a GOD coated CVD graphene electrode (via 1-PBASE) to serial glucose additions in agarose gel. Cyclic voltammograms demonstrate a clear increase in current with additions of glucose concentration at 0.7 V vs RE. The scan rate was 20 mV/sec, and the results were acquired after 3 scans. The insert is a calibration graph displaying the oxidative H_2O_2 current (at 0.7 V vs the platinum pseudo reference electrode) produced as a result of the enzymatic reaction, function of glucose concentration added in the gel.

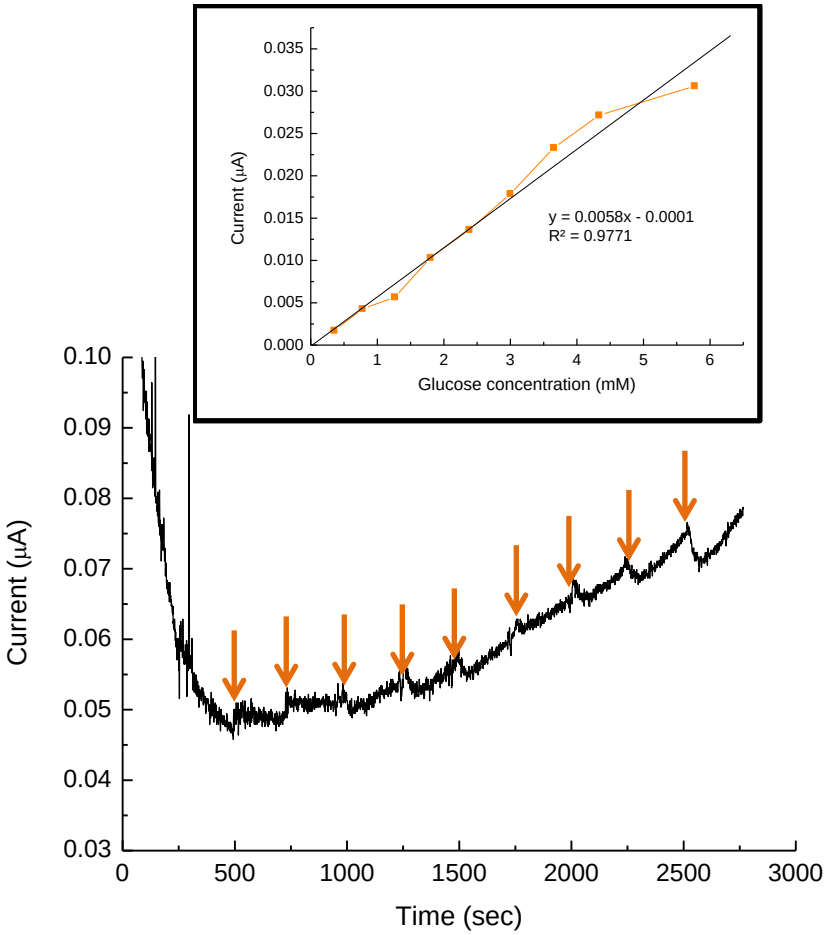

Figure 2.11. Chronoamperometric results from a GOD coated CVD graphene electrode (via 1-PBASE) to serial glucose additions (arrows) in agarose gel. Data were acquired at 0.7 V against a Pt pseudo reference electrode for H_2O_2 oxidation detection. The insert is a calibration graph presenting the catalytic current acquired as a function of the glucose concentration added in the gel. The sensor response is linearly proportional to the glucose concentrations. The linear regression is fitting the calibration well ($R^2 = 0.9771$).

Figures 2.10 and 2.11 clearly show the current to increase upon addition of glucose to the agarose gel. This indicates that the H_2O_2 produced in the glucose oxidation can be directly detected using electrochemical methods and the response is linear with respect to the concentration of glucose.

2.3.2.3 Response to glucose of GOD entrapped in an agarose gel

Figures 2.12 and figure 2.13 show, respectively, the cyclic voltammetry and chronoamperometry results obtained with GOD entrapped in agarose by the method described as *Entrapment 1*. The previous experiment showed that GOD immobilised onto the surface of the CVD graphene gave a good response to glucose additions. It is hoped that by

dispersing the enzyme in the gel, glucose could reach the enzyme active area from all sides whereas when it is immobilised on the graphene surface, glucose can only reach the top surface of the enzyme. Furthermore, this entrapment technique will allow an important enzymatic loading which will relate to the signal (see figure 2.14).

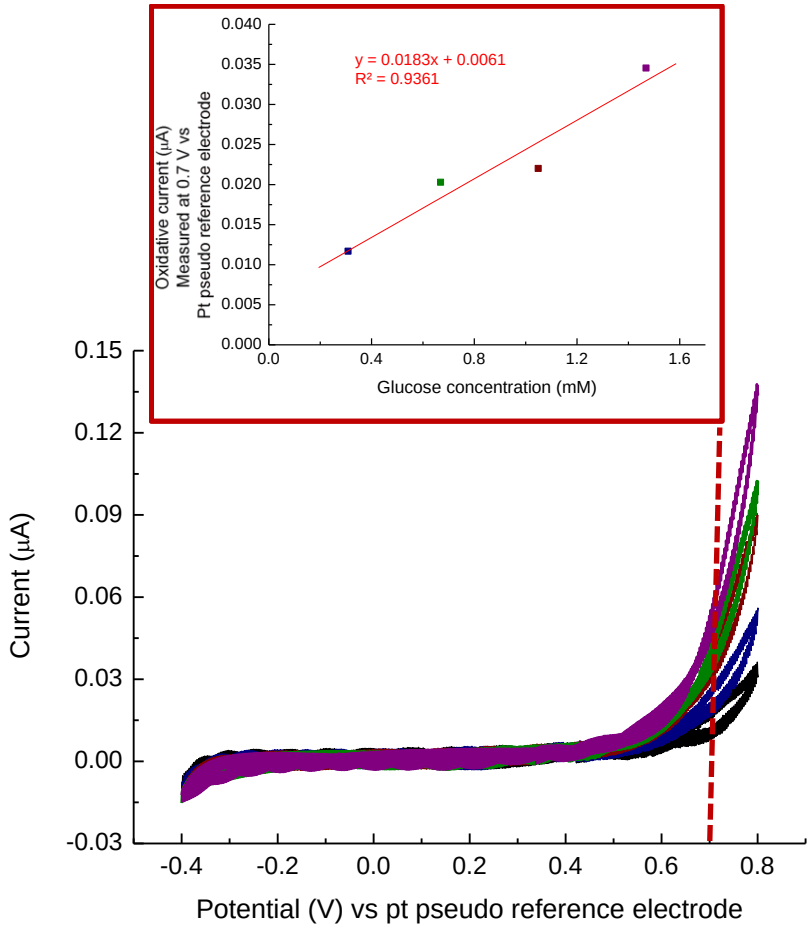

Figure 2.12. Cyclic voltammograms obtained in response to serial additions of glucose to GOD (6 mg/mL) entrapped (by method *Entrapment 1*) in an agarose gel. The scan rate was 20 mV/sec, and the results were acquired after 3 scans. The insert is a calibration graph displaying the oxidative H_2O_2 current (at 0.7 V vs the platinum pseudo reference electrode) produced as a result of the enzymatic reaction, function of glucose concentration added in the gel.

A.

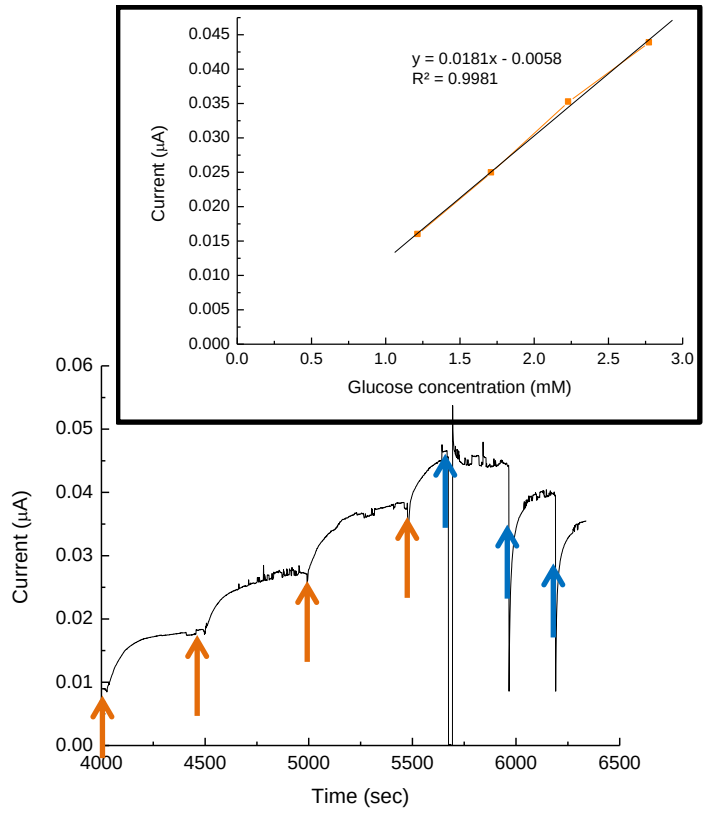

B.

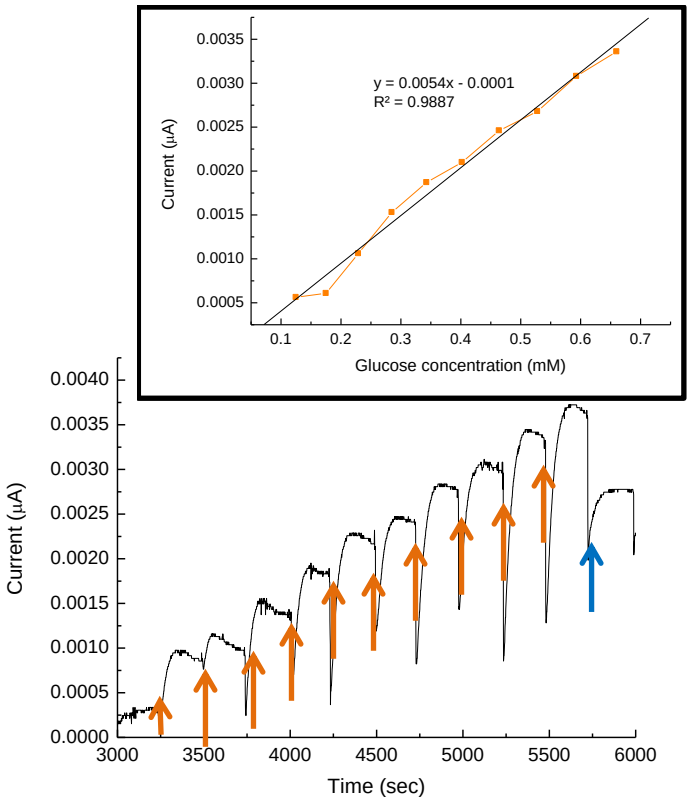

Figure 2.13. Chronoamperometry acquired in response to serial additions of glucose (orange arrows) to GOD entrapped (*Entrapment 1*) in an agarose gel. A: The glucose concentration in the gel ranged from 1.22 to 2.78 mM. B: The glucose concentration in the gel ranged from 0.125 to 0.66 mM. Blue arrows indicate additions of (blank) phosphate buffer. Data were acquired at 0.7 V against a Pt pseudo reference electrode. The inserts are calibration graphs presenting the catalytic current acquired as a function of the glucose concentration added in the gel. Again the signal fits linearly to the concentrations (especially in B, with an R^2 of 0.9887 for the linear regression of the calibration curve).

Figures 2.12 and 2.13 show a much better response to glucose additions with the currents being larger and less noisy with glucose additions. The entrapment method has clearly proven to be a better technique for GOD immobilisation and glucose detection.

2.3.2.4 Correlation of signal intensity with enzyme concentration entrapped in the gel

The intensity of the signal obtained from gels containing 0.21 and 6 mg/mL of enzyme were compared. Figure 2.14 demonstrates the direct correlation between the signal intensity observed with cyclic voltammetry and the level of enzyme present with the current measured increasing 22.2 times from the 0.21 mg/mL to the 6 mg/mL GOD concentraion.

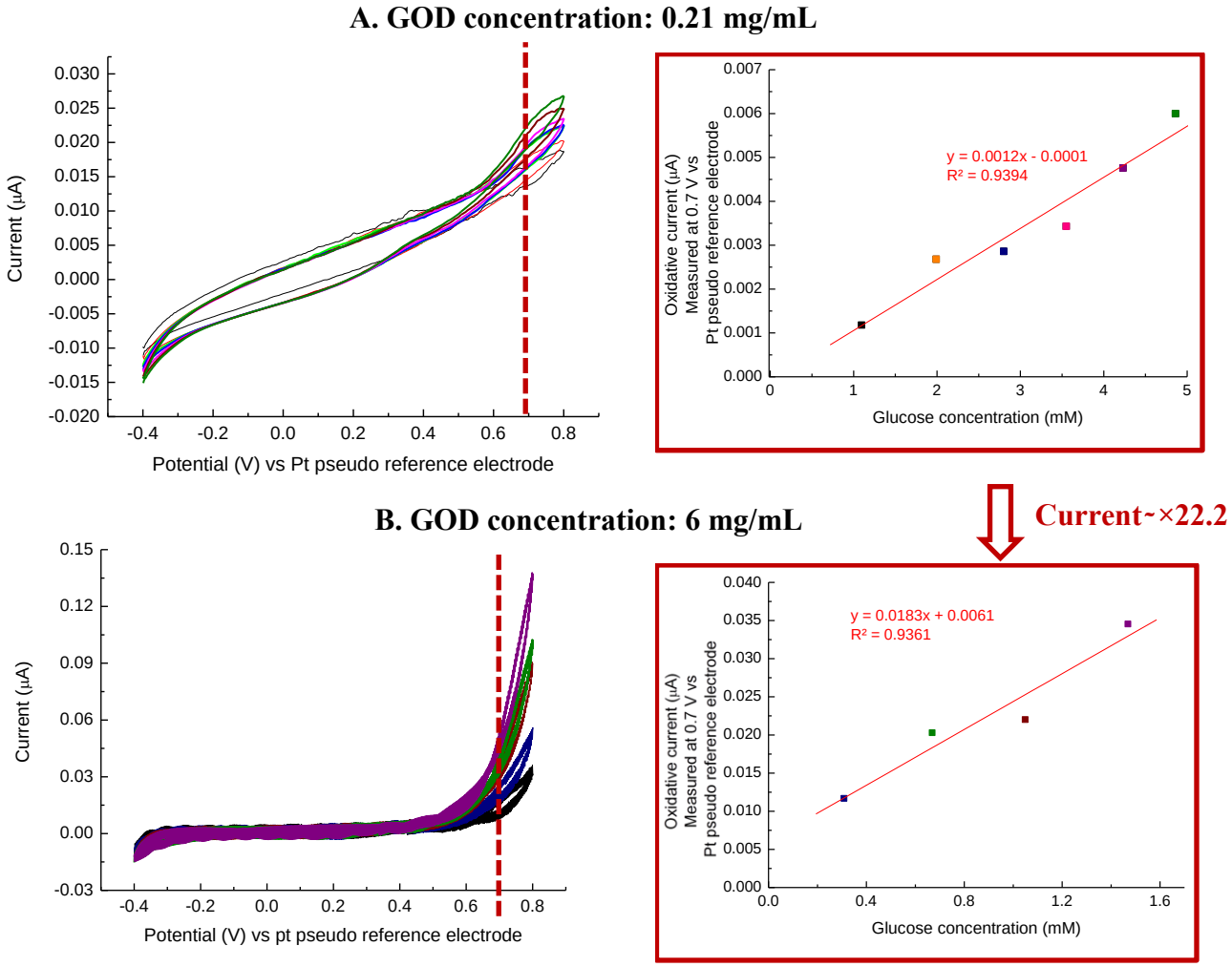

Figure 2.14. Correlation between signal intensity and enzyme concentration in the gel. A. Cyclic voltammetry obtained with GOD and glucose added on top of 32 µL+/- 2 µL piece of gel. B. Cyclic voltammetry obtained with GOD entrapped following "*entrapment 1*" and with glucose additions. The scan rate was 20 mV/sec, and the results were acquired after 3 scans. The inserts are calibration graphs displaying the oxidative H_2O_2 current (at 0.7 V vs the platinum pseudo reference electrode) produced as a result of the enzymatic reaction, function of glucose concentration added in the gel.

2.3.2.5 Glucose oxidase non-covalently coated on the surface and entrapped inside the gel

Next, serial additions of glucose were made to a GOD/1-PBASE coated graphene sample, and with GOD entrapped in the gel as well. Combining the two different immobilisation techniques should increase the signal as there is now twice the amount of enzyme; on the surface and in the gel. Figure 2.15 presents the chronoamperometric results again acquired at 0.7 V against a Pt pseudo-reference electrode.

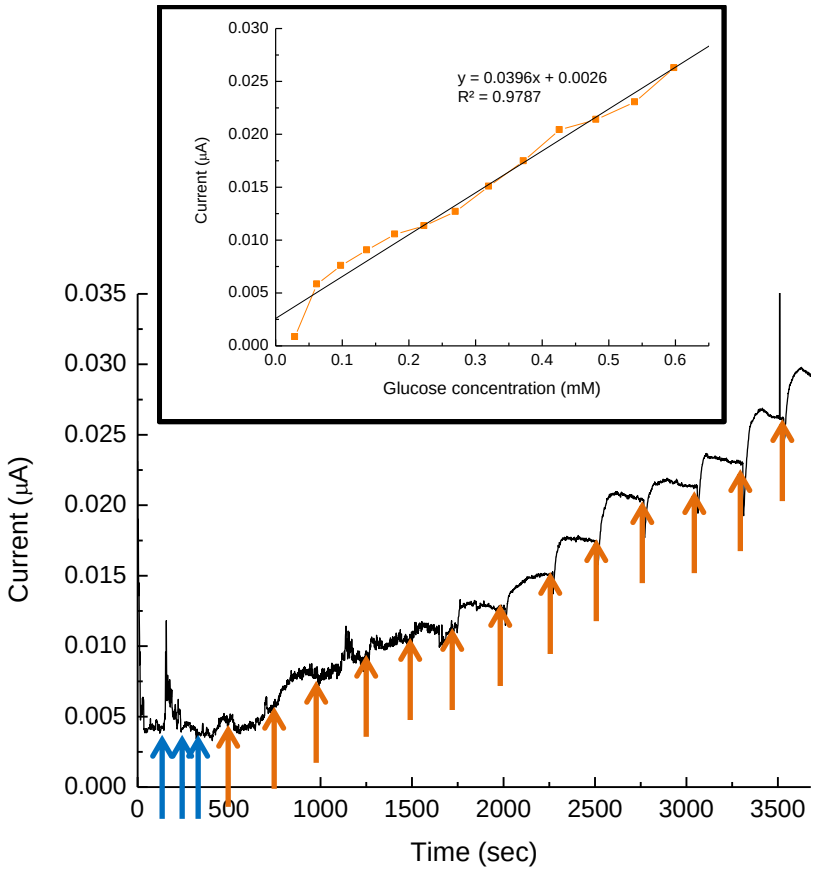

Figure 2.15. Chronoamperometry acquired in response to serial additions of glucose (orange arrows) to GOD coated on the surface and entrapped in the agarose gel (by method *Entrapment 1*). Blue arrows indicate additions of (blank) phosphate buffer. Data were acquired at 0.7 V against a Pt pseudo reference electrode. The insert is a calibration graph presenting the catalytic current acquired as a function of the glucose concentration added in the gel. The signal also fits linearly the concentrations here with an R^2 of 0.9787 for the linear regression of the calibration curve.

Figure 2.15 shows the current to increase further compared to only entrapping the enzyme in the gel indicating that the increase in the amount of GOD does have a direct effect on the currents measured as shown in section 2.3.2.4.

2.4 Discussion

2.4.1 LSCM characterisation of the transducer functionalization

The efficiency of the 1-PBASE functionalization of GOD was demonstrated (figure 2.6-A). LSCM revealed homogeneous fluorescence originating from the enzyme deposited on the nanomaterial (in contrast to the glass background, figure 2.6-B). Furthermore, the micro-contact printing of FITC labelled GOD on graphene was also effectively imaged by LSCM: a scan of micro-contact printed GOD on graphene that displayed fluorescent lines (distinguished from the graphene autofluorescent background) was obtained (figure 2.5). A patterned deposition of enzyme was confirmed. Then, a real-time glucose sensing was achieved by combining bioelectrochemistry with micro-contact printing and LSCM visualisation (figure 2.8). This detection takes advantage of the pH sensitivity of fluorescein and the reaction displayed in figures 2.7. During the reaction of glucose and glucose oxidase in oxygenated conditions and at an appropriate potential for the oxidation of the produced H_2O_2, 3 protons are produced. These will cause a local acidification of the medium and hence a decrease of fluorescence around the enzyme visualised in red in figure 2.8 (labelled with rhodamine). This phenomenon is demonstrated in figure 2.8-A and figure 2.8-D. An excess of glucose (>2 M) will cause a significant decrease of fluorescence around the rhodamine labelled GOD. The catalytic activity of the enzyme was hence visualised with a proof of concept technique. Although fluorescein's pH dependent behaviour had previously been used in sensor devices [29], and combined with electrochemistry [28], these results are the first to combine micro-contact printing, enzymatic/electrochemical sensing, and LSCM for real time imaging and detection of GOD activity on graphene. The experiment however suffered some drawbacks: (1) the potential was not fixed at the oxidation voltage of H_2O_2 but cycled. (2) Although a neat decrease of fluorescence was observed when adding an excess of glucose (figure 2.8-D), the fluorescence decay obtained in figure 2.8-B and figure 2.8-C were inconsistent with the glucose concentration added (5 and 10 mM respectively), the first fluorescence decrease being more intense than the second. This inconsistency might be explained by the diffusion of fluorescein in the buffer or the poor sensitivity of the detection. (3) The results were obtained from a single experiment. The aim of the thesis being the development of a non-invasive sensing glucose sensing platform, the direct visualisation and sensing of glucose was not studied further.

2.4.2 Electrochemical characterisation of the transducer functionalization

Figure 2.9 is a confirmation study of the stability of glucose stored in phosphate buffer pH 7.4 at 4 °C, over more than a month. This was done previous to chronoamperometric experiments in order to confirm the accuracy of the concentrations used and investigated in the rest of the experiments. The standard deviation obtained between the three measured concentrations was of 0.0025 mg/mL (i.e., 13.9 µM). This value only represents a total variation of 4.6% of the original sample concentration. The glucose solutions storage protocol is therefore appropriate for the rest of the analysis.

Figures 2.10 and 2.11 are first electrochemical demonstrations of catalytic activity with addition of glucose on a graphene electrode non-covalently functionalised with GOD and 1-PBASE. The additions were done in an agarose gel volume of 32 µL +/- 2 µL. The inserts of the respective figures display a linear increase of the catalytic current with additions of glucose. However the response current were relatively low (over 10 nA range), the signal was relatively noisy at low concentration of glucose and the chronoamperometric steps were not well-defined (figure 2.11). This suggested that the non-covalent coating of the electrode achieved was not optimal.

In an attempt to improve performance, the protein was entrapped inside the agarose gel. The device presented in figure 2.13 displayed an almost doubled catalytic oxidative current at 0.7 V vs a Pt pseudo reference electrode (1 mM of glucose gave a current of ~ 0.0057 µA in figure 2.11 while ~ 0.0123 µA was obtained in figure 2.13-A, providing an increase of ~2.17 times). Figure 2.13 also display linear calibration curves in two concentration ranges (1.22 to 2.78 mM in figure 2.13-A and 0.125 to 0.66 mM in figure 2.13-B). The chronoamperometric steps obtained in response to the glucose additions were also more defined than in figure 2.11. Both the stability and increase of the signal made the gel entrapment an appropriate design for the development of the sensor.

Figure 2.14 is a study of the effect of the concentration of GOD in the gel on the catalytic current with additions of glucose. Although the entrapment was slightly different, the outcome was an increase of oxidative current observed at 0.7 V against a Pt pseudo reference

electrode of ~ 22.2 between the low and high concentration of enzyme (the respective catalytic currents obtained for 1 mM of glucose were ~ 0.0011 µA for the lowest concentration of enzymes; figure 2.14-A and ~ 0.0244 µA for the highest concentration; figure 2.14-B). This value was in good agreement with the ratio of GOD concentrations: 28.6. The signal correlated therefore well with the amount of enzyme present.

Then the combination of both entrapment and electrode coating of the protein (figure 2.15) was also shown to improve the oxidative catalytic signal (the current for 0.5 mM of glucose was ~ 0.00325 µA and ~ 0.0224 µA for figure 2.13-B and figure 2.15 respectively). The GOD gel entrapment technique was hence selected for further analysis providing with a strong catalytic signal towards glucose. It is also an appropriate technique for implementation in a future non-invasive sensing design because the protocols involved are cheap and simple, the electrodes can be stored under ambient conditions and the gel platform will be adapted for extraction of glucose from the skin as demonstrated in chapter 5. The addition of the non-covalent technique to gel entrapment could however be studied in future work in an effort to improve the sensor signal.

Finally the use of agarose is justified by its' cheap price, its' availability and the simplicity to of its' gelling protocols and enzyme entrapment. It does however suffer some major issues that would need addressing in the future: (1) the enzyme is not fixed inside the gel but dissolved in the buffer of the hydrogel and will eventually diffuse out of the matrix, (2) being an hydrogel the structure is prone to dry under ambient conditions which will be the cause of problems in the development of the technology (in chapter 5 especially). Other gels have been used in the literature to entrap glucose oxidase in biosensing configurations. Table 2.1 enumerates some of the gels found in the literature along with their "enzyme entrapment properties". The focus here was however not placed onto the study of different gel formulation for the sensor but rather on the research of the best sensing operation (see chapter 3) and the optimisation of the sensor via miniaturization and addition of platinum nanoparticles (see chapter 4) in order to obtain a performant and adequate platform for non-invasive integration (see chapter 5).

Table 2.1: Comparison of gel enzyme "entrapment properties" for some glucose biosensors found in the literature and the developed sensor

Sensor	Gel	"Enzyme entrapment properties"	Ref.
Silica-dispersed GOD on platinized platinum (Pt) "Clark type amperometric sensor"	Silica sol-gel	• Maintain the enzyme stability • Reduced barrier to glucose diffusion	[30]
polypyrrole-polystyrensulfonate (PPy) embedded in polyacrylamide (PA) embedding GOD on top of a Pt electrode	Polyacrilamide/ polypyrrole microgel	• Inclusion of polypyrrole to facilitate electron transfer • Enzymatic activity preserved for at least nine months • Fast and easy producttion	[31]
Glucowatch sensor: Platinum/carbon ink electrode GOD embedded in the gel	polyethylene oxide, polyacrylic acid, polyvinyl alcohol, Carbopol®, and polyacrylamidomethylpropanesulfonate and copolymers	• Water loss from the gel: less than 70 % over 24 hours • Stability of the produced H_2O_2 (loss of H_2O_2 less than 20 % over 30 minutes) • Easily and economically produced • Disposable	[32]
CVD graphene sensor, GOD embedded in the gel	agarose	• Fast and easy production • High diffusion coefficient of glucose in agarose gels (0.5 %) $\sim 6 \times 10^{-10}$ m^2/s [33] • Conservation of the enzyme catalytic activity (see kinetic enzymatic parameters (Km) determined in chapter 4, figure 4.22)	This work

2.5 Conclusions

This chapter investigated one of the fundamental attributes of the development of a biosensor: the functionalization of the transducer with enzymes. The first presented technique involves non-covalent coating on graphene (covalent attachment of the GOD) via a linker: 1-PBASE. The enzyme coverage of CVD graphene was successfully demonstrated by LSCM with the GOD labelled with fluorescein (either on the entire surface of the electrode or in a patterned manner with the application of microcontact printing). The catalytic activity of this functionalization was assessed using real time sensing/LSCM visualisation and electrochemical measurements. This was an initial demonstration of glucose sensing, but due to lack of sensitivity at low concentration of glucose and because the design didn't fit the purpose of the project, the analysis wasn't carried further.

The later electrochemical evaluation of the activity performed via cyclic voltammetry and chronoamperometry displayed linear but small catalytic currents. Therefore the non-covalent coating that was used in this chapter as well as chapter 3, was replaced by GOD entrapment in an agarose gel. This second technique of sensor design demonstrated increased and linear oxidative catalytic signal, it was therefore selected as a good platform for the future non-invasive sensing application. Finally and even though the combination of both techniques was beneficial to the chronoamperometric signal, the latter technique was preferred for the design of the sensor and non-invasive integration described in chapter 4 and 5.

1. Brena, B.M. and F. Batista-Viera, *Immobilization of Enzymes*. 2006. p. 15-30.
2. Wang, L., et al., *Large thermoelectric power factor in polyaniline/graphene nanocomposite films prepared by solution-assistant dispersing method.* Journal of Materials Chemistry A, 2014. **2**(29): p. 11107-11113.
3. Trevan, M.D., *Enzyme Immobilization by Covalent Bonding*, in *New Protein Techniques*, J. Walker, Editor. 1988, Humana Press. p. 495-510.
4. Wadu-Mesthrige, K., N.A. Amro, and G.-Y. Liu, *Immobilization of proteins on self-assembled monolayers.* Scanning, 2000. **22**(6): p. 380-388.
5. Eliaz, N., *Applications of Electrochemistry and Nanotechnology in Biology and Medicine I*. 2011: Springer.
6. Song, J., X. Wang, and C.-T. Chang, *Preparation and Characterization of Graphene Oxide.* Journal of Nanomaterials, 2014. **2014**: p. 6.
7. Yu, Y., et al., *Direct electron transfer of glucose oxidase and biosensing for glucose based on PDDA-capped gold nanoparticle modified graphene/multi-walled carbon nanotubes electrode.* Biosensors and Bioelectronics, 2014. **52**(0): p. 147-152.
8. Kodali, V.K., et al., *Nonperturbative Chemical Modification of Graphene for Protein Micropatterning.* Langmuir, 2010. **27**(3): p. 863-865.
9. Huang, Y., et al., *Nanoelectronic biosensors based on CVD grown graphene.* Nanoscale, 2010. **2**(8): p. 1485-1488.
10. Ariga, K., et al., *Enzyme nanoarchitectonics: organization and device application.* Chemical Society Reviews, 2013. **42**(15): p. 6322-6345.
11. Alwarappan, S., et al., *Enzyme-Doped Graphene Nanosheets for Enhanced Glucose Biosensing.* The Journal of Physical Chemistry C, 2010. **114**(30): p. 12920-12924.
12. Kang, X., et al., *Glucose Oxidase–graphene–chitosan modified electrode for direct electrochemistry and glucose sensing.* Biosensors and Bioelectronics, 2009. **25**(4): p. 901-905.
13. Lu, J., et al., *Nanometal-Decorated Exfoliated Graphite Nanoplatelet Based Glucose Biosensors with High Sensitivity and Fast Response.* ACS Nano, 2008. **2**(9): p. 1825-1832.
14. Abraham, W., et al., *hydrogel formulations for use in electroosmoticextraction and detection of glucose*, 2004, US Patent 20040062759 A1.
15. Yang, W., et al., *Noncovalent Functionalization of Graphene in Suspension.* ISRN Organic Chemistry, 2013. **2013**: p. 7.

16. Li, D., et al., *Protein electrochemistry using graphene-based nano-assembly: an ultrasensitive electrochemical detection of protein molecules via nanoparticle-electrode collisions.* Chemical Communications, 2014. **50**(60): p. 8197-8200.
17. Leskovac, V., et al., *Glucose oxidase from Aspergillus niger: the mechanism of action with molecular oxygen, quinones, and one-electron acceptors.* The International Journal of Biochemistry & Cell Biology, 2005. **37**(4): p. 731-750.
18. Clark, L.C. and C. Lyons, *Electrode systems for continuous monitoring in cardiovascular surgery.* Annals of the New York Academy of Sciences, 1962. **102**(1): p. 29-45.
19. Chunyan, L., et al. *Brain-friendly amperometric enzyme biosensor based on encapsulated oxygen generating biomaterial*. in *Engineering in Medicine and Biology Society (EMBC), 2012 Annual International Conference of the IEEE*. 2012.
20. Putzbach, W. and N. Ronkainen, *Immobilization Techniques in the Fabrication of Nanomaterial-Based Electrochemical Biosensors: A Review.* Sensors, 2013. **13**(4): p. 4811-4840.
21. Li, X., et al., *Transfer of Large-Area Graphene Films for High-Performance Transparent Conductive Electrodes.* Nano Letters, 2009. **9**(12): p. 4359-4363.
22. The, T.H. and T.E.W. Feltkamp, *Conjugation of fluorescein isothiocyanate to antibodies.* Immunology, 1970. **18**(6): p. 865-873.
23. Mata, A., A. Fleischman, and S. Roy, *Characterization of Polydimethylsiloxane (PDMS) Properties for Biomedical Micro/Nanosystems.* Biomedical Microdevices, 2005. **7**(4): p. 281-293.
24. Zoldák, G., et al., *Irreversible Thermal Denaturation of Glucose Oxidase from Aspergillus niger Is the Transition to the Denatured State with Residual Structure.* Journal of Biological Chemistry, 2004. **279**(46): p. 47601-47609.
25. Bahl, A., *T.B. Of Organic Chemistry (M.E.)*. 2005: S. Chand Limited.
26. Veney, J.E., J.F. Kros, and D.A. Rosenthal, *Statistics for Health Care Professionals: Working With Excel*. 2009: Wiley.
27. Hazan, R., A. Levine, and H. Abeliovich, *Benzoic Acid, a Weak Organic Acid Food Preservative, Exerts Specific Effects on Intracellular Membrane Trafficking Pathways in Saccharomyces cerevisiae.* Applied and Environmental Microbiology, 2004. **70**(8): p. 4449-4457.

28. Rudd, N.C., et al., *Fluorescence Confocal Laser Scanning Microscopy as a Probe of pH Gradients in Electrode Reactions and Surface Activity.* Analytical Chemistry, 2005. **77**(19): p. 6205-6217.
29. Ma, L.Y., et al., *A long lifetime chemical sensor: study on fluorescence property of fluorescein isothiocyanate and preparation of pH chemical sensor.* Spectrochimica Acta Part A: Molecular and Biomolecular Spectroscopy, 2004. **60**(8–9): p. 1865-1872.
30. Harris, J.M., G.P. Lopez, and W.M. Reichert, *Silica-dispersed glucose oxidase for glucose sensing: in vitro testing in serum and blood and the effect of condensation pH.* Sensors and actuators. B, Chemical, 2012. **174**: p. 373-379.
31. Rubio Retama, J., et al., *Design of an amperometric biosensor using polypyrrole-microgel composites containing glucose oxidase.* Biosensors and Bioelectronics, 2004. **20**(6): p. 1111-1117.
32. Abraham, W., et al., *Hydrogel formulations for use in electroosmotic extraction and detection of glucose*, 2004, US Patent 20040062759 A1.
33. Weng, L., et al., *Transport of Glucose and Poly(ethylene glycol)s in Agarose Gels Studied by the Refractive Index Method.* Macromolecules, 2005. **38**(12): p. 5236-5242.

Chapter 3: Biosensor design and detection principles

3.1 Introduction

This chapter investigates the detection principle of two setups: (1) a potentiometric design: field effect transistor and (2) an electrochemical (voltammetric/amperometric) design. The latter was separated in two categories: a mediated detection using a redox mediator (second generation biosensor) and a direct sensing of the enzymatically produced H_2O_2 (first generation biosensor). Two additional sensing principles have been investigated in the literature: direct enzymatic oxidation and non-enzymatic sensing. These won't however be the subject of the presented work, (see 3.α footnote).

3.1.1 BioFET

A biological field effect transistor (BioFET) is able to detect small induced ionic variations in a solution as a result of (for example): (1) a change in gating potential due to a catalytic reaction product; (2) surface polarization effects or changes in dipole moment during DNA hybridisation or antigen/antibody immunoreaction; or (3) the complicated biochemical signals emitted by living cells. Clearly, the first category of BioFET is of most interest in this work, the so-called EnFETs (enzyme field effect transistor). EnFETs were first introduced in 1976 [4] and, included among the many enzymes studied, GOD. Several limitations have been noted, however, relative to their implementation: (i) buffer capacity and ionic strength of the solution can impact greatly on protonic detection, (ii) the sensors presents slow response and recovery times, (iii) the detection limit and linear range of ENFETs are not optimal, (iv) stability on storage and repeatability can be problematic and (v) the performance is very sensitive to enzyme immobilisation and patterning which are often far from optimal on silicon substrates [5].

[3.α] *Third generation biosensors (that rely on the direct electron transfer from the enzymatic active catalytic centre to the transducer) [1], or enzymeless glucose detection using transducer materials such as nanoporous gold [2] or silver oxide nanowalls [3] have been presented in the literature but will not be investigated further.*

The introduction of CVD graphene as a zero-gap semiconductor in the EnFET design was anticipated to solve at least some of these problems. One example of where graphene field effect transistors have been used in glucose detection is shown in [6]: A FET sensor made of graphene fonctionalised with a linker molecule (1-pyrenebutaoic acid succinimidyl ester) and immobilising GOD onto the surface of graphene was presented. The device could detect glucose levels in the range of 3.3-10.9 mM showing that CVD graphene FET devices are good biosensors.

3.1.2 "Bio"electrochemistry

The other detection platform is electrochemistry based. Several enzyme-based amperometric biosensors have been developed in the past 20 to 30 years including, of course, those with GOD [7]. GOD reacts with its β-D-glucose substrate producing H_2O_2 (chapter 2, figure 2.7), which is then oxidised at the WE (e.g., platinum [8] or glassy-carbon [9]) to generate an analytical current. On a Pt working electrode, H_2O_2 is oxidised at a potential between 0.5 and 0.7 V against a saturated calomel electrode [10]. A glucose sensor based on the direct electrochemistry of H_2O_2 at a graphene electrode was described in [11] with a linear glucose response up to 14 mM. This "first generation" detection of H_2O_2 is presented further.

An attempt at the development of a "second generation" sensor involving the use of a redox mediator is also investigated. 1,1-Ferrocenedimethanol (FDM) is a commonly used, electroactive mediator that facilitates electron transfer. Sensors using a redox mediator instead of molecular oxygen have been thoroughly studied and exploited over the past 30 years. Some of the most common redox mediators found in electrochemical biosensors are: ferrocene, ferricyanide, benzoquinones and methyl viologen. Redox mediators can be classified as either "inner" or "outer" sphere depending on their electron transfer properties. "Outer" sphere electron transfer is the most common in biological systems and is defined by electron passage between two non-connected redox entities separated by a few Ångstroms [12]. Electron transfer is highly dependent on the distance separating outer sphere redox entities as described by equation 3.1, derived from Marcus theory on electron transfer [12]:

$$k_{ET} = k_0 \exp[-\beta(d - d_0)] \qquad (3.1)$$

k_{ET} is the rate constant for outer sphere electron transfer, k_0 is the electron transfer rate at the closest distance d_0, d-d_0 is the distance between the two entities and β the distance decay factor, typically in the range of 0.8 to 1.4 $Å^{-1}$ [12, 13]. β depends on the nature of the

heterogeneous region between donor and acceptor of the electron: Electrons go through some materials in an easier way than others which is reflected in β [13].
In contrast, "inner" sphere electron transfer involves chemical bonding between the mediator and the electrochemical active site for the transfer to occur before the bond is cleaved to regenerate the mediator and substrate (being either oxidised or reduced) [14]. Typically, ferrocene has been described as an outer sphere redox mediator with respect to the catalytic activity of glucose oxidase [15], whereas benzoquinones are examples of inner sphere mediators [16]. The use of redox-mediators in second generation biosensors has significant advantages such as increasing electron transfer, shifting the electrode potential at which the redox signal is detected, and removing the oxygen dependence [17]. The latter, however also have negative consequences, specifically that involves working in anaerobic conditions to avoid oxygen competition with the mediator for the electron transfer [18, 19].

Some mediators are also toxic; for example methyl viologen can be converted into paraquat in solution, a compound which can have deleterious effects on the lungs, liver, kidneys and other organs [20]. To achieve optimal mediation, it is necessary to entrap the mediator with the enzyme, either in a hydrogel matrix [21] or even by covalent attachment to the enzyme [22]. Furthermore, an appropriate redox mediator must present the following characteristics: (1) a well-defined redox stoichiometry, (2) fast enzyme and electrode kinetics, (3) appropriate solvent solubility and redox/light stability, (4) no alteration of enzyme redox potential and (5) an adequate redox potential itself [23]. The latter must be such as to avoid other electro-active (interfering) species being oxidised or reduced at the electrode. FDM has a near reversible redox signal at a potential of 0.20 to 0.24 V versus Ag/AgCl [24]. It is very unlikely that common interfering molecules for the physiological detection of glucose such as ascorbic acid, uric acid or acetaminophen will be oxidised at this low potential [25]. FDM is water-soluble, is stable in the reduced form, insensitive to light and pH, with fast and quasi-reversible electron transfer. It is suitable for combination with enzymatic electrochemistry [26]. This redox species was therefore selected as a potentially useful mediator in this study.

3.1.3 Reduction of the receptacle volume

A final key objective of this chapter was the demonstration of the scaling down of the volume of the reaction reservoir. The rationale is self-evident: to facilitate mass transfer of the analyte to the sensor. Attention has therefore been focused on reducing the dimensions of the

electrochemical set-up combining a working graphene electrode with a small gel or liquid reservoir and wire, micro counter and reference electrodes (the gel design were already presented in chapter 2, sections 2.3.2.2 to 2.3.2.5).

3.2 Materials and experimental methods

3.2.1 Materials

Most of the materials are the same as the ones described in chapter 2, section 2.2.1. Additional includes: Silver (Ag), platinum (Pt) wires and gold pellets purchased from Advent (Oxford, UK). A Keithley 487 picoameter/voltage and a Keithley 230 programmable voltage source (Keithley instruments, Cleveland, OH, USA) were used as voltage and current controller in the transistor setup. 1,1-Ferrocenedimethanol (FDM), Ferrocene carboxylic acid, (2-aminoethoxy) acetic acid were obtained from Sigma-Aldrich (Dorset, UK). A SCE reference electrode was acquired from Radiometer Analytical (Lyon, France). The potentiostat used in the electrochemical experiments were Autolabs from Metrohom (Utrecht, The Netherland) except in figure 3.9 where an Ivium technology, CompactStat instrument (Eindhoven, The Netherland) was used. An AFM, Asylum Research (High Wycombe, UK) MFP-3D microscope was used for microscopic imaging of transferred CVD graphene.

3.2.2 Experimental methods

3.2.2.1 AFM imaging: CVD graphene microscopic visualisation

Atomic Force Microscopy images were acquired in tapping mode, using AC240TS-10, medium soft cantilevers from Olympus (Asylum Research, High Wycombe, UK). The tip approach was carefully monitored through a video camera and an optical microscope. The acquisition was controlled via the MFP-3D software provided (Asylum Research, High Wycombe, UK). The CVD graphene visualised had been transferred following the protocol presented in chapter 2, section 2.2.2.1.

3.2.2.2 CVD graphene transfer and GOD functionalization

See chapter 2, section 2.2.2.1 and section 2.2.2.2.

3.2.2.3 FET transistor

3.2.2.3.1 FET design

Conduction source (S) and drain (D) silver paint connection pads were deposited on graphene leaving a semiconductor conductive channel of ~ 1-2 mm (graphene flake dimensions were ~ 7×7 mm^2). Silicone rubber was deposited on the silver paint contact and formed an insulating "well" into which 20 µL of 0.1 M phosphate buffer pH 7.4 was introduced. A silver or platinum wire was used as a gate (G). The FET design is shown in chapter 1, figure 1.13.

3.2.2.3.2 FET results acquisition

During the acquisition, V_{SD} (*Voltage Source to Drain*) was set at 0.2 V and V_{GD} (*Voltage gate to Drain*) varied between -0.4 V and 0.8 V with voltage sources mentioned in the material section. Data were recorded using a LabView program written by Gavin Jones, Department of Physics, University of Bath. The acquisition measured $I_{SD} = f(V_{GD})$.

3.2.2.4 Electrochemical design

3.2.2.4.1 First generation sensing: detection of H_2O_2

The enzymatic coating, electrode design and electrochemical setup were the same for first generation and second generation sensing. The only variations are the addition of a mediator in the reaction receptacle or ferrocene coating in the second generation sensing experiments (see section 3.2.2.4.2).

The electrodes used for first generation sensing were functionalised with GOD as described in chapter 2, section 2.2.2.2. The electrochemical cell comprised three electrodes: a SCE or Ag pseudo reference electrode acting as a RE, a platinum wire for CE, and a working electrode made of CVD graphene (3×3 mm^2) deposited on silicon dioxide and non-covalently functionalized with GOD. Electrical conduction was achieved by evaporating titanium and gold (10 nm and 60 nm respectively) onto a part (approximately $1/6^{th}$) of the graphene flake. The active area of functionalized graphene was insulated via a layer of silicone rubber. As mechanical stirring was not optimised, the system relied on diffusion to attain equilibrium. An SCE electrode was first chosen for large volume electrochemistry, because it was made

available in the beginning of the project and adapted to the measurements. However with the decrease of the set-up dimensions (40 µL in figure 3.12) it was replaced by a pseudo Ag reference electrode which was more appropriate for manipulations. With improvement of the set-up this pseudo reference electrode will be replaced by an Ag/AgCl micro reference electrode as described in chapter 4. Glucose solutions used to test the sensor were allowed to mutarotate overnight at 4 °C before the electrochemical experiment. The electrochemical cell volumes were 21 mL for figure 3.7 and 8 mL for figure 3.9 to 3.11 and 40 µL for figure 3.12. Glucose calibration curves were obtained as described in chapter 2 section 2.2.3.

3.2.2.4.2 Second generation sensing: use of ferrocene as a redox mediator

A solution of 50 µM ferrocene dimethanol (FDM) in 0.1 M phosphate buffer pH 7.4 was used in figure 3.7 to detect glucose on a graphene electrode non-covalently coated with GOD. For the experiment displayed in figure 3.8, one step was added to the electrode treatment described in chapter 2, section 2.2.2.2 with the introduction of a ferrocene-amine compound synthesized from ferrocene-carboxylic acid and 2.2'-(Ethylenedioxy)bis(ethylamine) following the reaction displayed in figure 3.1 (*supplied by Sean Goggins, Department of Chemistry, University of Bath*). The newly synthetized compound was incubated with the GOD coated electrode at 0.27 mM for one hour, at room temperature, in a mixture of 1% DMSO and phosphate buffer pH 7.4, for coupling with the free 1-PBASE linkers on the electrode. The reaction between the succinimidyl ester of the linker and the amine of the compound is described in chapter 2, figure 2.2.

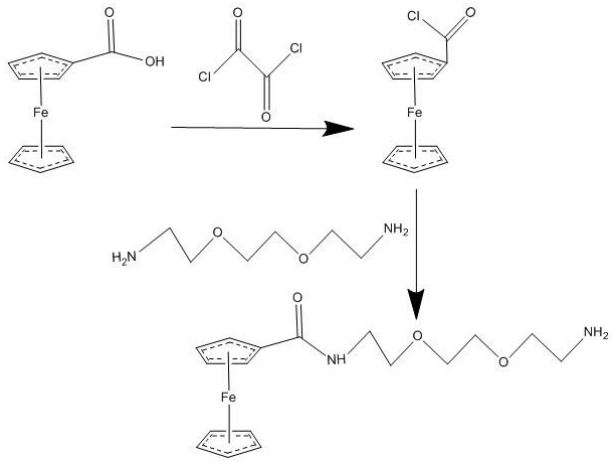

Figure 3.1: Synthesis of the ferrocene amine compound

3.3 Results

3.3.1 AFM imaging of CVD graphene transferred onto Si/SiO_2

Graphene was transferred onto a Si/SiO_2 substrate using the wet etching and transfer method outlined in chapter 2 section 2.2.2.1. Figure 3.2 shows AFM images taken after this transfer process had taken place to look at the surface morphology. It can be seen that there are both monolayer and multilayer regions on the graphene flake as well as folding of the flake. Figure 3.3 shows a height profile of the flake and the expected region of monolayer has a height of 0.445 nm which is close to the expected height for graphene of 0.34 nm reported in the literature [27]. Discrepancies in these values could be due to a water layer between the flake and the Si/SiO_2 substrate originating from the wet transfer technique used to place the flake on the substrate. Residues from the wet transfer technique are also evident from the AFM images as white lines appearing across the substrate which could be left over PMMA as well as drying circles.

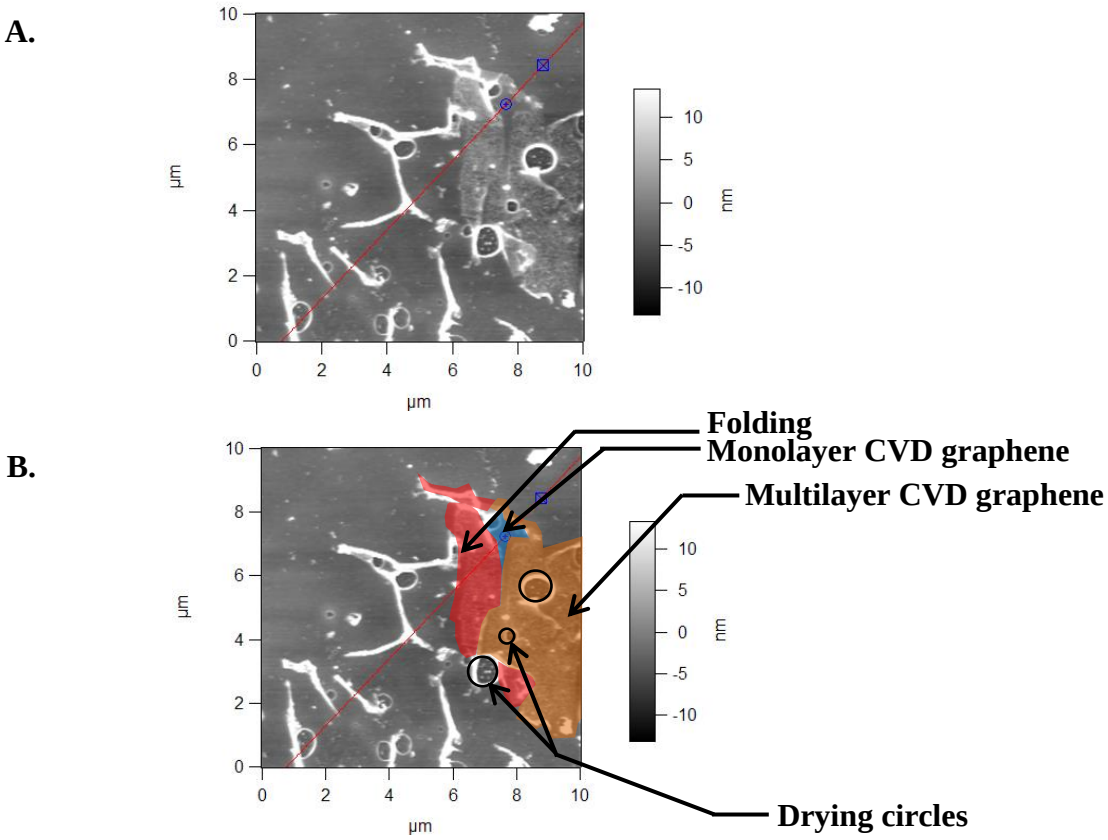

Figure 3.2. CVD graphene transferred onto Si/SiO_2. A: original image. B: specific patterns observed after the transfer procedure (i.e., folds, monolayer graphene, multilayer graphene and drying circles). The blue region presents a height of ~ 0.445 nm and is expected to be monolayer.

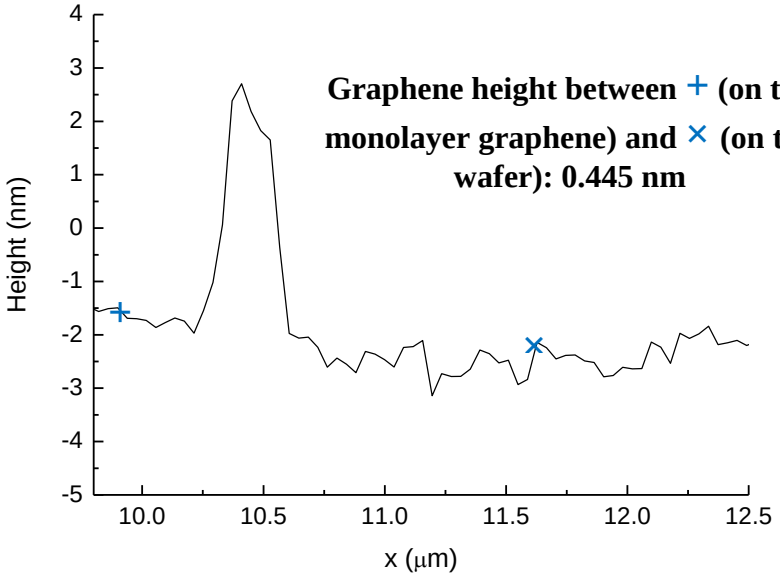

Figure 3.3. Height profile of CVD graphene. This height profile graph was obtained by analysing the AFM picture with the MFP 3D software (Asylum Research). The graphene thickness (presented between + and × on this figure and on figure 3.1) is an approximation and not a complete study of the structure of CVD graphene. It gives an indication of the representative graphene height.

3.3.2 Field effect transistor setup

3.3.2.1 Displacement of CVD graphene Dirac point as a function of solution pH

The graphene transistor coated with GOD was first tested with 0.1 M phosphate buffers at different pHs. Figure 3.4 to 3.6 presents $I_{SD} = f(V_{GD})$. The lowest I_{SD} point on the curve is the Dirac point of the semiconductor and is displaced as a function of pH or H^+ production in the enzymatic reaction between GOD and glucose. There is a noticeable hysteresis in figure 3.4, in the gate sweeps which is most likely to be caused by defects in the nanocarbon surface. It can be seen, in this figure, that the Dirac point shifts to higher gate potentials at lower pH phosphate buffer showing this to be a sensitive technique for studying pH changes on the surface of graphene.

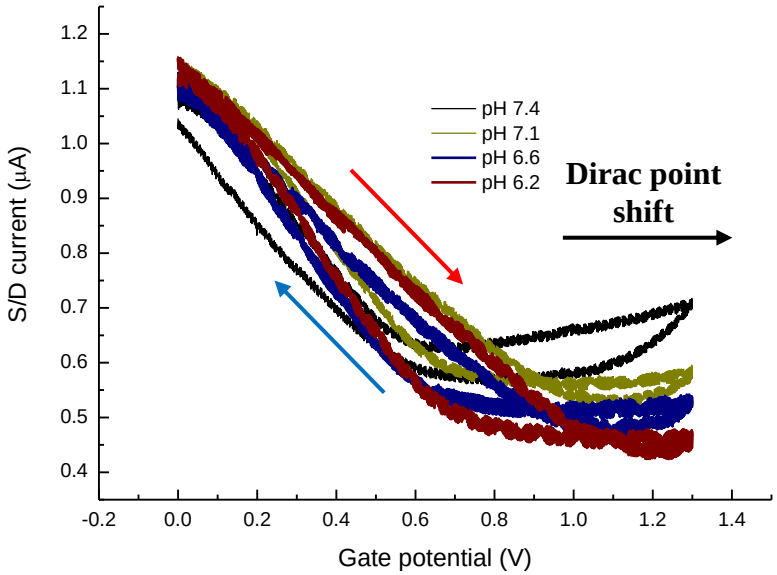

Figure 3.4: Displacement of the Dirac point of a GOD coated CVD graphene FET as a function of buffer pH. A range of pHs (0.1 M phosphate buffer) was tested on a CVD graphene FET functionalized with GOD and the I_{SD} and was reported as a function of V_{GS}. A slight hysteresis was observed between the forward signal (red arrow) and the reverse signal (blue arrow). The hysteresis is most likely caused by defects at the nanocarbon surface [28]. A noticeable trend was observed between each $I_{SD} = f(V_{GS})$ pH curves, displaying a shift in the Dirac point (lower I_{SD}) towards high V_{GS}.

3.3.2.2 $I_{SD} = f(V_{GD})$ with CVD graphene non-covalently coated with GOD

Figure 3.5 displays the differences in the FET signal obtained with GOD functionalization. The bare CVD graphene electrode (green line) has a Dirac point of 0.25 V, whereas when the GOD enzyme was non-covalently attached to the graphene surface, the Dirac point shifted by 0.07 V to a higher gate potential. This change in the Dirac point gives a clear indication of adsorption onto the surface of graphene changing the electronic properties of graphene.

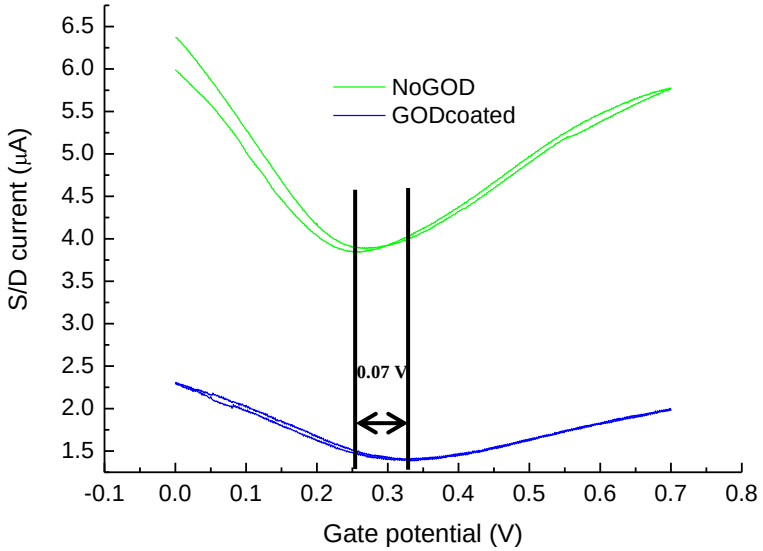

Figure 3.5. $I_{SD} = f(V_{GD})$ for graphene coated or not with GOD. This figure presents the shift in the Dirac point with non-covalent addition of GOD via 1-PBASE coating. A remarkable shift of around 0.07 V was observed between the bare graphene Dirac point and the GOD functionalized nanomaterial Dirac point. 20 µL of 0.1 M phosphate buffer pH 7.4 was used in this experiment.

3.3.2.3 GOD functionalized FET signal with glucose additions

The effect of different glucose concentrations was then studied by adding glucose at two different concentrations to the GOD/1-PBASE FET sensor. The Dirac point shifted at higher gate potentials with higher concentrations of glucose indicating that the production of protons, produced through the glucose oxidation, increases the pH and therefore shifted the Dirac point to higher potentials (see figure 3.6). The pH effect was already confirmed in figure 3.4 and shows the FET glucose sensor to be very effective at detecting glucose.

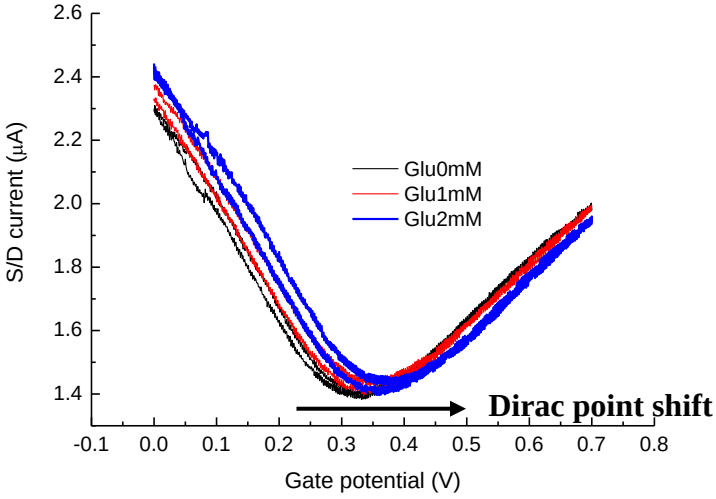

Figure 3.6. Glucose additions on a graphene FET coated with GOD. A 10 µL drop of 0.1 M phosphate buffer pH 7.4 served as the buffer/supporting electrolytes solution and was replaced for each glucose concentration. A shift of the Dirac point was observed towards higher V_{GD} was proportional to the amount of glucose added to the system.

3.3.3 Electrochemical setup

3.3.3.1 Second generation sensing

Cyclic voltammetry was performed on the GOD functionalised graphene electrode with different amounts of glucose added to the FDM solution (21 mL). The electrochemical response to additions of glucose, in the presence of 50 µM FDM in 0.1 M phosphate buffer (pH 7.4) is shown in figure 3.7. There is a clear peak at *ca*. 0.5 V (*vs*. SCE) which can be attributed to the oxidation of ferrocene dimethanol. The peak, however, decreases upon addition of glucose indicating that glucose oxidation is inhibiting the oxidation of FDM.

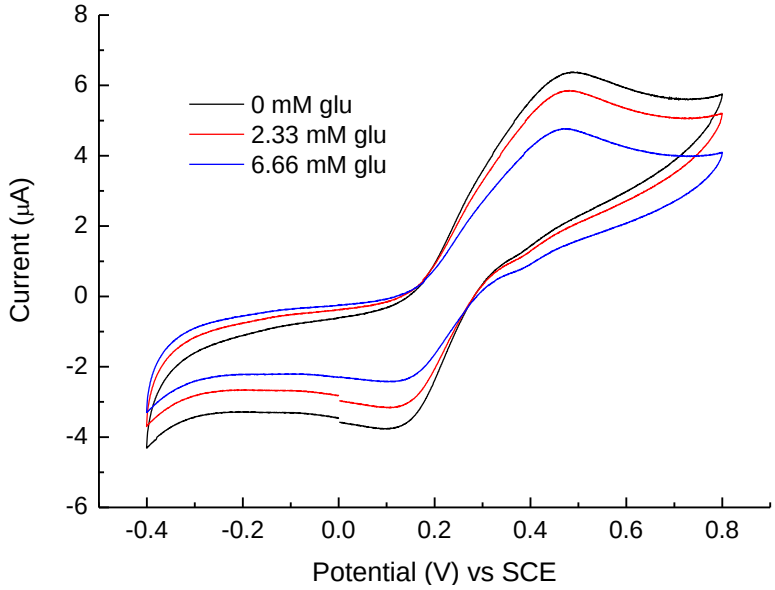

Figure 3.7. Signal detected on a GOD functionalised graphene electrode in response to additions of glucose to a FDM solution. The scan rate was 100 mV/sec.

In order to improve the ferrocene signal, ferrocene-carboxylic acid was reacted with (2-aminoethoxy) acetic acid according to the equation displayed in figure 3.1. The ferrocene mediator presented in figure 3.1 was then coated next to the enzyme to induce more efficient electron transfer by covalently bonding with free 1-PBASE linkers (figure 3.8). Tethering the redox mediator to the graphene surface means the ferrocene mediator is within close proximity to the GOD enzyme and it enables better electron transfer.

Figure 3.9 demonstrates cyclic voltammogram signals upon addition of glucose to the ferrocene-amine coated graphene electrode. The CVs were acquired in 8 mL of 0.1 M phosphate buffer drop (pH 7.4) to which glucose was added in varying concentrations. Again there is a peak at 0.5 V (*vs* SCE) corresponding to the ferrocene complex oxidation, however, no significant change in the signal is seen for different glucose concentrations. As the ferrocene-mediated detection did not display a significant catalytic signal, a simpler first

generation glucose biosensor (i.e., one relying on hydrogen peroxide with respect to redox detection) was tested in the next section (see figure 3.10).

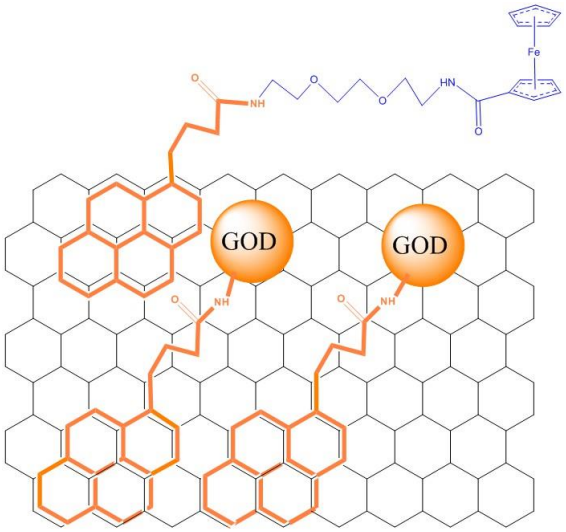

Figure 3.8. Ferrocene derived mediator (in blue) coated on "free" 1-PBASE linkers (in orange) alongside GOD coated with the same linker.

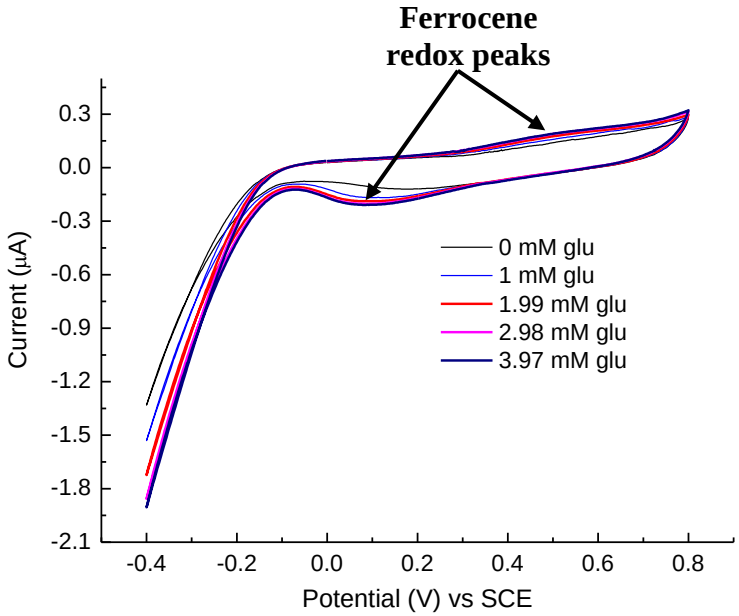

Figure 3.9. Response to glucose on a graphene electrode functionalised with GOD and 0.27 mM ferrocene-amine at a scan rate of 20 mV/sec. A small redox signal corresponding to ferrocene is observed at 0.5 V and 0.1 V vs SCE for the oxidation and reduction respectively. However no significant current change is observed with additions of glucose.

3.3.3.2 First generation sensing

3.3.3.2.1 "Large volume" electrochemistry

First generation sensing relies on detection of hydrogen peroxide produced during glucose oxidation. Figure 3.10 presents cyclic voltammetric results obtained following successive 20 µL additions of a concentrated glucose solution (500 mM in phosphate buffer pH 7.4) in 8 mL. An increase in the catalytic oxidative signal was identified at 0.7 V vs SCE with additions of glucose. Although lacking of linearity as displayed in the insert of figure 3.10, the increase of current seemed to be caused by the reaction of glucose with GOD producing H_2O_2 oxidised at the electrode. This was confirmed in figure 3.11 where serial additions of H_2O_2 were made on a bare CVD graphene electrode and the oxidative peak profile resembles the one obtained in figure 3.10.

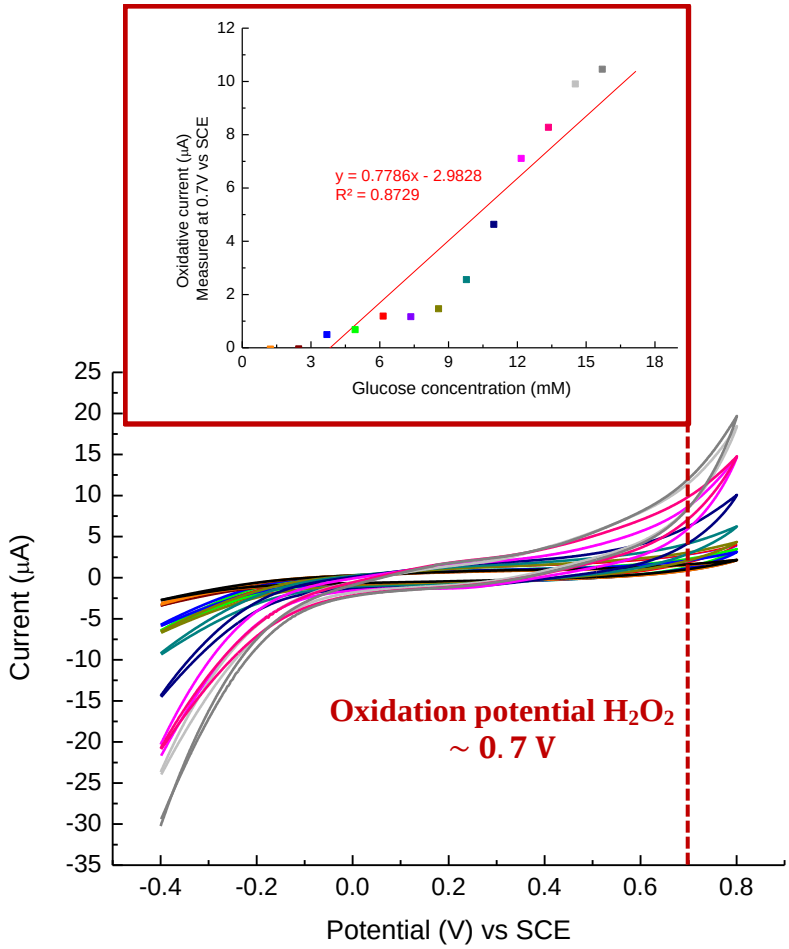

Figure 3.10. Response to glucose on a graphene electrode functionalised with GOD and detected via the redox properties of the enzymatically produced H_2O_2. The bulk solution was stirred mechanically. The insert is a calibration curves presenting oxidative current = f(glucose concentration) at 0.7 V against SCE. The scan rate was 20 mV/sec.

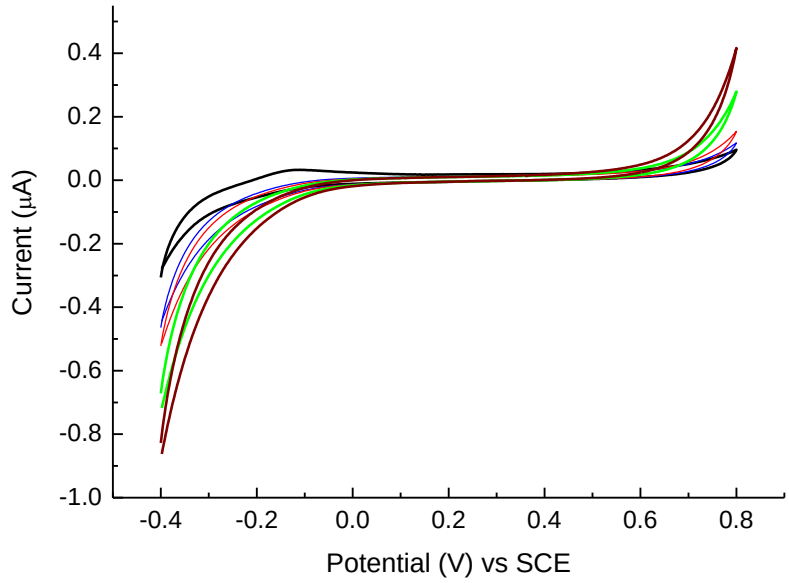

Figure 3.11. Cyclic voltammetry on a bare (i.e., no GOD) CVD graphene electrode as a function of H_2O_2 concentration in an 8 mL electrochemical cell. A characteristic oxidative signal is observed at ~ 0.7 V against a SCE. The scan rate was 20 mV/sec.

3.3.3.2.2 "Small volume" electrochemistry

To facilitate mass transfer of glucose to the electrode, the volume of the electrochemical 'cell' was reduced to 40 μL (0.1 M phosphate buffer pH 7.4). Figure 3.12 illustrates the cyclic voltammetric results obtained on a series of 40 μL drops containing increasing concentrations of glucose. The graphene flake was non-covalently coated with 1-PBASE and GOD. It again shows the characteristic H_2O_2 oxidation peak at *ca*. 0.7 V (*vs* Ag pseudo reference) which increases upon addition of glucose to the solution. The inset graph shows a clear linear trend of glucose concentration versus current measured indicating that the small volume of the test solution is a much more preferential set-up than the large volume case.

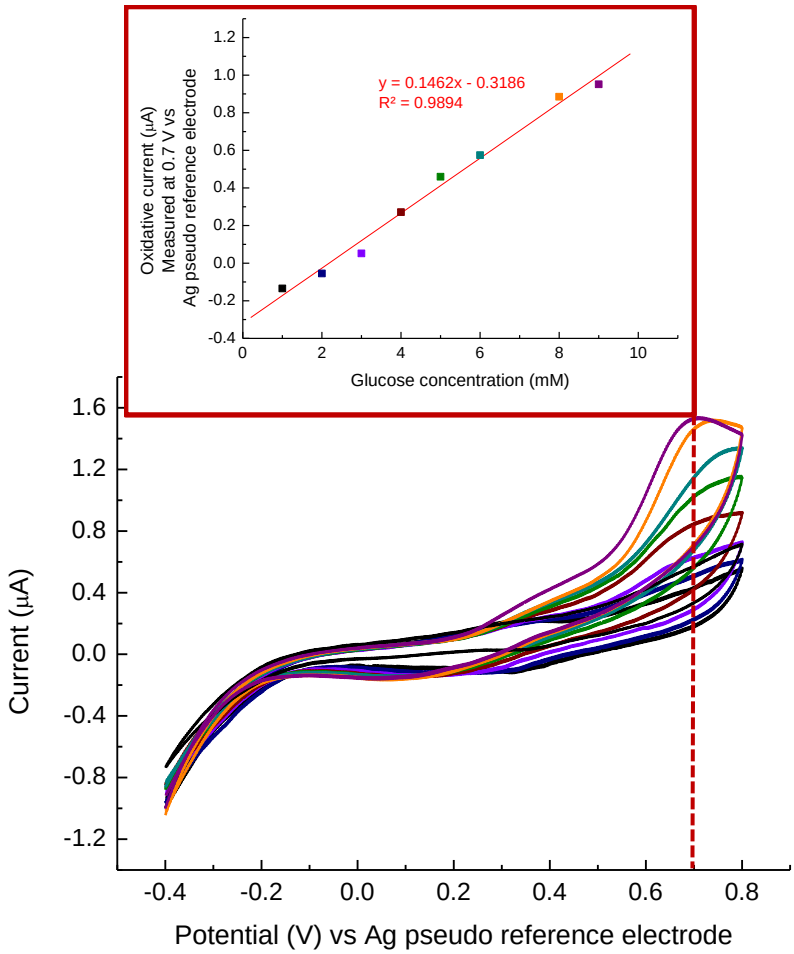

Figure 3.12. Cyclic voltammetry on a graphene electrode, non-covalently functionalised with GOD, as a function of glucose concentration in an "electrochemical cell" of 40 µL. The reference electrode was an Ag wire acting as a pseudo-reference electrode, the counter electrode was a Pt wire. The scan rate was 20 mV/sec. (The Ag wire was not ideal and was replaced by Pt in chapter 2 and 4 and later an homemade Ag/AgCl micro reference electrode because GOD is inhibited by metal ions (and especially Ag^{+}) in solution [29]).

3.4 Discussion

3.4.1 AFM imaging of CVD graphene transferred on Si/SiO_2

Figure 3.2 is a visualisation of a typical graphene sample transferred onto CVD graphene following the protocol exposed in chapter 2, section 2.2.2.1 and obtained via Atomic Force Microscopy. It displays several features identified as: monolayer graphene, multilayer graphene, foldings and drying circles. The blue region on figure 3.2 was estimated to be monolayer since its thickness (between this region and the wafer) was measured as 0.445 nm (figure 3.3).

The starting point of this thesis is the integration of chemical vapour deposited (CVD) graphene into a glucose sensing device. The reason behind the choice of graphene over other already studied electrode materials (glassy carbon, platinum, gold and, more recently, carbon nanotubes [30]) and other types of graphene (exfoliated graphene, graphene oxide, graphene grown on a support [31]) is principally related to the detection techniques to be used as presented in chapter 1. The basal plane monolayer visualised in blue in figure 3.2 would benefit a FET configuration, while other structures like cracks or folding would be of interest in an electrochemical design (the demonstration have been made that "graphitic islands" play a dominant role in the electrochemical signal of CVD graphene [32]). A sketch of CVD graphene is presented in figure 3.13 and corresponds to the AFM visualisation of a representative transferred sample (figure 3.2). It presents different regions of monolayer graphene, several layers of graphene and multi-layered graphite islands. From these observations it would appear that the nanomaterial could be of interest in both detection setups. Furthermore, it will be modified in chapter 4 with nanoparticles which will greatly improve the electron transfer to the nanomaterial and hence the catalytic signal (see chapter 4 section 4.1.1). Finally, several other interesting qualities of CVD graphene described in chapter 1 section 4 would also be highly beneficial to the final design (Flexibility, multiplexing, etc.).

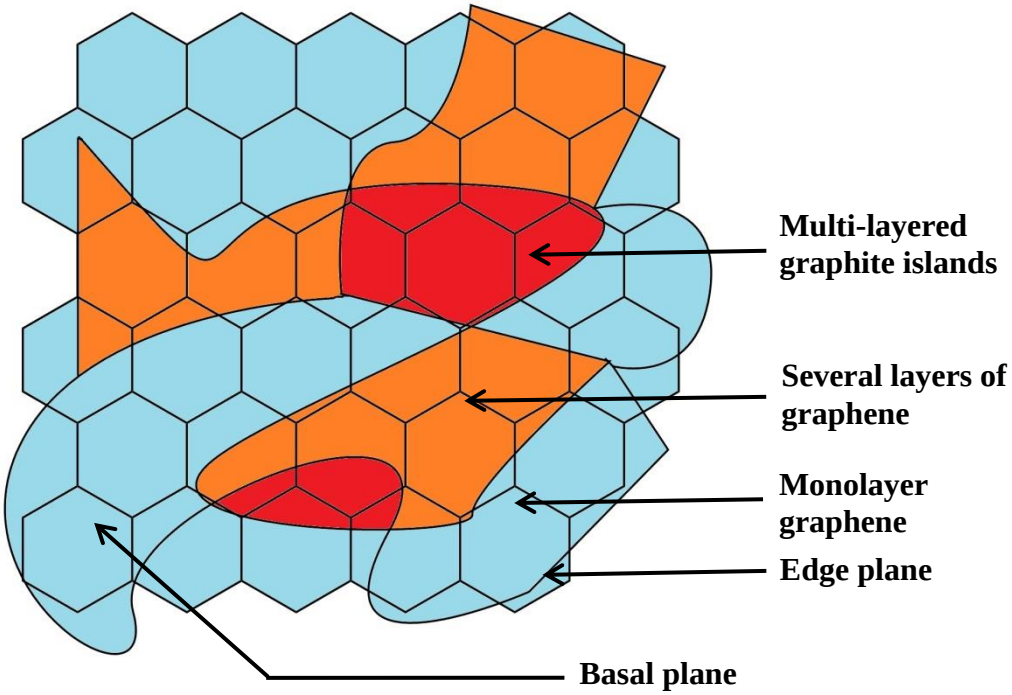

Figure 3.13. Sketch of graphitic/graphene islands formed when CVD graphene is deposited on a substrate.

3.4.2 Field effect transistor

Graphene presents two fundamental states (see chapter 1, figure 1.15), where either electrons (valence band) or holes (conduction band), are in the majority. When considering a $I_{SD} = f(V_{GD})$ representations, two fundamental characteristics regarding the doping of the nanomaterial and the charge carriers are identified in figure 3.14-A and figure 3.14-B.

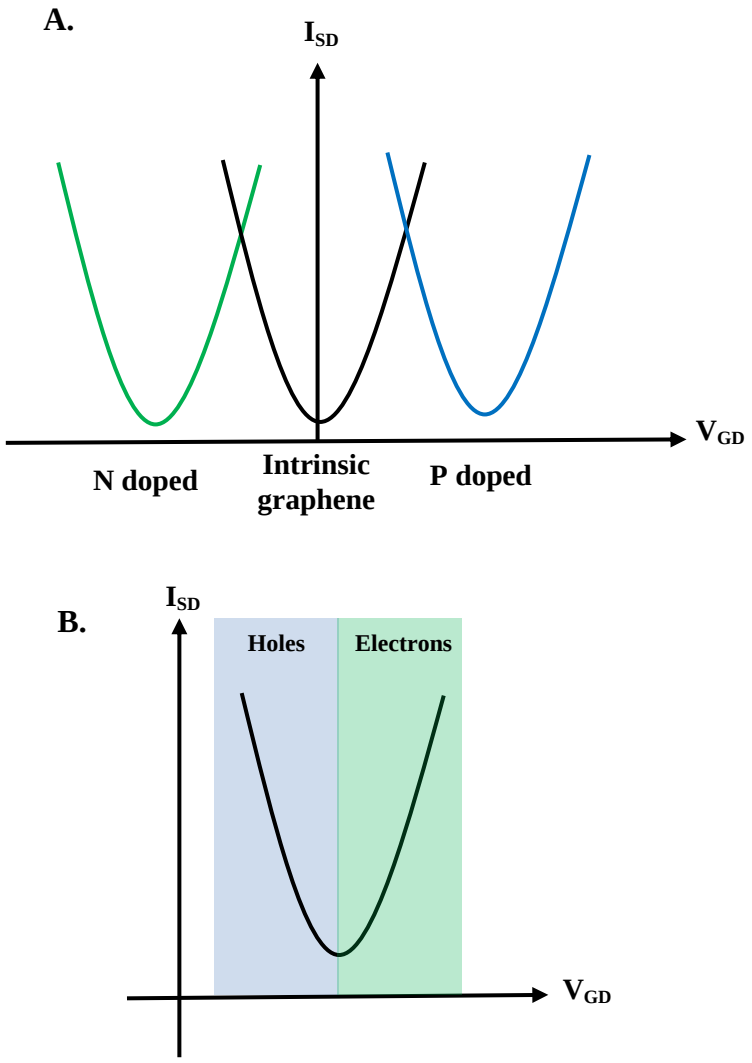

Figure 3.14. Electronic profile of a graphene FET. A: Representation of the Dirac point shift as a function of the N or P doping. Theoretically the Dirac point of intrinsic graphene sheet should be observed at V_{GD} = 0 and it would shift towards positive gate potential with a P doping (majority of holes) and towards negative gate potential with N doping (majority of electrons) [33, 34]. B: Representation of the two areas corresponding to a majority of holes or electrons on a $I_{SD} = f(V_{GD})$ curve [35].

CVD graphene presents a P type doping, with a Dirac point at around 0.3 V [36], (figure 3.5). Figure 3.6 introduces a shift in the Dirac point with glucose oxidase catalytic reaction (production of 3 H^+ at each enzymatic entity; chapter 2, figure 2.7). This shift is also observed with the same graphene FET tested with phosphate buffers of decreasing pH (figure 3.4). These experimental observations are in good agreement with the electronic properties exposed in figure 3.14: the more positive charges will be produced or present near the graphene surface the more it will shift the Dirac point towards high V_{GD}. The developed GOD/CVD graphene FET sensor was hence demonstrated to be sensitive to enzymatically produced proton.

Another noticeable effect was observed in figure 3.5 which displays a positive shift of around 0.07 V (V_{GD}) with GOD non-covalently linked to the graphene. GOD naturally bears a negative charge in phosphate buffer at pH 7.4 [37]. The Dirac point should therefore shift towards low V_{GD} but the opposite effect was observed. A conductance shift has been described to be caused by the enzymatic layer formed on top of the nanomaterial that would limit the access of the ions in solution to the transducer that could explain the depicted effect [38].

An H^+ sensitive transistor platform was therefore demonstrated. This design was however not appropriate for the aimed non-invasive application because of: (1) the complexity of manipulation and building of such sensors, (2) the internal limitations of any ISFET (buffer strength, storage, stability, etc…) and (3) the complicated integration with non-invasive detection techniques (top gating, multiplexing, etc…). The development of the FET configuration was hence not studied further, it was nevertheless promising (leading the way to the future enzymatic sensor development) and could be re-implemented in the final non-invasive sensor design along with the amperometric sensor as a single Na^+ detector for calibration of the device (see chapter 5, section 5.1.1 and chapter 6, section 6.2).

3.4.3 Electrochemical sensor (Second generation/First generation detection)

Figure 3.7 studies the ferrocene-mediated cyclic voltammetric detection of glucose. It was ineffective in the system studied: the oxidative signal decreasing with additions of glucose. This could be due to the hydrogen peroxide produced during glucose oxidiation inhibiting the oxidation of ferrocene and therefore decreasing the signal upon additions of glucose to the system. Similarly when the redox mediator was functionalized on the graphene there was no significant improvement in the catalytic activity of the glucose sensor (figure 3.9). The aim of the latter was to bring the mediator closer to the enzyme while benefiting from the free 1-PBASE sites (after GOD functionalization). Even though a ferrocene redox signal was identified (oxidation: ~ 0.5 V vs SCE and reduction ~ 0.1 V vs SCE) no increase of oxidative signal was observed with addition of glucose. This lack of ferrocene electro-activity may have been due to: (a) dissolved oxygen competing with the redox mediator for the electron

transfer [39], (b) the distance between the mediator and the catalytic redox centre being limiting [12]. (c) the synthesized ferrocene-amine being unstable [40].

In contrast, a promising sensing of glucose was obtained with a first-generation design involving H_2O_2 oxidation (production of electrons at the WE detected at 0.7 V vs the RE, see figure 3.10). The signal, although not entirely linear, showed great potential in terms of catalytic current increase and display a similar cyclic voltammetry behaviour than with addition of H_2O_2 on a bare CVD graphene electrode (figure 3.11). Remarkably, the catalytic oxidative signal obtained at 0.7 V vs SCE in figure 3.11 is particularly low compared to figure 3.10. This was most likely attributed to the poor quality of the electrode used in the experiment but did not impact on the attribute we wanted to study which was the shape of the redox signal of H_2O_2 on a CVD graphene electrode. The peak obtained in figure 3.11 appears to look like the redox signal obtained in figure 3.10, hence confirming the detection of H_2O_2.

It was therefore decided to develop and improve a H_2O_2 based CVD graphene sensor that will in turn be integrated into a reverse iontophoresis set-up for non-invasive transdermal glucose monitoring (chapter 5). Some of the preliminary results with different GOD entrapment had previously been exposed in chapter 2, section 2.3.2, and the capacity and performance of the final sensor design will be explored in chapter 4.

3.4.4 Miniaturization of the sensor reaction receptacle

The miniaturization of the volume of buffer for first generation sensing was finally demonstrated which led to the introduction of a small gel platform presented in chapter 2, section 2.3.2 and the rest of the thesis. First generation sensing was first introduced in a large volume reservoir of 21 mL (figure 3.10), however, intuitively this design was not ideal for two reasons: (1) it will be unpractical for future application as a non-invasive sensor and (2) the oxidation signal is more dependent on diffusion of H_2O_2 in a large volume electrochemical cell than in a miniaturized setup (diffusion is a function of the distance from the electrode, see equation 3.1). It was therefore decided to reduce the volume down to a drop (40 µL) in figure 3.12. This downscaling of the reaction reservoir provided a more defined peak at 0.7 V vs Ag pseudo reference electrode. While the origin of the difference in the oxidative shape is uncertain, the catalytic current from figure 3.10 to figure 3.12 was almost doubled: 4 mM of glucose gave a catalytic current of ~ 0.132 µA in figure 3.10 and ~ 0.266

µA in figure 3.12. However, a liquid receptacle was still inappropriate for skin implementation. The consistency of the drop volume itself was therefore changed to a hydrogel (see chapter 2, section 2.3.2). The new catalytic signal was promising and the detection platform was now appropriate for integration in the non-invasive device, as opposed to a liquid based reservoir.

3.5 Conclusions

This chapter presented different detection platforms for the design of the glucose biosensor. A FET was investigated and presented promising results towards the detection of enzymatically produced H^+. This setup was, however, discarded in the early stages of the development process due several drawbacks regarding the future implementation of the sensor. An electrochemical detection was instead preferred and again two glucose detection methods were compared: First generation and second generation sensing. The latter is a good strategy to replace H_2O_2 detection (and therefore the need for O_2) and enable to reduce the detection potential which will be beneficial to a specific detection of glucose (the lower the oxidation potential against the RE, the fewer oxidations from interferent molecules). The introduction of ferrocene in the design, however, failed to provide a catalytic signal, and mediated detection was therefore discarded. On the other hand, the first generation platform demonstrated promising catalytic activity towards glucose and was hence chosen as the basis for the rest of the sensing operations described in the other chapters. In an attempt to find an appropriate design for the integration of the sensor in a non-invasive device placed on the skin, the dimensions of the reaction receptacle were reduced to a droplet size (40 µL). The catalytic signal obtained from this miniature dimension setup was improved and led to the design of the agarose gel reservoir described in chapter 2, sections 2.2.2.7.2 and 2.3.2. The combination of the findings of chapter 2 on the enzymatic functionalization and chapter 3 on the sensor principle of detection provided a strong basis towards the study of the sensor performance in chapter 4.

1. Tang, W., et al., *Glucose Biosensor Based on a Glassy Carbon Electrode Modified with Polythionine and Multiwalled Carbon Nanotubes.* PLoS ONE, 2014. **9**(5): p. e95030.
2. Xia, Y., et al., *Nonenzymatic amperometric response of glucose on a nanoporous gold film electrode fabricated by a rapid and simple electrochemical method.* Biosensors and Bioelectronics, 2011. **26**(8): p. 3555-3561.
3. Fang, B., et al., *Silver Oxide Nanowalls Grown on Cu Substrate as an Enzymeless Glucose Sensor.* ACS Applied Materials & Interfaces, 2009. **1**(12): p. 2829-2834.
4. Janata, J. and S.D. Moss, *Chemically sensitive field-effect transistors.* Biomed Eng, 1976. **11**(7): p. 241-5.
5. Schoning, M.J. and A. Poghossian, *Recent advances in biologically sensitive field-effect transistors (BioFETs).* Analyst, 2002. **127**(9): p. 1137-51.
6. Kwak, Y.H., et al., *Flexible glucose sensor using CVD-grown graphene-based field effect transistor.* Biosensors and Bioelectronics, 2012. **37**(1): p. 82-87.
7. Guascito, M.R., et al., *Mediator-free amperometric glucose biosensor based on glucose oxidase entrapped in poly(vinyl alcohol) matrix.* Analyst, 2011. **136**(1): p. 164-173.
8. Guascito, M.R., et al., *Low-potential sensitive H_2O_2 detection based on composite micro tubular Te adsorbed on platinum electrode.* Biosensors and Bioelectronics, 2011. **26**(8): p. 3562-3569.
9. Horozova, E., et al., *Electrocatalytic Reduction of Hydrogen Peroxide on Palladium-Gold Codeposits on Glassy Carbon: Applications to the Design of Interference-Free Glucose Biosensor.* International Journal of Electrochemistry, 2011. **2011**: p. 8.
10. Chu, P.K. and X. Liu, *Biomaterials Fabrication and Processing Handbook*. 2008: Taylor & Francis.
11. Shan, C., et al., *Direct Electrochemistry of Glucose Oxidase and Biosensing for Glucose Based on Graphene.* Analytical Chemistry, 2009. **81**(6): p. 2378-2382.
12. Rusling, J.F., B. Wang, and S.-e. Yun, *Electrochemistry of Redox Enzymes*, in *Bioelectrochemistry*. 2008, John Wiley & Sons, Ltd. p. 39-85.
13. Kollipara, S. and T.T.U. Chemistry, *Theoretical Studies of Rates of Electron Transfer Between Cytochrome 5 Reductase and Cytochrome B5*. 2008: Tennessee Technological University.

14. Francke, R. and R.D. Little, *Redox catalysis in organic electrosynthesis: basic principles and recent developments.* Chemical Society Reviews, 2014. **43**(8): p. 2492-2521.
15. Lyons, M., *Mediated Electron Transfer at Redox Active Monolayers. Part 3: Bimolecular Outer-Sphere, First Order Koutecky-Levich and Adduct Formation Mechanisms.* Sensors, 2002. **2**(12): p. 473-506.
16. Xiao, X., et al., *Nanoporous gold assembly of glucose oxidase for electrochemical biosensing.* Electrochimica Acta, 2014. **130**(0): p. 559-567.
17. Herzog, G., Richard C. Alkire, Dieter M. Kolb and Jacek Lipkowski *(Eds): Bioelectrochemistry. Fundamentals, Applications and Recent Developments.* Chromatographia, 2014. **77**(1-2): p. 201-201.
18. Mano, N., F. Mao, and A. Heller, *Characteristics of a Miniature Compartment-less Glucose−O2 Biofuel Cell and Its Operation in a Living Plant.* Journal of the American Chemical Society, 2003. **125**(21): p. 6588-6594.
19. Prévoteau, A. and N. Mano, *Oxygen reduction on redox mediators may affect glucose biosensors based on "wired" enzymes.* Electrochimica Acta, 2012. **68**(0): p. 128-133.
20. Fukushima, T., et al., *Mechanism of Cytotoxicity of Paraquat.* Environmental Health and Preventive Medicine, 2002. **7**(3): p. 89-94.
21. Qu, F., et al., *Electrochemical Biosensing Platform Using Hydrogel Prepared from Ferrocene Modified Amino Acid as Highly Efficient Immobilization Matrix.* Analytical Chemistry, 2014. **86**(2): p. 973-976.
22. Battaglini, F., P.N. Bartlett, and J.H. Wang, *Covalent Attachment of Osmium Complexes to Glucose Oxidase and the Application of the Resulting Modified Enzyme in an Enzyme Switch Responsive to Glucose.* Analytical Chemistry, 1999. **72**(3): p. 502-509.
23. Göpel, W., et al., *Sensors, Chemical and Biochemical Sensors*. 2008: Wiley.
24. Bitri, N., et al., *Electrochemistry using single multiwalled carbon nanotubes – A step further.* Carbon, 2014. **69**(0): p. 113-121.
25. Harper, A. and M.R. Anderson, *Electrochemical Glucose Sensors—Developments Using Electrostatic Assembly and Carbon Nanotubes for Biosensor Construction.* Sensors, 2010. **10**(9): p. 8248.
26. Konash, A. and E. Magner, *Electrochemically Mediated Reduction of Horseradish Peroxidase by 1,1'-Ferrocenedimethanol in Organic Solvents.* Analytical Chemistry, 2005. **77**(6): p. 1647-1654.

27. Ishigami, M., et al., *Atomic Structure of Graphene on SiO2.* Nano Letters, 2007. **7**(6): p. 1643-1648.
28. Jin, S.H., et al., *Sources of Hysteresis in Carbon Nanotube Field-Effect Transistors and Their Elimination Via Methylsiloxane Encapsulants and Optimized Growth Procedures.* Advanced Functional Materials, 2012. **22**(11): p. 2276-2284.
29. Chen, C., et al., *Experimental Platform to Study Heavy Metal Ion−Enzyme Interactions and Amperometric Inhibitive Assay of Ag^+ Based on Solution State and Immobilized Glucose Oxidase.* Analytical Chemistry, 2011. **83**(7): p. 2660-2666.
30. Zhu, Z., et al., *A Critical Review of Glucose Biosensors Based on Carbon Nanomaterials: Carbon Nanotubes and Graphene.* Sensors, 2012. **12**(5): p. 5996-6022.
31. Soldano, C., A. Mahmood, and E. Dujardin, *Production, properties and potential of graphene.* Carbon, 2010. **48**(8): p. 2127-2150.
32. Brownson, D.A.C. and C.E. Banks, *CVD graphene electrochemistry: the role of graphitic islands.* Physical Chemistry Chemical Physics, 2011. **13**(35): p. 15825-15828.
33. Shanshan, C., et al., *Adsorption/desorption and electrically controlled flipping of ammonia molecules on graphene.* New Journal of Physics, 2010. **12**(12): p. 125011.
34. Guo, B., et al., *Controllable N-Doping of Graphene.* Nano Letters, 2010. **10**(12): p. 4975-4980.
35. Schwierz, F., *Graphene transistors.* Nat Nano, 2010. **5**(7): p. 487-496.
36. Suk, J.W., et al., *Enhancement of the Electrical Properties of Graphene Grown by Chemical Vapor Deposition via Controlling the Effects of Polymer Residue.* Nano Letters, 2013. **13**(4): p. 1462-1467.
37. Zhao, W., J.J. Xu, and H.Y. Chen, *Extended-range glucose biosensor via layer-by-layer assembly incorporating gold nanoparticles.* Front Biosci, 2005. **10**: p. 1060-9.
38. Besteman, K., et al., *Enzyme-Coated Carbon Nanotubes as Single-Molecule Biosensors.* Nano Letters, 2003. **3**(6): p. 727-730.
39. Wang, J., et al., *Comparison of oxygen-rich and mediator-based glucose-oxidase carbon-paste electrodes.* Analytica Chimica Acta, 2001. **441**(2): p. 183-189.
40. Bartlett, P.N., V.Q. Bradford, and R.G. Whitaker, *Enzyme electrode studies of glucose oxidase modified with a redox mediator.* Talanta, 1991. **38**(1): p. 57-63.

Chapter 4: Performance of the sensor

4.1 Introduction

This chapter builds on the work of the previous 2 chapters whereby previously it has been shown that the most promising way of measuring glucose concentrations with CVD graphene and GOD is through first generation sensing of H_2O_2. Glucose sensing can be improved through the use of metallic nanoparticles and this chapter aims to investigate their catalytic enhancement of glucose sensing. Chapter 2 also showed preliminary work on glucose sensing in a gel and this chapter will use the gel method developed in that chapter to make a sensor coupled with platinum nanoparticles.

4.1.1 Metal nanoparticles

In first-generation glucose sensors, H_2O_2 is a product of the enzymatic reaction of GOD with glucose. H_2O_2 is oxidised at an overpotential of 0.5 V to 0.7 V against SCE on a platinum electrode [1], and at ~0.7 V against SCE on graphene (Chapter 3, figure 3.10). There are three common interfering species associated with glucose biosensing: ascorbic acid (vitamin C), uric acid, and acetominophen (paracetamol). These three main interferents, which are often present in biological samples, are also oxidised at a similar potential [2]. It is therefore an important aim to reduce the potential at which H_2O_2 is oxidised so as to avoid such interferences. The typical use of a mediator to replace oxygen and lower the oxidation potential was ruled out early in the device development process, and attention was instead focused on the use of metallic nanoparticles.

Metallic nanoparticles combined with carbon nanomaterial electrodes have been shown to dramatically enhance electron transfer and electrocatalytic activity in biosensors. It was hence of interest to study the combination of nanoparticles with CVD graphene (already considered a useful nanomaterial for electron transfer [3]) that would potentially lower the potential for glucose detection.

An enhancement of electron transfer turnover rate was demonstrated with addition of gold nanoparticles alongside a reconstituted apo-glucose oxidase enzyme (from ~ 700 cm^{-1} to ~ 5,000 cm^{-1}) [4]. This effect is due to excellent electrical conductivity and the quantum size effect of the nanoparticles. A quantum size effect is observed when the dimension of the nanoparticles is of the order of the de Broglie wavelength of the valence electrons (wavelength associated with a particle, function of the mass *m* and the velocity *v* of the nanoparticle and the Planck constant *h*), [5]. A noble metal such as platinum also displays good electrocatalysis towards H_2O_2. Several authors have demonstrated the benefit of platinum nanoparticles for the study of the oxidation of H_2O_2 due to the electrochemical stability and the biocompatibility of the nanomaterial [6]. The oxidation of hydrogen peroxide is displayed in equation 4.1 [7]. Both the dimensions and electrocatalytic activity of the nanoparticles induce a synergetic effect with the enzymatic reaction towards the electrochemical detection of the produced H_2O_2 [8].

$$H_2O_2 \longrightarrow O_2 + 2\,H^+ + 2\,e^- \qquad (4.1)$$

4.1.2 Sensitivity

Sensitivity is a fundamental attribute of any sensor. It is defined as the slope of the change of current with increasing concentrations. This value, however, is only applicable if the sensor response is linear. The linear range of a calibration curve is the range at which the sensor signal is proportional to a change in concentration. The linear range is different from the dynamic range which describes the range at which a change in concentration will lead to any sort of noticeable change in signal. The linear range along with the limit of detection (LOD) are essential analytical tools to characterise a biosensor [9-11].

Any analytic assay, even extremely precise, cannot measure concentrations in a dynamic range down to zero. There is in every sensing device a limit of detection. It is defined by the International Conference of Harmonisation (ICH) as: “the lowest amount of analyte in the sample, which can be detected but not necessarily quantitated under stated experimental conditions”. It is differentiated from the limit of quantitation (LOQ) defined as: “the lowest amount of analyte in a sample, which can be quantitatively determined with suitable precision and accuracy” [12]. In the following, the interest will be focused on the LOD in order to

assess the lowest signal differentiated from the background noise. It was estimated using the linear regression method:

$$LOD = \frac{3.3\sigma}{S} \quad (4.2)$$

where σ is the standard deviation of the noise and S is the slope of the linear plot of the concentration curve [12].

Linear range and LOD are the most famous parameters to characterise the performance of any sensor since it introduces the working sensing range and the limit under which no signal will be differentiated from the background noise [13].

The following is an investigation of these characteristics for the developed sensor along with additional properties such as repeatability and stability. The repeatability refers to the "in-laboratory" precision with repeated measurements. It is differentiated from reproducibility which studies the "between-laboratory" precision. In order to achieve statistical significance the number of repeats, n, needs to be at least equal to 3. The stability of a sensor can be differentiated into 3 definitions: working stability, storage stability and long-term stability. The working stability is measured during a continuous operation. The storage stability relates to the stability obtained after storage. Finally, the long term stability describes the stability during an experiment in a sample solution that is not necessarily continuous. The stability of the sensor described in section 4.3.6 refers to the storage stability.

This chapter will determine the limit of detection and linear range for platinum nanoparticle catalysed glucose detection through a gel on CVD graphene to find out the sensitivity of the biosensor.

4.2 Materials and experimental methods

4.2.1 Materials

Hydrogen hexachloroplatinate (IV) hydrate, potassium chloride, H_2SO_4, glucose oxidase type X-S, (EC 1.1.3.4), 100,000-250,000 units/g solid (without added oxygen), low gelling temperature agarose, D-glucose, KCl, NaH_2PO_4 and Na_2HPO_4 were purchased from Sigma

Aldrich. Agarose was purchased from Fisher. Ag and Pt wires were purchased from Advent. Other materials (such as CVD graphene, 495 PMMA A3, etc.) were the same as the ones described in chapter 2, section 2.2.1.

4.2.2 Experimental methods

4.2.2.1 Preparation of a homemade micro Ag/AgCl electrode

A micro-Ag/AgCl electrode was used to maintain a relatively stable potential with respect to the working electrode. The electrode was prepared by coating a 0.25 mm diameter, 99.95% pure, silver wire with AgCl by chronoamperometry in a 3.5 M KCl solution with Pt as reference and counter electrodes, for 1 hour at 1 V. The wire was then encased in a 1% w/v agarose gel containing 0.1 M KCl in a 100 µL micropipette tip (figure 4.1). The electrode was stored in 0.1 M KCl (replaced every month) at 4 ˚C when not in use. The electrode held only a low (0.1 M) KCl concentration to limit the amount of glucose oxidase inhibitor present (see chapter 1 section 1.3.2). Stability of the electrode was checked every week against a solution of 0.1 mM ferrocene dimethanol in 0.1 M phosphate buffer pH 7.4, against a standard saturated calomel electrode (SCE) (figure 4.2 and 4.3). The reason behind this monitoring was to assess if the electrode, while not being in saturated KCl, kept a stable potential which will be appropriate for electrochemical measurements.

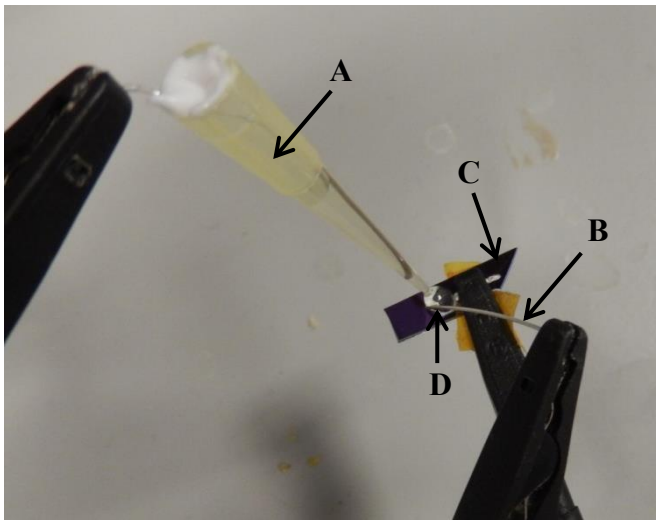

Figure 4.1. The electrochemical setup. A is the micro-Ag/AgCl reference electrode (encased in agarose gel), B is the Pt counter electrode, C is the working graphene electrode, and D is the GOD/Hydrogel. The setup is mounted with helping hands and flat connectors. The connection between the silver paint on the working electrode and the connector is achieved through a gold wire.

4.2.2.2 Electrode design

The sensing electrodes were first prepared as described in chapter 2 section 2.2.2.2 and then platinum nanoparticles were electrochemically deposited as followed.

4.2.2.3 Electrochemical deposition of platinum nanoparticles

Platinum nanoparticles were formed on the graphene electrodes by chronoamperometry for 1000 seconds in a 10 µL drop of a solution of 1.7 mM hydrogen hexachloroplatinate and 0.1 M H_2SO_4 at -0.5 V against a Pt pseudo-reference electrode, or -0.35 V against the Ag/AgCl micro reference electrode. Cyclic voltammetry was used to assess the chloride reduction potential before chronoamperometry was performed in the same solution and at the determined potential. A peak was observed at -0.5 V when using a Pt pseudo-reference electrode and at -0.35 V when using an Ag/AgCl micro reference (see figure 4.4-A) electrode which explains the difference of deposition potential. The deposition as well as characteristics of the nanoparticles are presented in figures 4.4 and 4.5.

4.2.2.4 GOD entrapment

GOD was incorporated into the gel when cited via the methods identified as *Entrapment 2* or *Entrapment 3*. These entrapment techniques were improvement of the previous *Entrapment 1* since the gel was formed directly on top of the electrode:

Entrapment 2: 12 µL of 1% w/v agarose in phosphate buffer pH 7.4 was heated (above 80 ºC) until a clear solution was obtained. It was then cooled down and directly casted onto the electrode at ~ 28 ˚C. 12 µL of an 8 mg/mL solution of GOD in phosphate buffer was immediately added on top of the gel at about 20 ˚C.

Entrapment 3: 12 µL of an 8 mg/mL solution of GOD was deposited directly on the electrode. Then 12 µL of 1 % w/v low gelling temperature agarose (which had been heated and cooled down in the same way as entrapment 2) was deposited on top of the enzyme at ~ 28 ˚C, i.e., a temperature low enough to maintain the enzyme's catalytic and structural properties [14] while enabling efficient entrapment in the gel.

4.2.2.5 Determination of the gradient concentration curves

To assess the sensitivity of the sensor, its performance was determined in a range of glucose concentrations prepared from a stock solution of 100 mM glucose in phosphate buffer 0.1 M pH 7.4 and left to mutarotate overnight. Glucose calibration curves were acquired as described in chapter 2 section 2.3.2.1. The background was averaged over the time period displayed in red in figure 4.16, and in figure 4.18.

4.2.2.6 Determination of the sensor LOD

The limit of detection was calculated using equation 4.2. It involved the determination of the sensor sensitivity (or slope of the linear plot) and the standard deviation of the background displayed over the period depicted in red in figure 4.16 and figure 4.18. This period was purposely chosen as the stabilised amperometric background.

4.3 Results

4.3.1 Set-up characteristics and modification of the sensor with platinum nanoparticles

4.3.1.1 Stability of the homemade micro Ag/AgCl reference electrode

The stability of the newly created Ag/AgCl reference electrode was regularly tested with a glassy carbon electrode (WE) in 10 mL of 0.1 mM ferrocene dimethanol (FDM). Figure 4.2 presents cyclic voltammograms obtained with the same WE and CE (platinum wire) and FDM solution but with different RE, respectively a saturated calomel electrode (SCE) and the created micro Ag/AgCl reference electrode. The difference of half peak potential ΔE between the SCE and the micro Ag/AgCl electrode is then plotted in figure 4.3.

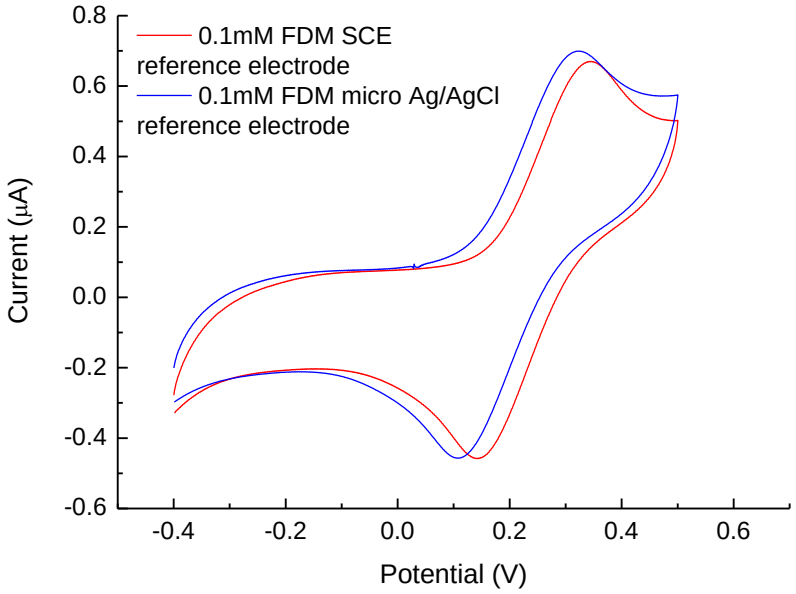

Figure 4.2. Comparison between the FDM redox signal (*ΔE*) measured against a traditional saturated calomel electrode (SCE) (red curve), and relative to a micro Ag/AgCl reference electrode (blue curve).

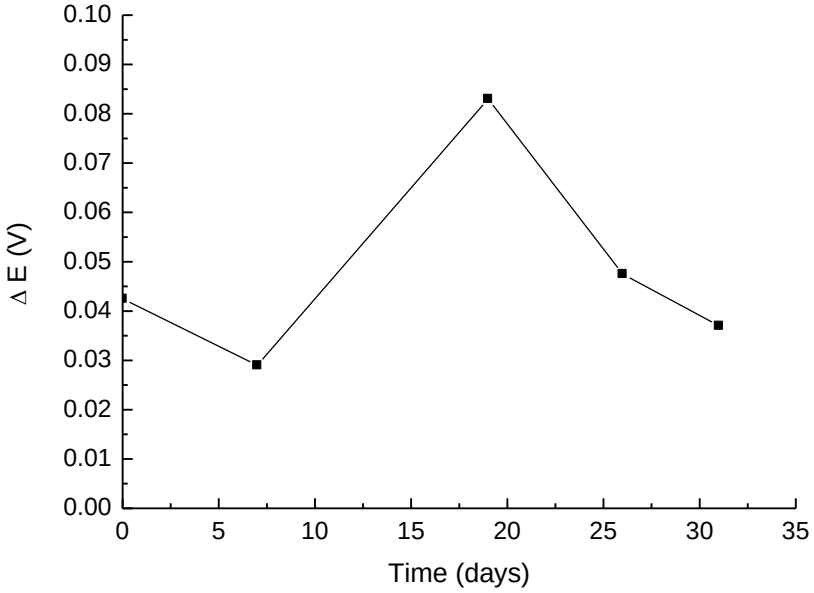

Figure 4.3. Stability of the micro Ag/AgCl electrode. The *ΔE* between the Ag/AgCl and a commercial SCE shows little variation over ~ 4 weeks.

The average *ΔE* was 47.8 mV (standard deviation: 20 mV), a reasonable value given that the typical potential variation between SCE electrode and Ag/AgCl electrode is 45 mV [15]. The electrode had a quite stable peak signal potential difference (Δ*E*), of only few mV, relative to the SCE (figure 4.3) and was therefore suitable for this study.

4.3.1.2 Platinum nanoparticle deposition

Figure 4.4-A shows a cyclic voltammogram obtained in a 10 µL drop of H_2SO_4 and hydrogen hexachloroplatinate. A clear reduction peak was identified at -0.35 V against Ag/AgCl and is attributed to platinum nanoparticle formation. Therefore this was the chosen potential for nanoparticle formation. The chronoamperometric signal was hence acquired for 1000 seconds at this potential (figure 4.4-B). The nanoparticles are formed following the reaction detailed in Figure 4.4-A (red insert), by aggregation at the electrode surface following chloride reduction.

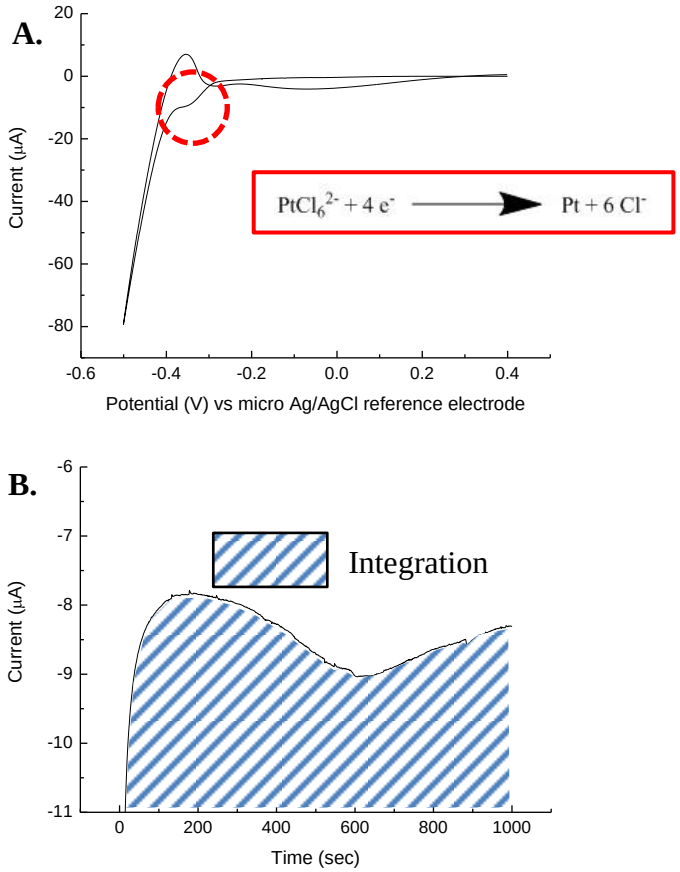

Figure 4.4. Deposition of platinum nanoparticles. A: cyclic voltammogram acquired in 10 µL of 0.1M H_2SO_4, 1.7 mM hydrogen hexachloroplatinate. There is a typical chloride reduction peak at about -0.35V against a micro Ag/AgCl reference electrode (red dotted circle). The scan rate was 20 mV/sec. B: Chronoamperometric signal corresponding to deposition of platinum at -0.35V against the micro Ag/AgCl electrode. The blue stripes, "area under the curve" (i.e. integration), will serve to calculate the mass of nanoparticles deposited using Faraday's law (equation 4.3).

The signal in figure 4.4-B was integrated (blue stripes) and gave a value for the charge Q of the deposition of 8.557 mC. This value was inserted in the Faraday's law (equation 4.3) and a mass of 9.086 µg was deduced for the nanoparticles produced.

$$m = \left(\frac{Q}{F}\right)\left(\frac{M}{z}\right) \qquad (4.3)$$

Faraday's law with Q the charge expressed in C, F the Faraday's constant expressed in C/mol, M the molar mass expressed in g/mol and Z the number of electrons involved to the reaction. The molecular weight of hydrogen hexachloroplatinate is 409.81 g/mol, 4 electrons are involved in the deposition reaction and the Faraday constant is 96485.34 C/mol.

Figure 4.5 shows cyclic voltammograms of a graphene electrode in phosphate buffer before and after platinum nanoparticle deposition. The bare graphene electrode shows a capacitive background response to the changing potential, however, upon deposition of platinum nanoparticles there is a clear oxidation peak at *ca*. 0.4 V (*vs*. Ag/AgCl) and a reduction peak at *ca*. 0 V (*vs*. Ag/AgCl). These peaks can be attributed to the formation of platinum oxide and reduction of platinum oxide nanoparticles respectively [16]. Scanning electron microscopy, figure 4.6, shows the nanoparticles to be of uniform size (*ca*. 375 nm) with some aggregates on the surface of the electrode but fairly uniformly distributed.

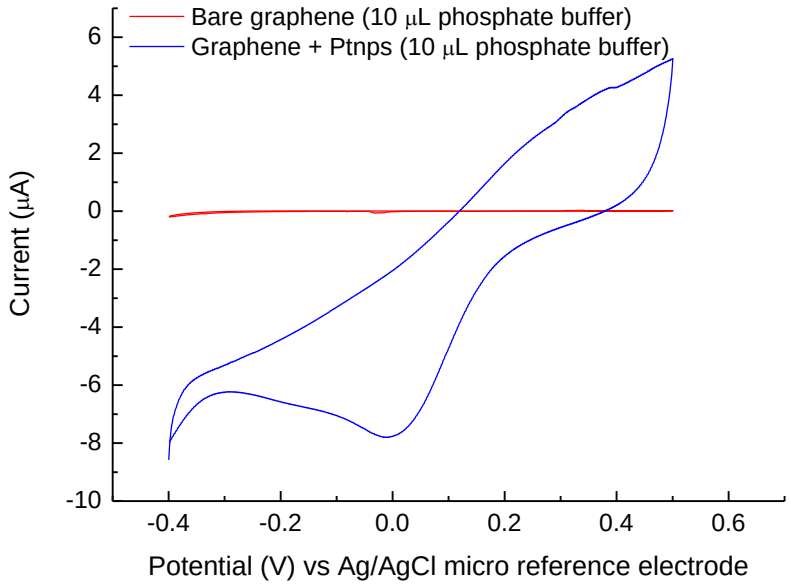

Figure 4.5. Cyclic voltammograms before and after platinum nanoparticle deposition. A significant increase in current and a characteristic redox signal is observed at *ca.* 0 V (reduction of platinum oxide) and *ca.* 0.4 V (platinum oxide formation) vs Ag/AgCl micro reference electrode, with addition of Pt nanoparticles. The scan rate was 20 mV/sec.

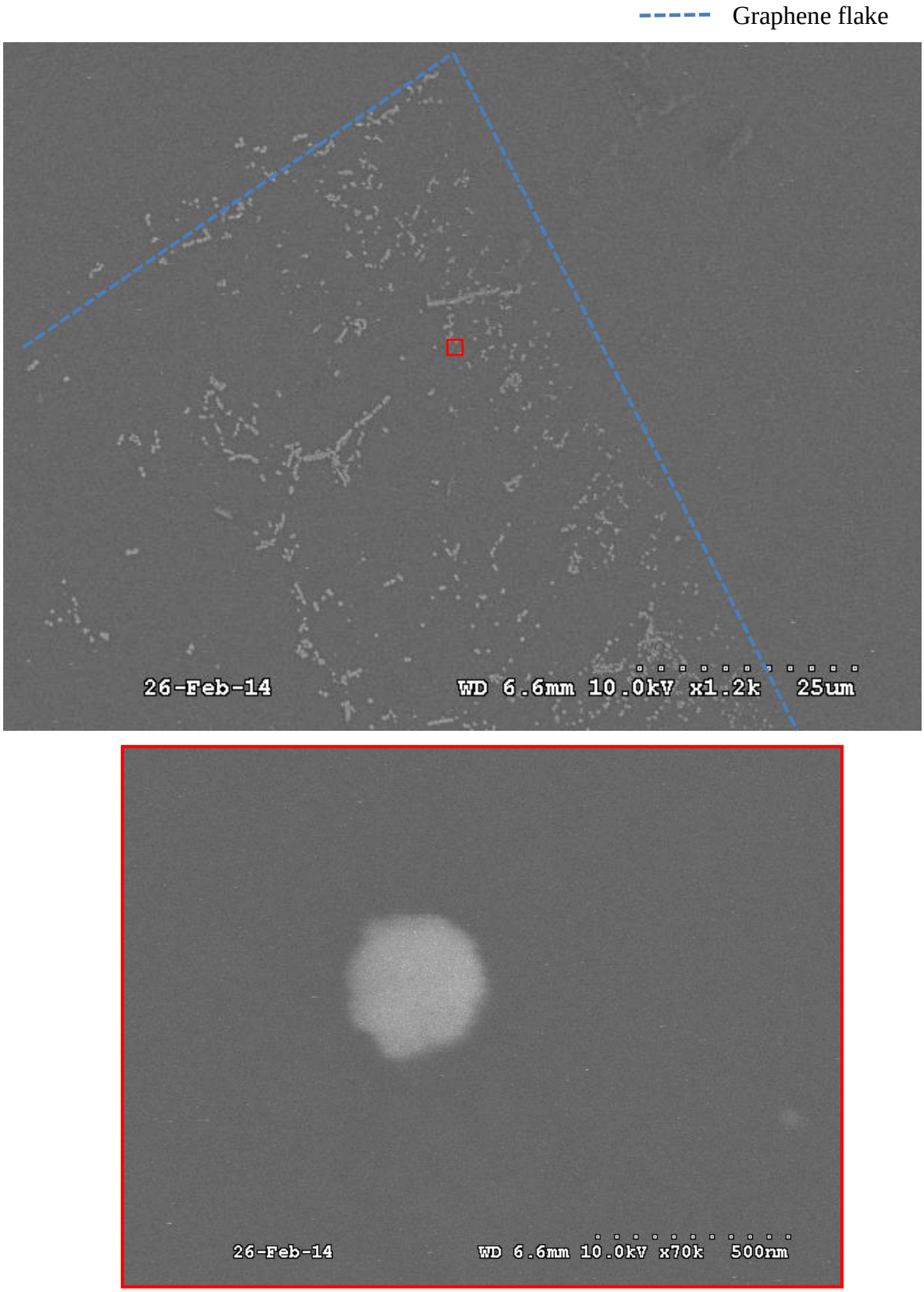

Figure 4.6. Scanning electron microscopy (SEM) pictures of Pt nanoparticles electrochemically deposited on CVD graphene. The red box is a zoom of a nanoparticle structure. This figure is not intended as an in depth characterisation of the nanoparticles, it rather provide an idea of the typical size and distribution of the nanoparticle structures.

4.3.2 Electrochemical catalytic activity with Graphene/Pt nanoparticles

The activity of the newly created graphene/Pt nanoparticle electrodes was first assessed against a series of glucose concentrations in 24 µL of a gel entrapping GOD using *entrapment method 1* (see chapter 2 section 2.2.2.7.2). Figure 4.7 shows the resulting cyclic voltammograms. A 1 µA level of increase in current is identified at ~0.4V against the Pt pseudo-reference electrode confirming the catalytic effect of platinum nanoparticles. The inset graph in figure 4.7 shows the increase in current with glucose additions to be non-linear in the all range of concentration while linear from 5 mM onwards. The reason for this could be because of interference effects from capacitive charging of the double layer during measurements.

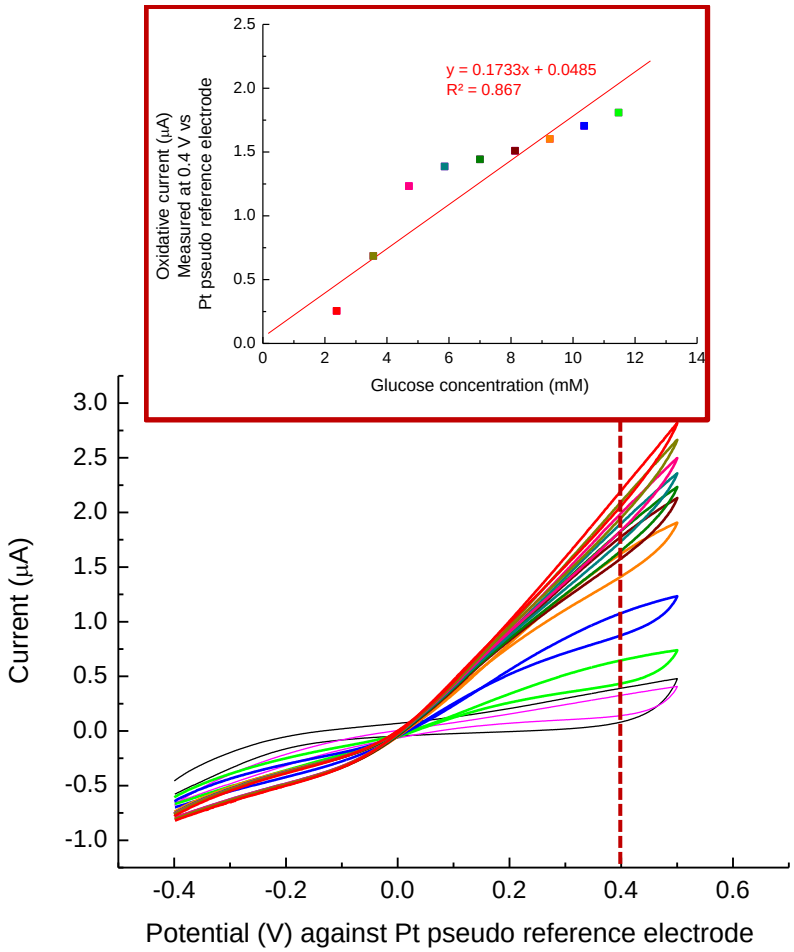

Figure 4.7. Cyclic voltammetry on a graphene/Pt nanoparticles electrode as a function of glucose concentration in a gel (24 µL) entrapping GOD - *Entrapment method 1*. Scan speed 20 mV/sec; one scan taken after each concentration step. The insert is a calibration graph displaying the oxidative H_2O_2 current (at 0.4 V vs the platinum pseudo reference electrode) produced as a result of the enzymatic reaction, as a function of glucose concentration added in the gel.

Chronoamperometric experiments were performed at 0.4 V (*vs.* Pt pseudo reference) as a function of glucose concentration (figures 4.8 and 4.9). First a series of 1 µL 0.1 M phosphate buffer additions (pH 7.4) were added to the gel to see if there was any effect of the mechanical addition of solution to the gel. Figure 4.8 shows the first 3 additions (blue arrows) to have no effect on the current indicating the sudden rush of solution into the gel has no effect. Next, a series of glucose additions to the gel (orange arrows) shows the current to clearly increase with each addition. The inset graph shows the trend to be linear in contrast to the cyclic voltammetry experiments (figure 4.7) indicating that chronoamperometry is a more reliable method to use. At the end of the experiment, 0.1 M phosphate buffer (pH 7.4) was again added to the gel. The current was shown to decrease slightly, possibly due to dilution effects, however, no significant change in the current was observed compared to glucose additions.

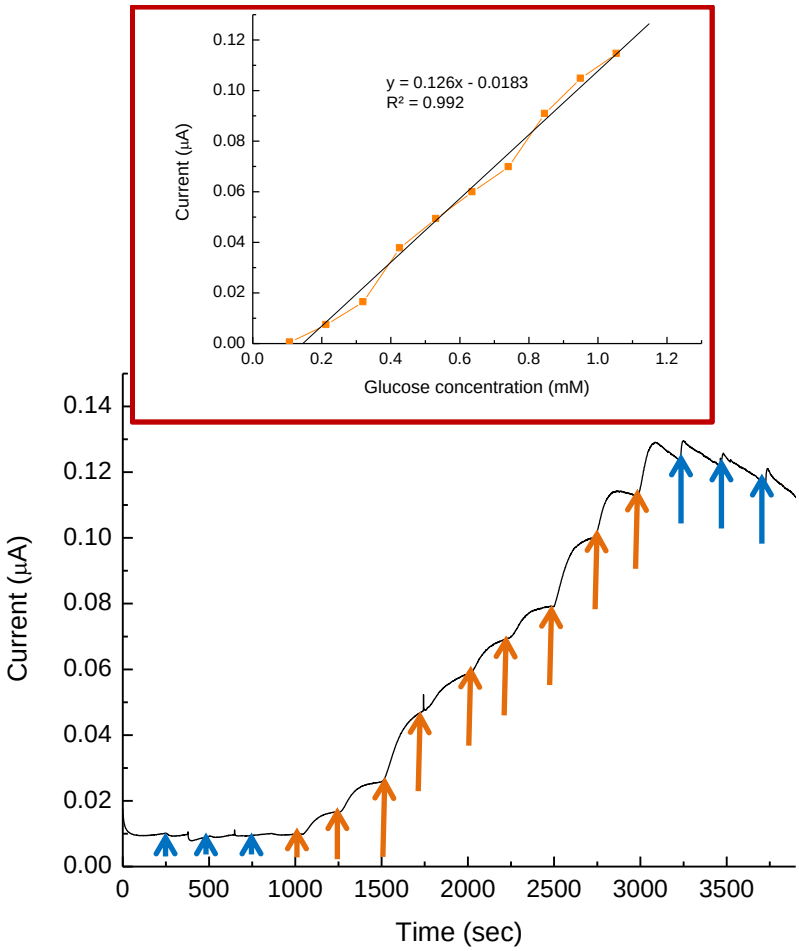

Figure 4.8. Chronoamperometry following successive (1µL) additions of glucose (orange arrows) to vary the concentration from 0.107 to 1.054 mM in a gel (24 µL) entrapping GOD - *Entrapment method 1.* Additions (1 µL) of phosphate buffer (blue arrows) acted as an appropriate control. Signals were acquired at 0.4 V against a Pt pseudo-reference electrode, 250 seconds separated successive additions. The insert is a calibration graph presenting the catalytic current acquired as a function of the glucose concentration added in the gel.

Figure 4.9 shows the chronoamperometry data obtained when a range of glucose concentrations are added to the gel. The smaller concentrations (1 μM and 10 μM) are barely visible on the chronoamperometry results. This would indicate that these concentrations are beyond the limit of detection. When concentrations of 100 μM and higher were added to the gel, the increase in current is clearly visible.

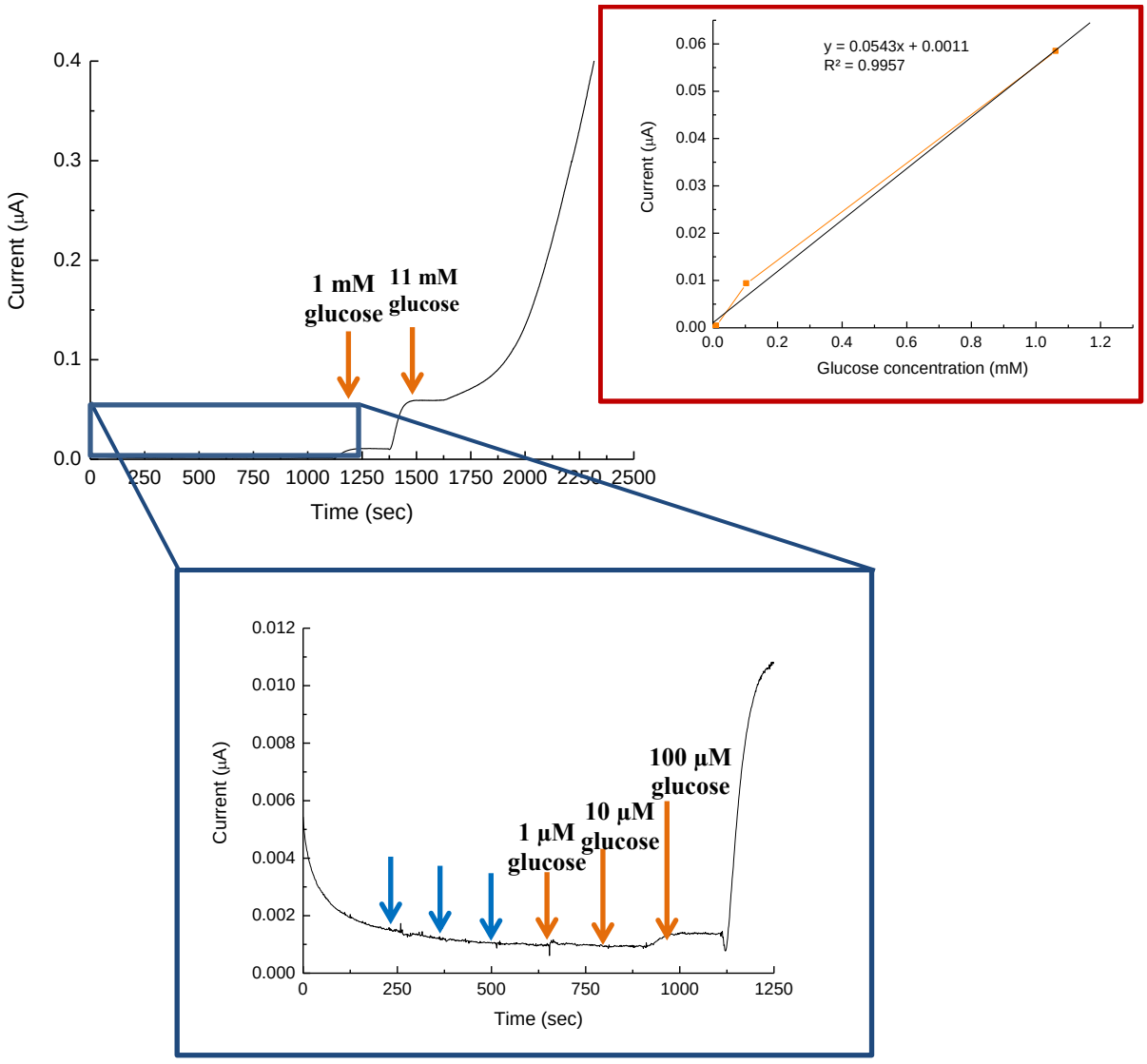

Figure 4.9. Chronoamperometry following successive additions of solutions of glucose at concentrations ranging from 1 μM to 10 mM (orange arrows) in a gel (24 μL) entrapping GOD – *Entrapment method 1*. Additions of 1 μL of phosphate buffer (blue arrows) acted as an appropriate control. Signals were acquired at 0.4 V against a Pt pseudo-reference electrode. The insert is a calibration graph of: catalytic current = f(glucose concentration).

4.3.3 Non enzymatic electrochemical detection of glucose

Because of the improved catalytic signal achieved with nanoparticles on the graphene surface, it was important to check for non-enzymatic glucose detection (which had been reported elsewhere [17]). The experiments reported in section 4.3.2 were therefore repeated using a gel, which did not contain GOD. However the results obtained (figure 4.10) showed that although there was an increase in the current with glucose additions, an increase in current was also seen for additions of 0.1 M phosphate buffer (pH 7.4). Therefore no selective glucose detection was possible.

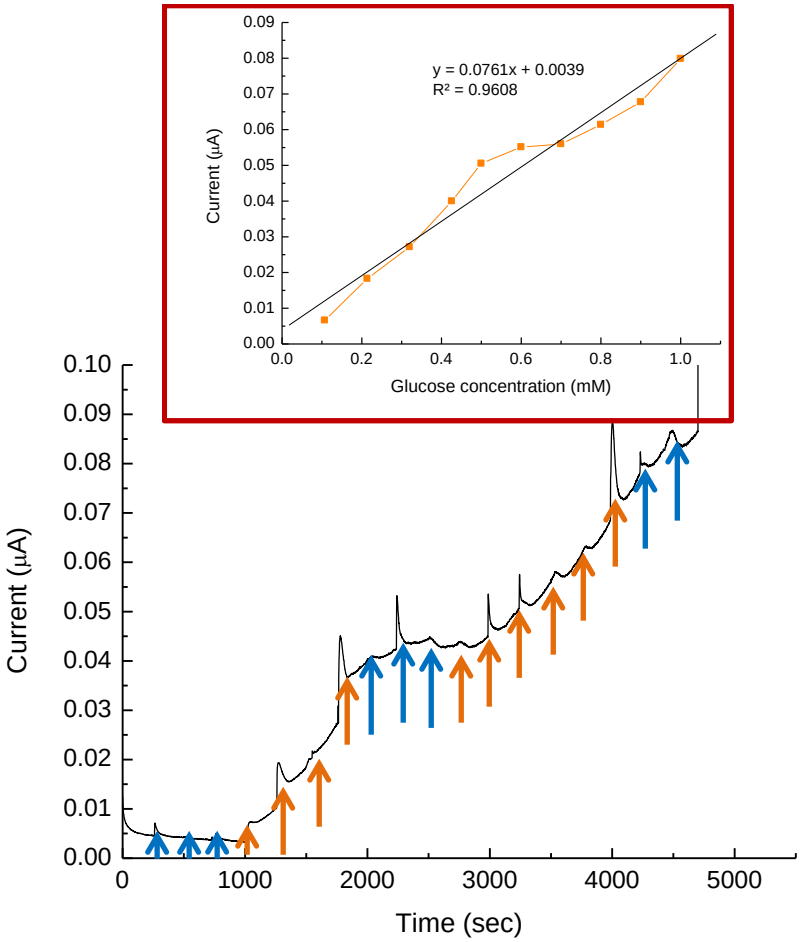

Figure 4.10. Chronoamperometry following successive (1 µL) additions of glucose (orange arrows) to vary the concentration from 0.107 to 1mM in a GOD-free gel (24 µL). Additions (1 µL) of phosphate buffer (blue arrows) acted as an appropriate control. Signals were acquired at 0.4 V against a Pt pseudo-reference electrode. The insert is a calibration graph of: catalytic current = f(glucose concentration).

4.3.4 Specificity of the sensor: the impact of potentially interfering compounds

Ascorbic acid (vitamin C), uric acid, and acetaminophen (paracetamol) are three compounds, often present in measurable concentrations in the body, and known to interfere with glucose detection. Given the potential of these compounds to oxidise relatively easily, it was important to test the new glucose sensor in the presence of these substances and to examine their impact (if any) on the glucose detection profiles (figure 4.11 to 4.14). Non-enzymatic detection was first tested with additions of ascorbic acid as well as glucose to the gel. As with the previous experiment (figure 4.10), the current further increased upon addition of ascorbic acid (purple arrows) showing the non-enzymatic sensor to be not specific enough.

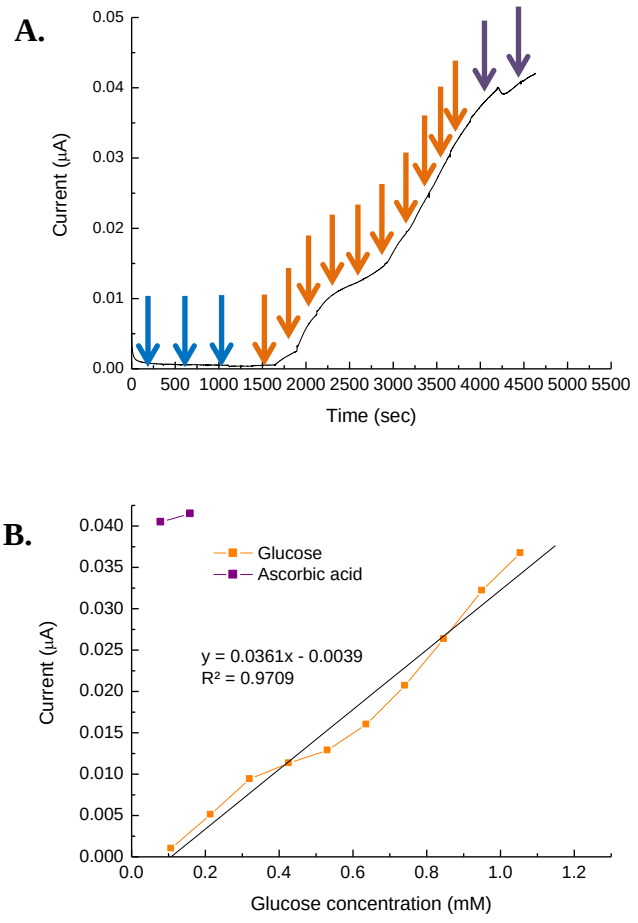

Figure 4.11. Regular additions of glucose and ascorbic acid on a non-enzymatic graphene Pt nanoparticles setup. A: Glucose (orange arrows) and ascorbic acid (purple arrows) were added to a 24 +/- 2 µL agarose gel. The current was measured at 0.4 V against a Pt pseudo reference electrode. Three additions of buffer (blue arrows) were made as a control before any additions. B: Calibration plot representing catalytic current = f(glucose concentration). The orange points refers to glucose additions and the purple points to ascorbic acid.

The GOD enzyme was reintroduced to the sensor design using *entrapment method 1*. This has shown to be a good glucose sensor in previous experiments (section 4.3.2) and therefore it was a good system to test with potentially interfering compounds. Figure 4.12-A shows a series of additions to the gel and its resulting chronoamperometric signal. After the initial spike in current, the plateau current was seen to increase with glucose additions. The addition of ascorbic acid and uric acid did not significantly increase the plateau current and figure 4.12 indicates that the current actually decreased when these compounds were added.

A.

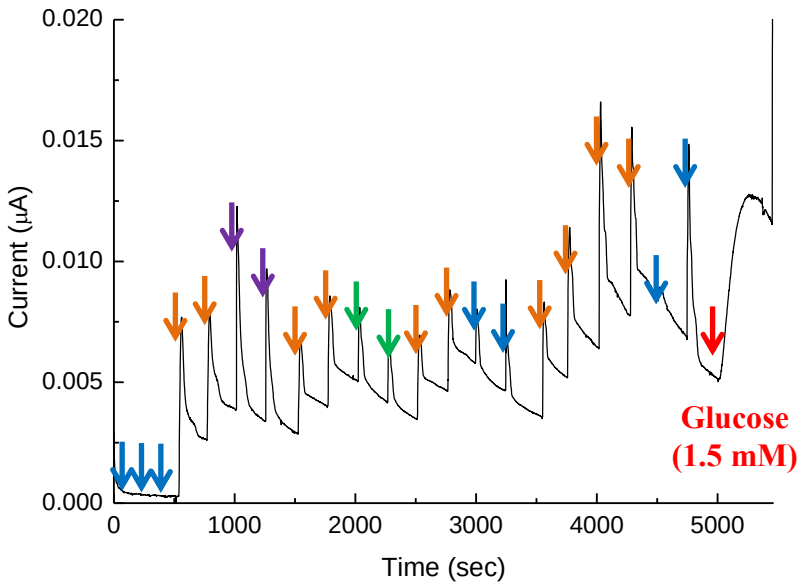

B.

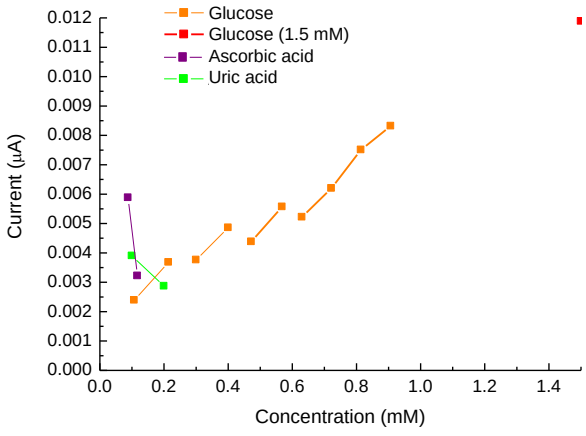

Figure 4.12. Chronoamperometry in response to glucose in the presence of ascorbic acid and uric acid in a gel (24 µL) entrapping GOD - *Entrapment method 1*. A: Additions of glucose (orange arrows), ascorbic acid (purple arrows) and uric acid (green arrows). Measurements were acquired at 0.4 V against a Pt reference electrode. The blue arrows represent additions of phosphate buffer (control). B: calibration graph representing catalytic current = f(concentration) with glucose in orange and red, ascorbic acid in purple and uric acid in green.

Due to the success of the enzymatic mediated glucose detection method, different methods of GOD enzyme entrapment methods were tested to see if they had any effect on the specificity of the sensor. Direct gel entrapment on the electrode *(Entrapment method 3)* was used to fabricate the glucose sensor tested in figure 4.13. This was an improvement on *entrapment method 1* in that the gel was directly formed on top of the electrode after a solution of the GOD enzyme had been deposited on top of the graphene. Interference experiments with ascorbic acid show the current to decrease, and after the first initial decrease in current, successive additions did not show a significant variation of the current (figure 4.13-B).

A.

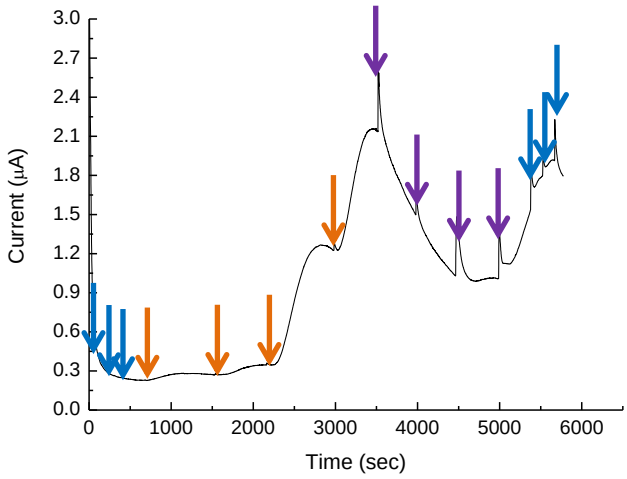

B.

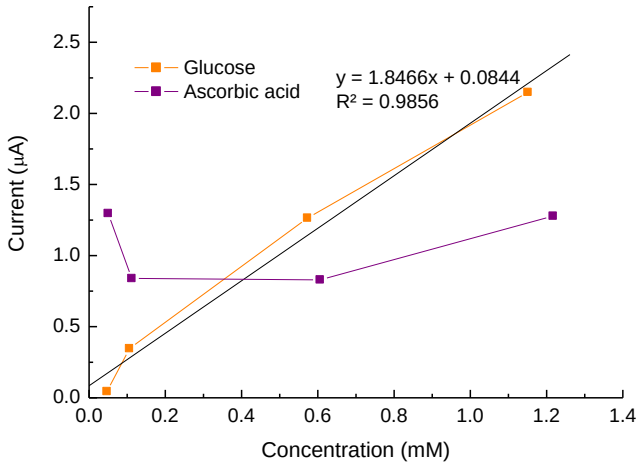

Figure 4.13. Chronoamperometry in response to glucose in the presence of ascorbic acid in a gel (24 µL) entrapping GOD – *Entrapment method 3*. A: additions of glucose (orange arrows) and ascorbic acid (purple arrows). Chronoamperometry acquired at 0.4 V against a micro Ag/AgCl electrode. Blue arrows indicate addition of phosphate buffer (control) B: calibration graph representing catalytic current = f(concentration) with glucose in orange and ascorbic acid in purple

The sensor made with enzyme *entrapment method 3* was then tested for interference with acetaminophen (figure 4.14). Once again additions of the interferent initially showed the current to decrease, and the current plateaued after further additions of acetaminophen indicating that it is only a minor interferent.

A.

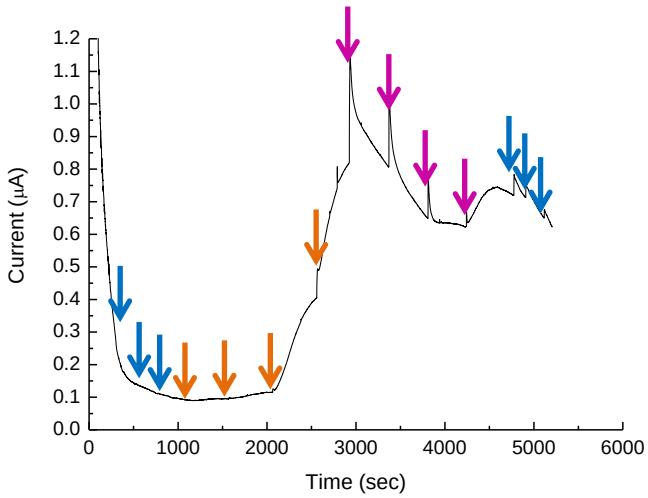

B.

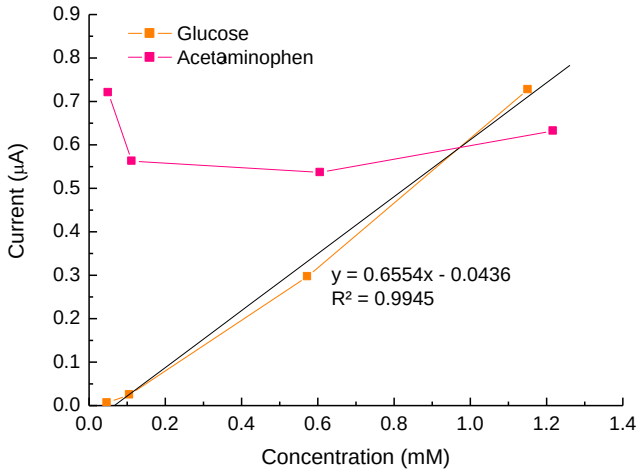

Figure 4.14. Chronoamperometry in response to glucose in the presence of acetaminophen in a gel (24 µL) entrapping GOD – *Entrapment method 3*. A: additions of glucose (orange arrows) and acetaminophen (magenta arrows). Chronoamperometry acquired at 0.4 V against a micro Ag/AgCl electrode. Blue arrows indicate addition of phosphate buffer B: calibration graph representing catalytic current = f(concentration) with glucose in orange and ascorbic acid in magenta.

It was mentioned in chapter 2 section 2.2.2.7.1 (footnote, 2.α), that a small amount of acetic acid was released from the silicone rubber during the design of the sensor. Although the sensor preparation and measurements involved washing steps, it was important to demonstrate that no interaction is observed with addition of acetic acid (see figure 4.15).

Addition of acetic acid, did show a decrease in the current upon successive additions but the concentrations added are well in excess of what would normally be found in a human body (42 µM in the serum [18]).

A.

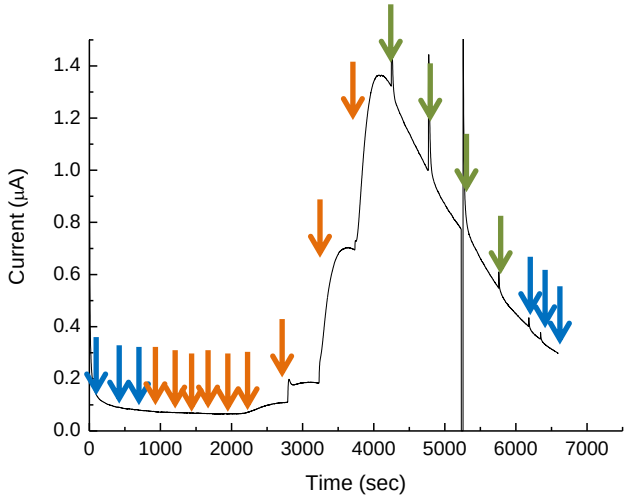

B.

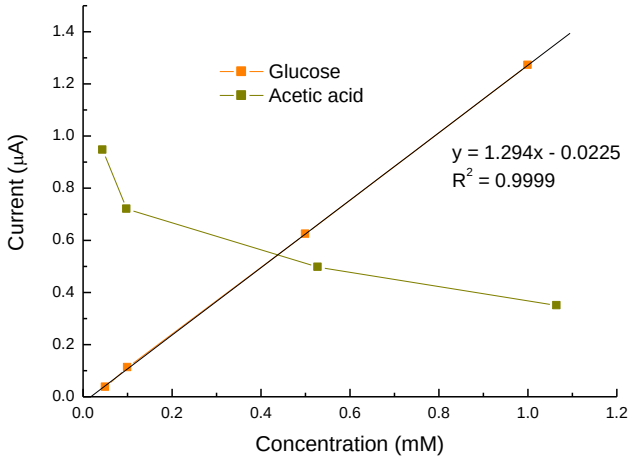

Figure 4.15. Chronoamperometry in response to glucose in the presence of acetic acid in a gel (24 µL) entrapping GOD – *Entrapment method 3*. A: additions of glucose (orange arrows) and acetic acid (brown arrows). Chronoamperometry acquired at 0.4 V against a micro Ag/AgCl electrode. Blue arrows indicate addition of phosphate buffer (control) B: calibration graph representing catalytic current = f(concentration) with glucose in orange and ascorbic acid in brown.

4.3.5 Sensitivity, linear range and limit of detection

It has now been established that the best design so far is to incorporate platinum nanoparticles on the surface of the graphene electrode as well as using a direct GOD/gel entrapment methods for the GOD integration into the gel (*entrapment 2 and 3*). Here, a broad range of glucose concentrations were added to the developed sensor in order to assess the sensitivity, linear range and limit of detection of the device. Figure 4.16 shows a series of glucose additions to the sensor over the concentration range of 0.001 mM to 1.89 mM. At the lower concentrations, only very small changes in current are observed in the chronoamperometry, however, higher concentrations show a clear increase in current. Figure 4.17 demonstrates a broad linear response over the concentration range from 1 µM to 1.89 mM. However, determination of the limit of detection of the sensor required the concentration range to be extended to sub micro molar concentrations (see figure 4.18).

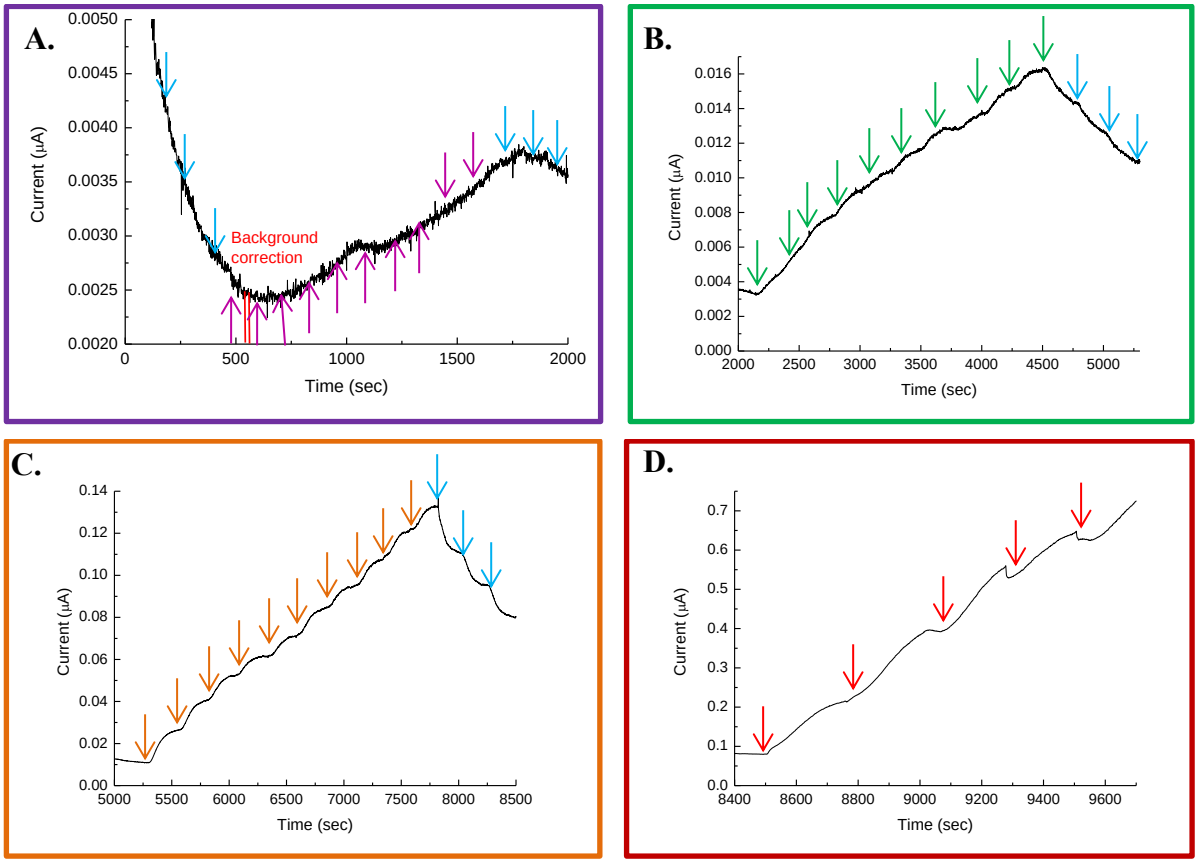

Figure 4.16. Chronoamprometry were acquired at 0.4 V against a micro Ag/AgCl electrode. Catalytic activity of the sensor over different concentration ranges: (A) 0.001 to 0.01 mM (purple arrows), (B) 0.016 to 0.081 mM (green arrows), (C) 0.127 to 0.652 mM (orange arrows), (D) 1.031 to 1.89 mM (red arrows). Blue arrows are glucose-free buffer acting as a positive control. The enzyme entrapment used was the *entrapment method 2*.

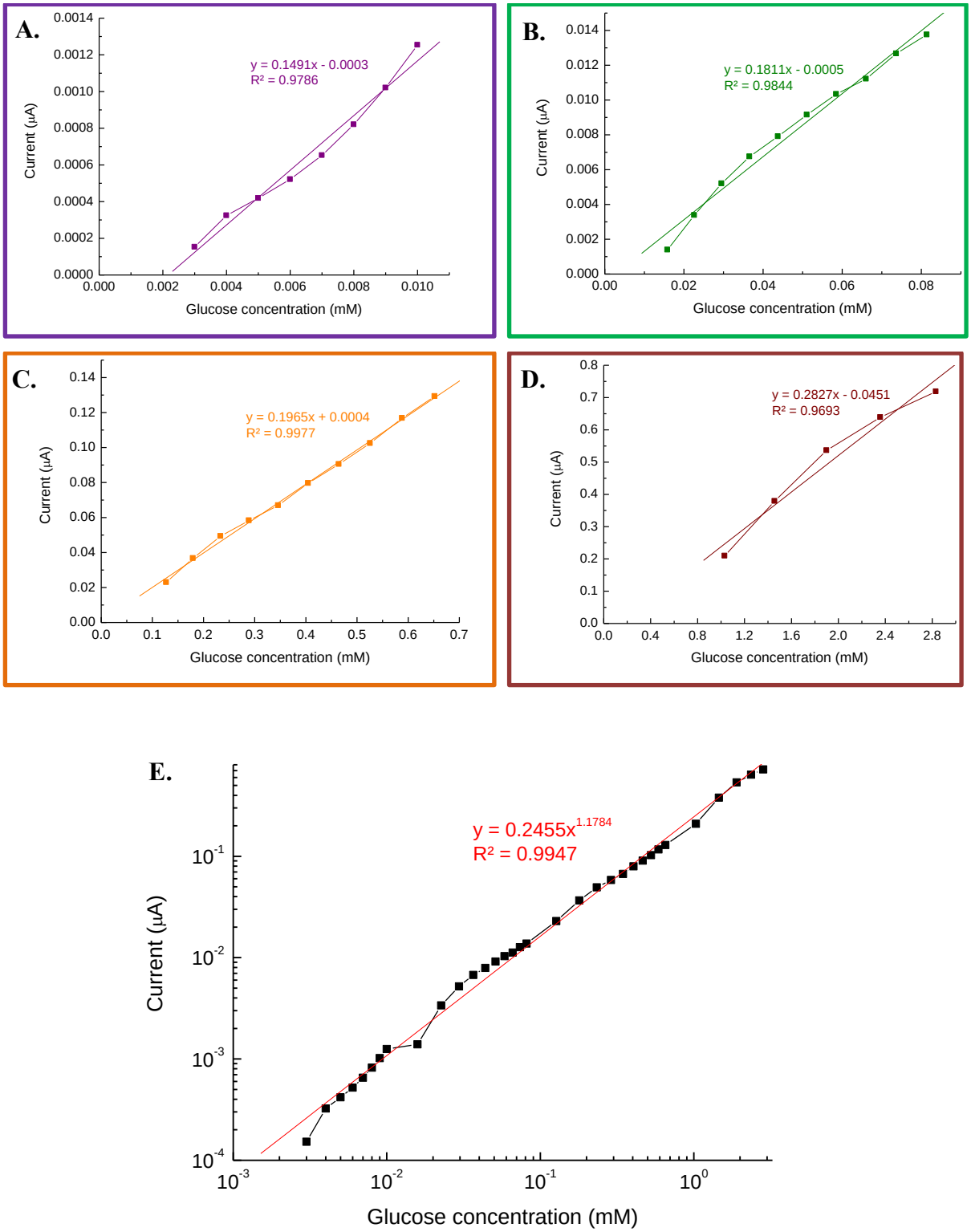

Figure 4.17. Determination of the linear range and sensitivity of the sensor. A-D: Calibration curves (catalytic current = f(glucose concentration)) for each of the glucose ranges. (A) 0.001 to 0.01 mM, (B) 0.016 to 0.081 mM, (C) 0.127 to 0.652 mM, (D) 1.031 to 1.89 mM. E: Measured catalytic current as a function of glucose concentration represented on a logarithmic graph. The enzyme entrapment used was the *entrapment method 2*.

Figure 4.18 shows the chronoamperometry data obtained when sub-micro molar concentrations of glucose were added to the developed sensor. At concentrations in the range of 0.1 µM to 1 µM it was very difficult to determine an increase in current because the signal was so noisy. It can be seen in figure 4.19 that the concentration dependence is linear with respect to the measured current, however, the very low concentrations do not follow this linear trend and are out of the range of the sensitivity of the device.

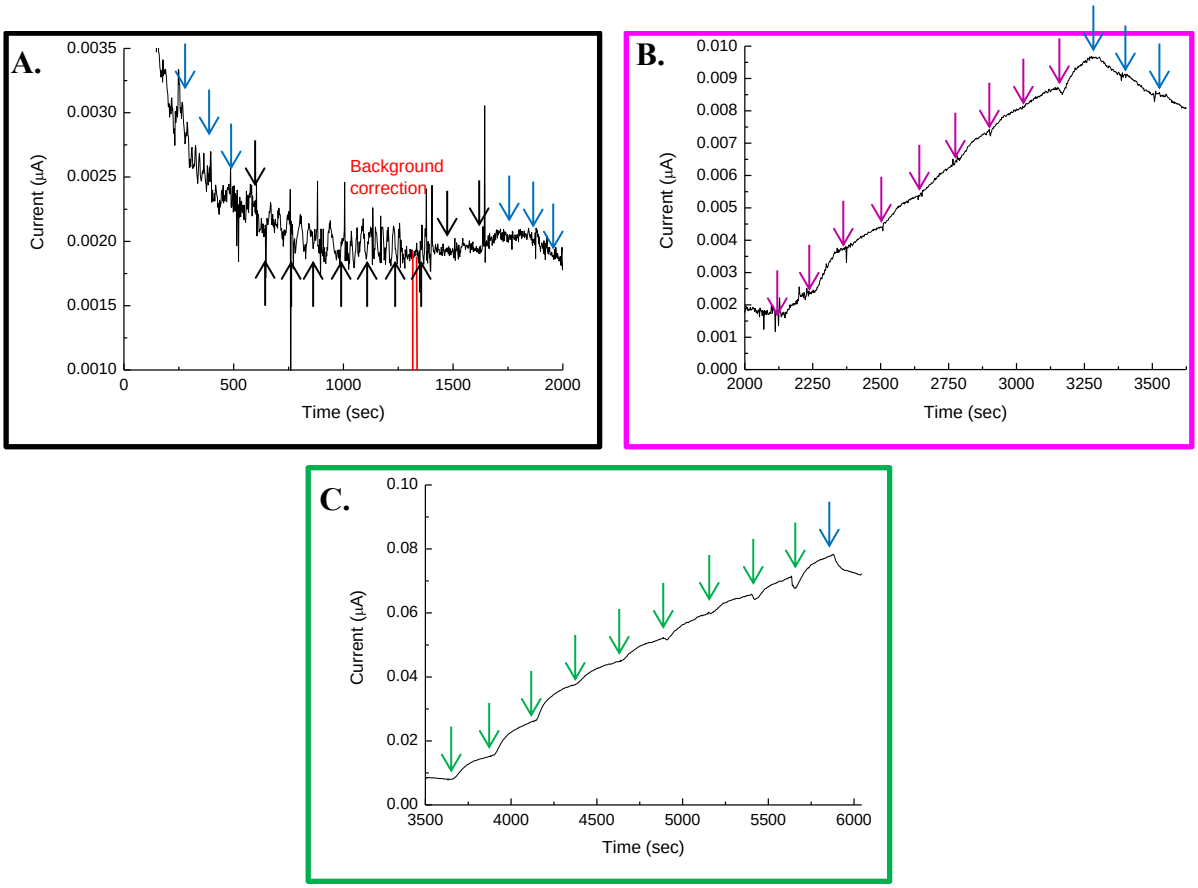

Figure 4.18. Chronoamprometry were acquired at 0.4 V against a micro Ag/AgCl electrode. The catalytic activity of the sensor was measured down to Sub-micro molar concentrations: (A) 0.1 µM to 1 µM (black arrows), (B) 1 µM to 10 µM (magenta arrows), (C) 10 µM to 100 µM (green arrows), blue arrows are additions of buffer. Similarly to figure 4.17, the enzyme entrapment used here was the *entrapment method 2*.

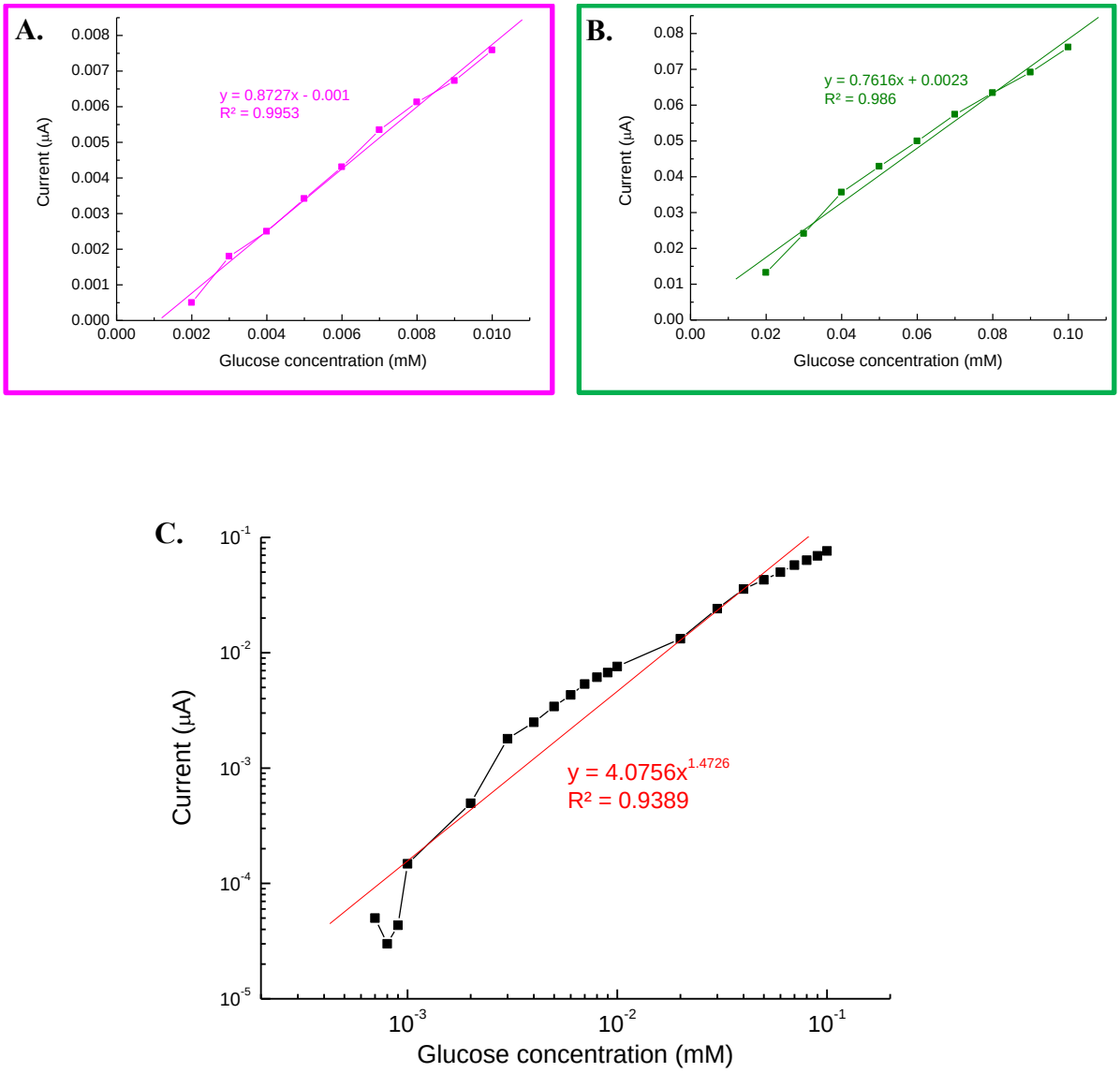

Figure 4.19. Determination of the limit of detection of the sensor. A-B: Calibration curves (catalytic current = f(glucose concentration)) for each of the glucose ranges, (A) 1 µM to 10 µM, (B) 10 µM to 100 µM C: Measured catalytic current as a function of glucose concentration represented on a logarithmic graph. The enzyme entrapment used was the *entrapment method 2*.

The performance of the sensor obtained from figures 4.16 and 4.18 are listed in table 4.1. Here the limit of detection has been calculated according to equation 4.2 and shows the limit to be 4 µM and 1 µM for each of the concentration ranges. These values are in close agreement with each other and discrepancies could be due to error in measurement of the current because of noise at the lower concentrations.

Table 4.1. Performance attributes of the sensor

Figure	Calibration curve gradient (sensitivity µA/mM)	Calculated LOD current µA	LOD (µM)	Linear range (mM)
4.17	0.263	0.00028	4	0.12 to 2.83
4.19	0.797	0.00009	1	0.003 to 0.1

4.3.6 Repeatability and stability of the sensor

Thus far, it has been shown that the graphene electrode with platinum nanoparticles electrodeposited on top and a gel containing GOD using *entrapment method 2* has an excellent limit of detection for glucose. To check the repeatability of the sensor, 3 sensors were tested with different concentrations of glucose and the current recorded with chronoamperometry. Figure 4.20 shows the average current obtained from the 3 sensors with error bars showing the standard deviation between the 3 different sensors. The error bars indicate a large variation in the current from sensor to sensor which is possibly due to the graphene wet transfer technique used to make the graphene electrode.

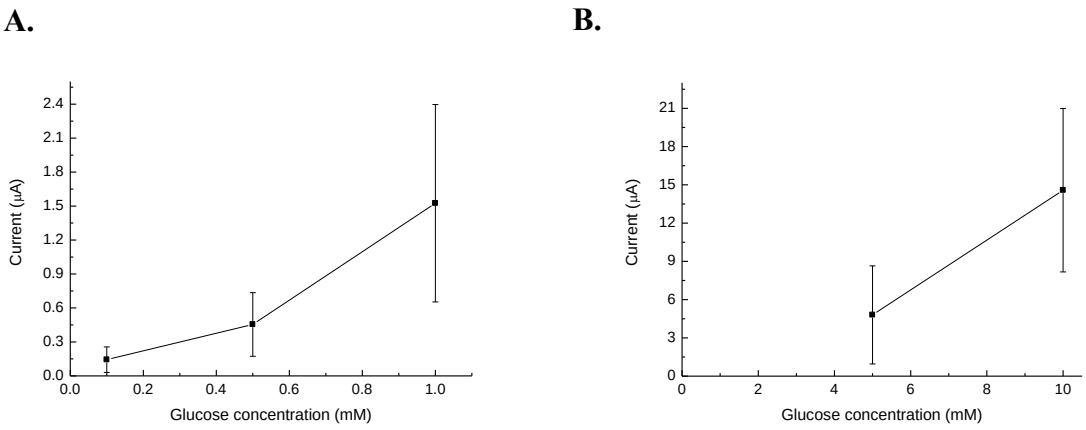

Figure 4.20. Repeatability of 3 sensors. The concentration graph was separated in two (A and B) in order to give a clear representation of the current increase over the entire concentration scale. A: glucose range going from 0.1 mM to 1 mM, B: glucose range going from 5 mM to 10 mM. Error bars correspond to standard deviation. The GOD/gel entrapment was *entrapment 3.*

Sensor stability was then assessed over a two week period by measuring its response as a function of glucose concentration (figure 4.21). The electrode was stored dry in a petri dish at room temperature when not in use. It can be seen that the data recorded on the first day gave

higher currents than data recorded after 5 and 14 days. Data obtained after 5 and 14 days gave similar currents indicating that the activity of the sensor had reached a plateau after 5 days. This could be due to mechanical damage of the electrode in the process of mounting the setup and discarding used gels.

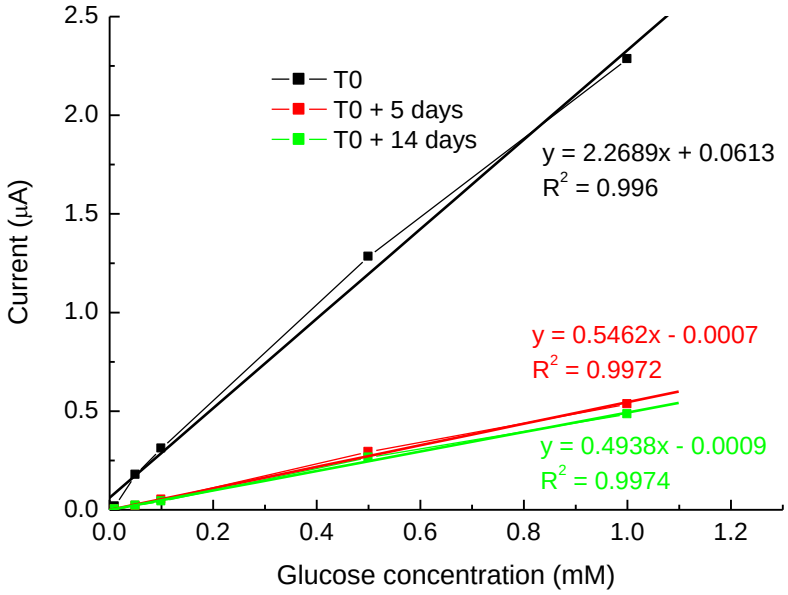

Figure 4.21. Stability of the catalytic current, for a representative electrode over two weeks. This figure represents catalytic current = f(glucose concentration) for a sensor at 0 (black curve), 5 (red curve) and 14 days (green curve). The GOD/gel entrapment was *entrapment 3*.

4.3.7 Sensor enzyme kinetics

From the data presented in figure 4.20, a Lineweaver-Burk plot was constructed for the new first generation glucose biosensor (figure 4.22). A Lineweaver-Burk plot is a graphical way of presenting the Michaelis-Menten equation:

$$V = \frac{V_{max}[S]}{K_m + [S]} \qquad (4.4)$$

where V is the reaction velocity, K_m is the Michaelis-Menten constant, V_{max} is the maximum reaction velocity and [S] is the substrate concentration. From this graph, K_m and I_{max} were assessed as 3.63 mM and 5.26 µA. The K_m value was in good agreement with the literature (for both amperometric first or second generation biosensors), see table 4.2.

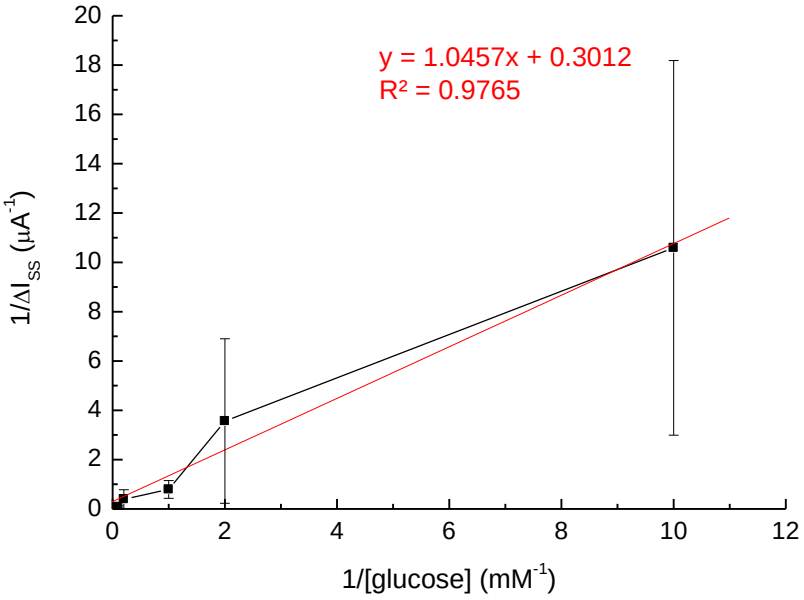

Figure 4.22. Lineweaver-Burk plot obtained from the results in figure 4.20. Averaged data from 3 freshly created sensors shown in figure 4.20. Error bars correspond to standard deviation.

Table 4.2. K_m values of 1st and 2nd generations glucose biosensors

K_m (mM)	1st/2nd generation glucose biosensor	Reference
0.186	1st	[19]
3.3	1st	[20]
10.94	1st	[6]
1.14	1st	[21]
8.94	2nd	[22]
38	2nd	[23]
3.63	1st	This work

4.4 Discussion

4.4.1 Effect of the addition of platinum nanoparticles

The Pt nanoparticles clearly improved the glucose detection providing increased current ranges at low detection potential compared to results presented in chapters 2 and 3. The detection potential was lowered from 0.7 V to 0.4 V against both a Pt pseudo reference electrode and a Ag/AgCl micro-reference electrode (see figures 4.7 to 4.9 and figures 4.16 and 4.18). As a comparison, the catalytic current obtained with 1 mM of glucose added to the nanoparticle functionalised electrode is ~ 0.108 µA (see figure 4.8) whereas the current previously obtained with addition of the same concentration of glucose on an electrode non-functionalised with nanoparticles was ~ 0.0123 µA (see chapter 2, figure 2.13-A). The current was increased (around 9 times) while the detection potential was decrease of 0.3 V, benefiting from the synergetic catalytic effect described in section 4.1.1. Chronoamperometry was also preferred to cyclic voltammetry as a detection technique providing with better linearity over a broad range of glucose concentrations (see the comparison between figure 4.7 and figures 4.8 and 4.9).

Having assessed the benefit of adding platinum nanoparticles to the catalytic detection, it was then important to study non enzymatic detection of glucose on the nanoparticle functionalized electrode. The non-enzymatic sensing of glucose on platinum nanoparticles has been demonstrated following the direct oxidation of the analytes on the nanoparticles presented in equation 4.5, [24].

$$\begin{aligned} Pt + 2OH^- - 2e^- &\longrightarrow Pt(OH)_2 \\ Pt(OH)_2 + 2OH^- &\longrightarrow PtO(OH)_2 + H_2O + 2e^- \\ PtO(OH)_2 + \text{glucose} &\longrightarrow Pt(OH)_2 + \text{gluconolactone} \end{aligned} \qquad 4.5$$

Based on this observation, direct glucose oxidation on the nanoparticles was investigated at 0.4 V against a Pt pseudo reference electrode. An increase of the catalytic current was observed with additions of glucose that demonstrated a good linear proportionality (see figure 4.10). However, the chronoamperometric steps observed didn't stabilize and an increase of current was observed with additions of buffer. Furthermore a signal was also obtained with additions of ascorbic acid (see figure 4.11). Non-enzymatic detection was therefore abandoned as not reliable enough and not sufficiently specific for glucose detection.

4.4.2 Impact of ascorbic acid, uric acid and acetominophen on the amperometric signal

The enzyme functionalized gel design was then tested with ascorbic acid, uric acid and acetaminophen along with addition of glucose to assess the impact of these interferents on the catalytic signal. A good selectivity towards glucose was demonstrated in figures 4.12 to 4.14. More specifically, figure 4.12-A presents the alternated additions of glucose and ascorbic and uric acid. Although displaying a current peak increase at each concentration steps (probably caused by the mechanical additions), the catalytic signal then stabilised after each initial spikes. The stable step signals were then plotted as a function of the concentration and a linear proportional increase was observed with glucose concentration whereas a decrease of catalytic current was identified with ascorbic and uric acid (see figure 4.12-B).

Figures 4.13 and 4.14 then present additions of ascorbic acid and acetominophen after glucose additions. In both cases the catalytic signal is linearly proportional to glucose additions whereas the additions of each interferents does not increase the signal up to an elevated concentration of ~ 1 mM. On the contrary the current seems to decrease with the additions of the interferents (with the exception of "high" 1 mM concentrations). This phenomenon is also observed when adding buffer after additions of glucose (as indicated in figure 4.12 to 4.17 by the blue arrows). The most likely explanation for both of these decrease is the dilution of the glucose already present (following the additions depicted in every picture in orange) and hence a decrease of catalysis at the electrode.

The design cannot be claimed to be totally specific towards glucose but it is selective enough for the integration into methodologies for glucose extraction/detection through the skin (chapter 5). This argument can be supported by several facts: Firstly, ascorbic acid in solution is in anionic form (ie, ascorbate bearing a negative charge), it is therefore very unlikely that a significant amount of this molecule will be extracted via reverse iontophoresis since the extraction is made from anode to cathode which induces a flux of cations (Na^+) towards the sensor (on the cathode), see chapter 1 section 1.3.4.5.2.4. Secondly, the physiological levels of ascorbic acid for a healthy human being is below 0.1 mM [25] and the typical plasma concentration of acetaminophen for a patient ingesting prescribed doses of the analgesic (1g every 6 hours) is 0.1 mM [11]. It is therefore highly unlikely that concentration at which a

signal is observed for both these molecules (1 mM) will be found at the surface of the epidermis after extraction by reverse iontophoresis. In conclusion, the sensor that is not altered by the presence of common interferents, presents a great selectivity towards glucose and is hence "highly specific" for the intended non-invasive sensing application.

4.4.3 Sensitivity, linear range and limit of detection

The performance characteristics of the sensor have then been evaluated. Figure 4.16 displays catalytic current steps obtained with additions of glucose over 4 ranges of glucose going from 0.001 mM to 2.83 mM. The steps in current appear to be well defined and stable. These were then plotted against glucose concentrations on linear and log-log graphs (figure 4.17). It demonstrated a broad linear range going from 0.12 to 2.83 mM and a LOD of 4 µM. Smaller glucose concentration were then added on a similar sensor configuration and a lower LOD of 1 µM was identified, with a broad linear range going from 3 to 100 µM as shown in figure 4.19.

The sensitivity of the sensor was assessed from the slope of the linear regression of figure 4.17 as 0.26 µA/mM (equivalent to 2.89 $\mu A.mM^{-1}.cm^{-2}$) for the 9 mm^2 area of the graphene flakes. These performance values are then compared with the graphene/metallic nanoparticles glucose sensors from the literature (table 4.3) and alternative glucose biosensor devices (to the fingerstick meters) in table 4.4. The sensor was determined to be competitive with respect to the literature (figures 4.17 and 4.19) and as presented in table 4.3 that compares the LOD and linear range of the graphene/Pt nanoparticle electrode developed here with similar amperometric designs reported in the literature. The sensitivity value of the sensor was slightly lower than those of nanoparticle-functionalized amperometric biosensors found in the literature [8, 26], but close to those of graphene sensors [13, 27]. Furthermore, with respect to the non-invasive extraction and detection of glucose via reverse iontophoresis through the skin, it would appear that the LOD and sensitivity are suitable. This conclusion is based on the fact that the gel used in the new sensor design has a volume of only 24 µL (compared to the 400 µL of the GlucoWatch ® Biographer [28]) and that the concentration extracted after 3 minutes of reverse iontophoresis into the large GlucoWatch ® Biographer gel volume was very low: 2.5 to 25 µM [29]. Much higher concentrations, and well above the LOD, are anticipated in the much smaller (17-fold) volume of the new sensor's gel.

Table 4.3. LOD and linear ranges of graphene/metallic nanoparticle glucose sensors

Electrode	Limit of detection (µM)	Linear range (mM)	Sensitivity ($\mu A.mM^{-1}.cm^{-2}$)	References
Pt nanoparticles/ graphene oxide/ glucose oxidase	0.6	sub µM to 5	-	[8]
PtPd nanoparticles/ graphene oxide/ glucose oxidase	1	2-12	26	[30]
Pt nanoparticles/ graphene oxide/ glucose oxidase/ nafion	25	3-15	-	[31]
Pt nanoparticles/ multilayered graphene petal nanosheet/ glucose oxidase	0.3	0.01-50	-	[32]
Pt nanoparticles/ exfoliated graphite nanoplatelet/ glucose oxidase/ nafion	1	1-20	61.5 ± 0.6	[26]
PdNps/ graphene oxide/ glucose oxidase/ glassy carbon electrode	33.7	Dynamic range up to 0.1	14.1 µA/mM	[33]
Graphene-bismuth nanoparticle (Bi) nanocomposite/ glucose oxidase/ glassy carbon electrode	350	1-12	2.243	[34]
Pt nanoparticles/ graphene oxide/ TiO_2 nanotube arrays	100	0.1-8	0.94	[35]
This work	1	0.003-0.1 and 0.1-3	2.89	

Table 4.4. Alternative devices (to fingerstick meters) performance characteristics

Device	Measurement design	Sensor characteristics	Detection	Measurement range (mM)	References
GlucoWatch ® Biographer (Cygnus Inc, Redwood City CA, USA)	Reverse iontophoresis	Platinum/carbon ink eleectrode	Amperometric/ GOD/ First generation sensor (detection of H_2O_2)	2.2-22.2 *Sensitivity:* $50\ \mu A.mM^{-1}.cm^{-2}$	[36]
FreeStyle Navigator (Abbott Diabetes Care, Alameda, CA, USA)	Invasive needle sensor	Carbon/ osmium wired electrode	Amperometric/wired GOD / second generation sensor, mediator: $Os^{2+/3+}$	1.11-27.75	[37]
Guardian Real-Time (Medtronic, MiniMed Inc., Northridge, CA, USA)	Invasive needle sensor	Platinum electrode/ Polyurethane poly urea polymer 22 gauge insertion needle	Amperometric/GOD/ First generation sensor (detection of H_2O_2)	2.22-22.2	[38]
DexCom STS™-7 (DexCom Inc., San Diego, CA, USA)	Invasive needle sensor	Platinum electrode/ membrane (hydrophobic polyurethane and a hydrophilic polyurethane mixture) 26 gauge insertion needle	Amperometric/GOD/ First generation sensor (detection of H_2O_2)	2.22-22.2	[15, 39]
GlucoDay® (A. Menarini Diagnostics, Florence, Italy)	Microdialysis set-up	Platinum electrode/ three membranes: cellulose acetate, nylon net with covalently linked GOD, and a polycarbonate protective membrane	Amperometric/ GOD/ First generation sensor (detection of H_2O_2)	up to 30	[40]

4.4.4 Repeatability, stability and kinetic parameters of the sensor

The repeatability and stability of the sensor were investigated in order to conclude on the robustness of the detection. The repeatability was not optimal over the range of concentrations possibly due to the process of transferring CVD graphene during sensor fabrication (see chapter 2, section 2.2.2.1) which would account for some electrode to electrode variability. However, this may be solved in the future by the use of dry transfer, for example [41]. While there was a significant drop in catalytic activity of the sensor over a 5-day period (figure 4.21) the signal then stabilized over the next 10 days. The initial drop of catalytic activity was potentially due to the deterioration of the transducer surface, caused by repeated washing and mechanical positioning of the enzymatic gel.

Finally, the enzyme kinetic parameters deduced for the sensor indicated that high affinity for the substrate was maintained. K_m was deduced from a Lineweaver-Burk plot based on a Michaelis-Menten kinetic presented in figure 4.22. From this representation it was possible to deduce a K_m of 3.63 mM which was in the order of the glucose sensor presented in the literature (table 4.2). The K_m value is defined as the concentration of substrate allowing the enzyme to achieve half of the maximal catalytic velocity (V_{max}). It follows that the lower the K_m value, the higher the affinity will be for the substrate [42]. Remarkably, a significant variation in K_m is observed in table 4.2 which can be attributed to the difference of entrapment of the enzyme, transducer, enzyme density, detection principle, etc.

4.5 Conclusions

In conclusion, the platinum nanoparticles and the direct GOD/gel entrapment on the graphene electrode *by method 2 or 3* acted synergistically towards the catalytic sensing of the enzymatically produced H_2O_2. It enabled to lower the detection potential and obtain an improved catalytic current with reaction of glucose on the GOD loaded gel electrode. The specificity regarding glucose was demonstrated by studying the impact on the signal of ascorbic acid, uric acid, acetominophen and acetic acid. The sensor performance (sensitivity, linear range and limit of detection) was then investigated. A sensitivity of 2.89 $\mu A.mM^{-1}.cm^{-2}$, a limit of detection of 1 µM and a linear range of 0.003 mM to 0.1 mM (and 0.1 mM to 3 mM on a separate experiment) was assessed. These attributes made the sensor competitive

with respect to platinum nanoparticles/graphene electrodes from the literature (table 4.3) and to alternative glucose monitoring technologies (table 4.4). The results however failed to demonstrate good reproducibility presenting high standard deviation error bars (attributed to the irregular quality of the transferred graphene). Furthermore, the electrode stability overtime showed an initial decrease of activity from day 0 to day 5 again possibly caused by the mechanical damages of the electrode during the multiple measurements. Finally a low K_m of 3.63 mM was obtained for the enzymatic reaction that was relatively low when compared to the literature and hence demonstrated good affinity for the substrate.

1. Chu, P.K. and X. Liu, *Biomaterials Fabrication and Processing Handbook*. 2008: Taylor & Francis.
2. Alegret, S. and A. Merkoci, *Electrochemical Sensor Analysis*. 2007: Elsevier Science.
3. Shao, Y., et al., *Graphene Based Electrochemical Sensors and Biosensors: A Review.* Electroanalysis, 2010. **22**(10): p. 1027-1036.
4. Xiao, Y., et al., *"Plugging into Enzymes": Nanowiring of Redox Enzymes by a Gold Nanoparticle.* Science, 2003. **299**(5614): p. 1877-1881.
5. Daniel, M.-C. and D. Astruc, *Gold Nanoparticles: Assembly, Supramolecular Chemistry, Quantum-Size-Related Properties, and Applications toward Biology, Catalysis, and Nanotechnology.* Chemical Reviews, 2004. **104**(1): p. 293-346.
6. Luhana, C., et al., *A novel enzymatic glucose sensor based on Pt nanoparticles-decorated hollow carbon spheres-modified glassy carbon electrode.* Journal of Nanoparticle Research, 2012. **14**(10): p. 1-9.
7. Gu, Y. and C.-C. Chen, *Eliminating the Interference of Oxygen for Sensing Hydrogen Peroxide with the Polyaniline Modified Electrode.* Sensors, 2008. **8**(12): p. 8237-8247.
8. Wu, H., et al., *Glucose biosensor based on immobilization of glucose oxidase in platinum nanoparticles/graphene/chitosan nanocomposite film.* Talanta, 2009. **80**(1): p. 403-406.
9. Thévenot, D.R., et al., *Electrochemical biosensors: recommended definitions and classification.* Biosensors and Bioelectronics, 2001. **16**(1–2): p. 121-131.
10. Borgmann, S., et al., *Amperometric Biosensors*, in *Advances in Electrochemical Science and Engineering*. 2011, Wiley-VCH Verlag GmbH & Co. KGaA. p. 1-83.
11. Fabry, P. and J. Fouletier, *Chemical and Biological Microsensors: Applications in Fluid Media*. 2013: Wiley.
12. Shrivastava A. and Gupta V. B., *Methods for the determination of limit of detection and limit of quantitation of the analytical methods.* Chron Young Sci 2011. **2**(1): p. 21-25.
13. Alkire, R.C., et al., *Bioelectrochemistry: Fundamentals, Applications and Recent Developments*. 2011: Wiley.
14. Zoldák, G., et al., *Irreversible Thermal Denaturation of Glucose Oxidase from Aspergillus niger Is the Transition to the Denatured State with Residual Structure.* Journal of Biological Chemistry, 2004. **279**(46): p. 47601-47609.

15. McGarraugh, G., *The Chemistry of Commercial Continuous Glucose Monitors.* Diabetes Technology & Therapeutics, 2009. **11**(s1): p. S-17-S-24.
16. Dai X. and R. G. Compton, *Detection of As(III) via oxidation to As(V) using platinum nanoparticle modified glassy carbon electrodes: arsenic detection without interference from copper* Analyst, 2006. **131**(4): p. 516-521.
17. Su, C., et al., *Nonenzymatic Electrochemical Glucose Sensor Based on Pt Nanoparticles/Mesoporous Carbon Matrix.* Electroanalysis, 2010. **22**(16): p. 1901-1905.
18. Psychogios, N., et al., *The Human Serum Metabolome.* PLoS ONE, 2011. **6**(2): e16957
19. Arslan, F., S. Ustabaş, and H. Arslan, *An Amperometric Biosensor for Glucose Determination Prepared from Glucose Oxidase Immobilized in Polyaniline-Polyvinylsulfonate Film.* Sensors, 2011. **11**(8): p. 8152-8163.
20. Chen, K.-J., et al., *Fabrication and application of amperometric glucose biosensor based on a novel PtPd bimetallic nanoparticle decorated multi-walled carbon nanotube catalyst.* Biosensors and Bioelectronics, 2012. **33**(1): p. 75-81.
21. Yu, J., T. Zhao, and B. Zeng, *Mesoporous MnO2 as enzyme immobilization host for amperometric glucose biosensor construction.* Electrochemistry Communications, 2008. **10**(9): p. 1318-1321.
22. German, N., et al., *Glucose biosensor based on graphite electrodes modified with glucose oxidase and colloidal gold nanoparticles.* Microchimica Acta, 2010. **168**(3-4): p. 221-229.
23. Luong, J.H.T., et al., *Monitoring the activity of glucose oxidase during the cultivation of Aspergillus niger using novel amperometric sensor with 1, 1'-dimethylferricinium as a mediator.* Biosensors and Bioelectronics, 1994. **9**(8): p. 577-584.
24. Su, C., C. Zhang, G. Lu and C. Ma, *Nonenzymatic Electrochemical Glucose Sensor Based on Pt Nanoparticles/Mesoporous Carbon Matrix,* Electroanalysis, 2010. **22**(16): p. 1901-1905
25. ICH. *Harmonized tripartite guidelines; Validation of analytical procedures: text and methodology*. Q2 R1 2005 [cited 2015]; Available from: http://www.ich.org/fileadmin/Public_Web_Site/ICH_Products/Guidelines/Quality/Q2_R1/Step4/Q2_R1__Guideline.pdf.

26. Lu, J., et al., *Nanometal-Decorated Exfoliated Graphite Nanoplatelet Based Glucose Biosensors with High Sensitivity and Fast Response.* ACS Nano, 2008. **2**(9): p. 1825-1832.
27. Lu, J., et al., *Simple Fabrication of a Highly Sensitive Glucose Biosensor Using Enzymes Immobilized in Exfoliated Graphite Nanoplatelets Nafion Membrane.* Chemistry of Materials, 2007. **19**(25): p. 6240-6246.
28. Leboulanger, B., R.H. Guy, and M.B. Delgado-Charro, *Reverse iontophoresis for non-invasive transdermal monitoring.* Physiological Measurement, 2004. **25**(3): p. R35.
29 Tierney, M.J. et al., *Electroanalysis of glucose for non-invasive transdermal monitoring. Physiological Measurement*, 2004, **25**(3): p. R35
30. Hossain, M.F. and J.Y. Park, *Amperometric Glucose Biosensor Based on Pt-Pd Nanoparticles Supported by Reduced Graphene Oxide and Integrated with Glucose Oxidase.* Electroanalysis, 2014: p. 940-951.
31. Liu, A. and S. Huang, *A glucose biosensor based on direct electrochemistry of glucose oxidase immobilized onto platinum nanoparticles modified graphene electrode.* Science China Physics, Mechanics and Astronomy, 2012. **55**(7): p. 1163-1167.
32. Claussen, J.C., et al., *Nanostructuring Platinum Nanoparticles on Multilayered Graphene Petal Nanosheets for Electrochemical Biosensing.* Advanced Functional Materials, 2012. **22**(16): p. 3399-3405.
33. Cheng, N., et al., *Amperometric Glucose Biosensor Based on Integration of Glucose Oxidase with Palladium Nanoparticles/Reduced Graphene Oxide Nanocomposite.* American Journal of Analytical Chemistry, 2012. **3**(4): p. 312-319.
34. Veerappan, M., et al., *A Novel Glucose Biosensor at Glucose Oxidase Immobilized Graphene and Bismuth Nanocomposite Film Modified Electrode.* Int.J.Electrochem.Sci, 2015. **10**: p. 691-700.
35. Feng, C., et al., *Facile Fabrication of Pt/Graphene/TiO2 NTAs Based Enzyme Sensor for Glucose Detection.* Journal of The Electrochemical Society, 2014. **161**(1): p. B1-B8.
36. Chan, M.-S., et al., *Materials for Fabricating Biosensors for Transdermal Glucose Monitoring.* Clinical Chemistry, 1999. **45**(9): p. 1689-1690.
37. Heller, A. and B. Feldman, *Electrochemistry in Diabetes Management.* Accounts of Chemical Research, 2010. **43**(7): p. 963-973.

38. Diabetes Research in Children Network (DirecNet) Study Group, *The Accuracy of the Guardian® RT Continuous Glucose Monitor in Children with Type 1 Diabetes.* Diabetes Technology & Therapeutics, 2008. **10**(4): p. 266-272.
39. Zisser, H.C., et al., *Accuracy of the SEVEN continuous glucose monitoring system: comparison with frequently sampled venous glucose measurements.* J Diabetes Sci Technol, 2009. **3**(5): p. 1146-54.
40. Poscia, A., et al., *A microdialysis technique for continuous subcutaneous glucose monitoring in diabetic patients (part 1).* Biosensors and Bioelectronics, 2003. **18**(7): p. 891-898.
41. Suk, J.W., et al., *Transfer of CVD-Grrown Monolayer Graphene Onto Arbitrary Substrates*. ACS Nano, 2011. **5**(9): p.6916-6924
42. Koolman, J. and K.H. Röhm, *Color Atlas of Biochemistry*. 2005: Thieme.

Chapter 5: Non-invasive glucose monitoring

5.1 Introduction

The glucose sensor developed so far in this thesis has shown excellent detection of glucose by coupling platinum nanoparticles with the GOD enzyme entrapped in a gel on top of a graphene flake. Integration of this sensor with in-vitro skin experiments was investigated next to study its practical applications to the real world.

Non-invasive sensing has been the subject of much research in the past 10 to 15 years and has aimed at the development of a solution that provides much needed physiological and biological information and helps avoid complicated or painful procedures. It has been demonstrated that in patients with both type 1 and type 2 diabetes, fingerstick glucose monitoring is associated with significant stress, pain, apprehension and physical symptoms that impair the daily life of an individual [1]. Diabetes mellitus is a metabolic disease originating from damaged pancreatic cells or induced insulin resistance that involves inefficient metabolic conversion of blood glucose leading to high blood glucose, i.e., hyperglycaemia (see chapter 1, section 1.2.1) [2]. The disease, if not managed correctly, can lead to problems ranging from minor symptoms to life threatening pathologies [2]. It is therefore fundamental for diabetics to be able to assess their blood glucose levels regularly in order to control their glucose intake or the requirement for an insulin injection.

The most widespread technique to monitor blood glucose to this date involves the use of a fingerstick meter as a self-monitoring blood glucose (SMBG) technology. This requires a small sample of blood (as low as 0.3 µL) deposited on an electrochemical sensor [3]. Improved monitoring technologies would be required to help patients with their disease management. Research in this area has followed two principal directions so far: implantable and non-invasive sensing, respectively. Implantable sensors provide continuous monitoring through devices surgically placed inside the body, mostly subcutaneously [4]. This research

area is however still controversial due to multiple limitations: it requires surgical interventions and calibrations while being plagued by short lifetime, lag time, biocompatibility issues and expensive costs (see chapter 1, section 1.3.5.1) [5].

An alternative is the promising research area of non-invasive sensing. This has attracted much interest in the past and several strategies have been proposed, such as glucose detection from tears [6] or transdermally [7] (based on multiple techniques listed in section 1.3.5.4); but the most notable and remarkable non-invasive system to have emerged is the GlucoWatch® Biographer developed by Cygnus in 2000 [8]. This device is based on a transdermal extraction technique, namely, *reverse iontophoresis* (RI), which involves the application of a low intensity current (i.e., 0.3 mA/cm^2) to the epidermis. The current creates a flux of ions in the anode-to-cathode direction. This flux will create a movement of H_2O molecules which will bring the solubilized glucose molecule to the epidermis level where it will be detected via a typical carbon paste/platinum electrochemical glucose sensor (the RI extraction principle is described in chapter 1, figure 1.5) [9]. The device was considered as an interesting competitor for the traditional fingerstick glucose technology, however, it failed commercially because of several drawbacks listed in chapter 1 section 1.1 [10, 11].

The aim of this chapter is to use the same extraction principle as the Cygnus device, but with the graphene-based sensor presented in chapter 4, and in a way that will help tackle some of the GlucoWatch ® Biographer failures and provide more accurate glucose monitoring. The electrodes therefore followed a design that would take advantage of both the CVD graphene properties and the principle of reverse-iontophoresis extraction. The latter is performed in the small volume of the sensor's gel receptacle. Essentially, the main attribute of the implementation is *iontophoretic glucose pathway targeting*, meaning that preferential transdermal glucose pathways will be accessed using an array of multiplexed sensing/extraction devices. Indeed, it has been demonstrated that when applying an iontophoretic current across the skin, charged molecules tend to follow preferential pathways, namely skin appendages (i.e., hair follicles or sweat ducts) [12, 13]. The skin itself is a complex barrier formed by several layers (see chapter 1, section 1.3.5.4.4) [14]. It therefore naturally acts as an efficient barrier to molecular extraction. It is however predicted that glucose will follow the path of preferential extraction through skin appendages (i.e., hair follicles) when applying reverse-iontophoresis extraction [15, 16]. In chapter 4 we demonstrated a competitive miniaturised sensor with 9 mm^2 active area and 24 µL enzyme

encased gel. Such miniature sensors could be used in a multiplex array that will target hair follicles, and give higher glucose concentrations, closer to the interstitial fluid glucose concentration than the GlucoWatch ® Biographer, which extracted glucose into a large reservoir (400 µL) [12]. The basic concept of this new technology is displayed in figure 5.1-B and compared to the GlucoWatch ® Biographer (figure 5.1-A). In figure 5.1-A the glucose extracted from the overall skin area is received in a large volume of gel and therefore diluted greatly before being detected by a disk platinum/carbon ink disk electrode. In figure 5.1-B even though every hair follicles pathway will not be detected, the multiplexed detections of the array ensure that at least several preferential pathways will be reached, while the smaller dimensions of the electrode and of the reduced gel volume can enable to obtain higher glucose concentrations to be detected.

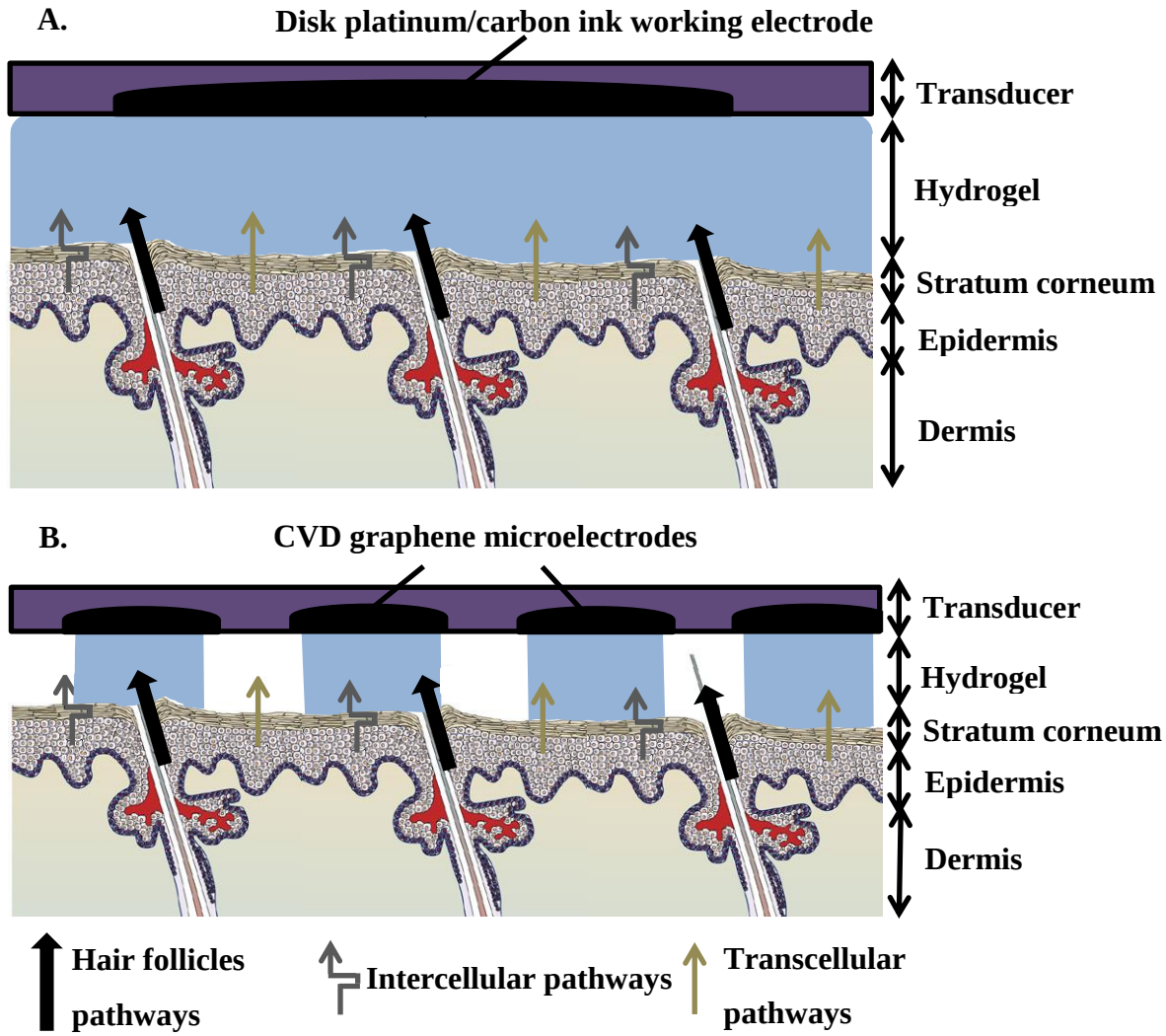

Figure 5.1. The principle of the "glucose path targeting" multiplexed device, contrasted with the GlucoWatch®. Skin depiction adapted from Prausnitz et al. [17]. A: RI extraction with the GlucoWatch ® Biographer. B: RI extraction with the proposed design.

5.1.1 GlucoWatch ® Biographer vs proposed technology

The main differences between our design and the GlucoWatch ® Biographer is the concept of targeting transdermal preferential pathways enabled by the reduction of the size and volume of the individual device. Nevertheless, other fundamental structural differences exist: (1) The GlucoWatch ® Biographer sensor consists of a screen printed platinum/carbon ink working electrode (on an alumina substrate) of relatively large area (i.e., 1.25 cm^2 [13], which is considerably larger than the sensor area, of 0.09 cm^2). (2) The material used for the electrode, as well as the fabrication process are radically different. The proposed technology uses CVD graphene leading to increased sensitivity, while the GlucoWatch ® Biographer relies on a traditional platinum electrode for its' electrochemistry [18]. (3) The GlucoWatch ® Biographer required an external calibration. In our design the extraction should be enhanced through the hair follicles and the dilution dramatically reduced, the concentration extracted should therefore be close to or similar to the interstitial glucose concentration, hence diminishing the need for an invasive calibration. This question is however debatable and dependant on the proportionality between blood glucose and interstitial fluid glucose already discussed in chapter 1, section 1.3.5.1.3. Nevertheless, if required, a calibrating sensor for Na^+ could be added to the multiplexed array. This uses the findings of Seig et al. who demonstrated that such ions could act as an internal calibration for the RI technique. The concentration of Na^+ is indeed constant in the skin, its' ratio with the extracted concentration would therefore provide the needed calibration for the technique [19]. This Na^+ could be designed as a field effect transistor and benefit from the findings presented in chapter 3 section 3.3.2. (4) The CVD graphene offers other interesting and important developments: (a) Large area of CVD graphene can be relatively easily deposited and patterned into small squares (structures) via photolithography and oxygen plasma etching [20], producing the intended multiplex array required for the targeting. (b) The nanomaterial is also remarkably flexible enabling the realisation of a skin-fitting flexible device which confers a big advantage over the GlucoWatch® Biographer designed on a solid, inflexible, substrate [21]. (c) Finally CVD graphene has very high conductivity (mobility of charge carriers of: 15,000 $cm^2\ V^{-1}\ s^{-1}$, see chapter 1, section 1.4.2.3) compared to traditional electrode materials. On the other hand, some similarities exist between the two concepts: both use reverse iontophoresis extraction, as well as gel entrapment [22] and are first generation in the detection method used. Table 5.1 summarises the differences and similarities between the two technologies:

Table 5.1. Attributes of the developed technology vs GlucoWatch® Biographer.

Sensor aspect	GlucoWatch ® Biographer	Developed sensor
Sensor material	Platinum on carbon ink [23]	CVD graphene/ Pt nanoparticles
Sensor construction	Screen printed electrodes	Wet/Dry transfer of CVD graphene.
Enzymatic glucose detection	First generation GOD/ electrochemical sensor	First generation GOD/ electrochemical sensor
Enzymatic entrapment	Hydrogel	Hydrogel
Reservoir volume	400 µL	24 µL (per sensor)
Sensor dimensions	1.25 cm^2	0.09 cm^2 (per sensor)
Substrate	Solid	Flexible substrate in a commercial form
Requirement for an invasive calibration	Yes	Not expected/ Possible integration of Na^+ standard sensor
Extraction principle	RI	RI
Transducing material	Detection using hydrogel enzyme entrapment	Detection using hydrogel enzyme entrapment
Reverse iontophoretic detection	No preferential pathway targeting	Hair follicles targeting

5.1.2 Proton NMR (^{1}H qNMR) spectroscopy as a quantitative comparative technique for RI extracted glucose concentrations

Several techniques have been used in the literature to assess the concentration of glucose in various samples. The most widely used and described involve the detection with GOD and horseradish peroxidase (POD) in a colorimetric test as described in chapter 2, section 2.2.4, but this technique is unsuitable here as a comparative test for the glucose extracted via RI since it relies on the same enzyme (GOD) used in the sensing detection (see chapter 4). ^{1}H

qNMR was thereafter implemented as a promising control technique for the developed technology.

5.1.2.1 ^{1}H qNMR principle

NMR spectroscopy is based on the spin of the atomic nucleus in a molecule and their behaviour in a set magnetic field. The most common NMR analysis are based on the spin of hydrogen and are referred as ^{1}H NMR. It focuses on the effect of the applied magnetic field on the spin of the different hydrogens and their emission energy. This last value depends on the neighbouring hydrogen atoms in the molecule. It is therefore possible to reconstruct a molecule with its' ^{1}H NMR spectra. In that sense, the technique appears to show very interesting qualitative information. This will be very useful in order to select glucose from a complex gel enzymatic extraction sample, but the main attribute of the reference technique should be the quantitative validation of glucose levels. qNMR or quantitative NMR was introduced in 1970 by Turczan *et al.* [24]. It is based on equation 5.1 describing the proportionality between the NMR signal intensity and the number of nuclei involved in a particular resonance [25].

$$\mathrm{I_x} = \mathrm{K_s} \times \mathrm{N_x} \qquad (5.1)$$

NMR intensity signal (I_x) described as a function of the nuclear number (N_x) and the spectrometer constant (K_s) which depends on pulse excitation, repetition time and broad band decoupling [25]. From this formula, relative or absolute quantification can be obtained. Relative quantification relates to equation 5.2. It is a molar ratio between the compound x and the other species present in solution.

$$\frac{n_x}{\sum_{i=1}^{m} n_i} = \frac{I_x/N_x}{\sum_{i=1}^{m} I_I/N_I} \times 100\% \qquad (5.2)$$

n_x/n_i represents the molar ratio between the molecule of interest *x* and the *m* compounds in solution, *I* is the intensity of the signal and *N* is the nuclear number.

On the other hand, absolute qNMR relates to the use of a standard of set NMR intensity, usually giving a singlet at low ppm. A good NMR standard should be inexpensive, stable, available in pure form, not hygroscopic, soluble in NMR solvents and displaying a simple singlet signal [26]. Absolute qNMR is used in this chapter, with the internal standard: 3-(trimethylsilyl)propionic-2,2,3,3-d4 acid sodium salt (TMSP-d4). It will be used to normalise the NMR signal obtained for glucose in the complex provided mixture, allowing to

effectively quantify the selected NMR peak and cancel the chemical shifts observed between measurements [27].

5.1.2.2 Advantages of ^{1}H qNMR over other quantification techniques

The main advantages of ^{1}H qNMR over other traditional quantitative techniques is the direct nuclear signal without interferences or the use of biological intermediates (enzymes). Several molecules can also be quantified from the same sample with only one standard. ^{1}H qNMR displays simple sample preparation, small analysed volumes and fast and easy procedures that will be appropriate to future analysis [27]. Finally, ^{1}H qNMR analysis was defined as "more precise and accurate than the chromatographic methods" [28]. The confidence in the choice of this reference technique for the new RI coupled sensor was therefore high.

5.1.2.3 Glucose ^{1}HqNMR

The singular identifiable resonance of glucose will come from its α or β proton on the terminal C-OH group. When studying glucose in a complex mixture, two fundamental aspects will direct the analysis to this particular proton. (1) Firstly, the α/β proton is connected to oxygen. It is deshielded by the electron withdrawing effect of the electronegative oxygen atom. (2) Secondly, the position of the proton (equatorial = β or axial = α) will shift the value at which the proton resonates [29]. The β form of the hydrogen displays a typical signal of 4.6 ppm while the α one was identified at 5.2 ppm [30].

5.1.3 Multiplexing of the graphene sensor

One of the very interesting properties of CVD graphene is its ability to be transferred in relatively "large dimensions" to arbitrary substrates, a useful feature in design development. Several techniques have been described to achieve the efficient transfer of large monolayer graphene sheets, including: the wet etching [31], roll to roll [32] and soak and peel techniques [33]. Multiplexed graphene sensors have been described in the literature, for example in the areas of pH sensing [34], cell proliferation study [35], and the detection of chemicals in the vapour phase [36]. To-date, however, while no amperometric multiplex CVD graphene sensor has been described, the scale-up of the sensor developed here to a multiplex array appeared realistic. In the final section of this chapter, a single large scale, unpattern CVD graphene sample is therefore examined to assess whether it may be used to sense glucose simultaneously in separated compartments without any "cross-talk" between the sensors.

5.2 Materials and experimental methods

5.2.1 Materials

NaCl, KCl, Na_2HPO_4, NaH_2PO_4, KH_2PO_4, ethylenediaminetetraacetic acid, BIS-TRIS hydrochloride, EDTA, NaOH, AgCl, glucose oxidase, D-glucose, low gelling temperature agarose, hydrogen hexachloroplatinate (IV) hydrate, H_2SO_4, $FeCl_3$, were purchased from Sigma Aldrich (Dorset, UK). Milli-Q water was used for all the solutions. CVD graphene was provided by the Univeristy of Bath, UK on copper, and transferred on a silicon dioxide substrate according to the procedure described in chapter 2, section 2.2.2.1. Abdominal pig skin was collected from a local abattoir, dermatomed (Zimmer®, Ohio, USA) to a nominal thickness of 750 µm, frozen within 24 hours of slaughter and thawed before use. β-agarase was purchased from Thermo Scientific (Loughborough, UK), TMSP-d4 from Goss Scientific (Shavington, UK) and Silcoset 151 ACC silicone rubber from Farnell (Leeds, UK).

5.2.2 Experimental methods

5.2.2.1 Electrode design

The sensing electrodes were first prepared as described in chapter 2 section 2.2.2.2, platinum nanoparticles were electrochemically deposited as presented in chapter 4 section 4.3.1.2 and a GOD entrapped gel was casted on top of the electrode following *entrapment method 3*.

5.2.2.2 Demonstration of dual function: reverse iontophoresis (RI) coupled with electrochemical sensing

10 and 100 mM glucose solutions were prepared in PBS and left to mutarotate overnight for use as the subdermal solutions for the RI experiment. The amount of chloride in the glucose/PBS solution was more than sufficient to supply the electrochemical demands (i.e. chloride requirement with Ag at the anode to create AgCl and one e^-). Indeed, the required amount was calculated as 0.9 mM which is well in the range of PBS. When starting a RI experiment, a piece of skin was placed on a 7.5 mL Franz cell, with the epidermis up. The cell was then filled with 7.5 mL PBS/glucose, placed on a magnetic stirrer and stirred for 1 hour before the operation. Ag/AgCl electrodes were prepared for the experiment by depositing molten AgCl on a silver wire. These would serve as cathodes placed on top of the

GOD/gel reservoir touching the epidermis. Some other electrodes were electrochemically treated in a solution of saturated KCl overnight to induce the formation of silver that will act as anodes placed inside the subdermal compartment. It is important to note at this point that the experiments presented were not done in a completely non-invasive situation, where both electrodes would need to be on top of the skin, but the reverse iontophoresis was executed with one electrode in the subdermal compartment and the other electrode touching the skin/gel reservoir. However, this was of minor importance considering that any change in the skin membrane resistance at a constant iontophoretic current is correlated with a change in the voltage across the resistor (decrease). So at constant current the amount of ions involved in the RI process will remain unchanged (only the voltage across the skin will double) and the amount of glucose extracted should be similar [37]. The model appears therefore appropriate for correlation with non-invasive analysis. Figure 5.3 displays the RI setup involving one electrode on each side of the skin sample.

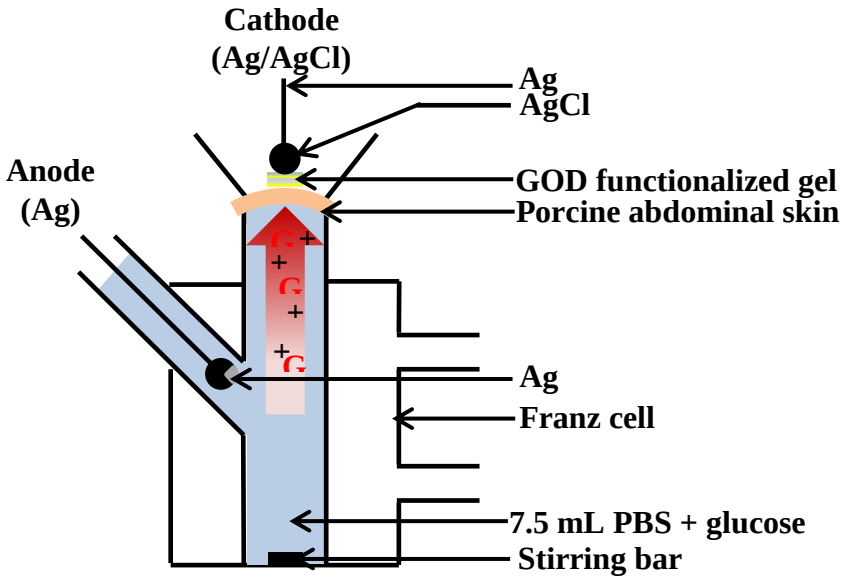

Figure 5.3. Reverse iontophoresis setup. The anode is placed in the subdermal compartment and the cathode in contact with the GOD/gel reservoir on top of the skin. During the RI process, oxidation occurs at the silver anode to form AgCl and one electron. Inversely, the cathode displays a reduction of AgCl to Ag + Cl^-. The red arrow symbolises the RI flow of glucose molecules G.

RI was performed by passing 0.2 mA (equivalent to 2.2 mA/cm^2) between the anode and cathode from a generator (Kepco power supply, MB electronic). Each RI extraction experiment lasted 1 hour. Chronoamperometry was obtained before and after each RI. Chronoamperometry was first performed before the RI experiment with a CVD graphene/ Pt nanoparticles electrode and 24 µL of gel containing 4 mg/mL GOD as described in chapter 4 (*entrapment method 3*).

The experiment was performed at 0.4 V against an Ag/AgCl micro-reference electrode (with a Pt counter electrode) for 700 seconds. The gel was then excised and RI was applied, as previously described. After the RI extraction was completed, the gel was placed on the electrode again and the chronoamperometry was repeated as before. Current results were averaged over 600 seconds (from 100 seconds to 700 seconds, *except for the point displayed in red in figure 5.5: averaged from 100 to 240 seconds*) and subtracted from the chronoamperometry current values obtained before the RI. This provided a ΔI current which was then plotted on a glucose gradient concentration curve (see section 5.2.2.3.2).

5.2.2.3 Data analysis

5.2.2.3.1 "Gradient concentration curves"

The glucose "gradient concentration curves"; catalytic current = f(concentration), were obtained by previously testing the sensor with several glucose concentrations. They are represented as dotted black curves. The increase of catalytic current with addition of glucose were analysed similarly to the calibration curves for sensitivity analysis presented in chapter 4 (method described in chapter 2 section 2.2.3.2). The current was then plotted as a function of the concentrations of glucose and fitted with linear regressions. For both sections 5.3.1 and 5.3.2 (see figures 5.7, 5.8 and 5.10) the "gradient concentration curves" were separated between the "*low concentration ranges*" and the entire range, because most of the calibration curves didn't fitted the linear regressions in the "*low concentration range*". When plotting a low ΔI, it therefore appeared more accurate to use this "*low concentration range*" in order to get the most realistic value of the extracted concentration.

5.2.2.3.2 chronoamperometric signal: "ΔI"

The chronoamperometric signal obtained before and after reverse iontophoresis for both experiments (see figure 5.6) presented different slopes. These differences relied on the experimental conditions: the drying of the gel (and therefore the diffusion of glucose) was not constant between experiments. The proposed solution was to take the average of the catalytic signal and hence account for each of the decays over 600 seconds (140 seconds for the red points in figure 5.8). The first 100 seconds were not analysed in order to cancel the initial decay of any chronoamperometric operation. This decay is described by the Cottrell equation (see chapter 2, section 2.1.2.7). The subtraction of the signal after and before reverse iontophoresis is designated as ΔI. The ΔI values were corrected for volumes of gel (*footnote 5.α*) and reported on the glucose gradient giving corresponding glucose concentrations.

[5.α] The initial volume of gel used for the glucose gradients was 27 µL (GOD concentration: 3.56 mg/mL), while the volume of gel during the RI process was 24 µL (GOD concentration: 4 mg/mL). The obtained ΔI results were hence corrected for volume before being plotted on the glucose gradients (by multiplying by a 27/24 factor).

5.2.2.4 Control experiment

A control experiment is presented in figure 5.8 in which the same experimental protocol is applied but without any glucose in the subdermal compartment during the RI.

5.2.2.5 Hair follicles targeting

In a second instance, abdominal porcine pieces of skin were classified into "less hairy" (LH) and "hairy" (H) samples. Typically the difference in hair frequency ranged from 2 to 6 times (LH samples were defined as presenting ≤ 22 hairs/cm^2 while H samples had a hair density ≥ 34 hairs/cm^2). The positioning of the gel was of utmost importance and was achieved using a binocular microscope. Gels were specifically positioned on top of a single or multiple hairs of the H samples whereas effort was made to avoid any hairs on the LH samples. Figure 5.4 shows the RI setup with the gels strategically placed for targeting the hair follicles (H sample) or avoiding them (LH sample). Depending on the hair follicle density, it was possible to achieve a comparison between hair/no-hair extraction (see table 5.2).

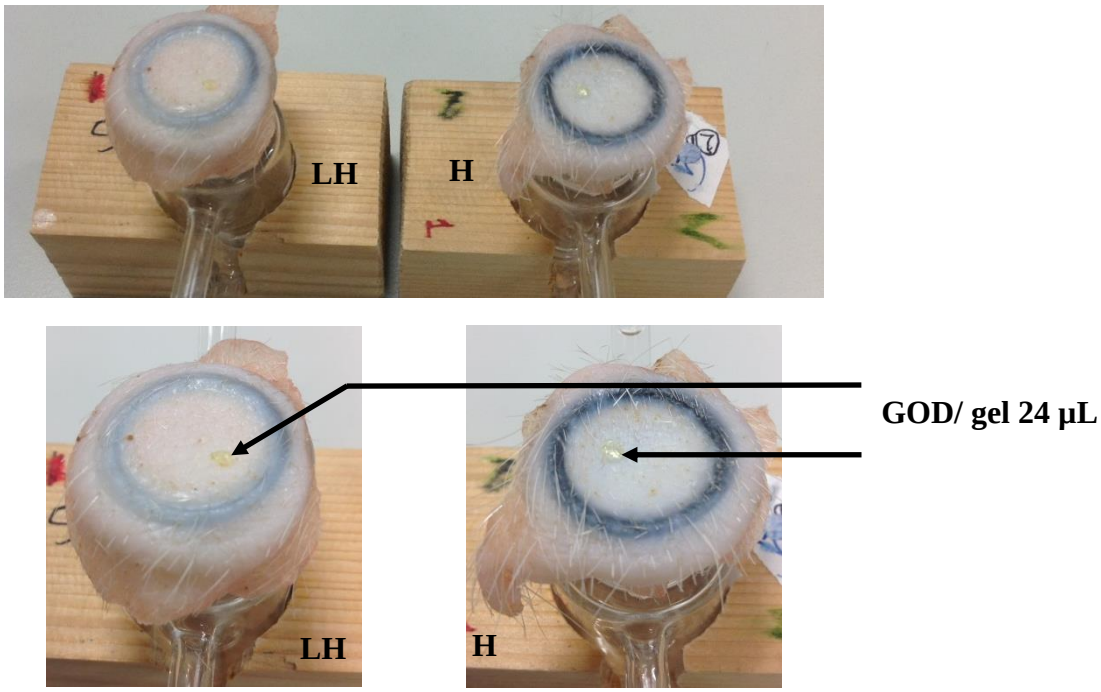

Figure 5.4. H and LH samples for reverse iontophoresis. Photography of the hair targeting setup on porcine skin: the yellow GOD-loaded gel is placed on top of a hair using the H sample, or in between hairs using the LH sample. In these pictures, the hair density was estimated to be 17 hairs/cm^2 for LH and 39 hairs/cm^2 for H.

The experiment followed three steps: First, two chronoamperometry were acquired at 0.4 V against an Ag/AgCl micro-reference electrode (with a Pt counter electrode) before reverse iontophoresis. The same electrode but two different GOD-loaded gel pieces were used that will then be placed on H and LH samples (see figure 5.4). Then, RI was performed for 1 hour with a 100 mM glucose subdermal concentration for both LH and H skin samples, in a similar set-up as figure 5.3. Finally, two chronoamperometry were again acquired at 0.4 V against an Ag/AgCl micro-reference electrode (with a Pt counter electrode), on the sensing electrode after RI. The increase of current ΔI between the chronoamperometry acquired before and after the RI were then reported on "glucose gradient concentration curves", see section 5.2.2.3.1, (*the concentration curves were obtained by previously testing the sensing electrode with glucose*). The concentrations corresponding to the ΔI fitted on the "glucose gradient concentration curves" will be the extracted concentrations.

5.2.2.6 ^{1}H qNMR spectroscopy

5.2.2.6.1 RI and sample preparation

Reverse iontophoresis was performed for 1 hour using the same setup as in figure 5.3, on H and LH skin samples (of 23 hairs/cm^2 and 8 hairs/cm^2 respectively), and with the subdermal glucose concentration set at 100 mM. The gels into which glucose was extracted (which did not contain GOD) were then diluted (1:5, vol/vol) in Bis-Tris/EDTA (10 mM/1 mM) buffer at pH 6.5. The mixture was warmed at 65 °C for 10 minutes, and subsequently cooled to 42°C before being incubated with one unit/100 µL of β-agarase for 1 hour at 42 °C. The β-agarase is an enzyme that is used to dissolve the low gelling temperature (LGT) agarose gel in order to obtain a liquid sample for ^{1}H qNMR analysis.

In parallel, a calibration curve displaying the NMR signal as a function of the glucose concentration was constructed with 24 µL samples of gel (without GOD) containing known concentrations of glucose : 250 µM, 1 mM and 19 mM respectively, (i.e., not obtained through RI) and dissolved in the same way (dotted black line in figure 5.11). Finally, the reverse iontophoresis values were reported on the calibration curve in order to assess the extracted glucose concentrations.

5.2.2.6.2 ^{1}H qNMR

120 µL of dissolved gel samples were inserted into a NMR analysis tube with TMSP-d4 *(as the internal standard)*. The NMR solvent was deuterium oxide (D_2O). Spectra were recorded on a Bruker Advance III NMR spectrometer operating at 500.13 mHz. Results were analysed with Topspin 2.1 software.

5.2.2.7 Multiplexing of the sensor

5.2.2.7.1 CVD graphene transfer

A Large piece of graphene of 36 mm^2 (figure 5.14) was transferred onto Si/SiO_2. The transfer via wet etching was obtained using the method described in chapter 2, section 2.2.2.1.

5.2.2.7.2 Pt nanoparticles treatment

The graphene sheet was then treated electrochemically for Pt nanoparticles deposition, with 50 µL of 1.7 mM hydrogen hexachloroplatinate and 0.1 M H_2SO_4, as described in chapter 4 section 4.2.2.3. Once transferred, the sample was patterned into 4 wells of 3×3 mm, using Silcoset 151, ACC silicone, Farnell (Leeds, UK).

5.2.2.7.3 Enzymatic gels

Glucose oxidase and then LGT agarose were cast on the graphene compartments up to a volume of 24 µL using *entrapment method 3*.

5.2.2.7.4 "Cross-talking" investigation

Sensor "cross talk" was assessed on a 2×2 multiplex. Unfortunately two of the four sensors did not display any conduction (probably due to problems on the graphene structure that occurred during the wet etching transfer). Attention was therefore focused on the two remaining functional sensors onto both of which were placed 24 µL of GOD-loaded gel. Chronoamperometry was performed on the first sensor (A) at 0.4 V against a micro Ag/AgCl electrode for 500 seconds. This was repeated on the other functional sensor (B) with the same conditions except that it was exposed to a series of increased glucose concentrations so that the characteristic step-like catalytic activity could be observed. Finally, the chronoamperometry experiment was repeated on sensor (A) to assess if any signal was detected due to the glucose additions to sensor (B).

5.3 Results

5.3.1 Demonstration of dual function: reverse iontophoresis coupled with electrochemical sensing

This section demonstrates that one individual sensor can perform both glucose extraction through reverse iontophoresis and electrochemical sensing of glucose. The device consisted of CVD graphene with the GOD entrapped gel and platinum nanoparticles placed on top (*entrapment method 3*). No specific targeting of skin appendages is undertaken at this stage.

5.3.1.1 Cyclic voltammograms before and after RI

Cyclic voltammograms of the gel were acquired before and after RI with 10 mM and 100 mM subdermal glucose used in the RI step. Figure 5.5 shows the data obtained for the different concentrations of glucose. A clear difference in the extraction was identified between the two different subdermal concentrations. It can be seen that in figure 5.5-A that the lower concentration (10 mM) shows almost no difference in the signal between the cyclic voltammetry before and after RI whereas at 100 mM (figure 5.4-B) there is a very clear difference in the cyclic voltammograms. Figure 5.4-B shows a peak at 0.4 V (*vs*. Ag/AgCl) indicating the presence of glucose extracted in the gel after RI.

A. 10 mM subdermal glucose

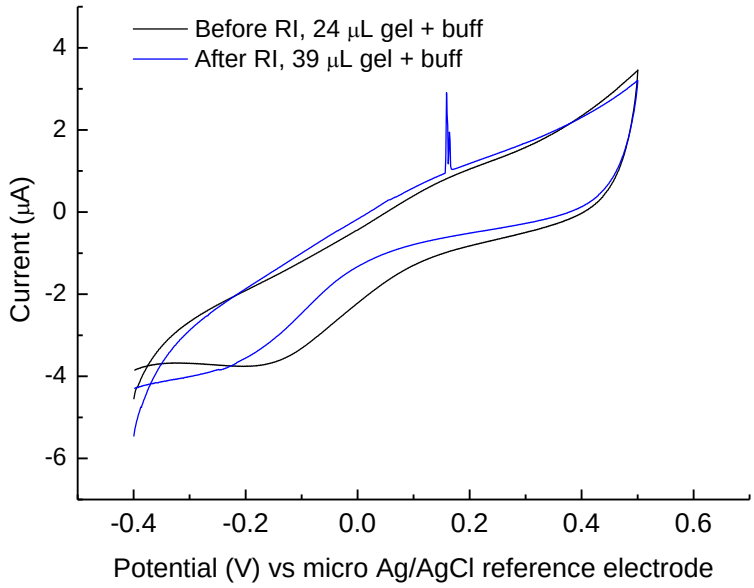

B. 100 mM subdermal glucose

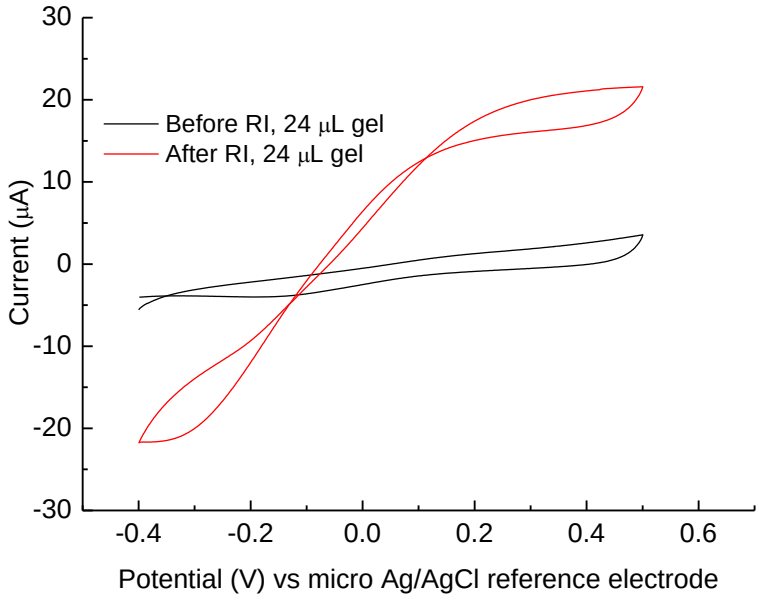

Figure 5.5. Cyclic voltammograms before and after reverse iontophoresis with 10 and 100 mM glucose subdermal concentration. A: RI applied with 10 mM subdermal glucose concentration. B: RI applied with 100 mM subdermal glucose concentration, scan rate 20 mV/sec.

Chronoamperometry was also carried out on the gel at a constant potential of 0.4 V (*vs.* Ag/AgCl) before and after RI. Differences ΔI were obtained by subtracting the chronoamperometric currents (before and after RI), figure 5.6 A and B (see section 5.2.2.3.2). This method of glucose detection seems to be more sensitive as even the 10 mM subdermal

glucose concentration shows an increase in current after reverse iontophoresis. ΔI values were then reported on a glucose concentration gradient. From there glucose extracted values were estimated as shown in figure 5.7 A and B.

A. 10 mM subdermal glucose

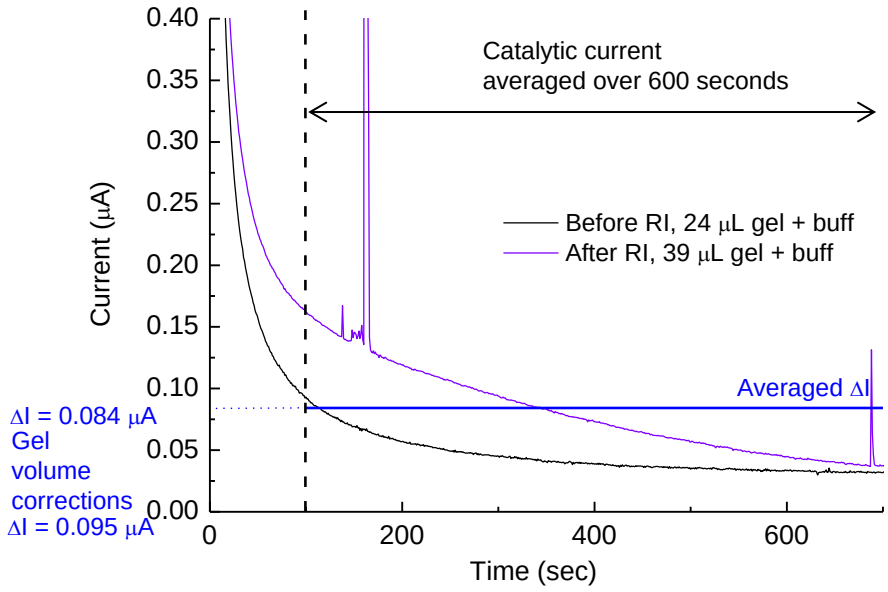

B. 100 mM subdermal glucose

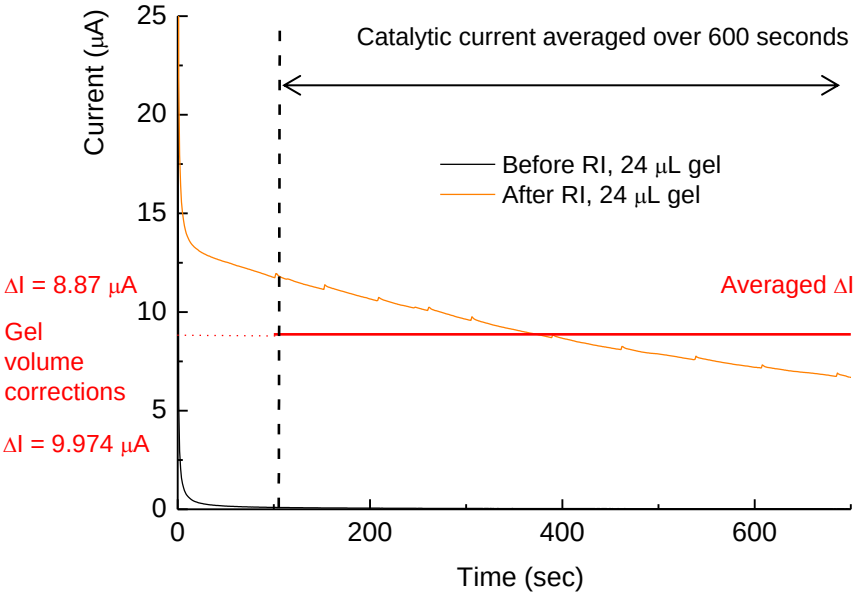

Figure 5.6. Chronoamperometric signal before and after reverse iontophoresis with 10 and 100 mM glucose subdermal concentration. A: RI applied with 10 mM subdermal glucose concentration. B: RI applied with 100 mM subdermal glucose concentration. Fixed potential vs micro Ag/AgCl reference electrode: 0.4 V.

A.

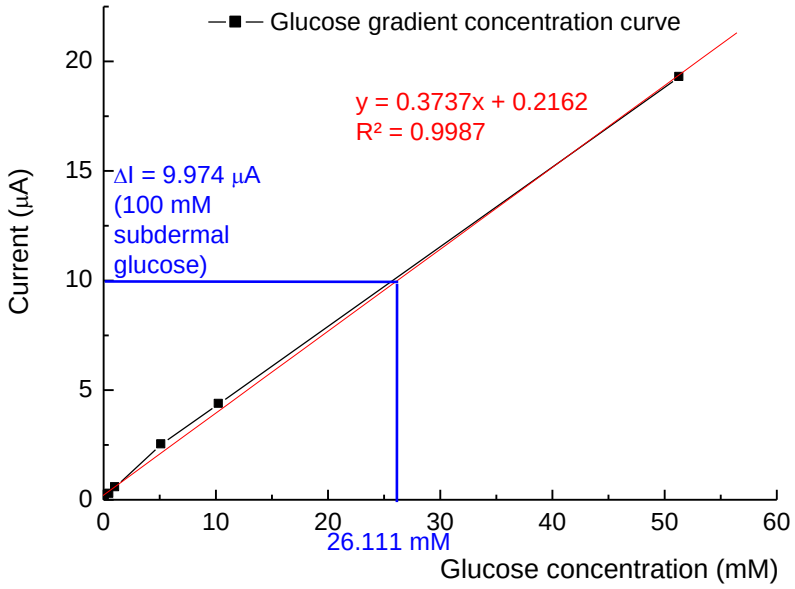

B.

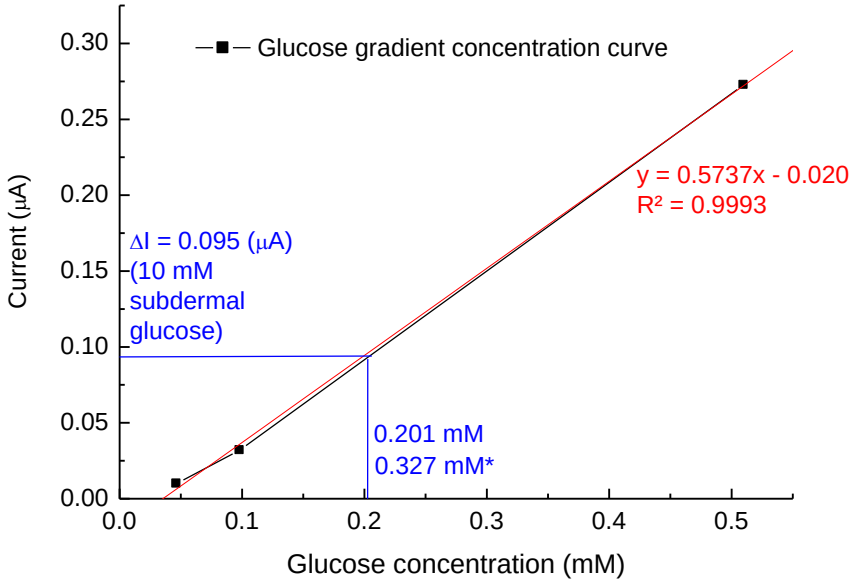

Figure 5.7. Chronoamperometric detection of extracted glucose via reverse iontophoresis with 10 and 100 mM subdermal glucose concentrations. The dotted black curves are gradient of glucose obtained with the sensor previous to the iontophoresis operation. The ΔI currents obtained from (A) and (B) in figure 5.6 were reported (in blue) on the sensor glucose gradient curve (black curves) and hence gave corresponding RI extracted glucose concentration values. A: plotting of the RI value obtained for 100 mM subdermal glucose on the entire glucose gradient curve (i.e. 0.05 mM to 50 mM). B: plotting of the RI value for 10 mM subdermal glucose for a *small concentration range* going from 0.05 mM to 0.5 mM. The * is a correction of the concentration following the dilution of the gel.

5.3.1.2 Repeatability of reverse iontophoresis detection

RI experiments were repeated under the same conditions as section 5.3.1.1, with different electrodes and different pieces of abdominal skin, from the same pig (see figures 5.8-A and 5.8-B). Even though the experimental conditions were variable the aim of this experiment was not to measure a repeatability on similar tissue models but rather assess if the extraction of glucose, differing ten times in concentration, was consistent with different sensor setups.

A.

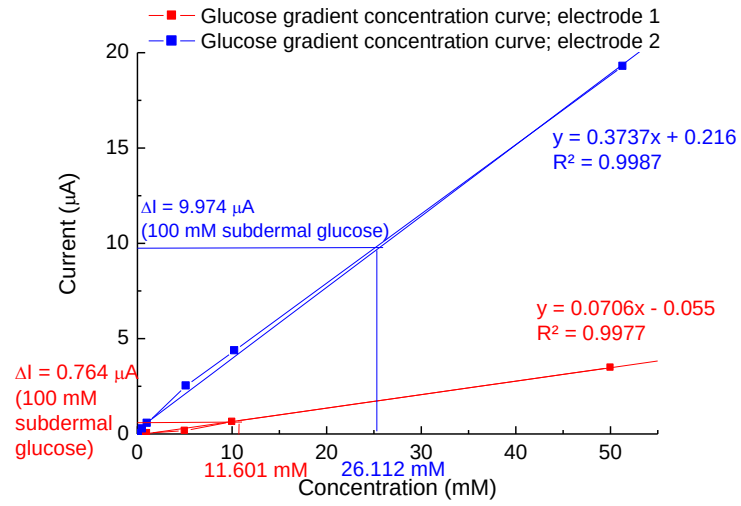

B.

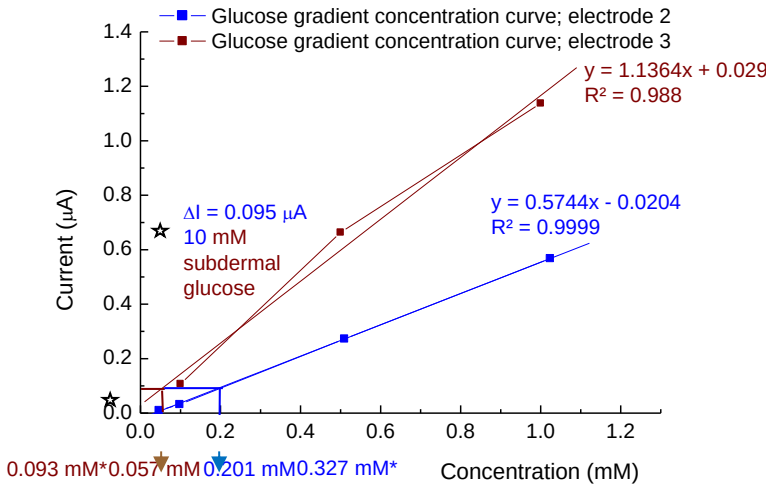

Figure 5.8. Repeatability of the reverse iontophoretic detection with 10 and 100 mM subdermal glucose concentrations. The blue curves are the glucose gradients presented in figure 5.7 with reported RI extraction current obtained from 10 and 100 mM subdermal glucose concentration. A. The red curve is the glucose gradient obtained with a second electrode with reported RI extraction current obtained from 100 mM subdermal glucose. B. The brown curve is the glucose gradient obtained with a third electrode with reported RI extraction current obtained from 10 mM subdermal glucose. These glucose gradients only present *small concentration ranges* going from 0.05 to 1 mM. The * is a correction of the concentration following the dilution of the gel.

5.3.1.3 Selectivity of the detection towards extracted glucose

Reverse iontophoresis was then undertaken in conditions similar to those described but without any glucose in the subdermal compartment to act as a control experiment. The GOD-loaded gel sensor (*entrapment method 3*) was tested, in figure 5.9, via chronoamperometry at 0.4 V (*vs*. Ag/AgCl) before and after the 1 hour of RI experiment. The control was positive since no significant increase in catalytic current was observed after the RI (blue curve).

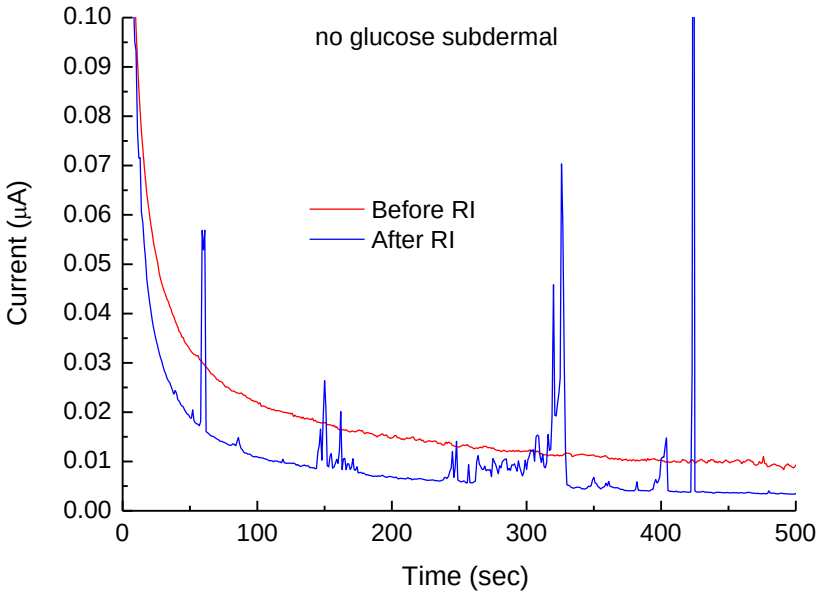

Figure 5.9. Selectivity of the RI extraction. The chronoamperometric current was obtained before and after RI without any glucose in the subdermal compartment. The RI and chronoamperometric experiments were acquired under the same conditions as used in figure 5.6. The spikes observed on the blue curve are most likely due to noise coming from the experimental setup.

5.3.2 Hair follicles targeting

The RI flux is not uniform over areas of the skin and appendages such as sweat, sebaceous glands or hair follicles appear to have a dominant role in the process. The structure of the skin as well as the preferential reverse iontophoresis extraction through hair follicles is presented in chapter 1 section 1.3.5.4.4.2. The following section focuses on hair follicle targeted extraction into micro-gels and glucose detection with the developed graphene sensing device.

5.3.2.1 Targeted RI

Chronoamperometry was performed on gel samples both before and after RI. The RI was operated on skin samples with lots of hairs (H) and less hairy samples (LH). A net increase in the current signal was observed, in figure 5.10, from sample H (i.e. hairy extraction; depicted in pink) as compared to sample LH (i.e. less hairy extraction; depicted in blue).

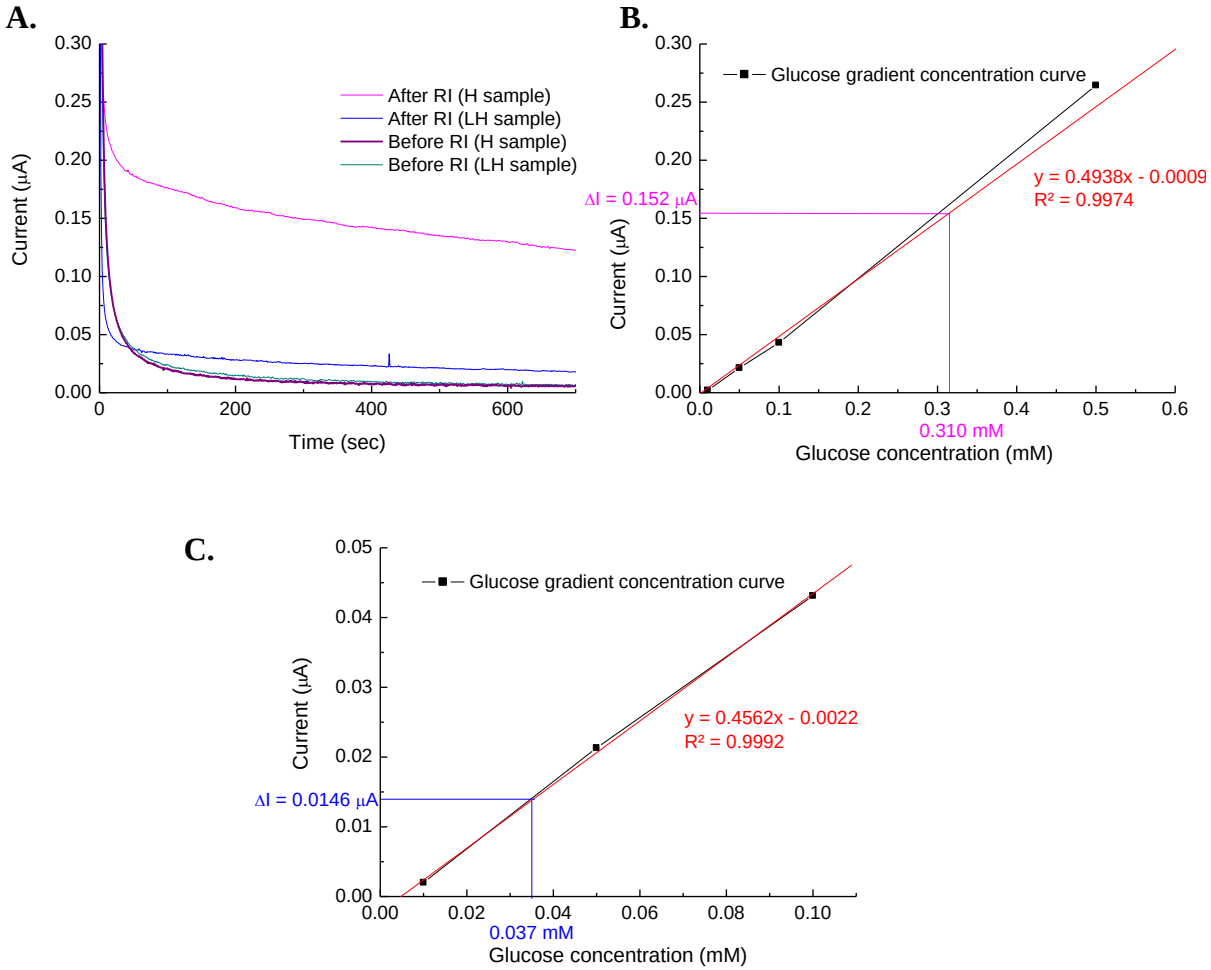

Figure 5.10. Extracted glucose concentrations from H and LH skin samples in a targeted hair/no-hair experiment. A: Chronoamperometric measurements acquired before and after RI from LH and H skin samples, of 6 and 34 hairs/cm^2 respectively. The signal was acquired at 0.4 V vs a micro Ag/AgCl reference electrode. B: Glucose concentration gradient curve (black dotted curve) obtained for the same sensing electrode used in (A). The extracted glucose concentrations ΔI for the H sample is indicated and plotted in magenta on the gradient curve. The glucose gradient curve displayed the all range of concentration tested (i.e. 0.01 mM to 1 mM). C: Glucose gradient curve displayed over a *low concentration range* (i.e. 0.01 mM to 0.1 mM). The extracted glucose concentrations ΔI for the LH sample is indicated and plotted in blue on the gradient curve.

5.3.2.2 Repeatability of targeted RI extraction

The same experiment was repeated with different LH and H samples and the same electrode. Extracted concentrations are displayed in Table 5.2 along with their average and standard deviation values. The hair density for each samples are also reported. The extracted concentrations didn't correlate with the densities of follicles (with high hair follicle density presenting low extracted concentrations). However, the concentration and hair density ratios showed similarity (i.e., average concentration ratio of the order of average hair density ratio). Moreover, even though the LH and H glucose extraction didn't show statistical difference (P(t.test)>0.05), H samples recurrently displayed increased concentrations (see Table 5.2).

Table 5.2. Comparison of extracted concentrations for LH and H samples. In addition with the concentration and hair density values the table also presents the student *P(t.test)* value used to assess the statistical difference between the two sets of concentrations (obtained from LH and H samples).

	Extracted concentrations (mM)		**Concentration ratios**	**Hair densities**		**Hair density ratios**
	LH	H		LH	H	
	0.017	0.031	1.824	22	46	2.091
	0.082	0.108	1.317	17	39	2.294
	0.037	0.310	8.378	6	34	5.667
Average concentrations	0.045	0.150				
Standard deviations	0.033	0.144				
Average concentration ratio			3.840	**Average hair density ratio**		3.351
***P(t.test)* applied to the extracted concentrations** *Two tailed, unpaired t.test, two sample, unequal variance*				0.336 (α=0.05)		

5.3.3 ^{1}H qNMR spectroscopy confirmation test

Reverse iontophoresis was then applied to H and LH samples in a similar way as section 5.3.2 but the samples (obtained in gel without enzymes) were analysed via ^{1}H qNMR which acted as an independent confirmation technique for the glucose extracted. The NMR results of these samples are shown in figure 5.11. They were then reported on a glucose calibration curve displaying normalised number of protons = f(glucose concentration) in figure 5.12 (black dotted curve). The measured doublet peak for glucose was observed at ~5.1 ppm (after TMSP normalization). The signal corresponds to the α-D-glucose [30]. β-D-glucose was then estimated from the proportionality between the two forms in solution at equilibrium: 64% β-D-glucose, 36% α-D-glucose [38] (the β glucose wasn't directly quantified due to the lack of specificity of the NMR signal in the gel mixture around 4.6 ppm). Table 5.3 displays the comparison between the ^{1}H qNMR β-D-glucose calculated extracted values and the ones obtained via electrochemical sensing.

A. H sample

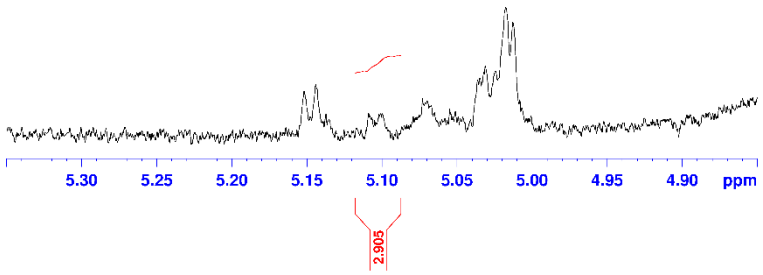

B. LH sample

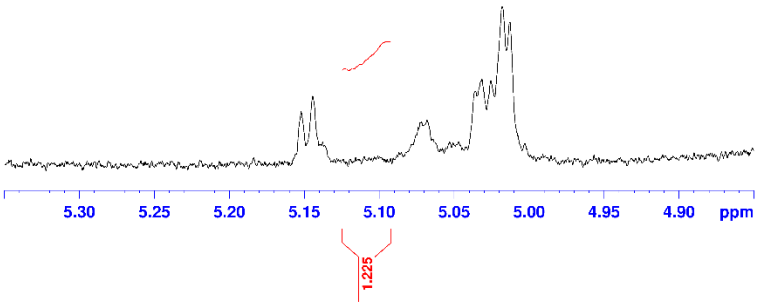

Figure 5.11. ^{1}H qNMR spectra from H and LH samples. Visualization of the α-D-glucose proton NMR signal at ~ 5.1 ppm and normalised for TMSP-d4. The signals were acquired after reverse iontophoresis (100 mM glucose subdermal concentration) on A: H samples and B: LH samples.

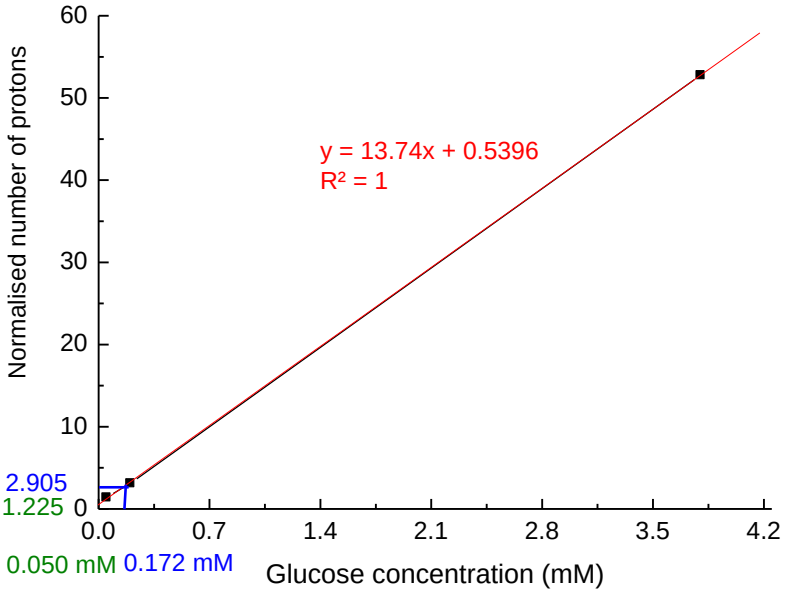

Figure 5.12. Extracted glucose concentrations from H and LH samples determined by NMR. The proton NMR signals of glucose extracted from H (blue) and LH (green) skin samples are converted to concentrations using the glucose calibration curve (black symbols). The glucose calibration curve was previously obtained by testing different concentration of glucose in the gels as described in section 5.2.2.6.1.

Different sets of skin samples (i.e., H and LH) have been used for the electrochemical (see figure 5.10) and ^{1}H qNMR evaluation of glucose extracted by RI. Again here even though different skin samples were used it didn't influence the problematic, which was to assess whether the extraction was preferential using both techniques or not. The concentration ratios are compared in table 5.3:

Table 5.3. Comparison between glucose analysis by electrochemical sensing and ^{1}H qNMR. The acquisition was conducted under the same RI conditions.

Technique	LH extracted concentration (µM)	H extracted concentration (µM)	Concentration ratio	Hair density ratio
^{1}H qNMR	α = 50 β = 89	α = 172 β = 306	3.438	2.875
Electrochemical (table 5.2)	17	31	1.824	2.091
	82	108	1.317	2.294
	37	310	8.378	5.667

The extracted glucose concentration ratios were then plotted as a function of their respective hair density ratios for both detection techniques (figure 5.13). The concentration ratios obtained via ^{1}H qNMR seems to fit on the same linear regression than the ones obtained electrochemically. A good proportionality between the two techniques was hence demonstrated.

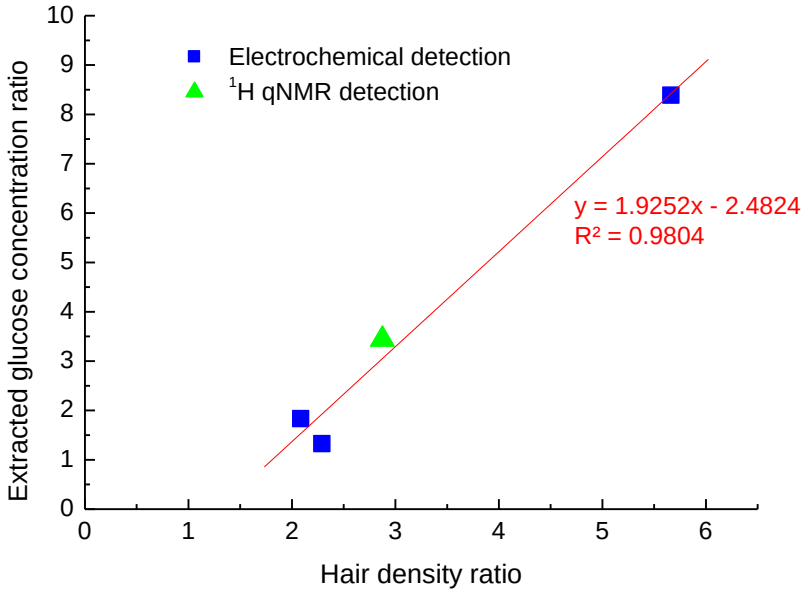

Figure 5.13. Extracted glucose concentration ratio = f(hair density ratio) obtained with electrochemical and ^{1}H qNMR detections.

5.3.4 "Cross-talk" experiment applied to a multiplex sensor configuration

The next step in the development of the non-invasive technology was the multiplexing of the sensor (on the same graphene sheet). Figure 5.14 depicts the chronoamperometric signal obtained in two sensors in which a GOD functional gel had been casted. Glucose was added in sensor (B) but no addition of glucose was made in sensor (A). A signal was acquired in (A) before and after additions in (B). The chronoamperometric signal difference ΔI at sensor (A) provoked by glucose exposure up to 1 mM in sensor (B) was about 0.13 µA. Based on the calibration curve (obtained in sensor (B), (see figure 5.14-B), the signal was only equivalent to 0.029 mM glucose (i.e., less than 3% of the total amount of glucose added to sensor B) and suggests very little cross talk between the sensors.

A.

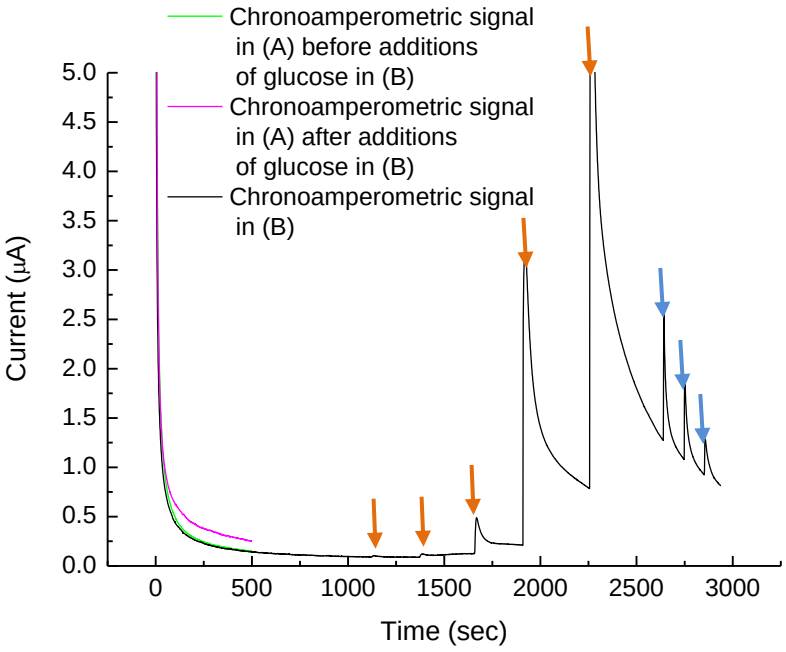

B.

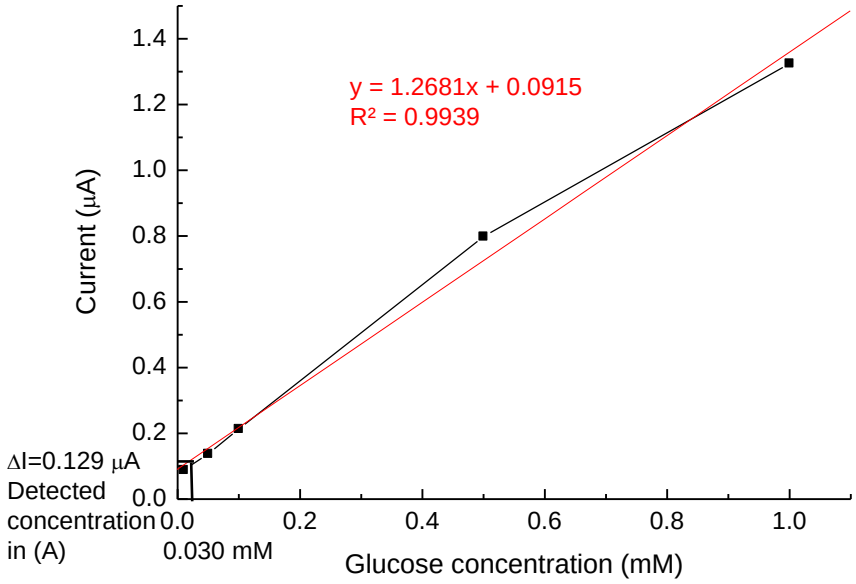

Figure 5.14. "Cross-talk" assessment between sensors on CVD graphene. A: Green and magenta lines are the chronoamperometric signals obtained on sensor (A) before and after, glucose additions in the sensor (B). The black line is the chronoamperometric signal observed in sensor (B) with additions of glucose concentration (the orange arrows are additions of glucose and the blue arrows are additions of buffer acting as a positive control in the experiment). B: The ΔI value from sensor (A) was reported on the glucose calibration (black dotted curves) obtained with sensor (B) and a "cross talking" concentration of 0.030 mM was found.

5.4 Discussion

5.4.1 Demonstration of dual function: reverse iontophoresis coupled with electrochemical sensing

From the first RI results described (Figures 5.5, 5.6 and 5.7) it was possible to validate two attributes of the technique: (1) the extraction of glucose through the skin, (2) the selective detection of glucose with the miniature sized sensor developed in chapter 4. Two subdermal concentrations differing by a factor of 10 were chosen for the initial test that provided a clear difference in the detection. The effectiveness of the extraction was demonstrated. The extracted concentration values (figure 5.7) were then converted into iontophoretic flux, respectively calculated as 39.2 nmol/h/mA and 3.13 μmol/h/mA for 10 and 100 mM subdermal concentrations. The ratio between the two fluxes was ~ 79.8. This value is significantly higher than the subdermal concentration ratio of 10. It could be explained by the drying of the gel not being controlled in the experimental protocol. This led to the re-dilution of the gel reservoir after reverse iontophoresis, but also and as presented in the next section to the overall overestimation of the extracted concentrations values of this section. The results nevertheless display a neat enhancement of extracted concentrations of glucose following the increase in subdermal concentration. Moreover, figure 5.8 indicated that a reproducible extraction of glucose was detected by different sensors that was within the sensitivity range. Noticeably, the 3 concentration gradients for electrode 1, 2 and 3 presented different slopes. This could be explained by the variability of signal from electrode to electrode itself influenced by many factors such as the quality of the deposited graphene, mechanical damage caused to the electrode while placing the gel, etc. Nevertheless, close concentration values were repeatedly obtained for extracted glucose: 93 μM and 327 μM for 10 mM subdermal concentration and 11.601 mM and 26.112 mM for 100 mM subdermal concentration. The selectivity of the sensor for glucose was finally demonstrated in figure 5.9 which didn't show any signal derived from RI samples treated without glucose. It was therefore possible to describe the glucose extraction and detection as highly selective (no interference coming from the skin itself). This section hence demonstrated the efficiency of the RI glucose extraction in small 24 μL volumes of GOD-loaded gel and the successful, coupled detection with the newly-developed sensor. However, thus far, no attempt to specifically target the hair

follicles had been made, the gels having been placed randomly onto the skin samples used. The next step, was therefore to investigate targeting of the hair follicles.

5.4.2 Hair follicles targeting

Hair follicle targeted extraction was then accomplished by placing the gels on top of hair follicles on H samples. Comparatively attention was placed to avoid any hair follicles on LH samples in order to compare the two collections of glucose (see figures 5.4 and 5.10). For both reverse iontophoresis experiments the subdermal glucose concentration was 100 mM. The respective extraction flux for H and LH extractions were then calculated as 37.2 nmol/h/mA and 4.4 nmol/h/mA. Following, are two aspects to be considered in the interpretation of the results: (1) The difference of order of magnitude between the values obtained here and in the previous section and (2) The preferential extraction through the hair follicles.

(1) The flux values obtained in this section are small when compared to the one obtained for 100 mM subdermal concentration in the previous section (i.e. 3.13 μmol/h/mA). Sieg et al. indicated in the literature that a glucose flux of 54.3 nmol/h/mA was obtained from a 10 mM subdermal glucose concentration [39]. In this study an iontophoretic current of 0.5 mA/cm^2 is passed through a skin area of 0.78 cm^2 for 6×1 h. The average hair density of a human subject in the thorax is 22 hairs/cm^2 [40]. Considering the area covered in the study, the average amount of hair involved in the extraction would be ~ 17. In our targeting experiment the hairy extraction flux is 37.2 nmol/h/mA for 100 mM subdermal concentration of glucose, it would therefore correspond to 3.72 nmol/h/mA for 10 mM subdermal. If this value is multiplied by the 17 hairs covered by Sieg et al., considering that the targeting only applies to a single hair, the resulting flux is 63.24 nmol/h//mA. This last result is close to the 54.3 nmol/h/mA obtained from the literature. It therefore appears that the results from the first section were over-estimated. The most logical explanation for these higher values is the drying of the gel during the experiment. As indicated by the * in Figures 5.7 and 5.8, the gel tended to dry during the experimental procedure (following mechanical pressure or longer time between experiments). This could have led to a significant increase in the glucose concentration of the sample from part one (however still proportional to the subdermal concentration of glucose).

(2) In a second instance, the results from figure 5.10 confirms the preferential extraction of glucose via the hair follicles pathways since a neat increase in extracted glucose concentration is observed for the hair targeting (H) when compared to no hair targeting (LH). The ratio between the obtained concentrations was ~ 8.4 which was in accordance with the hair density ratio between the two samples of ~ 5.7. In the same way, table 5.2 presents extracted glucose concentrations for H and LH samples obtained with different pieces of skin and hence different hair densities. The procedure did not allow for similar samples or hair densities between experiments. However, table 5.2 displays a resemblance between the average glucose extracted concentration ratio: 3.84 and the average hair density ratio: 3.351. These repeatability results were not, however, entirely consistent with the expected conclusion of preferential extraction of glucose through follicles since: (1) the H and LH extracted concentrations were not statistically different P(t.test)>0.05 and (2) the hair density of H samples didn't correlate with the extraction of glucose. This was likely due to the variability in the experimental protocol (positioning or drying of the gel) and related to the use of different abdominal pieces of skin acquired from the same pig. Nevertheless these experiments are a first demonstration of an already established theory of preferential extraction of neutral molecules (i.e. glucose) through follicles [16]: the extraction fluxes observed in figure 5.10 are indicative of this phenomenon.

5.4.3 ^{1}H qNMR spectroscopy confirmation test

An independent ^{1}H qNMR test was then developed for the quantitation of the glucose amounts extracted by a non-enzymatic method. The technique enabled the accurate quantification of the α glucose enantiomer concentration in RI samples. figure 5.11 displays the number of protons (normalised for TMSP-d4) for the α-D-glucose extracted by reverse iontophoresis with an H and LH sample. These values were then reported on a glucose concentration gradient and provided with the corresponding extracted concentrations values for α-D-glucose of 172 µM and 50 µM (figure 5.12). The respective β-D-glucose concentrations were then calculated from the proportion of enantiomers at equilibrium (see section 5.3.3) as 306 µM and 89 µM for H and LH samples respectively. The corresponding concentration ratio was 3.438 which resembled the skin samples hair density ratio of 2.875 (see Table 5.3). Moreover, when plotting the concentration ratios as a function of the hair density ratios, these fitted the same linear regression plot than the one obtained electrochemically with the sensor (see figure 5.13). A good agreement is therefore

demonstrated between the amounts of extracted glucose following different pathways measured with both detection techniques (electrochemical vs ^{1}H qNMR). Two conclusions could therefore be drawn: (1) ^{1}H qNMR spectroscopy is a good control technique for the developed technology and (2) the enhanced follicular extraction was confirmed by ^{1}H qNMR. This confirmation experiment however presented limitations: (1) the limited number of measurements in the glucose gradient curve (three; see figure 5.12) and (2) the lack of repeatability (single experiment). Hence, these results are not a statistically relevant demonstration of glucose sensing with ^{1}H qNMR, rather a promising step towards the implementation of a confirmation protocol for the developed sensor. To date, however, the combination of RI with ^{1}H qNMR detection for glucose detection has not yet been investigated in the literature, the procedure is therefore an original, state of the art technique. It is also a sensitive, specific and quantitative sensing of glucose in a mixture of enzymes and buffers *(with discrimination of the α and β enantiomers of the molecule)*, it does not require complicated sample preparation and small volumes can be analysed.

5.4.4 "Cross-talk" experiment applied to a multiplex sensor configuration

Figure 5.14 presents an attempt at building a multiplexed sensing device. Unfortunately half of the sensors failed probably due to an inefficient graphene transfer leading to the formation of defects and consequent conduction problems. However, several other graphene transfer techniques, as described before, could be investigated for further development [32, 33]. The figure studies the cross talking signal obtained in the compartment (A) when adding glucose in the compartment (B) (both being functional sensors). The chronoamperometric signal (ΔI: difference between the signal in (A) before and after glucose additions in (B)) is 3% of the total amount of glucose added in (B). It can therefore safely be concluded that the detections are well separated and independent from each other, even without patterning the graphene sheet (no physical separation/etching of the nanomaterial). Considering that a hair follicles extraction pathway glucose detection has already been demonstrated on one sensor, this multiplexing experiment will lead the way to an integrated RI-based targeting device.

5.5 Conclusions

The in-vitro application of the sensor from chapter 4 to transdermal glucose monitoring via RI was successfully demonstrated. The proportionality of the extracted detected glucose concentration in the micro-sized gels with the subdermal concentrations was first confirmed. The extracted results however overestimated (most likely due to drying) followed the increase in subdermal glucose concentrations. A hair targeting experiment was then implemented involving the positioning of the GOD containing gel on top of hair follicles or not. It was not however possible in the experimental procedure to be as precise as required to get the extraction from one hair only or no hair. The notion of hairy (H) samples and less-hairy (LH) samples was hence introduced in order to relate the hair density to the glucose extracted concentrations. Remarkably the glucose concentrations extracted from H samples were always higher than the ones extracted from LH samples. Furthermore, the ratio between the extracted concentrations (H/LH) were noticeably alike the hair density ratio (H/LH). Some discrepancies were however observed in between the results, principally in the concordance between the H samples hair density and the corresponding extracted concentrations. The extracted concentration for H and LH samples were also not significantly different (P(t.test) value > 0.05). Nevertheless, these results are a confirmation that the glucose is preferentially extracted through hair follicles and can successfully be detected with the miniature gel/sensor setup. Following this observation an independent confirmation test was necessary for the extracted concentration of glucose from H and LH samples that will act as a positive control towards the results obtained previously (i.e. section 5.3.2).

^{1}H qNMR was used following reverse iontophoresis with enzymeless gels on H and LH samples. The extracted concentration ratio (H/LH) detected with this technique fitted the linear regression of the extracted concentration ration (H/LH) obtained electrochemically. The control was hence positive and the conclusion obtained previously on the preferential extraction of glucose through hair follicles confirmed. The ^{1}H qNMR results were however obtained from a single experiment, attention will therefore be placed in the future work on repeating this control in order to attain satisfactory statistical significance. Finally, an attempt to multiplex the sensor was done that wasn't entirely successful: half of the four sensors failed to provide a signal. An important attribute was however studied that would be of major importance in a future multiple sensor configuration: the cross-talking between sensors signal. The last results of the chapter indicated that no such phenomenon is happening

significantly since only 3% of the signal was communicated from one sensor to the other on a continuous graphene sheet.

To summarize, the objective of demonstrating non-invasive targeted extraction coupled with the sensor technology was achieved and confirmed via an independent analytical tool. A multiplex sensor platform was also introduced that will provide an improved targeting of hair follicles and therefore high accuracy in the glucose detection.

1. Ong, W.M., S.S. Chua, and C.J. Ng, *Barriers and facilitators to self-monitoring of blood glucose in people with type 2 diabetes using insulin: a qualitative study.* Patient Preference and Adherence, 2014. **8**: p. 237-246.
2. Association, A.D., *Diagnosis and Classification of Diabetes Mellitus.* Diabetes Care, 2009. **32**(Supplement 1): p. S62-S67.
3. Yoo, E.-H. and S.-Y. Lee, *Glucose Biosensors: An Overview of Use in Clinical Practice.* Sensors, 2010. **10**(5): p. 4558.
4. Ghafar-Zadeh, E., *Wireless Integrated Biosensors for Point-of-Care Diagnostic Applications.* Sensors, 2015. **15**(2): p. 3236.
5. Cash, K.J. and H.A. Clark, *Nanosensors and nanomaterials for monitoring glucose in diabetes.* Trends in Molecular Medicine, 2010. **16**(12): p. 584-593.
6. Zhang, J., et al., *Noninvasive Diagnostic Devices for Diabetes through Measuring Tear Glucose.* Journal of Diabetes Science and Technology, 2011. **5**(1): p. 166-172.
7. Amir, O., et al., *Continuous Noninvasive Glucose Monitoring Technology Based on "Occlusion Spectroscopy".* Journal of Diabetes Science and Technology, 2007. **1**(4): p. 463-469.
8. Potts, R.O., J. A. Tamada, and M. J. Tierney, *Glucose monitoring by reverse iontophoresis.* Diabetes/Metabolism Research and Reviews, 2002. **18**(S1): p. S49-S53.
9. Chan, M.-S., et al., *Materials for Fabricating Biosensors for Transdermal Glucose Monitoring.* Clinical Chemistry, 1999. **45**(9): p. 1689-1690.
10. Eastman, R.C., et al., *Use of the GlucoWatch biographer in children and adolescents with diabetes.* Pediatr Diabetes, 2002. **3**(3): p. 127-34.
11. Iafusco, D., et al., *Usefulness or Uselessness of GlucoWatch in Monitoring Hypoglycemia in Children and Adolescents.* Pediatrics, 2004. **113**(1): p. 175-176.
12. Leboulanger, B., R.H. Guy, and M.B. Delgado-Charro, *Reverse iontophoresis for non-invasive transdermal monitoring.* Physiological Measurement, 2004. **25**(3): p. R35.
13. Tierney, M.J., et al., *Electroanalysis of Glucose in Transcutaneously Extracted Samples.* Electroanalysis, 2000. **12**(9): p. 666-671.
14. Baroni, A., et al., *Structure and function of the epidermis related to barrier properties.* Clinics in Dermatology, 2012. **30**(3): p. 257-262.
15. Cullander, C., *What are the pathways of iontophoretic current flow through mammalian skin?* Advanced Drug Delivery Reviews, 1992. **9**(2–3): p. 119-135.

16. Bath, B.D., H.S. White, and E.R. Scott, *Visualization and analysis of electroosmotic flow in hairless mouse skin.* Pharm Res, 2000. **17**(4): p. 471-5.
17. Prausnitz, M.R., S. Mitragotri, and R. Langer, *Current status and future potential of transdermal drug delivery.* Nat Rev Drug Discov, 2004. **3**(2): p. 115-124.
18. Berner, B., et al., *Monitoring of physiological analytes*, 2000, CA Patent 2332112 A1.
19. Sieg, A., R.H. Guy, and M.B. Delgado-Charro, *Noninvasive Glucose Monitoring by Reverse Iontophoresis in Vivo: Application of the Internal Standard Concept.* Clinical Chemistry, 2004. **50**(8): p. 1383-1390.
20. Kumar, S., et al., *Reliable processing of graphene using metal etchmasks.* Nanoscale Research Letters, 2011. **6**(1): p. 390.
21. Kwak, Y.H., et al., *Flexible glucose sensor using CVD-grown graphene-based field effect transistor.* Biosensors and Bioelectronics, 2012. **37**(1): p. 82-87.
22. Abraham, W., et al., *Hydrogel patch*, 1997, WO Patent 1997002811 A1.
23. Tierney, M.J., *Highly catalytic screen-printing ink*, 2006, US Patent 7018568 B2.
24. Turczan, J.W. and T. Medwick, *Qualitative and Quantitative Analysis of Amygdalin Using NMR Spectroscopy.* Analytical Letters, 1977. **10**(7-8): p. 581-590.
25. Bharti, S.K. and R. Roy, *Quantitative 1H NMR spectroscopy.* TrAC Trends in Analytical Chemistry, 2012. **35**(0): p. 5-26.
26. Griffiths, L., *Assay by nuclear magnetic resonance spectroscopy: quantification limits.* Analyst, 1998. **123**(5): p. 1061-1068.
27. Pauli, G.F., et al., *Quantitative 1H NMR. Development and Potential of an Analytical Method: An Update.* Journal of Natural Products, 2012. **75**(4): p. 834-851.
28. Wells, R.J., et al., *Quantitative Nuclear Magnetic Resonance (QNMR) Spectroscopy for Assessing the Purity of Technical Grade Agrochemicals: 2,4-Dichlorophenoxyacetic Acid (2,4-D) and Sodium 2,2-Dichloropropionate (Dalapon Sodium).* Journal of Agricultural and Food Chemistry, 2002. **50**(12): p. 3366-3374.
29. Drake, E.N. and C.E. Brown, *Application of nmr to biochemical kinetics. A laboratory experiment in physical biochemistry.* Journal of Chemical Education, 1977. **54**(2): p. 124.
30. Gurst, J.E., *NMR and the structure of D-glucose.* Journal of Chemical Education, 1991. **68**(12): p. 1003.
31. Li, X., et al., *Transfer of Large-Area Graphene Films for High-Performance Transparent Conductive Electrodes.* Nano Letters, 2009. **9**(12): p. 4359-4363.

32. Bae, S., et al., *Roll-to-roll production of 30-inch graphene films for transparent electrodes.* Nat Nano, 2010. **5**(8): p. 574-578.
33. Gupta, P., et al., *A facile process for soak-and-peel delamination of CVD graphene from substrates using water.* Sci. Rep., 2014. **4**.
34. Zaifuddin, N.M., et al., *pH Sensor Based on Chemical-Vapor-Deposition-Synthesized Graphene Transistor Array.* Japanese Journal of Applied Physics, 2013. **52**(6S): p. 06GK04.
35. Daly, R., et al., *Cell Proliferation Tracking Using Graphene Sensor Arrays.* Journal of Sensors, 2012. **2012**.
36. Nagelli, E., et al., *Sensor arrays from multicomponent micropatterned nanoparticles and graphene.* Nanotechnology, 2013. **24**(44): p. 444010.
37. Potts, R.O., *Mechanisms of Transdermal Drug Delivery*. 1997: Taylor & Francis.
38. Johnson, A.W., *Invitation to Organic Chemistry*. 1999: Jones and Bartlett Publishers.
39. Sieg, A., R.H. Guy, and M. Begoña Delgado-Charro, *Electroosmosis in Transdermal Iontophoresis: Implications for Noninvasive and Calibration-Free Glucose Monitoring.* Biophysical Journal, 2004. **87**(5): p. 3344-3350.
40. Otberg, N., et al., *Variations of Hair Follicle Size and Distribution in Different Body Sites.* J Investig Dermatol, 2004. **122**(1): p. 14-19.

Chapter 6: General conclusions and future work

6.1 General conclusions

This work presents a highly innovative method for non-invasive, transdermal glucose monitoring. The principle at its core is to target privileged reverse iontophoresis extraction pathways existing in the skin (such as hair follicles), through which glucose can be extracted directly from the interstitial fluid, and then detected by a coupled miniature, electrochemical glucose biosensor. Reverse iontophoresis enables even neutral molecules, such as glucose, to be extracted across the skin. The embodiment of multiple such sensors in a multiplexed array would provide a way to randomly reach such individual pathways by individual detectors in a future patch-like technology.

The main achievements of this work are:

(1) **The realization of a miniaturized, highly specific and sensitive first generation glucose biosensor based on glucose oxidase.** The sensor benefited from the incorporation of CVD graphene as a nanomaterial platform (advantageous for final implementations as patch-like technology due its mechanical resilience and flexibility), decorated with platinum nanoparticles to boost the electrochemical signal. The method of GOD enzyme entrapment into the gel put on top of the CVD graphene was found to be important in glucose detection and a suitable technique consisting of depositing a solution of the enzyme on top of the graphene and the gel dropped on top was found to be the best method. The miniature device displayed exquisite detection performance towards glucose and was later successfully multiplexed in a small-size array.

(2) **Successful integration of the electrochemical sensor with glucose extraction, *via* reverse iontophoresis, and demonstration of enhanced extraction *via* hair follicle targeting.** Proportionality between the source, sub-dermal concentration and the concentration of glucose extracted across the skin was demonstrated, with the extracted

glucose being detected electrochemically (by chrono-amperometry) by the coupled enzymatic sensor. The preferential hair follicle extraction was then confirmed with an experiment targeting the pathways and even though the results presented some discrepancies they tended to agree with the initial hypothesis of privileged extraction (as anticipated from the literature [1]). These results were further confirmed by correlation with measurements of extracted glucose concentrations via an independent ^{1}H qNMR technique. This confirmation experiment was not statistically significant (single experiment) but would lead the way to the implementation of an appropriate control for the developed technology.

Finally, some initial results were obtained on the multiplexed device based on the presented design. Although half of the sensor on the multiplex platform failed to give a signal, significant information was obtained: no cross linking was observed between two neighbouring sensor compartments on the same graphene sheet. These results are proof-of-concept of a future non-invasive, path-selective, highly sensitive and highly specific transdermal technology for glucose monitoring.

6.2 Future work

Future work is directed towards taking this proof-of-concept further and developing it into a complete technology, to be applied in real-life. This involves moving away from the current embodiment, which involved hard supporting substrates and macroscopic wiring, towards a patch-like technology, that requires flexible substrates and fully patterned, substrate-supported microelectrodes for both glucose extraction and detection.

Full size arrays of many (e.g. a 8×8 matrix) dual extraction/detection devices will need to be implemented to ensure that at least one hair follicle is reached by a sensor of the array in all cases of average density of hair follicles representative for human skin [2], as well as to provide some redundancy. Reaching this goal requires good uniformity in performance of all the sensors of the array, which is foreseen to be greatly influenced by the quality and uniformity of the supporting graphene layer. To this end, good control over the techniques for large area graphene transfer onto the desired, flexible substrates is highly important (this issue should be tractable in the same way as for other graphene-based flexible electronics, array-based applications that are being currently developed).

Some effort will also be made to further improve the sensor itself. Specifically further microscopic characterisation and optimization of the platinum nanoparticles deposition will be made. Some specific attributes will also be investigated or improved such as the speed of detection and the stability overtime respectively.

Another issue to be solved relates to the reproducibility of the characteristics of the enzyme-encasing gel; this requires higher control over the undesired process of gel drying that occurs during longer extraction times. This effect can be minimised by decreasing the glucose extraction time, which is a parameter linked to both the geometry of the sensor and the reverse iontophoresis process itself. It should also be solved by the integration of the sensor directly on top of the reverse-iontophoresis setup. This would also provide more control on the extraction and detection procedure since the gel receptacle will not have to be moved.

The preferential extraction through hair follicles and subsequent detection with the sensor although demonstrating promising results will have to be further repeated and the focus should be placed on the hair targeting with the gel (using microscopy for example). Similarly, ^{1}HqNMR was demonstrated to be an appropriate control test. However the results were only obtained from a single experiment. This control should hence be repeated to provide more robust comparison results.

A field effect transistor device for the detection of Na^{+} will also be developed (benefiting from the work presented in chapter 3 and the demonstration of Na^{+} as an internal standard for the reverse iontophoresis technique by Sieg et al. [3]) that will act as a calibration sensor for the technology (see chapter 5 section 5.1.1).

Finally, the developed multiplexed array monitor will need to be tested *in-vivo*, on human subjects, and several factors will need to be investigated such as the correlation between blood glucose and that extracted through the hair follicles by reverse iontophoresis, as well as variations between different skin areas or inter-individual variations.

1. Bath, B.D., H.S. White, and E.R. Scott, *Visualization and analysis of electroosmotic flow in hairless mouse skin.* Pharm Res, 2000. **17**(4): p. 471-5.
2. Otberg, N., et al., *Variations of Hair Follicle Size and Distribution in Different Body Sites.* J Investig Dermatol, 2004. **122**(1): p. 14-19.
3. Sieg, A., R.H. Guy, and M.B. Delgado-Charro, *Noninvasive Glucose Monitoring by Reverse Iontophoresis in Vivo: Application of the Internal Standard Concept.* Clinical Chemistry, 2004. **50**(8): p. 1383-1390.